Phenomenology of an odd scalar in a warped extra dimension

DISSERTATION

Submitted for the award of the title "Doctor of Natural Sciences" to the Faculty of Physics, Mathematics, and Computer Science of Johannes Gutenberg University Mainz in Mainz

JOHANNES GUTENBERG UNIVERSITÄT MAINZ

JG|U

Javier Castellano Ruiz

Born 25 November 1993 in Sevilla

Mainz, January 11, 2021

A mi abuela María.

Abstract

The Standard Model of particle physics has been tested to an unprecedented precision at the Large Hadron Collider, proving its success as the theory describing the laws of nature up to very short distances. However, there are still several open questions to which it cannot provide a viable answer, e.g. the unknown origin of fermion masses and the hierarchy problem. These questions inevitably point towards the presence of physics beyond the Standard Model.

Extensions of the Standard Model featuring a warped extra dimension compactified on an $S^1/\mathbb{Z}_2$ orbifold offer a convincing mechanism for addressing both the hierarchy problem and the flavor puzzle of the Standard Model. However, one aspect that has not been studied in detail so far is the coordinate dependence of bulk fermion masses. We propose a mechanism for dynamically generating these masses in warped extra dimensions by introducing an odd bulk scalar field, and demonstrate the feasibility of such proposal. Fermion 5D masses are obtained through Yukawa-like interactions after the odd bulk scalar acquires a vacuum expectation value. We can naturally reproduce the observed flavor structure and mass hierarchy of the Standard Model quark sector via different localizations of the fermion zero modes along the extra dimension, similarly to the conventional setup. The vacuum expectation value of the scalar field can induce backreaction effects on the Randal-Sundrum metric and deviations in the bulk fermion profiles. We study how such modifications can affect electroweak precision and flavor observables. We use the unsuppressed contributions to these parameters and up-to-date data to set a limit on the scale of new physics.

In addition, we argue that this extension of the Standard Model, featuring a warped extra dimension and a $\mathbb{Z}_2$-odd scalar singlet, provides a natural explanation, not only to the hierarchy problem and the nature of fermion bulk masses, but that it also has imprints in Higgs physics and introduces a new mediator between the Standard Model and any fermionic dark sector. The Kaluza-Klein excitations of the new scalar particle can be the leading portal to any fermion propagating in the bulk of the extra dimension playing the role of dark matter, therefore, contributing to reproduce the observed dark matter relic abundance. We show that the odd scalar excitations will necessarily mix with the Higgs boson, leading to modifications of the Higgs couplings and branching ratios and, at the same time, allowing the Higgs to mediate the coannihilation process of the fermionic dark matter. We study these effects and explore the viability of fermionic dark matter in the presence of the new heavy scalar mediators by considering different freeze-out scenarios.

Keywords: Randall Sundrum, Extra dimensions, Flavor Puzzle, Dark Matter

List of Abbreviations

In alphabetical order:

ADD	Arkani-Hamed, Dimopoulos and Dvali
AdS	anti-de Sitter
ATLAS	A Toroidal LHC ApparatuS
BC	boundary condition
BSM	beyond the Standard Model
BR	Branching ratio
CFT	conformal Field Theories
CKM	Cabibbo Kobayashi and Maskawa
CMS	Compact Muon Solenoid
d.o.f.	degrees of freedom
EM	electromagnetism
EOM	equation of motion
EW	electroweak
EWPT	electroweak precision tests
EWSB	electroweak symmetry breaking
GW	Goldberger and Wise
GR	General Relativity
IR	infrared
KK	Kaluza-Klein (KK)
LEP	Large Electron-Positron collider
LH	left-handed

LHC	Large Hadron Collider
NP	New Physics
PMNS	Pontecorvo-Maki-Nakagawa-Sakata
QED	Quantum electrodynamics
QFT	Quantum field theory
RH	right-handed
RS	Randall and Sundrum
SM	Standard Model
SSB	Spontaneous Symmetry Breaking
SVD	Singular-value decomposition
UV	ultraviolet
VEV	vacuum expectation value
VL	vector-like
WED	warped extra dimenson
WIMPs	weakly interacting massive particles
w.r.t.	with respect to
ZMA	Zero-mode approximation

Notations and conventions

We summarize here the notations and conventions used throughout this document. We use natural units, for which the Planck constant, h, and the speed of light, c, are set to the following values

$$\hbar = c = 1, \qquad \text{with} \qquad \hbar = \frac{h}{2\pi}.$$

We use greek indices, e.g. $\mu, \nu = 0, \ldots, 3$, to denote the four spacetime coordinates. We introduce Roman indices for denoting coordinates in 5 dimensions, where lower-case symbols $(a, b, \ldots)$ stand for local Lorentz indices, defined in the tangent flat space, while upper-case Roman indices $(M, N, \ldots)$ are used for objects defined in the curved space. In addition, we use Einstein's summation convention, i.e. indices that are repeated are summed over unless otherwise stated.

The Levi-Civita symbol is denoted by ϵ_{ijk}, and we use the following representation for the pauli matrices when necessary

$$\sigma_1 = \begin{pmatrix} 0 & 1 \\ 1 & 0 \end{pmatrix}, \qquad \sigma_2 = \begin{pmatrix} 0 & -i \\ i & 0 \end{pmatrix}, \qquad \sigma_3 = \begin{pmatrix} 1 & 0 \\ 0 & -1 \end{pmatrix}.$$

The transpose of a matrix A is denoted by A^T, the complex conjugate by A^* and the Hermitian adjoint is $A^\dagger = (A^*)^T$. The expression $+h.c.$ stands for "plus the hermitian conjugate" of the precedent quantity. Moreover, we denote the unitary group of degree n by $U(n)$ the special unitary group of same degree by $SU(n)$.

We employ the *time-like* convention for the metric tensor, i.e.

$$\eta_{\mu\nu} = \eta^{\mu\nu} = \begin{pmatrix} +1 & 0 & 0 & 0 \\ 0 & -1 & 0 & 0 \\ 0 & 0 & -1 & 0 \\ 0 & 0 & 0 & -1 \end{pmatrix}.$$

The gamma matrices are denoted as γ^μ and are defined by the anticommutation relations

$$\{\gamma^\mu, \gamma^\nu\} = \gamma^\mu\gamma^\nu + \gamma^\nu\gamma^\mu = 2\,\eta^{\mu\nu}.$$

Given a generic Dirac spinor Ψ, we define its adjoint by $\bar{\Psi} = \Psi^\dagger\gamma^0$.

Overview of publications

This thesis is based on the work appearing in the publications and preprints [1, 2]. Here we provide an overview of the work that is contained in them, and specify the contribution of the author.

[1] A. Ahmed, A. Carmona, J. Castellano Ruiz, Y. Chung, and M. Neubert, "*Dynamical origin of fermion bulk masses in a warped extra dimension*", JHEP 08 (2019) 045, [1905.09833].

In this work we consider an extension of the Standard Model featuring a warped extra dimension together with an odd bulk scalar field. We demonstrate the feasibility of dynamically generating fermion bulk masses with such scalar field. The bulk scalar acquires a vacuum expectation value, which is odd under the orbifold symmetry and gives rise to the fermion bulk masses through Yukawa-like interactions.

All authors contributed to the development of the equations of motion in section 3.1. A. Carmona and the author obtained the equations appearing in section 3.2 from the litterature and adapted them for our purposes. Sections 3.3, 3.4 and 3.5 are mostly work of the author, with the last mentioned section being based on a previous work by M. Neubert. The numerical calculations appearing in this work were all performed by the author, with the exception of the scans necessary for figures 3.11 and 3.12, that were performed by both A. Carmona and the author, and the cross-section $\sigma(gg \to S)$ in section 3.3, that was computed by A.Carmona. Section 3.6 corresponds almost entirely to M. Neubert's effort, whereas most of the formulae appearing in appendix C was derived by A. Carmona. Section 3.5.3 was developed by A. Carmona, M. Neubert and the author. All authors contributed to the text.

For the calculations the author used the program `Mathematica`, `python` and the library `flavio` [3]. The cross-section $\sigma(gg \to S)$ in section 3.3, was computed by A.Carmona using the `CT14nlo` PDF from LHAPDF6 [4]. Figures were done with *TikZ* and `Mathematica`. The scan necessary for figures 3.11 and 3.12 was done using `C++`, `Mathematica` and the High-Performance Computer, `Mogon`.

The majority of chapter 3 has been extracted from the publication (with minor modifications to the text), which can be distributed under the terms of the Creative Commons Attribution License CC-BY 4.0. All figures were remade for this thesis using `matplotlib` [5].

[2] A. Carmona, J. Castellano, and M. Neubert, "*A warped scalar portal to fermionic dark matter*", [2011.09492]. *Accepted for publication in EPJC*.

Here, we argue that the extension of the SM with a warped extra dimension together with a new $\mathbb{Z}_2$-odd scalar singlet presented in [1], provides a natural explanation not only for the hierarchy problem and the flavor puzzle, but also helps reproduce the observed dark matter relic abundance and can lead to modifications of Higgs couplings, because of the mixing between both scalars.

The author derived most of the equations from chapter 4 with advice from A. Carmona and M. Neubert, with the exception of the equations in sections 4.2.3, 4.2.4 and appendix D, that were extracted from the literature and adapted by the author. The numerical calculations appearing in this work were all performed by the author. All authors contributed to the text.

For the calculations the author used the program `Mathematica`. Figures were done with *TikZ* and `Mathematica`.

The majority of chapter 4 has been extracted from the e-print (with minor modifications to the text), which can be distributed under the terms of the Creative Commons Attribution License CC-BY 4.0. All figures were remade for this thesis using `matplotlib` [5].

Contents

Introduction

In July 2012 a press conference and the release of two preprints by both the ATLAS and CMS collaborations confirmed the discovery of a Higgs-like particle at the Large Hadron Collider (LHC) [6, 7]. As the interactions of this scalar seem to point to the SM Higgs boson, this discovery has been the final piece for establishing the Standard Model (SM) as the theory describing particles and their interactions, up to the scales so far explored. The SM allows us to understand three of the four fundamental forces of nature at the quantum level. It is able to combine the strong, the weak and the electromagnetic interactions within a single theory, where interactions are described by the exchange of spin-1 particles of the $SU(3) \times SU(2) \times U(1)$ gauge group. Moreover, chiral masses are introduced in the theory after spontaneous symmetry breaking (SSB) through the Higgs mechanism, explaining at the same time the origin of both fermion and gauge boson masses in the SM.

The origin of particle physics as we know it goes back to the early 1900s. We have gone a long way from there. We started by deriving the equations of special relativity and setting the foundation of quantum mechanics, later moving on to develop quantum field theory, necessary to reach the day we live today. We have built kilometers-long and multimillion-euro experiments such as the LHC or IceCube, with the aim of testing features of nature we would like to understand. Features that we initially thought we could never test experimentally. We started by doing *a terrible thing*,[1] and that led to the conviction of a whole community that this was indubitably the way to go. Soon after being developed in the early 1970s, the SM has successfully passed almost every test and correctly predicted a wide variety of phenomena, and is nowadays considered the most fundamental theory humankind has for describing nature at the smallest lenght scales.

However, the SM is not the last step on this path. Inevitably, questions such as *do we only need* $SU(3) \times SU(2) \times U(1)$ *to describe particle interactions?* or *would there be another sector, at another scale, accesible to us in the future?*, as well as many others, arised: the beyond the SM (BSM) era began. With the Higgs vacuum expectation value (VEV), at 246 GeV, being the highest scale in the SM, another question popped up, i.e. what would be the consequences for the SM when interacting with another sector sitting at a scale $\Lambda \gg \mathcal{O}(10^2)$ GeV. This is the so called *hierarchy problem*, which can also be presented as the question of how can the Higgs mass be of order GeV despite being possibly sensitive to any other scale interacting with the Higgs sector. Moreover, in the SM chiral fermion masses appear because of Yukawa couplings of fermions fields with the Higgs

[1] In reference to the famous quote by W. Pauli when he postulated the neutrino: *"I have done a terrible thing, I have postulated a particle that can not be detected"*.

doublet. However, experimental observations have told us that, even though these masses all share the same origin within the SM, they can differ by orders of magnitude. In particular, we know that mass the ratio between two different particles in the lepton sector can be up to $\mathcal{O}(10^4)$,[2] while in the quark sector the difference might be even larger, up to $\mathcal{O}(10^5)$. These features, together with the hierarchical mixings present in the quark sector are commonly refered to as the *flavor puzzle*. Moreover, there is experimental evidence that the amount of matter that can be infered via SM interactions does not account for all matter interacting gravitationally in the universe. This points towards the existence of dark matter (DM). What is the nature of the DM particles and how these sectors interact with the SM particles still remains unknown. These questions, as well as many others, triggered many different proposals to be studied and considered as candidates for theories describing physics BSM.

In particular, a class of models that was proposed as a solution of the hierarchy problem and that became important soon after is the one considering the Higgs as a composite state or additional spatial dimensions. In the case of composite Higgs models, the Higgs field is described as a pseudo-Nambu-Goldstone boson of the new sector, expected to lie within the few TeV range. Here, the dynamics of the model explain the parametrically small mass for the Higgs [8–17]. On the other hand, in extra dimensional theories the electroweak (EW) scale appears together with the Planck scale and is often allowed to interact with other sectors, appearing at a similar scale in the fundamental theory. However, it is the geometry of spacetime that explains the difference of scales in these models. For example, in theories considering a single extra dimension, the different coordinate suppressions or enhancements acting on the 5D parameters make these scales emerge as radically dissimilar effective quantities in the 4D theory [18–27]. Within the models considering extra spatial dimensions, the Randall and Sundrum (RS) proposal provides a setup with a plethora of possibilities, especially for addressing scale hierarchies [18]. In the RS model, the 5D EW scale is set near the Planck scale and presents an exponential suppression in the effective 4D theory because of the metric describing the 5D coordinate. The RS model considers a compactified fifth dimension featuring a $S^1/\mathbb{Z}_2$ symmetry, limited by two branes at the end-points of the extra dimension, separated by a bulk where 5-dimensional fields can propagate. When fields are allowed to propagate in the bulk, their 5D masses determine the shape of their profiles. In this scenario, SM fermion fields are described by the zero modes of the 5D fermion bulk fields. Therefore, the couplings of the SM fermions with the Higgs boson, whether the Higgs boson is constrained to live in the IR brane or we describe it as a bulk field, are determined by the overlap of the different 5D profiles, and consequently they depend exponentially on the 5D masses of such fields. This mechanism provides a geometrical solution to the SM flavor puzzle. Note thus, the relevance bulk fermion masses have for solving the flavor puzzle. Since chirality can not be defined in the 5D theory, in order to achieve a 4D effective chiral theory it is necessary to asign different $\mathbb{Z}_2$ transformations to the 5D fermion fields. The fact that the different 5D field chiralities have opposite $\mathbb{Z}_2$ transformations translates into the 5D bulk mass parameters of bulk fermions being odd under the orbifold coordinate transformation. This, in principle, can be solved by attaching a harmless sign-function to the mass parameters, guaranteeing the desired $\mathbb{Z}_2$-transformation. However, we claim that this dependence of a parameter on the fifth dimensional coordinate is calling for an origin, i.e. some dynamical reason behind the mentioned behaviour under the coordinate transformation.

We propose a mechanism for which the coordinate dependence of the bulk fermion masses is described by an odd bulk scalar field that propagates in the warped extra dimension (WED). This bulk scalar couples to the 5D fermion fields through Yukawa-like parameters. Once the scalar acquires a VEV, which is odd under the $\mathbb{Z}_2$-symmetry transformation, bulk fermions acquire 5D odd masses. Therefore, in our model fermion masses are no longer described by a sign-function, but as a VEV having a dynamical profile, which depends on the parameters of the model. We study the VEV solutions and encounter that it can induce a non-negligible backreaction on the metric for natural values of the gravity-scalar coupling, leading to modifications of the warp function in the

[2] Considering neutrinos as massless. When one considers massive neutrinos this difference could be up to $\mathcal{O}(10^7)$.

vicinity of both branes. Furthermore, we find that such modifications on the warp factor together with the different profile for the mass function, which is no longer described by a step-function, can induce notable deviations of the fermion profiles in our model, when compared to the profiles obtained in the traditional RS setup. Moreover, like in a conventional RS model, the observed flavor structure and the mass hierarchy of the SM fermions can be naturally explained by the different localizations of the fermion zero modes along the extra dimension, as it leads to different effective Yukawa couplings with the Higgs boson. In addition, we study the phenomenological implications the modified fermion profiles, as well as the backreaction on the metric caused by the VEV of the bulk scalar field, may have on the predictions of EW precision and flavor observables. In particular, we compute the predictions for the Peskin-Takeuchi S and T parameters and the CP violating flavor observable, ϵ_K, and analyze the dependence of the results on the model parameters and the strength of the backreaction on the metric. Moreover, we discuss possible flavor changing effects that might arise and discuss why these should not pose a problem in our model. We initially consider a brane-localized Higgs scenario, for which the portal coupling of the Higgs to the odd scalar is strongly suppresed.

We continue by analyzing the more general case, where the Higgs boson is allowed to propagate in the bulk of the extra dimension and for which the mixing between both scalars is unavoidable. We study the effect of this mixing and try to estimate the footprints such a mixing can have in Higgs physics, e.g. by leading to modified Higgs couplings. Moreover, since the odd scalar field is responsible for fermion bulk masses and therefore couples to any fermion field that propagates in the bulk, we argue that it acts as mediator between the SM model fermions and any femionic dark sector propagating into the bulk of the extra dimension. Models with extra dimensions already feature an inexorable mediator between visible and dark sectors, since gravity couples to matter through the energy-momentum tensor. However, we find that for some values of the dark fermion masses and model parameters, the odd scalar field becomes the most important mediator for the DM coannihilation cross section. We study these effects and explore the viability of fermionic dark matter in the presence of these new heavy scalar mediators both in the usual freeze-out scenario and in the case where the freeze-out happens during an early period of matter domination.

Structure of the dissertation

We begin this thesis by briefly introducing the SM, with the aim of setting some foundations for the rest of the text. Some open questions that are not addressed within the SM are also presented, as these are the main motivations for the rest of this work. This constitutes chapter 1.

Then, we take some time in chapter 2 to present the RS model and the theoretical background necessary for understanding the following chapters. We introduce the Kaluza-Klein (KK) decompositions and the equations of motion (EOM) for the different fields, where a special attention is payed to the fermion sector. In addition, we discuss how the RS model can naturally explain the mass and mixing structure of the quark sector of the SM and introduce the tools necessary for this task.

In chapter 3, we present a dynamical mechanism that can explain the coordinate dependence of fermion bulk masses by introducing an odd bulk scalar. We analyze the background solutions and how these solutions modify the profiles of the different fields, and compare it to the solutions we obtained in chapter 2. Then, we study the phenomenological implications of considering such an odd scalar in RS models. We understand how having a brane-localized Higgs scenario suppresses a portal coupling of the Higgs with the odd scalar.

Chapter 4 follows as a natural continuation to chapter 3. We allow the Higgs to propagate in the bulk and introduce a quartic term coupling it to the odd bulk scalar. We study the mixing that

could arise between the different scalar modes after the KK expansion and what this could imply for the Higgs sector, e.g. by modifying the Higgs couplings to other SM particles. We also discuss the possibility of having the odd bulk scalar acting as a mediatior between the SM and possible dark sectors containing fermion fields.

Finally, we draw our conclusions in chapter 5.

1 | The SM and open questions

It is impossible to point to a moment in the history of physics as the birth of the SM, since it is a theory that was built based on the effortful contribution of many physicists through many years, with the second half of the 20$^{\text{th}}$ century being of vital importance. Nevertheless, it is not fool to think of the contribution to the understanding of non-abelian gauge theories by Yang and Mills [28] in 1954 as a starting point, and of the SM becoming a theoretically complete theory with the contributions of Gross, Wilczek and Politzer [29, 30] and 't Hooft and Veltman [31, 32] in the early 1970s. The development of the SM led to many Nobel prizes being awarded to the field and to the most complete theory we have for describing particle interactions and physics at the most fundamental level we have been able to test to the day. Therefore, the SM is one of the greatest achievements of science in the modern era, within and outside physics. But it was a journey that theory did not cover without a companion. Experiments were as important and necessary as the theoretical developments, with the astonishing contributions of collaborations and experiments such as, first Large Electron-Positron collider (LEP), and then LHC, and with the discovery of the Higgs boson in 2012 by the CMS and ATLAS collaborations to reafirm the succesfull story of the SM.

In this chapter, we briefly present the SM of particle physics, with the aim of setting the theoretical background for this thesis, together with some conventions. In case a more detailed introduction is needed, the reader is encouraged to go to [33–38]. After introducing the SM, some of the open questions in particle physics are mentioned and discussed, with particular emphasis in the two problems that prompted the development of models with extra dimensions. In addition, we give a brief introduction to other open questions that make up the main motivation for the community to go beyond the SM and trying to understand particle physics at a even more fundamental level.

1.1 The SM of particle physics

The SM of particle physics [39–41] is a renormalizable gauge theory based on the local symmetry group $\mathcal{G}_{\text{SM}} = SU(3)_C \times SU(2)_L \times U(1)_Y$. Particles are represented by quantum fields that transform accordingly under the different representations of $\mathcal{G}_{\text{SM}}$ and under the Lorentz group, i.e. according to their spin. The SM gauge group describes the strong, weak and electromagnetic interactions by the exchange of spin-1 gauge fields corresponding to such groups. This correspond to 8 massless

gluons, g, for the strong interaction, 3 massive bosons, Z and $W^{\pm}$, and a massless photon, γ, for the EW interaction. The $SU(2)_L \times U(1)_Y$ gauge symmetry is broken by the Higgs vacuum, triggering the SSB of the EW group to the electromagnetic subgroup [42–45]. This can be summarized as follows

$$SU(3)_C \times SU(2)_L \times U(1)_Y \xrightarrow{\text{SSB}} SU(3)_C \times U(1)_{\text{QED}}\,, \tag{1.1}$$

where $Q = T_3 + Y$ stands for the electric charge generator, with T_3 being the third component of $SU(2)_L$ and Y the Hypercharge generator. After SSB the weak gauge bosons Z and $W^{\pm}$ become massive and the photon, i.e. the spin-1 gauge field corresponding to $U(1)_{\text{QED}}$, remains masless. Additionally, the fermion masses and mixings are also introduced, via Yukawa couplings of the Higgs scalar with the LH and RH fermion fields.

The fermion sector of the theory is chiral with respect to (w.r.t.) the EW gauge group, $SU(2)_L \times U(1)_Y$, with the left-handed (LH) and right-handed (RH) irreducible representations of the Lorentz group transforming as doublets and singlets of $SU(2)_L$, respectively. The fermionic matter is divided between leptons and quarks, which are organized in a three-fold family structure of identical gauge quantum numbers:

$(3,2,1/6)$	$(3,1,2/3)$	$(3,1,-1/3)$	$(1,2,-1/2)$	$(1,1,-1)$
$q_L = \begin{pmatrix} u_L \\ d_L \end{pmatrix}$	u_R	d_R	$l_L = \begin{pmatrix} \nu_L \\ e_L \end{pmatrix}$	e_R

where (C, L, Y) correspond to the gauge quantum numbers for the different families of SM fermions, according to their chiralities. Above, u, d, ν, e denote the three generations, being

$$\begin{aligned} \text{quarks}: &\qquad u = u, c, t, &\qquad d = d, s, b, \\ \text{leptons}: &\qquad \nu = \nu_e, \nu_\mu, \nu_\tau, &\qquad e = e, \mu, \tau. \end{aligned} \tag{1.2}$$

Adding a complex scalar doublet H charged under $SU(2)_L$ to the SM gauge group and fermion content and considering all possible renormalizable terms allowed by the symmetries defines the SM Lagrangian. This Lagrangian can be summarized as

$$\begin{aligned} \mathcal{L}_{\text{SM}} = &-\frac{1}{4}\left(G^a_{\mu\nu}G^{a,\mu\nu} + W^I_{\mu\nu}W^{I,\mu\nu} + B_{\mu\nu}B^{\mu\nu}\right) \\ &+ \bar{\Psi}^k i\not{D}\Psi^k + \left(D_\mu H\right)^\dagger \left(D^\mu H\right) - \mu^2 H^\dagger H - \lambda\left(H^\dagger H\right)^2 \\ &- \left[\lambda^u_{ij}\bar{q}_i u_j \tilde{H} + \lambda^d_{ij}\bar{q}_i d_j H + \lambda^e_{ij}\bar{l}_i e_j H + \text{h.c.}\right], \end{aligned} \tag{1.3}$$

with $a = 1, ..., 8$ and $I = 1, 2, 3$ being the $SU(3)_C$ and $SU(2)_L$ gauge indices, while i, j, k are used for the fermion generations. The first line contains to the kinetic terms of the gauge fields of each symmetry group. In the second line, the kinetic terms for the fermion fields are presented, where Ψ^k runs for all the fermion fields, i.e. $\Psi^k = u^k, d^k, \nu^k, e^k$, and additionally the complex Higgs doublet appears with its corresponding kinetic term and potential. Finally, in the third line the Yukawa interactions of the Higgs and fermion fields are introduced. There $\lambda^{u,d,e}_{ij}$ are the most general 3×3 matrices in flavor space. $\tilde{H}$ is defined as $\tilde{H} = i\sigma_2 H^*$, with σ_2 a Pauli matrix. Here, $\not{D} = D_\mu \gamma^\mu$ where D_μ denotes the covariant derivatives, being defined for the SM as

$$D_\mu = \partial_\mu - ig_S \frac{\lambda_a}{2} G^a_\mu - ig\frac{\sigma_I}{2} W^I_\mu - ig' Y B_\mu\,, \tag{1.4}$$

where g_S, g and g' are the $SU(3)_C$, $SU(2)_L$ and $U(1)_Y$ gauge coupling constants, and λ_a and σ_I the Gell-Mann and Pauli matrices, respectively. For fields that transform as a singlet under a given gauge group, the covariant derivative corresponds to the one presented in (1.4) but omitting the corresponding term. The fine-structure constant can be defined as $\alpha \equiv e^2/(4\pi)$, with e the QED coupling, which can be obtained as a linear combination of g and g' after EW symmetry breaking (EWSB). Similarly the strong coupling constant is $\alpha_S = g_S^2/(4\pi)$. The corresponding field strengths for the different gauge fields read

$$\begin{aligned} G^a_{\mu\nu} &= \partial_\mu G^a_\nu - \partial_\nu G^a_\mu + g_S\, f_{abc}\, G^b_\mu G^c_\nu, \\ W^I_{\mu\nu} &= \partial_\mu W^I_\nu - \partial_\nu W^I_\mu + g\, \epsilon_{IJK}\, W^J_\mu W^K_\nu, \\ B_{\mu\nu} &= \partial_\mu B_\nu - \partial_\nu B_\mu. \end{aligned} \tag{1.5}$$

The complex Higgs doublet has $(1, 2, 1/2)$ quantum numbers, such that it breaks the EW symmetry and at the same time couple to the LH and RH fermion pairs. This doublet can be written as

$$H(x) = \exp\left\{\frac{i}{v}\vec{\sigma}\cdot\vec{\varphi}(x)\right\}\frac{1}{\sqrt{2}}\begin{pmatrix}0\\ v+h(x)\end{pmatrix}. \tag{1.6}$$

The Higgs doublet appears in the SM lagrangian together with a non-trivial potential that triggers EWSB. This potential reads

$$V(H) = \mu^2 H^\dagger H + \lambda\left(H^\dagger H\right)^2 = \lambda\left(H^\dagger H - v^2/2\right)^2, \tag{1.7}$$

with $\mu^2 < 0$, so that a non-trivial VEV develops, and where v, the EW VEV, has been defined as

$$v = \sqrt{\frac{|\mu^2|}{2\lambda}}. \tag{1.8}$$

After the Higgs doublet prompts EWSB, the weak gauge bosons Z and $W^\pm$ become massive, as they *eat up* three goldstone bosons, this becomes explicit in the unitary gauge. The gauge boson masses are

$$M_W = M_Z\cos\theta_W = \frac{1}{2}gv, \tag{1.9}$$

where the gauge mixing angle, also known as weak mixing angle or Weinberg angle, sets the rotation of the Z and γ gauge fields as

$$\begin{pmatrix}W^3_\mu\\ B_\mu\end{pmatrix} = \begin{pmatrix}\cos\theta_W & \sin\theta_W\\ -\sin\theta_W & \cos\theta_W\end{pmatrix}\begin{pmatrix}Z_\mu\\ A_\mu\end{pmatrix}, \tag{1.10}$$

and corresponds to

$$\cos\theta_W = \frac{g}{\sqrt{g^2+g'^2}}. \tag{1.11}$$

Note that before EWSB the EW gauge bosons, $W^\pm$ and Z account for 6 degrees of freedom (d.o.f.), while the complex scalar doublet provides another 4. However, after SSB in the unitary gauge three d.o.f. from the Higgs doublet are rotated to become the longitudinal polarizations of the EW gauge bosons $W^\pm$ and Z, these spin-1 particles become massive and therefore account for 9 d.o.f., while there is a single d.o.f. from the scalar doublet that remains. This neutral scalar d.o.f. corresponds to the so-called Higgs boson, h. A scalar presenting a Higgs-like behavior was

discovered by the ATLAS and CMS collaborations [6, 7] at LHC in 2012, and according to the most updated results no significant deviations from the SM predictions have been observed [46].

Counting parameters from the EW gauge and scalar sectors of the SM Lagrangian, only four are necessary to fully determine the model, the two gauge couplings g and g' and the two parameters of the Higgs potential μ^2 and λ. However, it is useful to choose G_F, α, m_Z and m_h as free parameters. Once these parameters are obtained experimentally, the theory is able to make predictions and any other parameter or observable can be computed from them. The current experimental values for these parameters are [46]

$$\begin{aligned} G_F &= (1.1663787 \pm 0.0000006) \cdot 10^{-5}\,\mathrm{GeV}^{-2}, \\ \alpha^{-1} &= 137.035999084 \pm 0.000000021, \\ m_Z &= 91.1876 \pm 0.0021\,\mathrm{GeV}, \\ m_h &= 125.10 \pm 0.14\,\mathrm{GeV}, \end{aligned} \tag{1.12}$$

and the following relations are useful to determine the value of the desired quantities

$$\sin^2\theta_W = 1 - \frac{m_W^2}{m_Z^2}, \quad m_W^2 \sin^2\theta_W = \frac{\pi\alpha}{\sqrt{2}G_F}, \quad v = \left(\sqrt{2}\,G_F\right)^{-1/2}, \quad \lambda = \frac{m_h^2}{2v^2}. \tag{1.13}$$

The values derived for these parameters

$$\sin^2\theta_W = 0.212, \quad m_W = 80.94\,\mathrm{GeV}, \quad v = 246\,\mathrm{GeV}, \quad \lambda = 0.13, \tag{1.14}$$

are in good agreement with experimental data [46].

1.1.1 Yukawa interactions in the SM

One of the most interesting pieces of the SM Lagrangian are the terms corresponding to the Yukawa interactions. These terms of the SM Lagrangian are responsible for chiral fermion masses, which are obtained after EWSB from the interaction terms of LH and RH fermion fields with the Higgs doublet. In the unitary gauge, i.e. after substituting $H \to (0, v)^T/\sqrt{2}$ in (1.3)

$$-\mathcal{L}_Y \supset \left[\bar{u}_{iL}\mathcal{M}^u_{ij}u_{jR} + \bar{d}_{iL}\mathcal{M}^d_{ij}d_{jR} + \bar{e}_{iL}\mathcal{M}^e_{ij}e_{jR} + \mathrm{h.c.}\right], \tag{1.15}$$

with

$$\mathcal{M}^k_{ij} = \frac{v}{\sqrt{2}}\lambda^k_{ij}, \tag{1.16}$$

where k runs through all the u, d and e generations.

The mixings are introduced once the rotations are performed in the fermion fields, by taking the fields from the interaction to the mass basis. These rotations can be summarized as

$$\Psi^k_{iL} \to (\mathcal{U}^k_L)_{ij}\Psi^k_{jL}, \quad \Psi^k_{iR} \to (\mathcal{U}^k_R)_{ij}\Psi^k_{jR}, \tag{1.17}$$

where $\mathcal{U}^k_L$ and $\mathcal{U}^k_R$ are 3×3 unitary matrices in flavor space. These matrices diagonalize the fermion mass matrices as follows

$$(\mathcal{U}^k_L)^\dagger\mathcal{M}^k(\mathcal{U}^k_R) = \mathcal{D}^k = \mathrm{diag}\left(m^k_1, m^k_2, m^k_3\right). \tag{1.18}$$

Note that the whole flavor structure of the SM comes from the interaction of fermions with the Higgs boson. The SM lagrangian is invariant under $U(3)^5 = U(3)_{Q_L} \times U(3)_{u_R} \times U(3)_{d_R} \times U(3)_{l_L} \times$

$U(3)_{e_R}$ until Yukawa interactions of the Higgs boson with the fermion sector are introduced. Rotating the fermion fields from the interaction to the mass basis as presented in (1.17) introduces the full flavor structure of the SM. In other words, before EWSB the SM is flavor blind. The term in the lagrangian connecting the LH doublet, i.e. the weak interactions of the $W^{\pm}$ gauge boson with u_L and d_L fields, reads

$$\mathcal{L}_{\rm CC} = \frac{g}{\sqrt{2}} \left[W^{\dagger}_{\mu} \bar{u}^0_L \gamma^{\mu} d^0_L + \text{h.c.} \right] = \frac{g}{\sqrt{2}} \left[W^{\dagger}_{\mu} \bar{u}_L \gamma^{\mu} V d_L + \text{h.c.} \right], \tag{1.19}$$

where u^0 and d^0 represent the fields in flavor space, and

$$V = (\mathcal{U}^u_L)^{\dagger} \mathcal{U}^d_R = \begin{pmatrix} V_{ud} & V_{us} & V_{ub} \\ V_{cd} & V_{cs} & V_{cb} \\ V_{td} & V_{ts} & V_{tb} \end{pmatrix}, \tag{1.20}$$

is the Cabibbo Kobayashi and Maskawa (CKM) matrix [47, 48]. The CKM matrix appears as a consequence of requiring 4 field rotations in matrix form, corresponding to $\mathcal{U}^u_R$,$\mathcal{U}^d_R$,$\mathcal{U}^u_L$ and $\mathcal{U}^d_L$, to diagonalize the mass matrices, but having only three kinetic terms, i.e. covariant derivative terms, in the Lagrangian. Note that the piece corresponding to $\mathcal{U}^u_L$ and $\mathcal{U}^d_L$ terms appear in a doublet. Therefore, it is not possible to fully diagonalize the gauge interaction terms and the mass matrices at the same time.

The CKM matrix is a 3×3 unitary matrix that can be parameterized by three mixing angles and a CP-violating phase, using the convention [49]

$$V_{\rm CKM} \simeq \begin{pmatrix} 1 & 0 & 0 \\ 0 & c_{23} & s_{23} \\ 0 & -s_{23} & c_{23} \end{pmatrix} \begin{pmatrix} c_{13} & 0 & s_{13} e^{-i\delta_{\rm CP}} \\ 0 & 1 & 0 \\ -s_{13} e^{i\delta_{\rm CP}} & 0 & c_{13} \end{pmatrix} \begin{pmatrix} c_{12} & s_{12} & 0 \\ -s_{12} & c_{12} & 0 \\ 0 & 0 & 1 \end{pmatrix}, \tag{1.21}$$

where the quantities $s_{ij} = \sin\theta_{ij}$, $c_{ij} = \cos\theta_{ij}$ have been defined. In the SM, the parameter $\delta_{\rm CP}$ is the only source of CP-violating processes. It is experimentally known that the CKM presents a hierarchical structure (this is usually refered to as the *flavor puzzle*, and will be commented on the next section in more detail), which makes convenient to use the Wolfstein parametrization [50]

$$V_{\rm CKM} \simeq \begin{pmatrix} 1 - \lambda^2/2 & \lambda & A\lambda^3(\rho - i\eta) \\ -\lambda & 1 - \lambda^2/2 & A\lambda^2 \\ A\lambda^3(1 - \rho - i\eta) & -A\lambda^2 & 1 \end{pmatrix} + \mathcal{O}(\lambda^4), \tag{1.22}$$

where the CKM matrix is written in terms of an expansion parameter λ (together with A, ρ and η). The current experimental value of the Wolfstein expansion parameter is $\lambda = 0.22650 \pm 0.00048$ [51, 52], therefore justifying the expansion.

Furthemore, the rotations performed to diagonalize the mass matrices are done in the same fashion with the Yukawa matrices coupling the chiral fermion pairs to the Higgs boson and therefore, the Higgs boson has flavor-diagonal couplings to the physical fermions with a couplings proportional to the fermion masses

$$-\mathcal{L}_Y = \left(1 + \frac{h}{v}\right) \left[\bar{u}_L \mathcal{D}^u u_R + \bar{d}_L \mathcal{D}^d d_R + \bar{e}_L \mathcal{D}^e e_R + \text{h.c.} \right]. \tag{1.23}$$

1.1.2 Oblique parameters

The possibilities that appear in front of us while thinking of enlarging the SM are endless. In this regard, the Peskin-Takeuchi parameters S, T and U are a set of quantities that can help us constrain

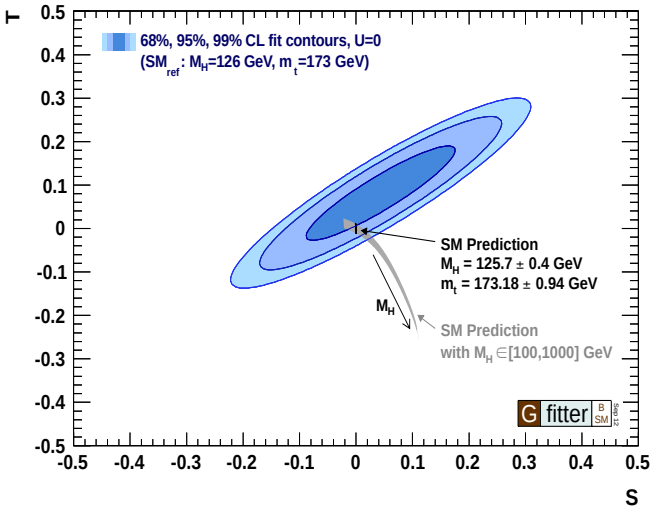

Figure 1.1: *Contours of 68%, 95%, and 99% confidence level in the TS-plane, for a fit done by constraining U to $U = 0$. Figure from [57].*

some of the contributions of the new physics (NP) [53]. Thus, allowing us to compare these models, as well as to understand them better. Even if NP appears at a significantly higher scale than the EW scale, it would contribute to the vacuum polarization corrections of the SM particles. In particular, corrections to the vacuum polarizations of the SM gauge bosons can become sizeable enough to be tested at experiments, imposing strong constraints on NP models. The EW precision parameters S, T and U allow us to measure these deviations from the SM predictions. These parameters read [53–56]

$$S = \frac{4s_W^2}{\alpha}\hat{S}, \qquad T = \frac{1}{\alpha}\hat{T}, \qquad U = \frac{-4s_W^2}{\alpha}\hat{U}, \tag{1.24}$$

with $s_W \equiv \sin\theta_W$. Here, the $\hat{S}$, $\hat{T}$ and $\hat{U}$ quantities are defined as

$$\hat{S} = \frac{\Pi'_{W^3B}(0)}{\Pi'_{W^+W^-}(0)}, \qquad \hat{T} = \frac{\Pi_{W^3W^3}(0) - \Pi_{W^+W^-}(0)}{-\Pi_{W^+W^-}(0)}, \qquad \hat{U} = 1 - \frac{\Pi'_{W^3W^3}(0)}{\Pi'_{W^+W^-}(0)}. \tag{1.25}$$

The quantities $\Pi_{V_1V_2}(p^2)$ correspond to the tree level transverse vacuum polarization amplitudes, with $V_1V_2 = \{W^+W^-, W^3W^3, BB, W^3B\}$. Moreover, for such expressions to hold we need to assume that these amplitudes allow for a Taylor series expansion in powers of p^2 around $p^2 = 0$, as

$$\Pi_{V_1V_2}(p^2) = \Pi_{V_1V_2}(0) + p^2\Pi'_{V_1V_2}(0) + \mathcal{O}(p^4). \tag{1.26}$$

It can also be helpful to think of S and T as being generated from higher-dimensional operators $\mathcal{O}_S$ and $\mathcal{O}_T$, e.g.

$$\mathcal{O}_S = H^\dagger\sigma^I H W^I_{\mu\nu}B^{\mu\nu}, \qquad \mathcal{O}_T = \left|H^\dagger D_\mu H\right|^2, \tag{1.27}$$

in this case, the contributions to S and T at tree-level are proportional to the Wilson coefficients for these operators. What one does in this case is to integrate out the new particles before EWSB of the corresponding NP model one would like to study. Thus, generating the coefficients C_S and C_T of the operators $\mathcal{O}_S$ and $\mathcal{O}_T$. In this case, the S and T parameters would have the expression

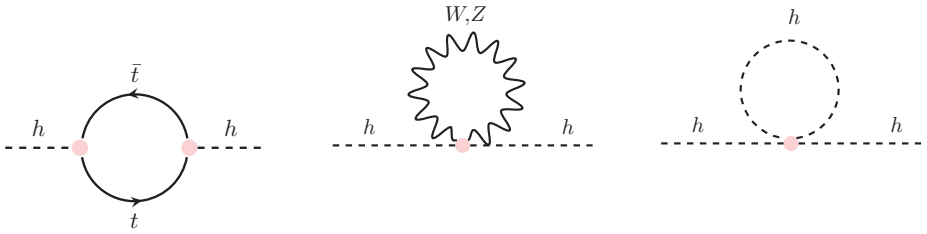

Figure 1.2: *Leading radiative contributions to the Higgs mass in the SM.*

$$S = \frac{4 s_W c_W v^2}{\alpha} C_S, \qquad T = \frac{-v^2}{2\alpha} C_T. \tag{1.28}$$

The current contours of the TS-plane at 68%, 95%, and 99% confidence level, for a fit done by the Gfitter Group by constraining U to $U = 0$, are shown in figure 1.1, see [58] for the most recent fit.

1.2 Hints for NP

The SM has been tested with an unprecedented precision at the LHC. The confirmation of the SM-like nature of the Higgs boson and the measurement of its interactions provides strong evidence of the robustness of the SM when describing the laws of nature up to very short distances. However, there are also several fundamental and open questions to which the SM is not able to provide a successful answer. A natural response is therefore to consider extensions of the SM that can solve or aliviate these questions or problems. Here, some of these problems that are currently triggering some interesting research in BSM physics, are presented.

In particular, two puzzles or unanswered questions within the SM provide the main motivation for the framework in which the work of this thesis has being developped. These two unsolved mysteries are *the hierarchy problem* and *the flavor puzzle*. Moreover, during the development of this thesis another issue that lacks of an explanation within the SM was addressed. Even if RS was not initially meant to solve questions on the scope of DM, we will show how it can address some of the problems in that area. Therefore, these are the first three topics covered here.

- ***The hierarchy problem:*** As mentioned before, one puzzeling question is why does the Higgs boson have a mass of ~ 100 GeV. This is the so-called hierarchy problem. Within the SM the main quantum corrections to the tree-level Higgs mass are

$$\delta m_h^2 = \frac{3\Lambda^2}{8\pi^2 v^2} \left[2m_W^2 + m_Z^2 + m_h^2 - 4m_t^2 \right], \tag{1.29}$$

  which can be derived from the diagrams shown in figure 1.2. There Λ would be the cut-off scale at which the SM would no longer be valid.[1] One could naively argue that this quadratic divergence is nothing but a byproduct of using a hard cut off, and that such dependency could simply be avoided by repeating the calculation using dimensional regularization. However, the main statement is totally independent of the regularization method used. This a consequence of not recovering any symmetry when the mass parameter of the Higgs is set to zero, as there is in general no symmetry associated to massless scalars with non-derivative

[1] Note that there is no problem if the SM would be the only theory describing nature.

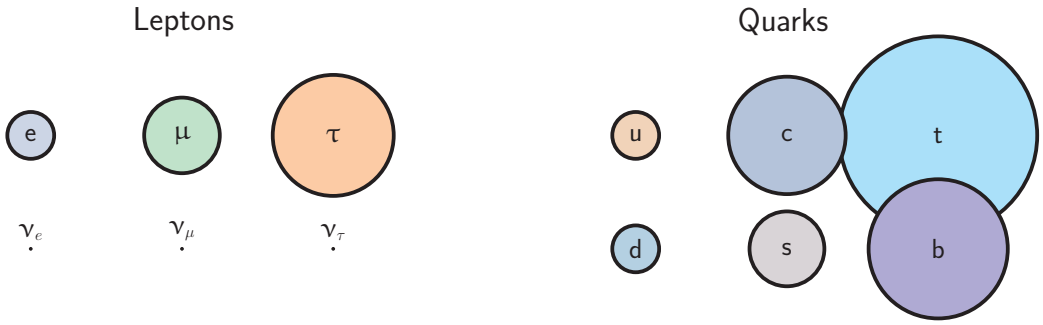

Figure 1.3: *Observed mass spectrum for SM fermions.*

couplings. The situation of the Higgs boson is unique within the SM, since that problem is not present for fermions or gauge bosons. Fermion masses are protected by chiral symmetry and gauge boson masses are protected by gauge symmetries. Corrections to the masses of fermions and gauge fields are proportional to themselves, as their masses are the parameters breaking the symmetry. Therefore, fermion and gauge masses are "technically natural". However, for the Higgs boson the story is completely different as no symmetry in the SM shields the Higgs mass from being sensitive to new heavy states.

Therefore, what this implies is that the Higgs is sensitive to new heavy states that could couple to it or that, if a new sector is added to the SM, some protection mechanism would be needed to keep the Higgs mass of order 10^2 GeV. Note that even if the Higgs would not couple directly to the new heavy states effective couplings at the loop level do usually appear, and therefore we still need to prevent these large corrections. In the effective field theory language this goes down to the fact that the Higgs mass operator, $H^\dagger H$, has mass dimension two and it is therefore a relevant operator. This implies that it would receive quadratic contributions from possible heavy states in the UV theory as [59]

$$\delta m_h^2 \propto \frac{1}{16\pi^2}|g_{\rm UV}|^2 m_{\rm UV}^2. \tag{1.30}$$

If the full theory is not able to protect the Higgs mass from quadratic contributions, a cancellation of large numbers $m_h^2, \delta m_h^2 \sim \mathcal{O}(m_{\rm UV}^2)$ would be required to give as a result a Higgs mass of 125 GeV, which would require a high level of *fine-tuning*.

When this happens in physics we expect to find a mechanism behind such an astonishing result and therefore, if NP appears at higher scales, we would like to understand why the value of the Higgs mass is much lower than the NP scale. This is the SM gauge hierarchy problem.

- ***The flavor puzzle:*** The SM presents a strong hierarchy in the fermion mass spectrum and in the mixing of the quark sector. These unexplained hierarchies receive the name of the flavor puzzle or flavor problem.

  In particular, there is a five orders of magnitud difference between the masses of the heaviest and lightests quarks in the SM, $m_{u,d}/m_t \sim 10^{-5}$. Furthemore, neutrinos are much lighter than any other fermion in the SM, with $m_\nu/m_e \lesssim 10^{-6}$. This observed difference between the fermion masses, primarly given that in the SM all masses have the same origin, is an enigma. The observed fermion masses are schematically shown in figure 1.3.

  Moreover, the CKM matrix presents a hierarchical structure, as commented in the previous section. The angles are such that $s_{13} \ll s_{23} \ll s_{12} \ll 1$, or equivalently $|V_{ud}|/|V_{us}| \sim$

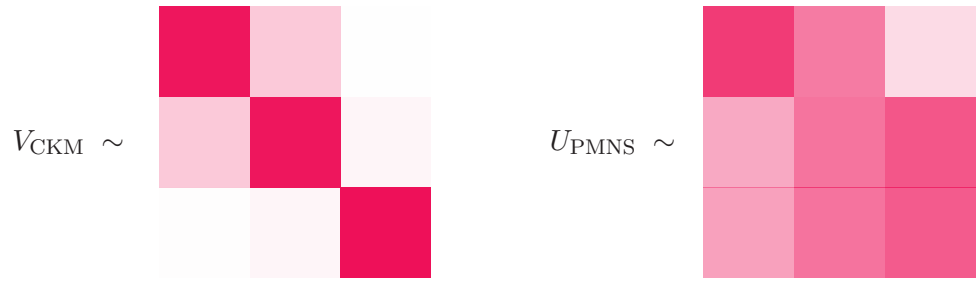

Figure 1.4: *Structure of the observed values for the CKM and PMNS matrices.*

$|V_{us}|/|V_{ub}| \sim \lambda$, where $\lambda \simeq 0.23$. Therefore the CKM presents an almost diagonal pattern, as can be seen in figure 1.4

In the SM fermion masses are given by the product of Yukawa couplings with the Higgs VEV, $v \sim \mathcal{O}(10^2)$ GeV. Being Yukawa couplings dimensionless parameters, one would expect them to have $\mathcal{O}(1)$ values. In that case, the SM flavor structure could be obtained after scanning these order-one parameters, by getting a probability distribution for the fermion masses and mixing angles. Without the presence of a dynamical mechanism or a symmetry constraint on the CKM, one would expect it to be obtained from anarchic $\mathcal{O}(1)$ entries. However, it is clear that nature chose Yukawa couplings to be much smaller than 1 and to they present a hierarchical structure, where only the top quark Yukawa is $y_t = \sqrt{2}\, m_t/v \sim 1$. On the other hand, the mixings appearing in the lepton sector are sizeable, and the Pontecorvo-Maki-Nakagawa-Sakata (PMNS) [60–63], i.e. the 3×3 unitary mixing matrix that relates the mass and flavour eigenstates in the lepton sector, presents a more natural structure, totally different from the observed in the quark sector as can be seen in figure 1.3. Therefore, such differences in the Yukawa couplings for the different fermions with the Higgs boson are demanding for an explanation.

- ***Dark matter:*** First noticed by Zwicky in 1933, the measurement of rotation curves of galaxies did not match the predictions obtained by considering the visible amount of matter that compose the galaxies [64]. Zwicky's findings were later confirmed by [65]. Another phenomena such as the collision of two clusters of galaxies, known as bullet clusters, and the cosmic microwave background power spectrum [66, 67] point to the same direction: Newtonian gravity and SM predictions are not able to account for the observations. These findings opened up the possibility that the amount of matter interacting gravitationally in the universe is higher than the one we can measure from SM interactions. This lead to a large number of DM models being proposed, which are expected to be tested in current and future experiments such as Xenon1T (see [68, 69] for a review). One of the most appealing candidates for DM are weakly interacting massive particles (WIMPs). An interesting feature of WIMPs is the fact that their interactions with the SM allow them to be tested at particle experiments. Moreover, it is not only the nature of the DM candidates that needs to be specified, we would also have to understand how dark sectors interact with the SM particles. It is possible that such sectors can interact not only gravitationally, in this case the so-called *mediators* would have a non-vanishing coupling with the DM candidates and the SM particles. One important constraint for determining the suitability of mediators is given by the DM relic abundance [64, 65, 67]. Unfortunately, no DM has been detected so far and their nature remains unknown. In addition, models of modified gravity have been proposed too to solve these issues [70–73].

In chapter 2 we will introduce the RS framework and see what are the advantages of working with such models. We will see what is the solution they provide to the hierarchy problem and why we find such models to be a natural playground to address the flavor puzzle. In chapter 3, we will further investigate on the mechanism that is often used to solve the flavor puzzle, proposing a feature that we think is essential for such mechanism. Moreover, we will see in chapter 4 how the model we proposed in chapter 3 introduces inevitably a DM mediator candidate, under the assumption of the existance of dark fermions propagating in the extra dimension.

In addition to these three topics, there are other problems that worth being mentioned but that have not being addressed in this thesis. These open questions, some of which are due to experimental observations that cannot be accounted for within the SM, point to the presence of NP. A brief comment on these topics follows.

- ***Neutrino masses:*** Another compelling hint for BSM are neutrino masses. Since within the SM only LH fields are introduced for neutrinos, neutrinos are massless and strictly left-chiral particles. With neutrino oscillations being observed, both from solar [74–77] and atmospheric [78] experiments, it is clear nowadays that neutrinos have non-zero masses. Although enlarging the SM trivially by adding three right-handed neutrinos, therefore allowing Dirac mass term, is allowed by phenomenology, the smallness of neutrino masses compared to other particles would remain unexplained for this setup. One class of attractive extensions of the SM that allows for non-zero neutrino masses and also predicts them to be light in comparison with the other SM fermions, made use of the so-called see-saw mechanism [79–85].
- ***The Strong CP problem:*** The vacuum structure of QCD is compatible with a term $\mathcal{L}_{\rm QCD} \sim \theta\tilde{G}G$, known as the QCD θ-term. This term leads to strong CP violating effects together with the prediction of a large value for the electric dipole moment of the neutron (EDMN), unless θ is tunned to be small. However, we know from EDMN experiments that $\theta < 10^{-10}$ [86]. The question of why θ is so small given that the SM does not have a mechanism to protect this term or similarly, why does not the strong interaction violate CP maximally, is known as the Strong CP problem. A solution to the strong CP problem is obtained by promoting the θ term to a dynamical d.o.f., whose minimum naturally relaxes to $\theta = 0$ after QCD condensation. This solution predicts a would-be pseudo-Goldstone boson, the axion [87, 88], that appears after a $U(1)$ Peccei-Quinn symmetry gets spontaneously broken [89].
- ***Baryogenesis:*** Another open question in particle physics is baryogenesis, i.e. what is the origin of the observed matter-antimatter asymmetry in the universe. For this to occur, Baryon number must be violated, at least for a short period in the early universe, and generally a significant amount of CP violation is required. In the SM the CKM-matrix is the only source of CP violation but however, it is not enough for most cases to reproduce the observed matter-antimatter asymmetry [46, 90–92].

There are many other unanswered questions or puzzles such as leptogenesis, whether grand unification is realized, or how can gravity be incorporated together with the SM into a full theory of nature. An instructive discussion on some other problems can be found in [93].

Furthemore, some new data might be currently pointing to NP in the flavor area. Some tension has been observed in semi-leptonic B meson decays, specially in the $b \to c\tau\nu$ and $b \to sl^+l^-$ transitions [94–97]. According to the SM the three lepton families are equivalent except for their masses, this is known as lepton flavor universality (LFU). LFU being violated in nature is an evident hint for NP. Many BSM models consider particles that do not present this universal behaviour and therefore could explain these anomalies, being models with leptoquarks of special interest in this area [98]. However, the experimental data is still not enough to come to a conclusion, since the current deviations lie at the $\sim 3\,\sigma$ level for individual observables, i.e. below the five sigma requirement to claim discovery.

2 | Extra dimensions

The idea of considering extra dimensions, i.e. more dimensions than the usual $3+1$ dimensions we are "used" to, dates back to the second decade of last century when Theodor Kaluza and Oscar Klein proposed a theory of unification of the electromagnetic (EM) theory and General Relativity (GR), by extending the latter one to five dimensions. Some of the main ideas had already been introduced by Gunnar Nordstöm in 1914 [99]. Gunnar's intended to unify the theories of EM and gravity by extending Maxwell's equations from 4 to 5 dimensions, a different perspective to what was proposed by T. Kaluza and O. Klein in 1921 and 1926 respectively [100,101]. The main reason of Gunnar's proposal of extending the EM theory instead of choosing GR as the starting point was simply due to the fact that his attempt was previous to Einstein's publishing of his theory of GR. In the KK theory in 4+1 dimensions EM appears as the new components of the five dimensional metric tensor. In that case, 4-dimensional gauge invariance could be obtained from a geometrical theory in 5D, as Kaluza proposed. This was extended in 1926, when Oskar Klein introduced the concept of compactification, allowing for a Fourier expansion of fields on an S^1 circular topology. However, this theory predicted the EM charge to be quantized and related to the nodes of the fields and therefore only allowing for modes with $n \neq 0$ to be charged under $U(1)_{\rm EM}$. In addition, the discovery of the nuclear forces shifted the attention away from the attempt of unifying GR and EM, since they were no longer the only forces to be understood.

Recently, and particularly by the end of the last century, models with an extra dimension gained importance again. In 1998, Arkani-Hamed, Dimopoulos and Dvali (ADD) [19] came out with a solution to the hierarchy problem by introducing n compact flat large extra dimensions. In this model the Planck scale is considered of order the EW scale in the full theory, i.e. in the $4+n$-dimensional theory, but a suppresion in the strength of gravity appears because of the behaviour of gravity once these extra dimensions are considered. However, in these models with flat extra dimensions setting the volume and the number of dimensions could be considered as a fine-tuning problem by itself.

Later in 1999, Randall and Sundrum [18] proposed a solution to the hierarchy problem by introducing a single extra dimension without requiring a large volume. In their work, the EW sector appears together with the Planck mass at a fundamental scale $\mathcal{O}(10^{15})$ TeV and the observed EW-Planck hierarchy is a result of an exponential suppression of the EW scale performed by the non-trivial geometry of the additional dimension. Models with a WED provide an elegant solution to the hierarchy problem, together with an attractive framework for implementing BSM theories. The geometry of such models is anti-de Sitter (AdS) and consist of two branes, which could be

understood as the limits of the extra dimension, and a bulk connecting both branes.

In the simplest versions of these models, the SM is confined to one of the branes, known as the infrarred (IR) or *visible* brane. In this brane, the fundamental scale, M_*, has been warped down because of the metric and has an effective value that lies around the EW scale. On the other hand, the effective Planck mass, $M_{\rm Pl}$, *lives* near or at the ultraviolet (UV) or hidden brane, and has a value $\mathcal{O}(10^{15})$ TeV.

Nonetheless, confining the full SM to the IR brane is not a necessary conditions for these models to reproduce the SM. 5D gauge boson [102–104] and fermion [20,21,25] fields can be allowed to propagate in the bulk of the extra dimension and still accommodate the SM. In that case SM fermions are represented by the zero-modes of the 5D fields after the KK-expansion. This configuration could lead to possible modifications of their SM-like behaviour, specially when the mixings of the zero-modes with the low-lying KK-modes of the SM fields are not suppressed [105–109]. In some cases, these modifications of the couplings could be large enough to be tested at current and future colliders [2, 105–111].

Once that 5D fermions are allowed to propagate in the bulk and the SM fermion fields correspond to the zero-modes of the 5D fields, the overlap of the fermion zero-mode profiles with the Higgs boson, whether it lives on the IR brane or propagates in the bulk, determines the SM 4D masses. These overlaps depend on the localization of the fermion profiles, which are set by their 5D mass parameters [20, 21, 25]. Since the profiles of the fermion zero-modes depend exponentially on their 5D masses, this mechanism provides an explanation of the hierarchy observed in the SM fermion masses from a geometrical perspective, naturally accommodating the hierarchical pattern of fermion masses and mixing angles present in the CKM.

Nevertheless, there is an issue concerning this class of models. While having a scale of NP around of ~ 1 TeV is preferred for solving the hierarchy problem and, in addition, making these models testable at the LHC, EW precision tests (EWPT) [1, 108, 109, 112, 113] and flavor [1, 110, 111, 114, 115] data point to the opposite direction, far out of the reach of current experiments. In particular, such constraints set the scale of NP, which in RS models corresponds to $M_{\rm KK}$, commonly designated as the KK-scale, to be at the $3-5$ TeV range, corresponding to new resonances appearing at the $\mathcal{O}(10)$ TeV. Having the scale for NP of $3-5$ TeV, whereas the EW scale is known to be 246 GeV is known as the *little hierarchy problem*, hard to avoid in models with extra dimensions or for which the Higgs appears as a pseudo-Nambu Goldstone boson [13, 14, 17, 116–123]. Nonetheless, there are some techniques that help us alliviate these bounds. The most common approaches are to introduce a custodial symmetry, for which the bulk gauge group and particle content of the model is enlarged to reproduce an $SO(4)$ symmetry, and models that consider a modified metric, for which the warp factor of the minimal RS model is deformed near the IR-brane [1, 124–136].

In addition, another aspect that makes these models interesting is that they can be seen as equivalent to models of conformal field theories (CFT) by means of the AdS/CFT duality [9, 10, 23, 137–139]. Such duality implies that a theory with fields living in an $(n+1)$-AdS space have a dual n-dimensional CFT. In the case of the RS model, an AdS geometry with the presence of UV brane at $y_{\rm UV}$ would correspond to a CFT with a cutoff $1/y_{\rm UV} \sim M_{\rm Pl}$, while the presence of an IR brane at $y_{\rm IR}$ implies the breaking of the CFT at the scale $1/y_{\rm IR} \sim M_{\rm KK}$. In other words, the breaking of the translational invariance in the AdS geometry corresponds to the breaking of scale invariance of the CFT, and therefore the radion, i.e. the Goldstone boson associated to the breaking of the translational invariance has a dual field in the broken CFT, the dilation [9, 116, 119, 123, 140, 141]. Moreover, it has been conjectured that the the scaling dimension of the operators in the 4D picture is closely related to the 5D bulk mass, i.e. the parameter determining the localization of the profiles for the bulk fields [9, 10, 22, 112]. Hence, the localization of the bulk fields is linked to the level of compositeness of the corresponding 4D fields. In particular, a field whose profile along the extra dimension points towards the IR brane could be considered as a composite field, while a field living close to the UV brane could be seen as elementary. Therefore, if we consider the SM fields

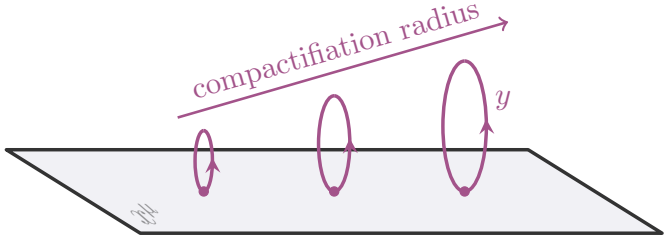

Figure 2.1: *Schematic representation of a fifth dimension compactificatified on S^1.*

to be confined to the TeV brane, such a choice corresponds to a broken CFT where the the SM fields are purely composite states. The advantage of the 5D theory is that is not strongly coupled and therefore calculations in the AdS theory are much simpler to perform than in the broken CFT [9, 10, 22, 112, 119, 142, 143].

Possibly having extra-dimensions arising at the TeV scale provides a strong motivation for a cutoff to exist near that scale. However, finding such phenomena would not be the end of the story, as we would still be lacking of an explanation for the separation of the compactification and EW scales. Nevertheless, it would certainly provide solid step towards a deeper understanding of particle physics in particular, and nature in general.

In this chapter we will review the most important aspects of RS models. We will start by describing the geometry of the extra dimension in section 2.1, where we will try to justify the choice of $S^1/\mathbb{Z}_2$ as the topology defining the extra dimension. We will introduce the RS metric in 2.2 showing under which conditions this metric is a solution of Eintein's equations. In section 2.3 we will analyze how the Higgs field is described in WED and how the hiearchy problem is solved, for both the brane Higgs and bulk Higgs scenarios. We will then shortly introduce bulk gauge fields in 2.4 and continue with bulk fermion fields in section 2.5, on which we will ellaborate more later in section 2.7, where we will describe the flavor structure of RS models and how they can handle hierarchies in the fermion sector. Section 2.6 will contain a short comment on how the size of the extra dimension can be stabilized with the presence of a single scalar field, commonly known as the Goldberger-Wise (GW) scalar. And in 2.8, we will close the chapter by discussing how important 5D fermion bulk masses are for solving the flavor puzzle, and why we think there are issues within the RS prescription for solving such a puzzle that should be addressed.

2.1 Compactification

The fact that we are not able to detect extra dimensions directly means that (if they exist) they have to be of sufficiently small size so that they cannot be directly observed, in other words, they must be *compactified* down to a very small length scale. But what does being compactified mean? It means that the additional dimension(s) must have a finite length.

One possibility would be to consider a periodic extra dimension, in such a way that by moving along the extra dimension, after a certain *length* is covered, we must return to our initial position. An example of this would be a circle, i.e. an extra dimension defined on an S^1 topology. If the radius of the circle is small enough, we would not be able to access the extra dimension experimentally, as $\sqrt{s} \sim R^{-1}$. Therefore, we could imagine that at every point in our well known Minkowski spacetime, there exists an additional circle of radius R, orthogonal to the 4D Minkowski spacetime. We have sketched this in figure 2.3.

However, for phenomenological purposes it is more interesting to consider an orbifold compactification. In this case an extra constraint is imposed onto the S^1, in this case a $\mathbb{Z}_2$ symmetry. This means that we passed from a manifold to an orbifold compactification. The particularity of the orbifold, in opposition to a manifold, is that it has non-identified points, also known as fixed points. This is interesting to us because of two reasons. Firstly, the extra $\mathbb{Z}_2$ symmetry allows us to impose parities in the 5D fields, which would lead to different 4D phenomenology. In addition, the fixed points would correspond to the localization of the branes, with two fixed points in our particular case.

Therefore, our 5D spacetime can be defined as follows

$$\text{AdS}_5 = \mathcal{M}_4 \times S^1/\mathbb{Z}_2\,, \tag{2.1}$$

where $\mathcal{M}_4$ is the usual four-dimensional (4D) Minkowski spacetime, and $S^1/\mathbb{Z}_2$ describes the topology of the extra spatial dimension, which presents an orbifold compactification. The $S^1/\mathbb{Z}_2$ orbifold compactification is obtained via $\mathbb{R} \to \mathbb{R}/\mathbb{Z} \approx S^1 \to S^1/\mathbb{Z}_2$. This configuration has the following identifications along the extra dimension

$$\begin{aligned} &y \sim y + 2\pi r n, \quad n \in \mathbb{N}, \\ &y \sim -y, \end{aligned} \tag{2.2}$$

which are schematically shown in figure 2.2. For an extended discussion on orbifold compactifications see [144].

2.2 The RS set-up

The idea of the RS model is to explain the hierarchy between the Planck and EW scales without recurring to a formulation based on gauge interactions, but as the geometrical consequence of having the field theory defined on a slice of a AdS_5 spacetime (see figure 2.3 for a sketch). The bulk of the extra dimension has two D3-branes localized at the fixed points of the orbifold, a UV-brane at $y = y_{\text{UV}} = 0$ and an IR-brane at $y = y_{\text{IR}} = r\pi$, where y is the coordinate describing the position along the fifth-dimension and r is the radius of S^1. Moreover, the 5D metric is

$$ds^2 = e^{-2\sigma(y)}\,\eta_{\mu\nu} dx^\mu dx^\nu - dy^2, \tag{2.3}$$

where $\sigma(y)$ is known as the warp factor and $\eta_{\mu\nu} = \text{diag}(+1, -1, -1, -1)$ is the 4D Minkowski metric. This metric ansatz (2.3) has a non-factorizable form and is the most general 5D metric which preserves 4D Poincaré invariance. As will become clear, this metric satisfies Einstein's equations if appropriate cosmological terms are chosen.

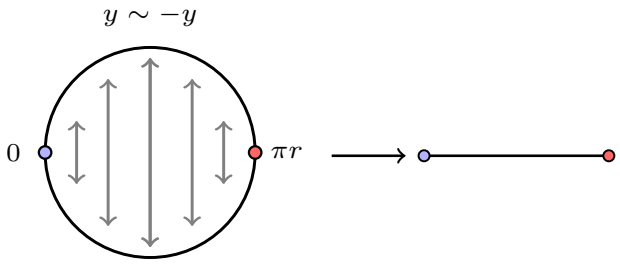

Figure 2.2: *Sketch of the orbifold identification used in RS models.*

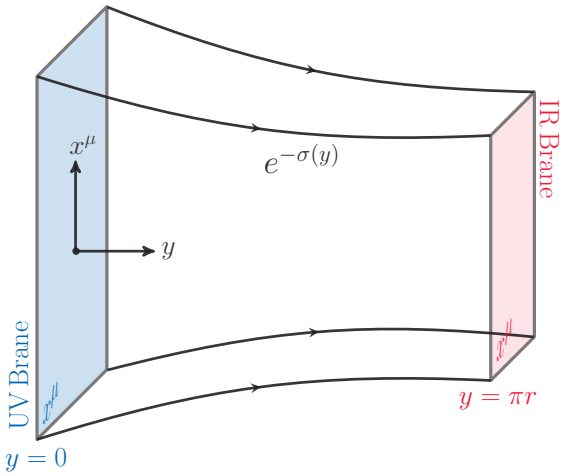

Figure 2.3: *Schematic representation of a fifth dimension compactificatified on S^1.*

The action for RS model can be written as

$$S = \int d^4x \int_0^{y_{\text{IR}}} dy\, \sqrt{g} \left\{ -\frac{\mathcal{R}}{2\kappa^2} - \Lambda_B - \frac{\sqrt{|\hat{g}_{\text{UV}}|}}{\sqrt{g}} \lambda_{\text{UV}} \delta(y) - \frac{\sqrt{|\hat{g}_{\text{IR}}|}}{\sqrt{g}} \lambda_{\text{IR}} \delta(y - y_{\text{IR}}) \right\}, \tag{2.4}$$

where $\mathcal{R}$ is the 5D Ricci scalar, $\kappa^{-2} \equiv 2M_*^3$ with M_* the 5D Planck mass, and Λ_B is the bulk cosmological constant. In addition, λ_{UV} and λ_{IR} are the brane tensions at the UV and IR fixed points and $\hat{g}_{\text{UV}}$ and $\hat{g}_{\text{IR}}$ are the determinant of the 4D induced metrics $\hat{g}^{\mu\nu}_{\text{UV}}$ and $\hat{g}^{\mu\nu}_{\text{IR}}$ on the corresponding brane.

The backround solution for the geometry is obtained by introducing the ansatz (2.3), where σ is a generic y-dependent warp function, into Einstein's equations. The action (2.4) leads to

$$\mathcal{R}_{MN} - \frac{1}{2} g_{MN} \mathcal{R} = \kappa^2 T_{MN}, \tag{2.5}$$

where the energy-momentum tensor T_{MN} corresponds to

$$T_{MN} = g_{MN} \Lambda_B + \frac{\sqrt{|\hat{g}_{\text{UV}}|}}{\sqrt{g}} \lambda_{\text{UV}}\, \hat{g}^{\text{UV}}_{\mu\nu} \delta^\mu_M \delta^\nu_N\, \delta(y) + \frac{\sqrt{|\hat{g}_{\text{IR}}|}}{\sqrt{g}} \lambda_{\text{IR}}\, \hat{g}^{\text{IR}}_{\mu\nu} \delta^\mu_M \delta^\nu_N\, \delta(y - y_{\text{IR}}). \tag{2.6}$$

Einstein's equations can be reduced to

$$\begin{aligned} \sigma'^2 &= \frac{-\kappa^2}{6} \Lambda_B, \\ \sigma'' &= \frac{\kappa^2}{3} \left[\lambda_{\text{UV}}\, \delta(y) + \lambda_{\text{IR}}\, \delta(y - y_{\text{IR}}) \right], \end{aligned} \tag{2.7}$$

where prime stands for the derivative w.r.t. the fifth-dimensional coordinate. Note that the set of equations in (2.7) satisfy the orbifold symmetry $y \to -y$, as was expected from the ansatz. We can easily solve the first equation in (2.7), obtaining

$$\sigma(y) = k|y|, \qquad \text{with} \qquad k \equiv \sqrt{\frac{-\kappa^2}{6} \Lambda_B}. \tag{2.8}$$

requiring the bulk cosmological constant to be negative, i.e. $\Lambda_B < 0$.

Moreover, the above equations have singularities due to the presence of the branes at $y = 0$ and $y = y_{\text{IR}}$, represented by the delta functions in (2.7). This leads to the warp factor satisfying the *jump* conditions

$$\big[\sigma'(y)\big]_i = \frac{\kappa^2}{3}\lambda_i, \tag{2.9}$$

where the *jump* of a function $f(y)$ is defined as

$$\big[f(y)\big] \equiv \lim_{\epsilon\to 0}\Big[f(y+\epsilon) - f(y-\epsilon)\Big]. \tag{2.10}$$

Therefore, (2.9) can be rephrased into the following boundary conditions (BC)

$$\sigma'(0_+) = \frac{\kappa^2}{6}\lambda_{\text{UV}}, \qquad \sigma'(\pi_-) = \frac{-\kappa^2}{6}\lambda_{\text{IR}}, \tag{2.11}$$

with $y_\pm \equiv y \pm \epsilon$.

Note that in order for the solution to satisfy the BC and the EOM the brane tensions need to be of equal magnitude and opposite sign, as

$$\lambda_{\text{UV}} = -\lambda_{\text{IR}} = \frac{6k}{\kappa^2}. \tag{2.12}$$

The definition of the warp parameter k allows to write the three quantities $\lambda_{\text{UV}}, \lambda_{\text{IR}}$ and Λ_B in terms of the same scales, k and M_*. Note that the following conditions need to be fulfilled

$$\lambda_{\text{UV}} = -\lambda_{\text{IR}} = 12M_*^3 k, \qquad \Lambda_B = -12M_*^3 k^2. \tag{2.13}$$

It becomes now clear that the brane potentials are crucial to ensure that the ansatz is a solution of Einstein's equations.

Now the solution allows to relate the 5D Planck mass M_* to the 4D effective reduced Planck mass $M_{\text{Pl}} \simeq 2.4 \cdot 10^{15}$ TeV

$$M_{\text{Pl}}^2 = M_*^3 \int_0^{y_{\text{IR}}} dy\, e^{-2\sigma(y)} = \frac{M_*^3}{2k}\left(1 - e^{-2ky_{\text{IR}}}\right). \tag{2.14}$$

Note that taking k of the same order as the fundamental Planck, $k \sim M_*$, leads to $M_{\text{Pl}} \sim M_*$ for values of $ky_{\text{IR}} > 1$. In addition, (2.14) implies that once $ky_{\text{IR}} > 1$ is satisfied, the 4D Planck mass depends weakly on the size of extra dimension y_{IR}.

However, y_{IR}, together with k, plays an important role determining the suppresion of the EW scale and the Higgs mass w.r.t. the fundamental masses of the theory, of order M_{Pl}. This will become clear in section 2.6.

2.3 The Higgs boson

It is understood nowadays that there are many viable prescriptions within RS models, considering different localizations for the Higgs boson, that are able to solve the hierarchy problem. Initially, RS models considered the Higgs to be confined to the IR brane [18, 21, 25, 145, 146]. In that simplified case, one find the Higgs scale to lie at around the IR-brane scale, i.e. $\sim \mathcal{O}(1)$ TeV. A tuning is therefore needed in these models to realize this little hierarchy problem, but the Higgs is protected from heavy resonances as these resonances coupling to the Higgs will all appear at the TeV scale.

However, soon after models in which the Higgs was allowed to propagate in the bulk emerged [11, 109–113, 147, 148]. It was found that if the Higgs parameters are chosen such that the profile

of the Higgs describing its behavior along the extra dimension is peaked towards the IR brane, then the suppresion on the couplings of the Higgs to heavy resonances are more relaxed but similar to the IR brane case.

Some work consider the case where the Higgs can propagate in a small portion of the bulk located near the IR, this is known as the narrow bulk Higgs scenario. Such scenario has been explored e.g. in [149, 150], where a relation between the bulk, narrow and brane-localized Higgs cases have been discussed, and how one can take the limit from one case to the other.

However, to understand how the hierarchy problem is solved in RS for any of the setups we have just discussed, one needs to understand the role $y_{\rm IR}$ plays for determining the hierarchy. It is instructive as well to see how the 4D effective Higgs mass and the effective EW scale emerge from the 5D fundamental parameters. For this, the most illustrative derivation can be done in the case of a brane-localized Higgs, and this will be therefore the first scenario here presented. In addition, the ϕ and t-coordinates will be introduced (see appendix A for a summary of how the different coordinates are defined), which will become handy for the next sections.

2.3.1 The brane-localized Higgs case

In this section, we will analyze the simplest configuration for the Higgs in RS models. In this set-up the Higgs is confined to a IR brane and is therefore a pure 4D-field. However, the quantities appearing in the Higgs action even though they are defined to lie at the Planck scale, get a suppresion because of the 5D metric and appear as 4D effective parameters at the TeV scale.

To study the brane-localized Higgs we will introduce the ϕ-coordinates, which will be useful for the rest of the manuscript. Then, the metric in (2.3) can be rewritten in terms of the new coordinates as

$$ds^2 = e^{-2\sigma(\phi)}\,\eta_{\mu\nu}dx^\mu dx^\nu - r^2 d\phi^2, \tag{2.15}$$

where the warp factor is now $\sigma(\phi) = kr|\phi|$, and $\phi \in [-\pi, \pi]$. Here, r is the compactification radius of the extra dimension, with $\pi r = y_{\rm IR}$, and the localization of the branes are now $\phi = 0$ for the UV brane, and $\phi = \pm\pi$ for the IR brane.

In these coordinates, the action for a IR-brane-localized Higgs doublet reads

$$S_H^{(4D)} = \int d^4x \sqrt{|\hat{g}_{\rm IR}|}\left\{\hat{g}_{\rm IR}^{\mu\nu}\left(D_\mu H\right)^\dagger\left(D_\nu H\right) - m^2\left(H^\dagger H\right) - \lambda\left(H^\dagger H\right)^2\right\}, \tag{2.16}$$

where the 4D induced metric on the IR-brane corresponds to $\hat{g}_{\rm IR}^{\mu\nu} = e^{2kr\pi}\eta^{\mu\nu}$. Defining $L \equiv kr\pi$ and writing explicitely the metric factors, the previous action reads

$$S_H^{(4D)} = \int d^4x \left\{e^{-2L}\left(D_\mu H\right)^\dagger\left(D^\mu H\right) - m^2 e^{-4L}\left(H^\dagger H\right) - \lambda e^{-4L}\left(H^\dagger H\right)^2\right\}. \tag{2.17}$$

Note that the Higgs doublet is not canonically normalized in (2.17). The following field redefinition is necessary for the Higgs doublet to have a canonically normalized kinetic term

$$H \to He^L. \tag{2.18}$$

Defining

$$\mu \equiv m\,e^{-L}, \qquad \lambda_H \equiv \lambda\,e^{-2L}, \tag{2.19}$$

together with the field redefinition in (2.19) leads to

$$S_H^{(4D)} = \int d^4x \left\{ (D_\mu H)^\dagger (D^\mu H) - \mu^2 \left(H^\dagger H\right) - \lambda_H \left(H^\dagger H\right)^2 \right\}, \tag{2.20}$$

where μ is the effective Higgs mass parameter at the IR-brane and is related to the fundamental quantity m in the 5D theory by the warp factor. Therefore, if the fundamental parameter m is considered to sit at the scale of the Planck mass, i.e. $m \sim \mathcal{O}(10^{15})$ TeV, it can get warped down to the EW scale for the appropiate value of L and therefore $\mu \sim \mathcal{O}(10^2)$ GeV for values of $L = kr\pi \sim \mathcal{O}(30)$, or $ky_{\text{IR}} \sim \mathcal{O}(30)$ in the y-coordinates. Therefore, in the RS model, the hierarchy between the EW and the Planck scales gets resolved in terms of the curvature and size of the extra dimension.

Moreover, note that the same suppresion can be obtained for the Higgs VEV

$$v_h \equiv v_0\, e^{-L}, \tag{2.21}$$

which becomes trivial after rewritting the potential appearing in (2.16) as

$$V_H(H) = m^2 \left(H^\dagger H\right) - \lambda \left(H^\dagger H\right)^2 = \lambda \left(H^\dagger H - v_0^2\right)^2. \tag{2.22}$$

2.3.2 The bulk Higgs case

Soon after the RS model was introduced, it was noticed that the Higgs boson could also be promoted to a 5D field if the parameters of the model are such that allow the Higgs to be localized towards the IR brane [113,149–155]. Once the bulk Higgs is close enough to the IR brane the hierarchy problem is solved similarly to the brane-Higgs scenario and therefore it presents no problem from the naturalness perspective.

The action for a 5D complex scalar field, Φ, in generic 5D coordinates, considering a bulk and brane potentials reads

$$S_\Phi^{(5D)} = \int d^5x \sqrt{g} \left\{ g^{MN} (D_M \Phi)^\dagger (D_N \Phi) - V(\Phi) - \frac{\sqrt{|\hat{g}_k|}}{\sqrt{g}} V^k(\Phi) \delta(x_5 - x_{5k}) \right\}, \tag{2.23}$$

where $V(\Phi)$ denotes the bulk scalar potential and $V^k(\Phi)$ the brane potentials at x_{5k} with $x_{5k} = x_{5,\text{UV}}$ and $x_{5,\text{IR}}$. Here, the generic metric is defined as

$$ds^2 = a(x_5)^2 \eta_{\mu\nu} dx^\mu dx^\nu - b(x_5)^2 dx_5^2, \tag{2.24}$$

where are writing the metric in a generic form. The factors $a(x_5)$ and $b(x_5)$ would take appropriate values for any given choice of the x_5-coordinate, e.g. $a(y) = e^{-\sigma(y)}$ and $b(y) = 1$ when choosing the y-coordinate representation for the extra dimension.

Integrating by parts in the action (2.23), the EOM for the scalar field Φ can be obtained. It reads

$$a^{-4} b^{-1} \partial_5 \left(a^4 b^{-1} \partial_5 \Phi\right) - a^{-2} \Box\, \Phi - \frac{\partial V}{\partial \Phi} = 0, \tag{2.25}$$

together with BC

$$\delta\Phi \left\{ \pm b^{-1} \partial_5 \Phi + \frac{\partial \hat{V}^k}{\partial \Phi} \right\} \Bigg|_{\Phi = \Phi(x_{5k})} = 0. \tag{2.26}$$

Here, the goal of writing (2.25) and (2.26) from the generic metric (2.24) is to have a simple way of translating EOM from a specific set of coordinates into another.

For the bulk Higgs scenario it is convenient to introduce the t-coordinates. These coordinates are defined in terms of the ϕ-coordinates as $t = \epsilon\, e^{kr\phi}$, where $\epsilon = e^{-kr\pi}$. In this case, the metric reads

$$ds^2 = \frac{\epsilon^2}{t^2}\left(\eta_{\mu\nu}dx^\mu dx^\nu - \frac{1}{M_{\text{KK}}^2}dt^2\right), \tag{2.27}$$

where $M_{\text{KK}} = k\epsilon$, and the metric factors correspond to $a(t) = \epsilon/t$ and $b(t) = \epsilon/(tM_{\text{KK}})$. Here, $t \in [\epsilon, 1]$, with $\epsilon \sim \mathcal{O}(10^{-14})$ for $L = kr\pi \sim \mathcal{O}(30)$.

The Higgs doublet in the unitary gauge can be defined as follows

$$H(x,t) = \frac{t}{\epsilon\sqrt{2r}}\begin{pmatrix}0\\1\end{pmatrix}\left[\varphi_H(t) + h(x,t)\right], \tag{2.28}$$

where $\varphi_H(t)$ is the profile of the Higgs VEV, which only depend on the coordinates of the extra dimension, and $h(x,t)$ is the 5D Higgs field [113, 149, 150, 154, 155]. The prefactor $t/(\epsilon\sqrt{2r})$ is introduced for convenience. This will become clear later when the normalization condition for the Higgs modes after the KK-expansion is obtained.

In addition, the bulk and brane localized potentials for the bulk higgs field take the following form

$$\begin{aligned} V &= \mu_H^2|H|^2, \\ V^{\text{UV}} &= \sigma_{\text{UV}}|H|^2, \\ V^{\text{IR}} &= -\sigma_{\text{IR}}|H|^2 + \rho_{\text{IR}}|H|^4. \end{aligned} \tag{2.29}$$

Let's analyze the dimension of the fields and the parameters of the bulk and brane potentials. First of all, the mass dimension of the bulk scalar fields can be infered from the kinetic term of the action, in (2.23). Moreover, a similar derivation can be done with the parameters of the potentials in (2.29), given that the dimension of the potentials are well known. The mass dimensions of the scalar sector of a 5D bulk theory can be summarized as

$$[\mathcal{L}_{5\text{D}}] \Rightarrow [\Phi] = 3/2, [V] = 5, \left[V^{\text{UV}}\right] = \left[V^{\text{IR}}\right] = 4, \tag{2.30}$$

which leads to

$$[\mu] = [\sigma_{\text{UV}}] = [\sigma_{\text{IR}}] = 1, \quad \text{and} \quad [\rho_{\text{IR}}] = -2. \tag{2.31}$$

For simplicity, a quartic term is only introduced at the IR brane, in order to induce EWSB near that brane [113, 149–155]. However, the same could be done for the bulk and UV branes if the Higgs is peaked towards the IR brane. In that case, the quartic term contributions would be negligeable and therefore, could be omitted.

The EOM for the Higgs VEV is derived from (2.25) by omitting the 4D term

$$\left[t^2\partial_t^2 + t\partial_t - \beta^2\right]\frac{\varphi_H(t)}{t} = 0, \tag{2.32}$$

where the effective mass parameter β has been defined as

$$\beta^2 \equiv 4 + \frac{\mu_H^2}{k^2}. \tag{2.33}$$

Note that the effective mass parameter $\mu^2 + 4k^2$ in (2.33) is precisely the one appearing in the Breitenlohner-Freedman (BF) bound in AdS space [156, 157]. The BF bound

$$\beta^2 = 4 + \frac{\mu_H^2}{k^2} \geq 0, \tag{2.34}$$

is related to the absence of tachyonic modes for the scalar fluctuations for a free field. Note that the Higgs has a quartic parameter located at the IR brane, however and since it has the potential of a free field in the bulk, it is usually assummed that β is real and positive. Note that this allows for negative values of μ_H^2, as long as (2.34) is satisfied.

Moreover, the BC corresponding to the UV and IR branes are

$$\begin{aligned} \partial_t \left[t\, \varphi_H(t) \right]_{t=\epsilon^+} &= m_{\text{UV}}\, \varphi_H(\epsilon), \\ \partial_t \left[t\, \varphi_H(t) \right]_{t=1^-} &= m_{\text{IR}}\, \varphi_H(1) - \frac{2\lambda_{\text{IR}}}{M_{\text{KK}}^2} \varphi_H(1)^3. \end{aligned} \tag{2.35}$$

The notation ϵ^+ and 1^- refers to the orbifold fixed points, approached from the appropriate side. In addition, the following quantities have been defined

$$m_{\text{UV}} = \frac{\sigma_{\text{UV}}}{2k}, \quad m_{\text{IR}} = \frac{\sigma_{\text{IR}}}{2k}, \quad \lambda_{\text{IR}} = \frac{\rho_{\text{IR}} k}{4r}. \tag{2.36}$$

Solving the EOM and BC set leads to the well known solution [149, 154, 155]

$$\varphi_H(t) = N_v \left[t^{1+\beta} - r_v t^{1-\beta} \right], \tag{2.37}$$

with r_v and N_v defined as

$$\begin{aligned} r_v &= \epsilon^{2\beta} \frac{2+\beta-m_{\text{UV}}}{2-\beta-m_{\text{UV}}}, \\ N_v^2 &= \frac{M_{\text{KK}}^2}{2\lambda_{\text{IR}}} \frac{(m_{\text{IR}}-2-\beta) + r_v\,(m_{\text{IR}}-2+\beta)}{(1-r_v)^3}. \end{aligned} \tag{2.38}$$

Note that, unless β is very small or the denominator in r_v is fine-tuned to $m_{\text{UV}} \sim 2-\beta$, it is safe to consider r_v to be small, i.e. $r_v \propto \epsilon^{2\beta} \ll 1$, and therefore can be set to zero for all practical purposes. In that case, (2.37) simplifies to

$$\varphi_H(t) \approx N_v\, t^{1+\beta}, \tag{2.39}$$

where it comes explicit that the Higgs VEV is peaked towards the IR brane, as it was previously discussed that $\beta \geq 0$. As can be seen, the fact that the Higgs VEV is localized near the IR brane is not a consequence of a fine-tuning. On the contrary, it is avoiding the Higgs VEV to point towards the IR brane that requires such fine-tuning, since it would become necessary to adjust m_{UV} so that $m_{\text{UV}} \simeq 2-\beta$.

In the approximation (2.39), the profile at $t=1$ can be indentified as

$$\varphi_H(1) \simeq N_v \simeq M_{\text{KK}} \sqrt{\frac{m_{\text{IR}}-2-\beta}{2\lambda_{\text{IR}}}}, \tag{2.40}$$

given by the BC at the infrarred brane. Therefore, it follows

$$\varphi_H(t) \simeq \varphi_H(1)\, t^{1+\beta}. \tag{2.41}$$

Furthemore, the normalization such that the SM W, Z masses are obtained (see [149, 150, 154, 155]) leads to

$$v_4^2 = \frac{2\pi}{L} \int_\epsilon^1 \frac{dt}{t} \varphi_H^2(t) = \frac{\pi N_v^2}{L} \left[\frac{1}{1+\beta} + \mathcal{O}(\epsilon) \right] \simeq \frac{\pi}{L} \frac{\varphi_H^2(1)}{1+\beta}, \tag{2.42}$$

where the zero-mode profiles of the gauge bosons have been assumed to be flat, up to $\mathcal{O}(v_4^2/M_{\text{KK}}^2)$ corrections [150]. The reason why this assumption can be made will become clear in the next section. In that case, the Higgs VEV reads

$$\varphi_H(t) \approx v_4 \sqrt{\frac{L}{\pi}(1+\beta)}\, t^{1+\beta}, \tag{2.43}$$

where v_4 corresponds with $v_{\rm SM}$ at leading order in both $x_4 \equiv v_4/M_{\rm KK}$ and ϵ.

Let's move now to the study of the scalar KK excitations. The profiles of these resonances can be computed by inserting the KK decompositions

$$h(x,t) = \sum_{n=0}^{\infty} h_n(x)\chi_n^h(t), \tag{2.44}$$

into the action (2.23). They correspond to the solutions of a mass eigenvalue problem for the $h_n(x)$ modes, the 4D resonances satisfying the Klein-Gordon equation, while $\chi_n^h(t)$ are their corresponding profiles along the extra dimension. In that expansion, the zero mode $h(x) \equiv h_0(x)$ corresponds to the SM Higgs boson. Demanding these fields to have canonically normalized kinetic terms leads to the profile orthogonality condition

$$\frac{2\pi}{L}\int_\epsilon^1 \frac{dt}{t}\chi_m^h(t)\chi_n^h(t) = \delta_{mn}. \tag{2.45}$$

The EOM for the 5D profiles correspond to the following Sturm-Liouville equation

$$\left[t^2\partial_t^2 + t\partial_t + t^2x_n^2 - \beta^2\right]\frac{\chi_n^h(t)}{t} = 0, \tag{2.46}$$

with BC

$$\begin{aligned} \partial_t\left[t\,\chi_n^h(t)\right]_{t=\epsilon^+} &= m_{\rm UV}\,\chi_n^h(\epsilon), \\ \partial_t\left[t\,\chi_n^h(t)\right]_{t=1^-} &= m_{\rm IR}\,\chi_n^h(1) - \frac{2\lambda_{\rm IR}}{M_{\rm KK}^2}\chi_n^h(1)^3. \end{aligned} \tag{2.47}$$

where x_n, the eigenvalue of the EOM, denotes the mass of the 4D particle in units of $M_{\rm KK}$, as

$$x_n \equiv m_n/M_{\rm KK}\,. \tag{2.48}$$

The fact that (2.46) is a Sturm-Liouville equation (as will be the case for the gauge boson and fermion fields) guarantees that the profiles, corresponding to eigenfunctions of such Sturm-Liouville problem, are orthogonal to each other. In this case, the most general solution to equation (2.46) is a linear combination of Bessel functions as

$$\chi_n^h(t) = N_n t\left[J_\beta(x_n t) - r_n Y_\beta(x_n t)\right], \tag{2.49}$$

where the BC on the UV brane does again imply that $r_n \propto \epsilon^{2\beta}$ is extremely small and can be set to zero. In this case, the profiles for the n-modes of the 5D Higgs field can be written as

$$\chi_n^h(t) = \sqrt{\frac{L}{\pi}}\frac{tJ_\beta(x_{h_n}t)}{\sqrt{J_\beta^2(x_{h_n}) - J_{\beta+1}(x_{h_n})J_{\beta-1}(x_{h_n})}}, \tag{2.50}$$

where $J_\beta(x)$ is a Bessel function, and $\chi_n^h(t)$ satisfy the orthogonality condition and normalization from (2.45).

The eigenvalues x_{h_n} are obtained from the relation

$$\frac{x_{h_n}J_{\beta+1}(x_{h_n})}{J_\beta(x_{h_n})} = 2\left(m_{\rm IR} - 2 - \beta\right) \equiv 2\delta, \tag{2.51}$$

which has been derived form the BC at the IR brane, by using properties of the J_β Bessel functions. The eigenvalues resulting from equation (2.51) are $\mathcal{O}(1)$. However, for the zero-mode a smaller

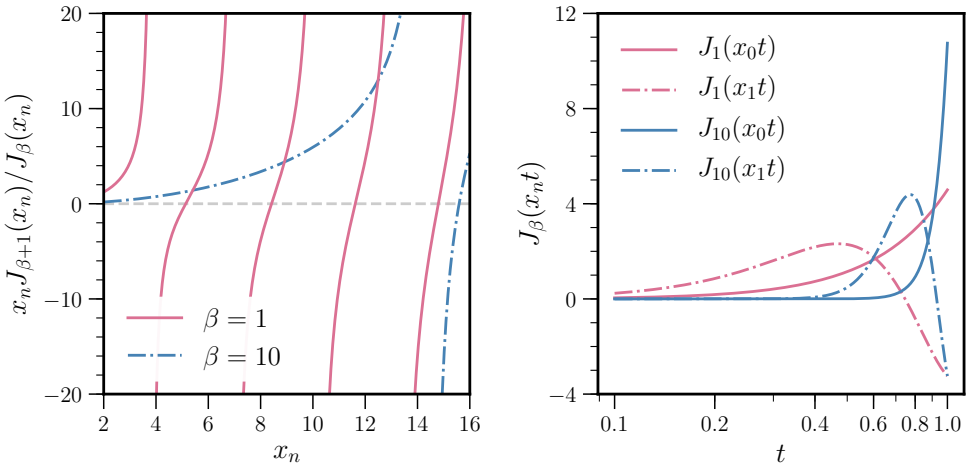

Figure 2.4: *Left: Representation of the function that sets the eigenvalues x_n for the Higgs n-modes. Right: Profiles of the zero and first KK modes of the Higgs field.*

value can be obtained if a fine-tuning is performed. This is equivalent to the little hierarchy problem appearing in the brane-Higgs scenario, since in these models the intrinsic IR-brane is $\mathcal{O}(5)$ TeV, and therefore to obtain the Higgs mass requires some tuning. In this case, it is $\delta \ll 1$ the tuning required to obtain the appropriate x_0 so that $m_h = 125$ GeV and therefore $x_0 = m_h/M_{\text{KK}} \ll 1$.

In particular, in [150] the authors expanded the zero-mode mass in a power series of δ

$$x_0^2 = \frac{m_h^2}{M_{\text{KK}}^2} = 4(1+\beta)\delta + \mathcal{O}(\delta^2), \tag{2.52}$$

making the tunning on δ explicit.

In addition, since the eigenvalue for the zero-mode is a small parameter, it is possible to expand the zero-mode profile for the Higgs in powers of x_0^2. Such expansion reads

$$\chi_0^h(t) = \sqrt{\frac{L}{\pi}(1+\beta)}\, t^{1+\beta}\left[1 - \frac{x_0^2}{4}\left(\frac{t^2}{1+\beta} - \frac{1}{2+\beta}\right)\right] + \mathcal{O}(x_0^4), \tag{2.53}$$

and therefore, at first order it can be approximated as

$$\chi_0^h(t) \simeq \sqrt{\frac{L}{\pi}(1+\beta)}\, t^{1+\beta}. \tag{2.54}$$

In this limit, the zero-mode profile for the Higgs corresponds with the Higgs VEV profile up to a v_4 factor, as can be seen from (2.43).

We show in the left plot of figure 2.4 the ratio of Bessel function from (2.51) that allows to obtain the mass eigenvalues x_n. For $x_0 \ll 1$, $2\delta \sim 0$ and therefore the zeros of that ratio correspond to the eigenvalues as a good approximation. In particular, for $M_{\text{KK}} = 5$ TeV we find $2\delta \sim \mathcal{O}(10^{-3})$ for $\beta = 1$ and $2\delta \sim \mathcal{O}(10^{-4})$ for $\beta = 10$, if we want to reproduce the SM Higgs mass for $n = 0$. Note that in general $x_n \sim \mathcal{O}(1)$ and $J_{\beta+1}(x_n)/J_\beta(x_n) \sim \mathcal{O}(10^{-1})$. In the right plot, we show the profiles for the zero and first KK modes of the Higgs field for $\beta = 1$ and $\beta = 10$.

2.4 Gauge fields

We continue now with the discussion of gauge fields. We will be focusing here on a $U(1)$ gauge field as our purpose in this section is to give an overview on how the gauge profiles are obtained and what are their orthogonality conditions and in that case, the derivation for a non-abelian gauge field is substantially the same. Moreover, we will be only interested in the quadratic part of the action, where there is no distinction between the abelian and non-abelian cases. Therefore, we can define our gauge field tensor as $F_{MN} = \partial_M A_N - \partial_N A_M$.

The 5D action for the $U(1)$ gauge field reads

$$S_A^{(5\mathrm{D})} = \int d^4x \int_{-\pi}^{\pi} d\phi \, \sqrt{g} \Big\{ -\frac{1}{4} g^{MN} g^{KL} F_{MK} F_{NL} \Big\} + S_{\mathrm{GF}}, \tag{2.55}$$

where S_{GF} is a gauge-fixing term, necessary to cancel the mixed kinetic terms the gauge bosons, A_μ, and the scalar components, A_5, [110, 158]. Such cancellations are not a feature of the abelian case, and can also be achieved for a non-abelian theory, see [110].

The covariant derivative for a field charged under the $U(1)$ is defined as

$$D_M = \partial_M - i g_5 A_M. \tag{2.56}$$

The mass dimensions of the gauge fields and the coupling constant can be inferred from the definition of the covariant derivative in (2.57) and the action in (2.55), being

$$[A_M] = 3/2, \qquad [g_5] = -1/2. \tag{2.57}$$

We can now write the KK decomposition for the 5D $U(1)$ gauge field A_M in terms of the A_μ and A_5 components, as

$$\begin{aligned} A_\mu(x,\phi) &= \frac{1}{\sqrt{r}} \sum_n A_\mu^n(x) \chi_n^A(\phi), \\ A_5(x,\phi) &= \frac{-1}{\sqrt{r}} \sum_n \frac{1}{m_n^A} A_5^n(x) \partial_\phi \chi_n^A(\phi). \end{aligned} \tag{2.58}$$

Inserting the KK decomposition into the action leads to the EOM for the χ_n^A profiles

$$\left[\partial_\phi \, e^{-2\sigma(\phi-\pi)} \partial_\phi + (x_n^A)^2 (kr)^2 \right] \chi_n^A(\phi) = 0, \tag{2.59}$$

together with BC

$$\left[\partial_\phi \chi_n^A(\phi) \right] \big|_{\phi=0,\pi} = 0. \tag{2.60}$$

Again, being the profiles, χ_n^A, the eigenfunctions of a Sturm-Liouville problem, it is guaranteed that the profiles are orthogonal to each other. In particular, they satisfy the following orthonormality condition

$$\int_{-\pi}^{\pi} d\phi \, \chi_m^A(\phi) \chi_n^A(\phi) = 2 \int_0^{\pi} d\phi \, \chi_m^A(\phi) \chi_n^A(\phi) = \delta_{mn}. \tag{2.61}$$

The solutions for the gauge boson profiles is given in terms of Bessel functions for the KK modes

$$\chi_n^A(\phi) = N_n e^{\sigma(\phi)} \left[J_1\left(x_n^A e^{\sigma(\phi-\pi)} \right) + b_n Y_1\left(x_n^A e^{\sigma(\phi-\pi)} \right) \right]. \tag{2.62}$$

However, for the zero-mode the solution is trivially $\chi_0^A(\phi) = N_0$, where the value of N_0 is set by the condition (2.61), and therefore [103, 104, 110]

$$\chi_0^A(\phi) = \frac{1}{\sqrt{2\pi}}. \tag{2.63}$$

As we can see from the BC in (2.60), the profiles corresponding to the A_μ components satisfy Neumann BC, while the profiles corresponding to A_5 satisfy Dirichlet BC. Note that this only makes it possible for the A_μ fields to have a non-vanishing zero-mode, while the Dirichlet BCs for the 5D profiles of the A_5 fields do not allow them to have a zero-mode.

As was mentioned in the previous section, for determining the normalization of the Higgs VEV in (2.43), the zero-modes for the gauge bosons are flat. This is due to the fact that there is no free parameter that can control the localization of the gauge zero-modes. In addition, the fact that the zero-mode is flat is necessary for gauge invariance and the universality of gauge interactions. Note that the effective 4D gauge coupling of the SM gauge bosons, which corresponds to the effective coupling of the gauge boson zero-modes with the Higgs and the SM fermions, is obtained from the 5D theory after the profiles of the Higgs boson and fermions are integrated out together with the profile of the particular gauge boson zero-mode. Since gauge bosons appear in kinetic term of such fields through the covariant derivative, it is guaranteed that in the absence of a coordinate-dependent gauge bosons profiles, i.e. when setting χ_0^A equal a constant, the overlaps with the Higgs bosons and SM fermions are all normalized the same way and are therefore universal. Notice however that, if the gauge zero-mode is not flat, the non-trivial localizations of fermions or scalars, once these are integrated out together with the non-flat profile of the gauge bosons, would lead to arbitrary 4D gauge couplings for every field.

However, once the gauge bosons have a non-vanishing 5D mass, their profiles deviate from $\chi_0^A = 1/\sqrt{2\pi}$. In particular, for the SM gauge fields the Higgs introduces a mass term, and therefore one could think that the profiles would no longer be described by the trivial solution given in (2.63). However, being the scale of the new 5D mass $v = 246$ GeV much smaller than M_{KK}, such deviations can be computed as perturbations of $\mathcal{O}(v_4/M_{\text{KK}})$ and therefore, the flat solutions still provide a very good approximation [103, 104].

Let us consider the case of the brane-localized scalar, ϕ_A, that lives in the IR brane and its charged under the $U(1)$ gauge symmetry. If such scalar acquires a VEV, it would introduce a new mass term for the A_M gauge bosons, and this new term would appear in the BC for the IR brane. In this case, the BC for the gauge bosons read

$$\left[\partial_\phi \chi_n^A(\phi)\right]\big|_{\phi=0} = 0, \qquad \left[\partial_\phi + \pi r^2 M_A^2 e^{2\sigma(\pi)}\right] \chi_n^A(\phi)\big|_{\phi=\pi} = 0, \tag{2.64}$$

where we have introduced

$$M_A^2 \equiv \frac{g_A^2}{2\pi r}\frac{v_\phi^2}{4}, \tag{2.65}$$

with $\langle \phi_A \rangle \equiv v_\phi$.

Moreover, if we consider now the case where ϕ_A is a bulk scalar, the new 5D mass for the gauge bosons would have a dependence on the fifth dimensional coordinate. In this case, the mass for the zero-mode becomes

$$m_A^2 \approx \frac{2\pi}{L}\int_\epsilon^1 \frac{dt}{t} M_A^2(t). \tag{2.66}$$

where we have used the approximation $\chi_0^A(\phi) \approx 1/\sqrt{2\pi}$ and

$$M_A^2(t) \equiv \frac{g_A^2}{2\pi r}\frac{v_\phi^2(t)}{4}, \tag{2.67}$$

where now $\langle \phi_A \rangle \equiv v_\phi(t)$. Note that we have changed from ϕ to t coordinates here. It could have been shown using the ϕ coordinates, however it is convenient to have this formulae in t coordinates, so that the Higgs VEV solution from (2.43) can be inserted directly.

To obtain the masses of the SM gauge bosons, $Z, W^\pm$, from the previous derivations, it can be easily done by identifying $v_\phi = v_0$ for the brane-Higgs case, and $v_\phi^2(t) = \varphi_H^2(t)$ for the bulk Higgs scenario. In both cases, to derive $M_{Z,W}$ and $M_{Z,W}(t)$, the gauge couplings g_A should be traded for $g_Z^2 = g_5^2 + g_5'^2$ and $g_W^2 = g_5^2$. For photons and gluons the masses are naturally $M_\gamma = M_g = 0$ and the profiles are therefore purely flat, where note that this result holds for all orders in v_4/M_{KK}.

2.5 Fermion fields

In 4D fermions are described through an irreducible representation of two-dimensional Weyl spinors. However, in 5D the smallest irreducible representation for fermions has 4 complex components, and therefore the 2-component Weyl spinors are connected through Lorentz transformations. Another way to understand this is by the fact that in 5D γ_5 is part of the five-dimensional Dirac algebra, therefore it does no longer commute with all the generators of the Lorentz group, i.e. the 4D chiral components are now connected by the Lorentz transformations. This means that 5D fermions are described by vector-like fields and that we cannot build a chiral gauge theory in 5D. Even if we initially asign vanishing gauge charges to one of the two components, and a non-vanishing charge to the opposite chirality, we can always transform the LH modes into the RH modes and *vice versa*, and therefore by rotating one chirality into the other we would always be able to charge both LH and RH fields under the gauge symmetry [143, 158, 159].

However, we will see that it is still possible to obtain a 4D chiral spectrum from the 5D vector-like theory. Because the compactification of the extra dimension breaks down the 5D Lorentz invariance, only one of the massless modes from the 4D chiralities remains, and therefore the 4D theory differentiates left and right [1, 21, 24, 25, 143, 158–160].

In particular, the 5D Clifford algebra is given by

$$\left\{\Gamma^a, \Gamma^b\right\} = 2\eta^{ab}, \tag{2.68}$$

where Γ^a and Γ^b are the five 4×4 anticommuting Dirac Γ-matrices and the symbols $(a, b, \ldots)$ correspond to local Lorentz indices, defined in the tangent flat space. These Gamma-matrices can be transformed into quantities defined in the AdS_5 space by

$$\Gamma^M = e_a^M \, \Gamma^a, \tag{2.69}$$

where e_a^M is the inverse *fünfbein*. We will use upper-case Roman indices $(M, N, \ldots)$ to denote objects defined in the curved space. The *fünfbeins* are defined so that they satisfy

$$g_{MN} = e_M^a e_N^b \, \eta_{ab}. \tag{2.70}$$

Here, the *fünfbeins* allow to transform quantities from the 4D vector tangent space to the AdS_5 spacetime [123, 143, 158, 161]. In addition, the inverse *fünfbein* must fulfill

$$e_a^M e_M^b = \delta_a^b. \tag{2.71}$$

For an AdS_5 space, these quantities correpond to

$$e_M^a = \text{diag}\,(e^{\sigma(y)}\delta_\alpha^a, 1). \tag{2.72}$$

Therefore, the 5D Clifford algebra in an AdS_5 space satisfies

$$\left\{\Gamma^M, \Gamma^N\right\} = 2g^{MN}. \tag{2.73}$$

To summarize, our 5D Dirac Γ-matrices, which provide a 4D irreducible representation of the 5D Clifford algebra in flat space, are

$$\Gamma^a = (\gamma^\alpha, i\gamma_5)\,, \tag{2.74}$$

with $\alpha = 0, \ldots, 3$, and where γ^α are the usual Dirac matrices and γ_5 is defined as $\gamma_5 = i\gamma^0\gamma^1\gamma^2\gamma^3$.

In addition, for a general backgrounds we need to include a spin connection to define the covariant derivative. The covariant derivative for an uncharged fermion is defined as

$$D_M = \partial_M + \omega_M = \partial_M + \frac{1}{8}\omega_{Mab}\left[\Gamma^a, \Gamma^b\right], \tag{2.75}$$

where ω_M is spin connection and the coefficients ω_{Mab} are defined as in [123, 143, 158, 161]

$$\omega_M^{ab} = \frac{1}{2}g^{RP}e_R^{[a}\,\partial_{[M}e_{P]}^{b]} + \frac{1}{4}g^{RP}g^{TS}e_R^{[a}e_T^{b]}\,\partial_{[S}e_{P]}^{c}e_M^d\eta_{cd}. \tag{2.76}$$

For the RS background, given that the metric is diagonal, the spin connection is simply

$$\omega_M = \left(-\frac{\sigma(\phi)}{2r}e^{\sigma(\phi)}\gamma_\mu\gamma_5, 0\right). \tag{2.77}$$

Even though we can always rotate the fields of one chirality to the other in 5D, we can still define the chirality projectors as usual, being $P_{L,R} = (1 \mp \gamma_5)/2$. In this case, we can decompose the five-dimensional Dirac spinor into the two chiralities as $\Psi = \Psi_L + \Psi_R$ with $\Psi_{L,R} \equiv P_{L,R}\Psi$ and $\gamma_5\Psi_{L,R} = \pm\Psi_{L,R}$. As we mentioned before, the idea is to asign a different $\mathbb{Z}_2$ transformation, even or odd, to each chirality of Ψ, in such a way that only one of the zero modes can fulfill the BC and therefore survives. This will be explicitly shown in section 2.5.1, where we will introduce the zero-mode solutions.

We can now define the action for Dirac fermion fields. Note that in 5D fermions can have a mass term in the action, since as we mentioned before, 5D fermions are described by vector-like fields. However, since the opposite-chirality components would transform differently under the $\mathbb{Z}_2$ orbifold symmetry, such a mass term needs to appear together with a *sign* function. Otherwise, the action would no longer be invariant under the orbifold symmetry. Taking this into account, the action for 5D fermions can be written as [21, 25]

$$S_\psi^{(5\mathrm{D})} = \int d^4x \int_{-\pi}^{\pi} d\phi\sqrt{g}\left\{E_a^N\left[\frac{i}{2}\bar\Psi\,\Gamma^a(\partial_N - \overleftarrow{\partial}_N)\Psi + \frac{\omega_{bcN}}{8}\,\bar\Psi\{\Gamma^a, \sigma^{bc}\}\Psi\right] - m_\psi\,\mathrm{sgn}(\phi)\bar\Psi\Psi\right\}, \tag{2.78}$$

where the derivatives have been written such that the action is explicitly hermitian. We are considering here free fermions, but gauge charges could be considered by replacing the partial derivatives for covariant derivatives. Note however that the spin connection has already been written explicitely.

The mass dimensions of the fields and the mass parameter in the action are

$$[\Psi] = 2, \qquad [m_\psi] = 1. \tag{2.79}$$

Applying the principle of least action and integrating by parts in (2.78) leads to the EOM for the Ψ field

$$\begin{aligned} e^\sigma i\not{\partial}\Psi_L + \left[-\partial_5 - m_\psi + 2\sigma'\right]\Psi_R = 0, \\ e^\sigma i\not{\partial}\Psi_R + \left[+\partial_5 - m_\psi - 2\sigma'\right]\Psi_L = 0, \end{aligned} \tag{2.80}$$

and to the BC

$$\delta\bar\Psi_L\,\Psi_R\Big|_{\phi=0,\pi} = \delta\bar\Psi_R\,\Psi_L\Big|_{\phi=0,\pi} = 0. \tag{2.81}$$

We now perform the following KK decomposition

$$\Psi_{L,R}(x,\phi) = \sum_n \psi_n^{L,R}(x) \frac{e^{2\sigma}}{\sqrt{r}} f_n^{L,R}(\phi), \tag{2.82}$$

and requiring in (2.83) that the $\psi_n^{L,R}(x)$ modes satisfy the 4D Dirac equation for massive fermions leads to the EOM for the $f_n^{L,R}$ profiles

$$\left(\pm\frac{\partial_\phi}{r} - m_\psi\right) f_n^{L,R}(\phi) = -m_n e^{\sigma} f_n^{R,L}(\phi), \tag{2.83}$$

where m_n are the masses of the 4D resonances. Note that the LH and RH resonances of the same n-mode have indentical masses. We define the dimensionless mass

$$c \equiv m_\psi / k, \tag{2.84}$$

allowing us to write the EOM in a dimensionless form

$$(\pm\partial_\phi - ckr)\, f_n^{L,R}(\phi) = -x_n\, kr\, e^{\sigma(\phi-\pi)} f_n^{R,L}(\phi), \tag{2.85}$$

where x_n is the dimensionless mass eigenvalue, as defined in (2.48).

The BC (2.81) can be rewritten in term of the profiles of the fermion modes as

$$\delta f_n^{L*}(\phi)\, f_n^R(\phi)\Big|_{\phi=0,\pi} = \delta f_n^{R*}(\phi)\, f_n^L(\phi)\Big|_{\phi=0,\pi} = 0. \tag{2.86}$$

The BC guarantees either $f_n^{L*}(0) f_n^R(0) = 0$, or $f_n^{L*}(\pi) f_n^R(\pi) = 0$, i.e. for a given fermion field Ψ if we assume the same $\mathbb{Z}_2$ behavior for the field at both branes, either the LH or the RH component of the field must be $\mathbb{Z}_2$-odd. That allows us to identify the orbifold $\mathbb{Z}_2$-parity of the fermion field with its projection with γ_5, in agreement with what was previously discussed.

The set of $f_n^L(\phi)$ and $f_n^R(\phi)$ span two complete and orthonormal eigenfunctions of the just presented Sturm-Liouville problem. Therefore, they must satisfy the orthonormality conditions

$$\int_{-\pi}^{\pi} d\phi\, e^{\sigma} f_m^{L*}(\phi) f_n^L(\phi) = \int_{-\pi}^{\pi} d\phi\, e^{\sigma} f_m^{R*}(\phi) f_n^R(\phi) = \delta_{mn}. \tag{2.87}$$

2.5.1 Fermion zero-modes

The EOM in (2.85) couples the LH and RH modes of equal n through their eigenvalue m_n. Therefore, when such eigenvalue vanishes, the EOM decouples the LH and RH modes and can be solved analytically. The zero-modes, i.e. the $n = 0$ modes with $m_0 = 0$, satisfy

$$\big(\pm\partial_\phi - ckr\big) f_n^{L,R}(\phi) = 0, \tag{2.88}$$

which can be easily integrated, giving

$$f_0^{L,R}(\phi) = f_0^{L,R}(0)\, \exp\big(\pm\, c\, kr|\phi|\big), \tag{2.89}$$

where the normalization condition from (2.87) gets absorbed in $f_0^{L,R}(0)$. We can see that the BC at the UV brane, $f_0^{L*}(0) f_0^R(0) = 0$, implies that only one of the two zero-modes remains, i.e. the $\mathbb{Z}_2$-even profiles, while the $\mathbb{Z}_2$-odd components of the Ψ zero-mode vanish. In addition, note that the EOM and the solutions are the same for the LH and RH modes for for $c \to -c$.

The value of $f_0^{L,R}(0)$ can be obtained from (2.87), being

$$\left|f_0^{L,R}(0)\right|^2 = \frac{kr}{2}\frac{1 \pm 2c}{e^{(1\pm 2c)kr\pi} - 1}. \tag{2.90}$$

Therefore, even if the 5D theory is vector-like, we can obtain a 4D chiral theory by relating the $\mathbb{Z}_2$-parity of the fermion fields with the chirality operator, e.g. by assigning Ψ_L to be $\mathbb{Z}_2$-even and Ψ_R to be $\mathbb{Z}_2$-odd. The theory in 5D remains vector-like but at low energies only one of the two chiralities is present, i.e. the one whose zero-mode survived. In other words, at $\sqrt{s} \ll M_{\text{KK}}$ the theory is chiral.

Let's go back to the KK decomposition we proposed in (2.82). The $e^{2\sigma}$ factor appearing there is totally arbitrary and is introduced with the purpose of not encountering derivatives of the metric in the EOM for the profiles. However, if we look at the orthonormalization condition in (2.87), we can see that the profiles we have defined do not give us a good idea about the "true" localization of the fermion profiles along the fifth dimension, since the quantities $f_n^{L,R}$ we have defined require exponential factors of the metric to normalize to 1 in (2.87). Let us see what happens if we choose a different definition for the profiles. Let us define

$$\hat{f}_0^{L,R}(\phi) = e^{\sigma/2} f_n^{L,R}(\phi), \tag{2.91}$$

in such a way that the orthogonality condition for such profiles reads

$$\int_{-\pi}^{\pi} d\phi\, \hat{f}_m^{L*}(\phi)\hat{f}_n^{L}(\phi) = \int_{-\pi}^{\pi} d\phi\, \hat{f}_m^{R*}(\phi)\hat{f}_n^{R}(\phi) = \delta_{mn}. \tag{2.92}$$

In this case, the EOM for the zero modes can be written as

$$\left[\partial_\phi - kr\left(\frac{1}{2} \pm c\right)\right] \hat{f}_n^{L,R}(\phi) = 0, \tag{2.93}$$

leading to the zero-mode profiles

$$\hat{f}_0^{L,R}(\phi) = \hat{f}_0^{L,R}(0)\, \exp\Big(\,(1/2 \pm c)\, kr|\phi|\Big). \tag{2.94}$$

We can see now that there is a special value of the dimensionless mass parameter c for which the LH or RH zero-mode profiles are flat, i.e. for $c = -1/2$ for the LH profiles and $c = 1/2$ for the RH profiles. In the case of a LH profiles, for $c > -1/2$ the zero-modes are pointing towards the IR brane, while the profile would be UV localized for $c < -1/2$ [25, 158]. This behavior has been illustrated in figure 2.5.

It is useful again to present the equations and solutions for the fermion zero-modes in t-coordinates. Let's first rescale the fermion profiles as

$$f_0^{L,R}(t) = \sqrt{kr\epsilon}\,\tilde{f}_0^{L,R}(t). \tag{2.95}$$

Now, the EOM (2.88) reads

$$\big(\pm t\partial_t - c\big)\tilde{f}_n^{L,R}(t) = 0, \tag{2.96}$$

and the solution now is simply

$$\tilde{f}_0^{L,R}(t) = \tilde{f}_0^{L,R}(1)\, t^{\pm c}, \tag{2.97}$$

where the $\tilde{f}_n^{L,R}(t)$ profiles must satisfy the orthonormality condition

$$2\int_{\epsilon}^{1} dt\, \tilde{f}_m^{L*}(t)\tilde{f}_n^{L}(t) = \int_{\epsilon}^{1} dt\, \tilde{f}_m^{R*}(t)\tilde{f}_n^{R}(t) = \delta_{mn}. \tag{2.98}$$

Finally, the normalization for the zero modes that satisfies (2.98) is

$$\left|\tilde{f}_0^{L,R}(1)\right|^2 = \frac{1 \pm 2c}{1 - \epsilon^{1\pm 2c}}. \tag{2.99}$$

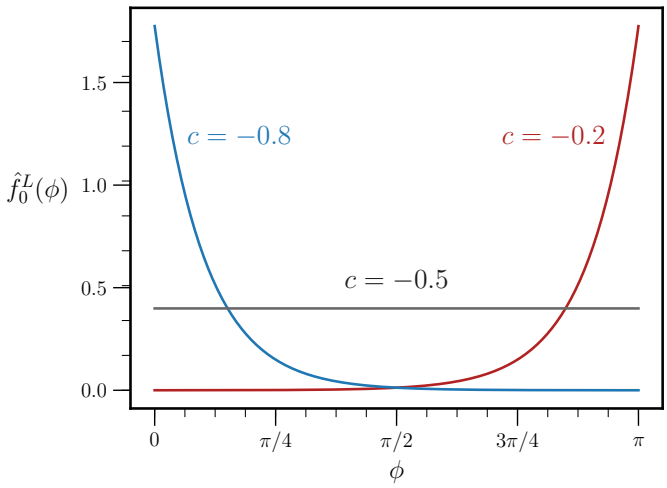

Figure 2.5: *Schematic representation of the localization of the fermion zero-modes, depending on the c mass parameter defined in equation* (2.84).

2.5.2 Fermion KK-modes

We will focus here on the KK resonances with $n \geq 1$. In this case the EOM (2.85) can be decoupled by taking a derivative w.r.t. the fifth coordinate and inserting the first order EOM. This way, a second-order EOM for the KK resonances is obtained

$$\left[\partial_\phi^2 - kr\,\partial_\phi + x_n^2 (kr)^2\, e^{2\sigma(\phi-\pi)} - c\,(kr)^2 (c \mp 1)\right] f_n^{L,R}(\phi) = 0. \tag{2.100}$$

This EOM can be written in t-coordinates for the $\tilde{f}_n^{L,R}(t)$ profiles, being

$$\left[t^2\partial_t^2 + t^2 x_n^2 - c\,(c \mp 1)\right] \tilde{f}_n^{L,R}(t) = 0. \tag{2.101}$$

where the eigenvalues x_n are expected to be $\mathcal{O}(1)$, corresponding to fermion resonances with masses of $\mathcal{O}(M_{\text{KK}})$ in the 4D theory.

$$\tilde{f}_n^{L,R}(t) = \sqrt{t}\, N_\psi \left[J_{c\mp 1/2}(x_n t) + b_\psi Y_{c\mp 1/2}(x_n t)\right] , \tag{2.102}$$

where N_ψ is a normalization condition while the eigenvalue x_n and the coefficient b_ψ are obtained from requiring that (2.102) satisfies the BC (2.86). Moreover, the profile functions for the fermion KK modes can also be written in terms of only J Bessel functions, as in [25].

In addition, the eigenvalues x_n for the heavy fermions can be obtained as the zeroes of Bessel functions. These Bessel functions correspond to $J_{|1/2-c|}(x_n) = 0$ for even RH-fields and odd LH-fields, while for even LH-fields and odd RH-fields the eigenvalues are found as zeroes of $J_{|1/2+c|}(x_n) = 0$.

We show in figure 2.6 the Bessel function function $J_{|1/2-c|}(x_n)$, which defines the eigenvalues x_n, in the left plot and the profiles of the RH and LH first KK modes, computed using the eigenvalues obtained from the zeroes of the left-side plot, in the middle and right plots.

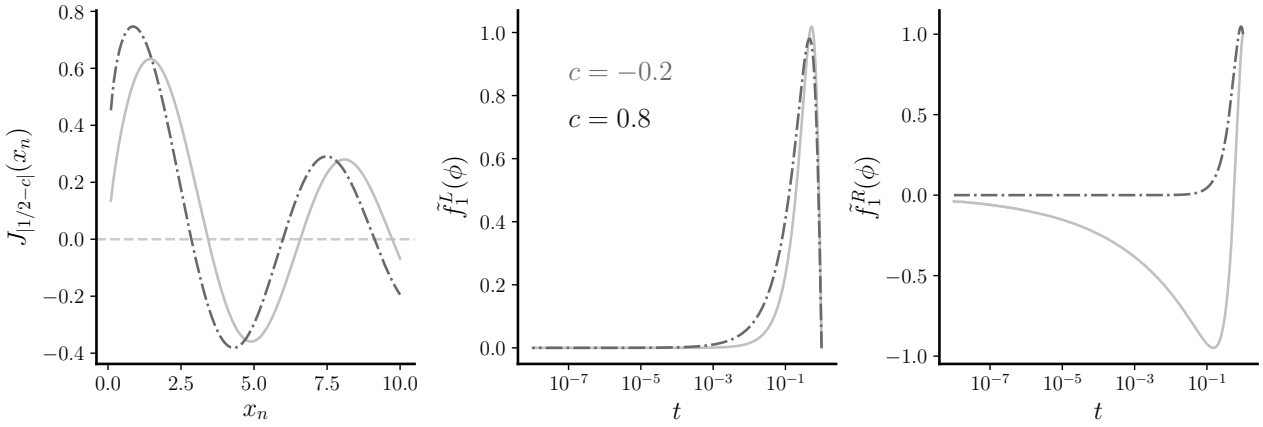

Figure 2.6: *In the left plot, we show $J_{|1/2-c|}(x_n)$, the function that sets the eigenvalues x_n from demanding the LH-fields to be odd. In the center and right plots we show the profiles of the first KK modes for LH and RH fields respectively, where the eigenvalues of x_n corresponding to the zeroes of the left plot have been used. The mass parameter c has been set to $c = -0.2$ (solid) and $c = 0.8$ (dot-dashed) for the three plots.*

2.6 GW stabilization

We have seen how the RS model is able to solve the hierarchy problem with a extra dimension of size $y_{\text{IR}} = \pi r$. However, in the original set-up no reason is given for why to set the length of the extra dimension to the value proposed in [18], nor a dynamical mechanism for setting this size is mentioned. Moreover, in theories with extra dimensions the fluctuations of the radius of the extra dimension are identified with a 4D scalar field, the so-called radion. In this case, having no dynamical mechanism explaining why the radius of the extra dimension is fixed to a determined value of y_{IR}, is associated to this particle being massless in the effective theory, i.e. the radion represents a flat direction of the theory and any size of the extra dimension becomes possible, since no particular value for y_{IR} is preferred. This is phenomenologically intolerable, since it would lead to violations of the equivalence principle by long-range modifications of the Newtonian potential.

In this section, we introduce the mechanism proposed by W. Goldberger and M. Wise [162] to stabilize the size of the extra dimension in the RS model with a bulk scalar field. In their work, the bulk scalar field acts as a moduli field and generates an effective potential $V_r(kr)$ which depends non-trivialy on the size of the extra dimension. It is found that the combination of the bulk and brane parameters from the scalar action set the minimum of V_r to be found for values of $kr \sim \mathcal{O}(10)$ for natural values of the model parameters. This section is just a summary of the findings presented in [162] followed by a discussion of the possible backreaction of the GW field on the metric. Some pedagogical introductions to this topic can be found in [123, 140, 158, 163].

The scalar action for the bulk real scalar field $\hat{\Phi}$ reads

$$S_{\text{GW}}^{(5\text{D})} = \int d^4x \int_{-\pi}^{\pi} d\phi \, \sqrt{g} \Big\{ g^{MN} \frac{1}{2} \partial_M \hat{\Phi} \partial_N \hat{\Phi} - \frac{m^2}{2} \hat{\Phi}^2 - \frac{\sqrt{|\hat{g}_{\text{UV}}|}}{\sqrt{g}} \lambda_{\text{UV}} \left(\hat{\Phi}^2 - v_{\text{UV}}^2 \right)^2 \delta(\phi) \\ - \frac{\sqrt{|\hat{g}_{\text{IR}}|}}{\sqrt{g}} \lambda_{\text{IR}} \left(\hat{\Phi}^2 - v_{\text{IR}}^2 \right)^2 \delta(\phi - \pi) \Big\}, \tag{2.103}$$

where m is the 5D bulk mass, $\lambda_{\rm UV}$ and $\lambda_{\rm IR}$ are the brane quartic couplings and $v_{\rm UV}$ and $v_{\rm IR}$ are the VEV of the field at the branes. The parameter have mass dimensions

$$[\lambda_{\rm UV}] = [\lambda_{\rm IR}] = -2, \qquad \text{and} \qquad [v_{\rm UV}] = [v_{\rm IR}] = 3/2. \tag{2.104}$$

The EOM for the VEV of $\langle\hat{\Phi}(x,\phi)\rangle \equiv \Phi(\phi)$ can be derived from the action, reading

$$\Phi''(\phi) - 4\,kr\,\Phi'(\phi) - m^2\Phi(\phi) = 0, \tag{2.105}$$

for which the most general solution is given by

$$\Phi(\phi) = e^{2\sigma(\phi)}\left[Ae^{\beta\sigma(\phi)} + Be^{-\beta\sigma(\phi)}\right], \tag{2.106}$$

with $\beta = \sqrt{4 + m^2/k^2}$, as defined in (2.33).

Integrating over the fifth dimension leads to the effective potential

$$\begin{aligned} V_r(kr) =& k(\beta+2)A^2\left(e^{2\beta kr\pi} - 1\right) + k(\beta-2)B^2\left(1 - e^{-2\beta kr\pi}\right) \\ &+ \lambda_{\rm IR}e^{-4kr\pi}\left(\Phi(\pi)^2 - v_{\rm IR}^2\right)^2 + \lambda_{\rm UV}\left(\Phi(0)^2 - v_{\rm UV}^2\right)^2. \end{aligned} \tag{2.107}$$

The coefficients A and B are determined by the BC, being

$$\begin{aligned} A &= v_{\rm IR}\,e^{-(2+\beta)kr\pi} - v_{\rm UV}\,e^{-2\beta kr\pi}, \\ B &= v_{\rm UV}\left(1 + e^{-2\beta kr\pi}\right) - v_{\rm IR}\,e^{-(2+\beta)kr\pi}, \end{aligned} \tag{2.108}$$

where subleading powers of ϵ have been neglected. Assumming that $m \ll k$ in such a way that $\beta = 2 + \delta$ with $\delta \simeq m^2/(4k^2)$, and assumming $kr \gg 1$, leads to the minimum of the potential V_r to be located at the values of kr

$$kr = \frac{4}{\pi}\frac{k^2}{m^2}\log\left(\frac{v_{\rm UV}}{v_{\rm IR}}\right), \tag{2.109}$$

which can be $\mathcal{O}(10)$ for $m^2/k^2 \sim 10$, while it only depends logarithmically on the values of $v_{\rm UV}$ and $v_{\rm IR}$.

However, in this previous derivation we have not considered the possible modifications that the GW scalar could induce on the background metric from the RS model. We will see now why in the case of the GW field such modifications are not important, if the parameters of the model fulfill certain conditions.

In general, the modifications of the RS metric caused by contributions of fields to the stress energy tensor are referred as *backreaction*. In the particular case of the GW field, we find [164]

$$\begin{aligned} \sigma'' &= \frac{\kappa^2}{3}\left[\Phi'^2 + \lambda_{\rm UV}\left(\Phi^2 - v_{\rm UV}^2\right)^2\delta(\phi) + \lambda_{\rm IR}\left(\Phi^2 - v_{\rm IR}^2\right)^2\delta(\phi-\pi)\right], \\ \sigma'^2 &= \frac{\kappa^2}{12}\left[\Phi'^2 - m^2\Phi^2\right], \\ \Phi'' - 4\,\sigma'\,\Phi' &= m^2\Phi + 4\left[\lambda_{\rm UV}\Phi(\Phi^2 - v_{\rm UV}^2)\delta(\phi) + \lambda_{\rm IR}\Phi(\Phi^2 - v_{\rm IR}^2)\delta(\phi-\pi)\right], \end{aligned} \tag{2.110}$$

Note that we are only describing here the modifications of the metric solution of (2.7) as

$$\hat{\sigma} = \bar{\sigma} + \sigma, \tag{2.111}$$

where $\hat{\sigma}$ would be the complete solution and $\bar{\sigma}$ is the RS solution. Therefore, we do not consider here the bulk cosmological constant and the brane tensions.

The BC for the metric are now

$$\begin{aligned}
[\sigma'(\phi)]_{\phi=0} &= \frac{\kappa^2 \lambda_{\text{UV}}\, r}{3}\left(\Phi^2 - v_{\text{UV}}^2\right)^2, & [\Phi'(\phi)]_{\phi=0} &= 4\lambda_{\text{UV}}\, r\, \Phi(0)\left(\Phi(0)^2 - v_{\text{UV}}^2\right), \\
[\sigma'(\phi)]_{\phi=\pi} &= \frac{\kappa^2 \lambda_{\text{IR}}\, r}{3}\left(\Phi^2 - v_{\text{IR}}^2\right)^2, & [\Phi'(\phi)]_{\phi=\pi} &= 4\lambda_{\text{IR}}\, r\, \Phi(\pi)\left(\Phi(\pi)^2 - v_{\text{IR}}^2\right),
\end{aligned} \tag{2.112}$$

where the *jump* conditions are defined as in (2.10).

We have three coupled equations involving σ and Φ and at first sight the system might seem to be overdetermined. However, it can be proven that the system does not require the three of them since they are not linearly independent. In addition, there is a method that allows to separate the system of equations (2.110) into a set of first order ordinary differential equations. This is known as the *superpotential* method [165].

The only assumption we need to make is that the scalar potential $V(\Phi)$ can be expressed in terms of the superpotential $W(\Phi)$ as

$$V(\phi) = \frac{1}{8}\left(\frac{\partial W(\Phi)}{\partial \Phi}\right)^2 - \frac{\kappa^2}{6} W(\phi)^2. \tag{2.113}$$

If this is the case, then it can be shown that the following ansatz for σ and Φ are solutions of (2.110)

$$\begin{aligned}
\sigma' &= \frac{\kappa^2 r}{6} W(\Phi), \\
\Phi' &= \frac{r}{2}\frac{\partial W(\Phi)}{\partial \Phi}.
\end{aligned} \tag{2.114}$$

In addition, the superpotential must satisfy the BC

$$\begin{aligned}
\frac{1}{2}\left[W(\Phi)\right]_{\phi=0} &= \lambda_{\text{UV}}\left(\Phi^2 - v_{\text{UV}}^2\right)^2, & \frac{1}{2}\left[\frac{\partial W(\Phi)}{\partial \Phi}\right]_{\phi=0} &= 4\lambda_{\text{UV}}\, \Phi(0)\left(\Phi(0)^2 - v_{\text{UV}}^2\right), \\
\frac{1}{2}\left[W(\Phi)\right]_{\phi=\pi} &= \lambda_{\text{IR}}\, r\left(\Phi^2 - v_{\text{IR}}^2\right)^2, & \frac{1}{2}\left[\frac{\partial W(\Phi)}{\partial \Phi}\right]_{\phi=\pi} &= 4\lambda_{\text{IR}}\, \Phi(\pi)\left(\Phi(\pi)^2 - v_{\text{IR}}^2\right),
\end{aligned} \tag{2.115}$$

as can be derived from (2.112) and (2.113).

In general, finding an ansatz for $W(\Phi)$ for any given $V(\Phi)$ can be complicated, depending on the specific model we would like to describe. However, for the GW case we can propose a solution of the following form

$$W(\Phi) = a - u\Phi^2. \tag{2.116}$$

This ansatz leads to

$$V(\Phi) = \frac{u^2}{2}\Phi^2 - \frac{\kappa^2 u^2}{6}\Phi^4, \tag{2.117}$$

which corresponds to the GW potential, see (2.103), for $u = m$ only in the limit of $\kappa^2 u^2 \Phi^4 \to 0$, what is required for this to happen will be clear once we get the solutions for Φ and σ.

The solution for Φ can be obtained from

$$\Phi' = \frac{r}{2}\frac{\partial W(\Phi)}{\partial \Phi} = -mr\Phi, \tag{2.118}$$

leading to

$$\Phi(\phi) = \Phi(0)e^{-mr\phi}. \tag{2.119}$$

In the large λ_{UV} and λ_{IR}, we can identify $\Phi(0) = v_{\text{UV}}$ and $\Phi(\pi) = v_{\text{IR}}$. Therefore, we find [123, 140, 158, 163, 165]

$$mr\pi = \log\left(\frac{v_{\text{UV}}}{v_{\text{IR}}}\right) \Rightarrow kr = \frac{1}{\pi}\frac{k}{m}\log\left(\frac{v_{\text{UV}}}{v_{\text{IR}}}\right), \tag{2.120}$$

along the same lines to what was found in (2.109). The factor $4k/m$ difference is due to the fact that in [162], some approximations are performed during the derivation, whereas in [165], the result obtained by using the super-potential method is exact. The assumption in the potential of $\kappa^2 u^2 \Phi^4 \to 0$ is therefore satisfied for $m \ll M_*$ as long as v_{UV}^2 and $v_{\text{IR}}^2 \leq M_*^3$.

In the case of the metric, we find

$$\sigma' = \frac{\kappa^2}{6}W(\Phi) = -\frac{\kappa^2 mr}{6}v_{\text{UV}}^2 e^{-2mr\phi}, \tag{2.121}$$

which, once (2.121) is integrated from 0 to ϕ, to the following solution for σ

$$\sigma(\phi) = \frac{\kappa^2 v_{\text{UV}}^2}{12}e^{-2mr\phi}, \tag{2.122}$$

where we have been working on $\phi \in [0, \pi]$. The full metric then reads

$$\hat{\sigma}(\phi) = kr|\phi| + \frac{\kappa^2}{12}\Phi(\phi)^2, \tag{2.123}$$

where, since m can be positive or negative, but in both cases Φ is monotonous

$$\max \Phi(\phi) = \max\left(v_{\text{UV}}, v_{\text{IR}}\right), \tag{2.124}$$

therefore the contribution of the backreaction of the GW field can be neglected as long as $v_{\text{UV}}^2/M_*^3 \ll 1$ and $v_{\text{IR}}^2/M_*^3 \ll 1$ is satisfied. Therefore, there is no need to consider possible backreaction effects on the metric caused by the bulk scalar field and the RS metric $\sigma(\phi) = kr|\phi|$ remains as a solution even when the extra dimension gets stabilized by the GW field.

To study the full theory, one would have to still consider the scalar fluctuations of the background solutions we have just described. In that case, the linearized Einstein equations of the following 5D scalar-gravity system need to be solved

$$\begin{aligned} ds^2 &= e^{-2(\sigma(\phi)+\alpha(x,\phi))}\eta_{\mu\nu}dx^\mu dx^\nu - \left[r^2 + \beta(x,\phi)\right]^2 d\phi^2, \\ \hat{\Phi}(x,\phi) &= \Phi(\phi) + \varphi(x,\phi), \end{aligned} \tag{2.125}$$

where the scalar perturbations to the metric $\alpha(x,\phi)$ and $\beta(x,\phi)$, and the scalar field $\varphi(x,\phi)$ have been introduced, these apparently independent fields describe a single d.o.f. , the radion. However, radion physics is beyond the scope of this thesis. Some interesting references on the radion can be found in [116, 123, 140, 141, 163, 166–169].

2.7 The flavor puzzle in WED

We introduced in the section 1.2 the problem of the huge hierarchy present in the masses of the SM fermions. In addition, we also discussed how the diagonal structure of the CKM matrix is not explained in the SM. In this section, we will see how these questions are addressed within the RS framework. For the purpose of presenting in detail the flavor structure of RS models, we will consider the IR-brane-localized Higgs boson scenario. Even if the mechanism shown here for the IR-brane case could be extrapolated for the bulk Higgs case, the mathematical derivation becomes

much more complex, and therefore the solutions and relations would not be as simple and straight forward as in the ones we will obtain for the brane-localized case. This section will follow the arguments and for most part the notation of [110, 160].

It is usually stated that providing a solution to the hierarchy problem is the main feature of RS models, leaving aside many times that it can also naturally explain the large hierarchies observed in the fermion spectrum of the SM, particularly in the quark sector [21,25,110,114,115,170–172]. By a similar mechanism to the one that solves the hierarchy problem, RS models can naturally lead to hiearchical structures in the quark masses and the CKM mixing angles. Finding a solution for the lepton case is a bit more problematic, since the PMNS mixing matrix features large mixing angles. We will explain why this is tricky later, once the solution for the quark sector has been presented and understood.

2.7.1 The setup

Let's explain here how this mechanism works for the quark sector. Consider N generations of 5D fermions in the bulk interacting with the Higgs doublet, localized on the IR brane. We will consider $SU(2)_L$ doublets and singlets, denoted by Q and $q^c = u^c, d^c$, respectively. Each of this fields, Q, u^c and d^c is an N-component vector in flavor space. Like in the SM, these fields couple to the Higgs on the IR brane with Yukawa matrices $\boldsymbol{Y}_u^{(5\mathrm{D})}$ and $\boldsymbol{Y}_d^{(5\mathrm{D})}$. The SM fermions correspond to the zero modes of the 5D theory. However, after EWSB takes place on the IR brane, the zero-modes acquire a non-zero mass.

The action for the SM fermion fields in 5D can be written as [1, 21, 25, 110]

$$\begin{aligned} S_\psi^{(5\mathrm{D})} = \int d^4x \int_{-\pi}^{\pi} d\phi \sqrt{g} \Bigg\{ & \frac{i}{2} E_a^N \left(\bar{Q}\, \Gamma^a (D_N - \overleftarrow{D}_N) Q + \sum_{q=u,d} \bar{q}^c\, \Gamma^a (D_N - \overleftarrow{D}_N) q^c \right) \\ & - \mathrm{sgn}(\phi) \left(\bar{Q} \boldsymbol{M}_Q Q + \sum_{q=u,d} \bar{q}^c\, \boldsymbol{M}_q\, q^c \right) \\ & - \delta(|\phi| - \pi)\, \frac{\sqrt{|\hat{g}_i|}}{g}\, \frac{v_h\, e^{\sigma(\pi)}}{\sqrt{2}} \left[\bar{u}_L\, \boldsymbol{Y}_u^{(5\mathrm{D})}\, u_R^c + \bar{d}_L\, \boldsymbol{Y}_d^{(5\mathrm{D})}\, d_R^c + \mathrm{h.c.} \right] \Bigg\}, \end{aligned} \tag{2.126}$$

where $v_h \approx 246$ GeV has already been defined in (2.21). Here, $\boldsymbol{M}_Q$ and $\boldsymbol{M}_q$ stand for the 5D real bulk masses, which can be taken to be diagonal. The choice can be justified as follows. In the most general definition of (2.126), the action would contains positive hermitian matrices $\boldsymbol{Z}_A$ and $\boldsymbol{M}_A$, with $A = Q, u, d$, corresponding to the kinetic and bulk mass terms respectively. The matrices $\boldsymbol{Z}_A$ are not only hermitian but positive, necessary to guarantee that the kinetic terms are positive. Making the kinetic terms diagonal would require an unitary transformation of the form

$$\boldsymbol{U}_A^\dagger \boldsymbol{Z}_A \boldsymbol{U}_A = \mathrm{diag}\,(Z_{A_1}, \ldots, Z_{A_N}) \equiv \boldsymbol{D}_A, \tag{2.127}$$

with $Z_{A_i} > 0$. This transformation defines the canonically normalized fields, after the appropiate rescaling. At the same time, the bulk mass matrices get rotated into

$$\boldsymbol{M}_A \to \boldsymbol{M}'_A = \boldsymbol{D}_A^{-1/2} \boldsymbol{U}_A^\dagger \boldsymbol{M}_A \boldsymbol{U}_A \boldsymbol{D}_A^{-1/2}. \tag{2.128}$$

These new mass matrices can be diagonalized by another set of unitary transformations, as

$$\boldsymbol{U}_A'^\dagger \boldsymbol{M}'_A \boldsymbol{U}'_A = \mathrm{diag}\,(M_{A_1}, \ldots, M_{A_N}). \tag{2.129}$$

Therefore, it is always possible to switch to a basis in which the bulk mass terms are diagonal in flavor space without loss of generality. Such basis is usually known as the *bulk mass basis*. For the

rest of this document, we will consider diagonal bulk mass matrices, which we will denote by $\boldsymbol{M}_A$. Consequently, the Yukawa matrices of the bulk fermions with the Higgs doublet, $\boldsymbol{Y}_u^{(5\mathrm{D})}$ and $\boldsymbol{Y}_d^{(5\mathrm{D})}$, will correspond to the Yukawa matrices in this particular basis, unless otherwise stated.

Remember that the chiral components of each spinor field are defined as usual, i.e. $\Psi = \Psi_L + \Psi_R$, as discussed in section 2.5 and note that the 5D bulk mass terms in (2.126) consider LH and RH fields belonging to the same 5D field. This implies that, unlike in the 4D theory, bulk masses can be positive or negative, since a complex phase transformation of the 5D fields cannot reverse the sign of the Dirac mass. The consequence of having both positive and negative masses is that it allows for different localizations of the fermion profiles. Phenomenologically, we will find that the dimensionless mass parameters $c_{Q_i} = M_{Q_i}/k \approx -0.5$, while $c_{q_i} = M_{q_i} \approx 0.5$. The LH (RH) components of the $SU(2)_L$ doublet Q are even (odd) under the $\mathbb{Z}_2$ orbifold symmetry and the opposite assignment is performed for the 5D fields corresponding containing the RH SM fields, i.e. the RH (LH) components of the u^c and d^c singlet fields are even (odd).

As was discussed previously, before the Yukawa interactions with the Higgs are turned on and EWSB takes place, each 5D fermion would lead to the presence of a massless mode in the effective 4D theory accompanied by a tower of massive KK excitations ($m_n \sim M_{\mathrm{KK}}$). However, after EWSB the Yukawa couplings give mass ($m_n \ll M_{\mathrm{KK}}$) to the zero-modes and now they are accompanied by two chiral towers of KK modes.

Moreover, if we analyze the mass dimension of the 5D Yukawa couplings we find

$$[\boldsymbol{Y}_u^{(5\mathrm{D})}] = [\boldsymbol{Y}_d^{(5\mathrm{D})}] = 1, \tag{2.130}$$

therefore, it is convenient to define a dimensionless Yukawa couplings as

$$\boldsymbol{Y}_q = \frac{k}{2}\boldsymbol{Y}_q^{(5\mathrm{D})}, \quad \text{with } q = u, d\,. \tag{2.131}$$

We would like to obtain the profiles for the different modes corresponding to the KK decomposition of the 5D fields. For doing so we need to solve the eigenvalue problem. We will show here the derivation only for the case of the up-type quarks, however a similar discussion holds for down-type quarks.

We write the KK decomposition of the 5D fields in the form

$$\begin{aligned}
u_L(x,\phi) &= \frac{e^{2\sigma(\phi)}}{\sqrt{r}}\sum_n \boldsymbol{C}_n^{(Q)}(\phi)\, a_n^{(U)}\, u_L^{(n)}(x)\,, \quad u_R(x,\phi) = \frac{e^{2\sigma(\phi)}}{\sqrt{r}}\sum_n \boldsymbol{S}_n^{(Q)}(\phi)\, b_n^{(U)}\, u_R^{(n)}(x)\,, \\
u_L^c(x,\phi) &= \frac{e^{2\sigma(\phi)}}{\sqrt{r}}\sum_n \boldsymbol{S}_n^{(u)}(\phi)\, b_n^{(u)}\, u_L^{(n)}(x)\,, \quad u_R^c(x,\phi) = \frac{e^{2\sigma(\phi)}}{\sqrt{r}}\sum_n \boldsymbol{C}_n^{(u)}(\phi)\, a_n^{(u)}\, u_R^{(n)}(x)\,,
\end{aligned} \tag{2.132}$$

where $m_n > 0$ are the masses of the Dirac fermions and $u^{(n)}(x) = u_L^{(n)}(x) + u_R^{(n)}(x)$ are spinor fields. We use $\boldsymbol{C}_n^{(Q,u)}$ to denote the $\mathbb{Z}_2$ even profiles and $\boldsymbol{S}_n^{(Q,u)}$ for the odd profiles. In addition, the $u_{L,R}(x,\phi)$ and $u_{L,R}^c(x,\phi)$ spinors denote N-component vectors in flavor space. This information is contained on the $a_n^{(U,u)}$ and $b_n^{(U,u)}$ on the RH side of the equation. Note that the $N \times N$ profile matrices $\boldsymbol{C}_n^{(Q,u)}$ and $\boldsymbol{S}_n^{(Q,u)}$ are diagonal in the bulk mass basis, where each entry corresponds to a different bulk mass parameter $c_{Q,u}$. Moreover, the index n labels the mass eigenstates corresponding to the eigenvalues m_n and to the Dirac spinors $u^{(n)}(x)$. In our notation $n = 1, 2, 3$ denote the 3 SM u-type quarks u, c and t, while the KK excitations correspond to $n \geq 4$.

In (2.132) note that $u(x,\phi) = u_L(x,\phi) + u_R(x,\phi)$ corresponds to the 5D field whose zero mode will correspond to a LH u-type quark, while $u^c(x,\phi) = u_L^c(x,\phi) + u_R^c(x,\phi)$ is such that its zero mode will be RH. One remark should be done here. In (2.132), the bulk profiles for the u and d

quarks from to the same $SU(2)_L$ doublet, $\boldsymbol{C}_n^{(Q)}$ and $\boldsymbol{S}_n^{(Q)}$ are the same. However, the vectors $a_n^{(U)}$ and $a_n^{(D)}$ associated with these profiles in the KK decomposition are different, as they contain the flavor information (they will become the coefficients of the flavor eigenvectors).

Inserting the decomposition (2.132) into the action, and restricting the analysis to the region of the orbifold defined by $\phi \in [0, \pi]$, the following EOM are obtained

$$\begin{aligned}\left[\frac{1}{r}\,\partial_\phi - \mathcal{M}\right] \mathcal{F}_L^n(\phi) &= -\,m_n\, e^{\sigma(\phi)}\, \mathcal{F}_R^n(\phi) + \delta(\phi-\pi)\, e^{\sigma(\phi)}\, \frac{\sqrt{2}\, v_h}{kr} \mathcal{Y}_u \mathcal{F}_L^n(\phi) \\ \left[-\frac{1}{r}\,\partial_\phi - \mathcal{M}\right] \mathcal{F}_R^n(\phi) &= -\,m_n\, e^{\sigma(\phi)}\, \mathcal{F}_L^n(\phi) + \delta(\phi-\pi)\, e^{\sigma(\phi)}\, \frac{\sqrt{2}\, v_h}{kr} \mathcal{Y}_u \mathcal{F}_R^n(\phi)\end{aligned} \tag{2.133}$$

where we have defined

$$\mathcal{F}_L^n(\phi) = \begin{pmatrix} \boldsymbol{C}_n^{(Q)}(\phi)\, a_n^{(U)} \\ \boldsymbol{S}_n^{(u)}(\phi)\, a_n^{(u)} \end{pmatrix}, \qquad \mathcal{F}_R^n(\phi) = \begin{pmatrix} \boldsymbol{S}_n^{(Q)}(\phi)\, a_n^{(U)} \\ \boldsymbol{C}_n^{(u)}(\phi)\, a_n^{(u)} \end{pmatrix}, \tag{2.134}$$

and $\mathcal{M} = \text{diag}\,(\boldsymbol{M}_Q, \boldsymbol{M}_u)$ and $\mathcal{Y}_u = \sigma_1 \text{diag}\,(\boldsymbol{Y}_u^\dagger, \boldsymbol{Y}_u)$, with σ_1 the first Pauli matrix [150, 173]. Requiring the $u_{L,R}^{(n)}(x)$ spinors to satisfy the 4D Dirac equation has allowed us to use $a_n^{(U,u)} = b_n^{(U,u)}$. In addition, the following relations need to be fulfilled [110]

$$\begin{aligned} a_n^{(U)\dagger}\, a_n^{(U)} + a_n^{(u)\dagger}\, a_n^{(u)} &= 1\,, \\ a_m^{(U,u)\dagger}\, \boldsymbol{\Delta C}_{mn}^{(Q,u)}\, a_n^{(U,u)} + a_m^{(u,U)\dagger}\, \boldsymbol{\Delta S}_{mn}^{(u,Q)}\, a_n^{(u,U)} &= 0. \end{aligned} \tag{2.135}$$

Away from the branes, i.e. for $\phi \neq \pi$, and for the special case of a single generation, these EOM are equivalent to (2.85), and the solutions for such EOM are Bessel functions, as shown in section 2.5. The effect of the IR brane-localized terms is only present through the BC at this brane. Therefore at $\phi = 0$ we still find

$$\boldsymbol{S}_n^{(Q,u)}(0) = 0\,. \tag{2.136}$$

For deriving the BC at the IR brane we integrate the EOM around $\phi = \pi$. The IR BC read [110]

$$\left(1 \quad -\frac{v_h}{\sqrt{2} M_{\text{KK}}}\, \boldsymbol{Y}_u\right) \mathcal{F}_R(\pi) = 0, \qquad \left(-\frac{v_h}{\sqrt{2} M_{\text{KK}}}\, \boldsymbol{Y}_u^\dagger \quad -1\right) \mathcal{F}_L(\pi) = 0, \tag{2.137}$$

where the odd profiles in $\mathcal{F}_R(\pi)$ and $\mathcal{F}_L(\pi)$ are evaluated at $\phi = \pi^-$. We solved the EOM for the fermion profiles in section 2.5 and we obtained that, without the presence of brane-localized Yukawa terms, the profiles $\boldsymbol{C}_n^{(Q,u)}(\phi)$ and $\boldsymbol{S}_n^{(Q,u)}(\phi)$ form complete sets of even and odd functions on the orbifold, satisfying the orthonormality conditions given in (2.87). However, introducing the brane terms with a delta function in the EOM together with these orthonormality conditions leads to inconsistencies. Therefore, we need to introduce the generalized orthonormality conditions

$$\int_{-\pi}^{\pi} d\phi\, e^{\sigma(\phi)}\, \boldsymbol{A}_m^{(Q,u)}(\phi)\, \boldsymbol{A}_n^{(Q,u)}(\phi) = \delta_{mn}\, \mathbf{1} + \boldsymbol{\Delta A}_{mn}^{(Q,u)}\,, \qquad \text{with } \boldsymbol{A} = \boldsymbol{C}, \boldsymbol{S}. \tag{2.138}$$

The derivation of the quantities $\boldsymbol{\Delta C}_{mn}^{(Q,u)}$ and $\boldsymbol{\Delta S}_{mn}^{(Q,u)}$ was done in [110] and we gather the explicit expressions in appendix B.

The BC (2.137) can be written as a system of $2N$ linear equations for the vectors $a_n^{(U,u)}$, for which the eigenvalues are obtained from the resulting $2N \times 2N$ matrix. Using that the matrices $\boldsymbol{C}_n^{(Q,u)}$, $\boldsymbol{S}_n^{(Q,u)}$ are non-singular, we can write the system of linear equations as

$$\begin{aligned} \boldsymbol{S}_n^{(Q)}(\pi^-)\, a_n^{(U)} &= -\,\frac{v_h^2}{2M_{\text{KK}}^2}\, \boldsymbol{Y}_u\, \boldsymbol{C}_n^{(u)}(\pi) \left[\boldsymbol{S}_n^{(u)}(\pi^-)\right]^{-1} \boldsymbol{Y}_u^\dagger\, \boldsymbol{C}_n^{(Q)}(\pi)\, a_n^{(U)}\,, \\ \boldsymbol{S}_n^{(u)}(\pi^-)\, a_n^{(u)} &= -\,\frac{v_h^2}{2M_{\text{KK}}^2}\, \boldsymbol{Y}_u^\dagger\, \boldsymbol{C}_n^{(Q)}(\pi) \left[\boldsymbol{S}_n^{(Q)}(\pi^-)\right]^{-1} \boldsymbol{Y}_u\, \boldsymbol{C}_n^{(u)}(\pi)\, a_n^{(u)}\,. \end{aligned} \tag{2.139}$$

Therefore, the mass eigenvalues are found from the roots of the following equation

$$\det\left(\mathbf{1}-\frac{v^2}{2M_{\rm KK}^2}\left[\boldsymbol{S}_n^{(Q)}(\pi^-)\right]^{-1}\boldsymbol{Y}_u\,\boldsymbol{C}_n^{(u)}(\pi)\left[-\boldsymbol{S}_n^{(u)}(\pi^-)\right]^{-1}\boldsymbol{Y}_u^\dagger\,\boldsymbol{C}_n^{(Q)}(\pi)\right)=0\,, \tag{2.140}$$

where $\boldsymbol{C}_n^{(Q,u)}(\phi)$ and $\boldsymbol{S}_n^{(Q,u)}(\phi)$ are the solutions of EOM (2.133). Finally, the solutions from (2.140) allow us to compute the eigenvectors $a_n^{(U,u)}$ using (2.139).

We introduce now the expression for the functions $(C_n^{(Q,q)})_{ii}$ and $(S_n^{(Q,q)})_{ii}$, corresponding to the profiles associated with bulk mass parameters M_{Q_i,q_i} (with $q=u,d$), see [25, 110]. For the SM fermions, i.e. in the approximation $x_n \ll 1$, these functions read

$$\begin{aligned} C_n^{(Q,q)}(t) \approx& \sqrt{\frac{L\epsilon}{\pi}}\,\frac{F(c_{Q,q})}{\sqrt{1+\delta_n(c_{Q,q})}}\,\left[t^{c_{Q,q}}-\delta_n(c_{Q,q})\,t^{1-c_{Q,q}}\right],\\ S_n^{(Q,q)}(t) \approx& \pm\sqrt{\frac{L\epsilon}{\pi}}\,\frac{x_n F(c_{Q,q})}{\sqrt{1+\delta_n(c_{Q,q})}}\,\frac{t^{1+c_{Q,q}}-\epsilon^{1+2c_{Q,q}}\,t^{-c_{Q,q}}}{1+2c_{Q,q}}\,, \end{aligned} \tag{2.141}$$

where we have dropped the i-index and switched to t-coordinates, since the expressions for the profiles have a simple dependence on t. We will do so for the remaining piece of the section. We have as well defined the function

$$F(c)\equiv \mathrm{sgn}[\cos(\pi c)]\,\sqrt{\frac{1+2c}{1-\epsilon^{1+2c}}}\,, \tag{2.142}$$

known as the "zero-mode profile" [21, 25, 110], and the parameter

$$\delta_n(c)\equiv\frac{x_n^2}{4c^2-1}\,\epsilon^{1+2c}\,. \tag{2.143}$$

whose definition is valid for any value of c but for $|c|=1/2$.

The quantities $F(c)$ and $\delta_n(c)$ depend strongly on the parameters c and x_n. In particular, one finds that for $-1/2<c<1/2$

$$F(c)\approx\sqrt{1+2c}\,,\qquad \delta_n(c)\approx 0\,, \tag{2.144}$$

is a good approximation. On the other hand, if one limits itself to the range $-3/2<c<-1/2$

$$F(c)\approx -\sqrt{-1-2c}\,\epsilon^{-c-1/2}, \tag{2.145}$$

which is exponentially suppresed by positive powers of ϵ. In that same case however, δ_n is a positive quantity and can be large for some combinations of c and x_n. Therefore, dropping the δ-terms in (2.141) cannot be justified, as happened for $-1/2<c<1/2$. However, it was discussed in [110] that (only when considering more than one generation of fermions), after the fermion profiles appear together with the corresponding mixing parameters $a_n^{(U,u)}$, these terms can only lead to very small effects on the fermion masses and on the flavor-changing couplings of the model.

2.7.2 Quark masses and mixings

For studying the quark sector of the SM, it can be illustrative to analyze how the mechanism we have presented for the RS model works for the lightest generations. Therefore we will shorten the expansion down to $N=3$. In this case, the $n=1,2,3$ terms correspond to the zeroth-order terms in a series expansion of the bulk profiles in powers of $v_h^2/M_{\rm KK}^2$. The advantage of doing so is that the profile expression from (2.141) for these fields simplify notably, as δ_n appears there

as a $\mathcal{O}(v_h^2/M_{\rm KK}^2)$ quantity. This approach is commonly known as the *zero-mode approximation* (ZMA), [21, 25, 110, 171].

In this approximation we can solve for the fermion bulk profiles without taking into account the Yukawa couplings, since these appear as a first order perturbation in $v_h^2/M_{\rm KK}^2$. In particular, if we evaluate the profiles from (2.141) at the IR brane, using this approximation we find

$$C_n^{(Q,q)}(1) \approx \sqrt{\frac{L\epsilon}{\pi}}\, F(c_{Q,q})\,, \qquad S_n^{(Q,q)}(1^-) \approx \pm\sqrt{\frac{L\epsilon}{\pi}}\, \frac{x_n}{F(c_{Q,q})}\,. \tag{2.146}$$

We can now define the 4D effective Yukawa matrices

$$\left(Y_u^{\rm eff}\right)_{ij} \equiv F(c_{Q_i})\, (Y_u)_{ij}\, F(c_{u_j}), \tag{2.147}$$

in such a way that we can demand the BC (2.137) to fulfill

$$\frac{\sqrt{2}\, m_n}{v_h}\, \hat{a}_n^{(U)} = \boldsymbol{Y}_u^{\rm eff}\, \hat{a}_n^{(u)}\,, \qquad \frac{\sqrt{2}\, m_n}{v_h}\, \hat{a}_n^{(u)} = (\boldsymbol{Y}_u^{\rm eff})^\dagger\, \hat{a}_n^{(U)}\,, \tag{2.148}$$

where we have used the expressions of the profiles at the IR brane from (2.146) and we have rescaled the $a_n^{(A)}$ vectors to $\hat{a}_n^{(A)} \equiv \sqrt{2}\, a_n^{(A)}$. The rescaled vectors obey the normalization conditions [110]

$$\hat{a}_n^{(U)\dagger}\, \hat{a}_n^{(U)} = \hat{a}_n^{(u)\dagger}\, \hat{a}_n^{(u)} = 1\,. \tag{2.149}$$

In addition, note that in the ZMA the $a_n^{(A)}$ and $\hat{a}_n^{(A)}$ vectors belonging to different n are orthogonal on each other, which does not hold in the general case.

From (2.148), we can obtain the equations for the $\hat{a}_n^{(A)}$ vectors

$$\left(m_n^2\, \mathbf{1} - \frac{v_h^2}{2}\, \boldsymbol{Y}_u^{\rm eff}\, (\boldsymbol{Y}_u^{\rm eff})^\dagger\right) \hat{a}_n^{(U)} = 0\,, \qquad \left(m_n^2\, \mathbf{1} - \frac{v_h^2}{2}\, (\boldsymbol{Y}_u^{\rm eff})^\dagger\, \boldsymbol{Y}_u^{\rm eff}\right) \hat{a}_n^{(u)} = 0\,, \tag{2.150}$$

which can be written into matrix form, leading to the following eigenvalue equation

$$\det\left(m_n^2\, \mathbf{1} - \frac{v_h^2}{2}\, \boldsymbol{Y}_u^{\rm eff}\, (\boldsymbol{Y}_u^{\rm eff})^\dagger\right) = 0\,, \tag{2.151}$$

determining the masses of the SM quarks at first order in $v_h^2/M_{\rm KK}^2$.

Note that the derivation we have shown here also holds for d-type quarks. Therefore, we show now the results for the general case, i.e. by identifying $U \to Q$ and $u \to q$. We find that the vectors $\hat{a}_n^{(Q)}$ and $\hat{a}_n^{(q)}$ are the eigenvalues of the matrices $\boldsymbol{Y}_q^{\rm eff}\left(\boldsymbol{Y}_q^{\rm eff}\right)^\dagger$ and $\left(\boldsymbol{Y}_q^{\rm eff}\right)^\dagger \boldsymbol{Y}_q^{\rm eff}$, respectively, where we have $Q = U, D$ and $q = u, d$, where remember that we are restricting to $n = 1, 2, 3$ with $m_n = m_u, m_c, m_t$ for $q = u$ and $m_n = m_d, m_s, m_b$ for $q = d$. Moreover, the eigenvalues $\hat{a}_n^{(Q)}$ and $\hat{a}_n^{(q)}$ correspond to the columns of the unitary matrices $\boldsymbol{U}_q$ and $\boldsymbol{W}_q$ appearing in the singular-value decomposition (SVD)

$$\boldsymbol{Y}_q^{\rm eff} = \boldsymbol{U}_q\, \boldsymbol{\lambda}_q\, \boldsymbol{W}_q^\dagger\,, \tag{2.152}$$

with

$$\boldsymbol{\lambda}_u = \frac{\sqrt{2}}{v_h}\, \text{diag}\,(m_u, m_c, m_t)\,, \qquad \boldsymbol{\lambda}_d = \frac{\sqrt{2}}{v_h}\, \text{diag}\,(m_d, m_s, m_b)\,. \tag{2.153}$$

Finally, the CKM mixing matrix is defined as in the 4D as

$$\boldsymbol{V}_{\rm CKM} = \boldsymbol{U}_u^\dagger\, \boldsymbol{U}_d\,, \tag{2.154}$$

where the matrices $\boldsymbol{U}_q$ and $\boldsymbol{W}_q$ in the RS model and in our approximation rotates between the original 5D fields into the SM mass eigenstates.

Now, one would expect that we are in a similar situation to that of the SM, where we can obtain the CKM matrix from the Yukawa matrices and masses, with the drawback of having three fundamental parameters, i.e. $c_{Q_i}, (Y)_{ij}$ and c_{u_j}, for every value of the 4D Yukawa. Therefore one could think that the model is only losing some predictivity. However, the idea of the RS model when addressing the hierarchies within the flavor sector is to avoid building in the hierarchies into the model as a choice, but to generate the flavor structure starting by $\mathcal{O}(1)$ parameters. To do so we can start with anarchic Yukawa matrices with $\mathcal{O}(1)$ inputs, and requiring the model to reproduce the correct quark masses and CKM elements; we fit the dimensionless mass parameters, which can always be found to have values of $|c| \sim 1$. Therefore, with both Yukawa inputs and c-parameters of $\mathcal{O}(1)$ we can replicate the hierarchical structure of the quark sector present in the SM [110, 114, 119].

Hence, we will consider anarchic 5D Yukawa couplings with complex-valued entries. In particular, we make use of the Froggat-Nielsen mechanism [174], as it allows to reproduce the SM quark mass hierarchies by assuming the zero-mode profiles evaluated at the IR brane to have a hierarchical structure, as

$$|F(c_{A_1})| < |F(c_{A_2})| < |F(c_{A_3})|\,. \tag{2.155}$$

This is a natural assumption in our model, as it can be easily obtained by considering similar values of c_{A_i}.

Looking at (2.152), we can see that the products of the quark masses can be written as

$$\begin{aligned} m_u\, m_c\, m_t =& \frac{v_h^3}{2\sqrt{2}} |\det\left(\boldsymbol{Y}_u\right)| \prod_{i=1,2,3} |F(c_{Q_i})\, F(c_{u_i})|, \\ m_d\, m_s\, m_b =& \frac{v_h^3}{2\sqrt{2}} |\det\left(\boldsymbol{Y}_d\right)| \prod_{i=1,2,3} |F(c_{Q_i})\, F(c_{d_i})|. \end{aligned} \tag{2.156}$$

The assumption $|F(c_{A_i})| < \left|F(c_{A_{i+1}})\right|$ allows us to consider hierarchic eigenvalues. Thus, we can write

$$\begin{aligned} m_u =& \frac{v_h}{\sqrt{2}} \frac{|\det(\boldsymbol{Y}_u)|}{|(M_u)_{11}|} |F(c_{Q_1})F(c_{u_1})|\,, & m_d =& \frac{v_h}{\sqrt{2}} \frac{|\det(\boldsymbol{Y}_d)|}{|(M_d)_{11}|} |F(c_{Q_1})F(c_{d_1})|\,, \\ m_c =& \frac{v_h}{\sqrt{2}} \frac{|(M_u)_{11}|}{|(Y_u)_{33}|} |F(c_{Q_2})F(c_{u_2})|\,, & m_s =& \frac{v_h}{\sqrt{2}} \frac{|(M_d)_{11}|}{|(Y_d)_{33}|} |F(c_{Q_2})F(c_{d_2})|\,, \\ m_t =& \frac{v_h}{\sqrt{2}} |(Y_u)_{33}|\, |F(c_{Q_3})F(c_{u_3})|\,, & m_b =& \frac{v_h}{\sqrt{2}} |(Y_d)_{33}|\, |F(c_{Q_3})F(c_{d_3})|\,, \end{aligned} \tag{2.157}$$

where $(M_q)_{ij}$ denotes the minor of the $\boldsymbol{Y}_q$ matrix. Moreover, the matrices $\boldsymbol{U}_q$ and $\boldsymbol{W}_q$ can be defined at leading order in the hierarchies as

$$(U_q)_{ij} = (u_q)_{ij} \begin{cases} \dfrac{F(c_{Q_i})}{F(c_{Q_j})}\,, & i \le j\,, \\ \dfrac{F(c_{Q_j})}{F(c_{Q_i})}\,, & i > j\,, \end{cases} \qquad (W_q)_{ij} = (w_q)_{ij}\, e^{i\phi_j} \begin{cases} \dfrac{F(c_{q_i})}{F(c_{q_j})}\,, & i \le j\,, \\ \dfrac{F(c_{q_j})}{F(c_{q_i})}\,, & i > j\,. \end{cases} \tag{2.158}$$

Note that at leading order the matrices $\boldsymbol{U}_q$ do not depend on the localization of the RH profiles $F(c_{q_i})$, i.e. on the dimensionless 5D bulk masses of the 5D fields whose zero modes are RH. Therefore, the CKM entries do not depend on the c_{q_i} parameters at first order [110, 114].

Furthermore, using the Wolfenstein parametrization of the CKM matrix one can write the values of the parameter (λ, A, $\bar{\rho}$ and $\bar{\eta}$) in terms of the projections of the 5D fermion profiles at the IR brane, $F(c_{A_i})$, together with the Yukawa matrix elements $(Y_q)_{ij}$, or the corresponding minors. The necessary formulae is summarized in appendix B.

In particular, one finds the following hierarchical structure for the quark LH profiles [110, 114, 119]

$$\frac{|F(c_{Q_1})|}{|F(c_{Q_2})|} \sim \lambda\,, \qquad \frac{|F(c_{Q_2})|}{|F(c_{Q_3})|} \sim \lambda^2\,, \qquad \frac{|F(c_{Q_1})|}{|F(c_{Q_3})|} \sim \lambda^3\,, \tag{2.159}$$

while for the RH quark these hierarchies are set by the observed quark-masses, being

$$\begin{aligned} &\frac{|F(c_{u_1})|}{|F(c_{u_3})|} \sim \frac{m_u}{m_t}\,\frac{1}{\lambda^3}\,, \qquad \frac{|F(c_{u_2})|}{|F(c_{u_3})|} \sim \frac{m_c}{m_t}\,\frac{1}{\lambda^2}\,, \\ &\frac{|F(c_{d_1})|}{|F(c_{u_3})|} \sim \frac{m_d}{m_t}\,\frac{1}{\lambda^3}\,, \qquad \frac{|F(c_{d_2})|}{|F(c_{u_3})|} \sim \frac{m_s}{m_t}\,\frac{1}{\lambda^2}\,, \qquad \frac{|F(c_{d_3})|}{|F(c_{u_3})|} \sim \frac{m_b}{m_t}\,. \end{aligned} \tag{2.160}$$

We have found that this mechanism, which we will implement in the following chapter for our own model, allows us to describe the observed hierarchies of the CKM matrix from $\mathcal{O}(1)$ fundamental parameters of the 5D theory and by starting from anarchic Yukawa matrices.

One could then think that this is an appealing mechanism for describing the masses and mixing in the lepton sector of the SM. However, this mechanism would not be able to reproduce the PMNS matrix if we apply it directly. The lepton sector of the SM features large mixings and therefore, for this mechanism to work, it would require ratios of the fermion profiles at the IR brane of $|F(c_{L_i})|/\left|F(c_{L_j})\right| \sim \mathcal{O}(1)$, which could be understood as requiring a fine-tuning of the different c_{L_i} parameters [119]. Therefore, for this mechanism to work for describing the lepton fields of the SM we would have to introduce some constraints on the dimensionless masses c_{L_i}, e.g. by imposing some symmetries for these fields.

2.8 Short commment on fermion bulk masses

In the previous section, we have shown how important 5D bulk masses are to reproduce the SM model from a 5D theory, and how we can explain the hierarchical structure of the quark sector in the SM departing from anarchic Yukawa matrices. However, one important question arises when examining this mechanism more closely. We have seen how this whole mechanism relies on a term of the action that was introduced by hand, as we can see from (2.78). We discussed that fermion bulk mass terms need to be odd under the orbifold $\mathbb{Z}_2$ symmetry and that, in order to incorporate such a behaviour, we attached a sign-function (i.e. a function of the fifth-dimensional coordinate) to the mass parameter. However, this feature feels completely unnatural and it demands for a better explanation, and maybe for a more fundamental origin. Studying this possibility is the goal of the next chapter.

3 | A dynamical origin of fermion masses in WED

The bulk fermion localization mechanism we introduced in the previous chapter relies on the fact that hierarchical 4D Yukawa couplings can be generated via different localizations of the zero-mode profiles, corresponding to the SM chiral fermions, along the extra dimension. We have explained that such localizations are controlled by the values of the fermion bulk masses in such a way that starting with an anarchic 5D Yukawa matrix, we can compensate the different entries through exponentially different overlaps of the fermion profiles with the IR brane, where the Higgs field is localized, leading to a completelly hierarchical effective Yukawa matrix, providing therefore a natural explanation of the SM fermion mass hierarchy.

However, the 5D bulk masses must be $\mathbb{Z}_2$-odd functions on the orbifold, which implies that they should be *fields* on the extra dimension. The reason is that the 5D Dirac fermion bilinear $\bar{\Psi}_i\Psi_i$ is odd under the orbifold $\mathbb{Z}_2$ symmetry and therefore a constant mass term is forbidden by the orbifold symmetry. In existing implementations of RS models, these $\mathbb{Z}_2$-odd bulk masses are introduced by hand simply by multiplying constant mass parameters with a *sign* function of the 5D coordinate. However, we consider that in any consistent field-theoretic implementation of the fermion localization mechanism one should obtain the coordinate-dependent 5D mass parameters from the VEV of a $\mathbb{Z}_2$-odd bulk scalar field. Here, we will show how the VEV of such scalar can be dynamically generated and that, by coupling it to the bulk fermions, the corresponding zero modes can reproduce the observed SM fermions masses with $\mathcal{O}(1)$ parameters. Consider a bulk scalar field $\Sigma(x,\phi)$ which develops a non-trivial ϕ-dependent VEV. This scalar field couples to 5D Dirac fermions through Yukawa interactions such that when the scalar acquires a VEV the bulk fermion masses are generated dynamically, i.e.

$$\mathcal{Y}_i\Sigma(x,\phi)\bar{\Psi}_i(x,\phi)\Psi_i(x,\phi) \xrightarrow{\langle\Sigma(x,\phi)\rangle} M_i(\phi)\bar{\Psi}_i(x,\phi)\Psi_i(x,\phi), \tag{3.1}$$

where now $M_i(\phi) \equiv \mathcal{Y}_i \langle\Sigma(x,\phi)\rangle$, in contrast to $M_i(\phi) = M_i\,\text{sgn}(\phi)$.

We will first discuss the vacuum solutions of the odd bulk scalar in a flat geometry, where intuition allows us to understand how the problem can be solved and where we can compare our solutions to the ones presented in [24], where a similar approach to generate the bulk fermion masses was discussed in the context of flat extra dimensions. Then, we will extend the discussion to the warped geometry. Moreover, we will study the possible effects on the background geometry that adding a scalar field with a non-trivial VEV may have on the metric. In some previous work, without any connection to generating bulk fermion masses, odd bulk scalars acquiring a non-trivial VEV were studied in the context of both flat and WED in [175–177].

The phenomenological implications of our mechanism are important and lead to modifications w.r.t. the conventional RS model (in this chapter we will refer as conventional RS to the RS models considering a sign-function in front of the fermion bulk masses) in the fermion zero-mode profiles of the SM fermions, the spectrum of KK modes, and on the background geometry through back-reaction on the metric, i.e. the warp factor). These effects are potentially important for deriving constraints on the model from precision measurements, such as EWPT [105, 106, 117] and flavor observables [119, 170, 178–181]. We stress that the existence of a $\mathbb{Z}_2$-odd bulk scalar field should be seen as a generic feature of *any* realistic WED model with bulk matter fields. As a consequence, such models predict the existence of a new type of scalar KK states, whose masses are significantly larger than the masses of other KK resonances.

This chapter is based on what was initially published in [1]. Here, it is organized as follows: In section 3.1, we study the background solution of the odd bulk scalar field in flat and WED, while backreaction effects on the background geometry are discussed in 3.1.3 for the warped case. In section 3.2, we discuss the KK decomposition of the gauge sector assuming minimal, i.e. non-custodial, and custodial bulk gauge symmetries to study the implications on the EWPT due to the backreaction on the metric by the bulk scalar field. Furthermore, in appendix C we complement the conventions and derivation of EW precision observables for the custodial case. The scalar sector is analyzed in section 3.3, where we study the dependence of the profiles of its KK modes in terms of the model parameters. In section 3.4, we show how fermion bulk masses can be generated from an odd bulk scalar and we examine the fermion zero modes and the corresponding KK modes of the fermion fields. The phenomenological implications of our model on the fermion mass hierarchies and mixings and on flavor observables are presented in section 3.5. In particular, we take a look at how the new features of our model can affect our prediction for ϵ_K. In section 3.6, the Higgs portal coupling to the bulk scalar is briefly discussed. Finally, section 3.7 contains a summary of the chapter.

3.1 Non-trivial background solution for an odd bulk scalar field

We consider a RS model with an odd bulk scalar in a warped extra-dimensional geometry. We will work in ϕ-coordinates in this chapter. Therefore, we define the 5D metric as

$$ds^2 = e^{-2\sigma(\phi)}\,\eta_{\mu\nu}dx^\mu dx^\nu - r^2\,d\phi^2, \tag{3.2}$$

with $\sigma(\phi)$ the warp factor and r is the compactification radius of the extra dimension. In the case, when the backreaction of the bulk fields is neglected the warp factor is given by the RS solution, i.e. $\sigma(\phi) \equiv kr|\phi|$, where k is curvature of the AdS space. We assume that both k and r are set by the 5D Planck scale M_*, and that the product of both quantities is $kr \simeq \mathcal{O}(10)$, which is needed in order to solve the gauge hierarchy problem, as was discussed previously in chapter 2. Note that taking the limit $k \to 0$ recovers the flat case of an extra dimension.

As mentioned in the introduction, our goal is to generate the $\mathbb{Z}_2$-odd bulk fermion masses dynamically through Yukawa interactions with a $\mathbb{Z}_2$-odd scalar field $\Sigma(x,\phi)$ which develops a ϕ-dependent VEV. The scalar action for the $\mathbb{Z}_2$-odd real bulk scalar on a slice of a AdS spacetime reads

$$S_\Sigma^{(5\mathrm{D})} = \int d^4x \int_{-\pi}^{\pi} d\phi\sqrt{g}\,\Big\{\frac{1}{2}g^{MN}(\partial_M\Sigma)(\partial_N\Sigma) - V(\Sigma) - \sum_i \frac{\sqrt{|\hat{g}_i|}}{\sqrt{g}}V_i(\Sigma)\delta(\phi-\phi_i)\Big\}, \tag{3.3}$$

where g is the determinant of the 5D metric and $\hat{g}_i$ are the determinant of 4D metric defined on the branes, as defined in section 2.2. V_i are possible brane-localized potentials and $V(\Sigma)$ is the bulk scalar potential. Note that the bulk scalar field Σ is $\mathbb{Z}_2$-odd w.r.t. the orbifold fixed points,

therefore it must vanish at both brane locations. Hence, the brane potentials $V_i(\Sigma)$ could only be constants, which we choose to be the same as in the original RS setup [18]. As we will see later, the bulk scalar potential $V(\Sigma)$ induces a background solution for the scalar field in the bulk, i.e. a ϕ-dependent VEV. Taking this into account, the scalar field can be defined as

$$\Sigma(x,\phi) = \omega(\phi) + \frac{e^{\sigma(\phi)}}{\sqrt{r}} S(x,\phi), \qquad \text{with} \qquad \langle \Sigma(x,\phi) \rangle \equiv \omega(\phi), \tag{3.4}$$

where $S(x,\phi)$ is the scalar fluctuation around the VEV. Now we can rewrite the above scalar action as

$$\begin{aligned} S_{\Sigma}^{(5\mathrm{D})} = 2 \int d^4x \int_0^{\pi} d\phi\, e^{-4\sigma} \left\{ \frac{1}{2} e^{4\sigma}\, \partial_\mu S\, \partial^\mu S - \frac{1}{2r} \left[\frac{1}{r} \Big(\partial_\phi\, e^{\sigma} S \Big)^2 + \, (\partial_\phi\, \omega)^2 \right] \right. \\ \left. + \frac{e^{5\sigma}}{r^{3/2}}\, S\, \partial_\phi \Big(e^{-4\sigma}\, \partial_\phi\, \omega \Big) \, - r V(\Sigma) \right\} - \int d^4x\, e^{-4\sigma} \left\{ \frac{2e^{\sigma}}{r^{3/2}}\, S\, \partial_\phi\, \omega + \sum_i V_i \right\} \Bigg|_{\phi=0}^{\pi}. \end{aligned} \tag{3.5}$$

In the tadpole term an integration by parts has been performed. However, since $\Sigma(x,\phi)$ is odd, the corresponding boundary terms simply vanish. We now introduce the explicit form for the scalar potential

$$V(\Sigma) = \Lambda_B + \frac{\mu^2}{2}\Sigma^2 + \frac{\lambda}{4!}\Sigma^4, \tag{3.6}$$

where Λ_B is the bulk cosmological constant required for having the RS metric as a solution of Einstein's equations and $\mu^2 < 0$ is required for non-trivial background solutions being realized by the scalar field. From here on, we use the notation $|\mu| \equiv \sqrt{|\mu^2|}$. The parameters have mass dimension $[\mu] = 1$ and $[\lambda] = -1$, while the scalar field has mass dimension $[\Sigma] = 3/2$ (which implies $[S] = 1$ and $[\omega] = 3/2$).

We now use the variational principle to obtain the following EOM for the background field

$$\omega''(\phi) - 4\sigma'(\phi)\, \omega'(\phi) - r^2 \frac{\partial V(\Sigma)}{\partial \omega}\Big|_{S=0} = 0, \tag{3.7}$$

where primes denote derivatives w.r.t. the fifth-coordinate ϕ. It can be easily seen that the trivial ansatz, $\omega(\phi) = 0$, is a solution of (3.7). However, our goal is to find out if there exists a non-trivial solution with a lower energy, while still satisfying the Dirichlet BC

$$\omega(0) = \omega(\pi) = 0. \tag{3.8}$$

One can define a 4D energy density from the Hamiltonian associated with the scalar action (3.5). Using the EOM (3.7), we find

$$\rho_E = -\frac{\lambda r}{12} \int_0^{\pi} d\phi\, e^{-4\sigma(\phi)} \omega^4(\phi). \tag{3.9}$$

This implies that if a non-trivial VEV is developed, it will always correspond to a lower energy state than that of the trivial solution $\omega(\phi) = 0$.

In order to understand the dynamics leading to a non-trivial background solution for the bulk odd scalar field Σ, we need to solve (3.7). This is the equation of a damped anharmonic oscillator, however with a "wrong sign" damping term for $\sigma'(\phi) > 0$. In order to fix this, we can redefine the coordinate of the orbifold to $\varphi \equiv \pi - \phi$, such that the UV and IR branes are located at $\varphi = \pi$ and $\varphi = 0$, respectively. Without loss of generality we can restrict our study to $\varphi \in [0, \pi]$. Denoting derivatives w.r.t. φ by dots, we can rewrite (3.7) with (3.6) as

$$\ddot{\omega}(\varphi) - 4\dot{\sigma}(\varphi)\, \dot{\omega}(\varphi) + |\mu r|^2 \omega(\varphi) - \frac{\lambda r^2}{6} \omega^3(\varphi) = 0, \tag{3.10}$$

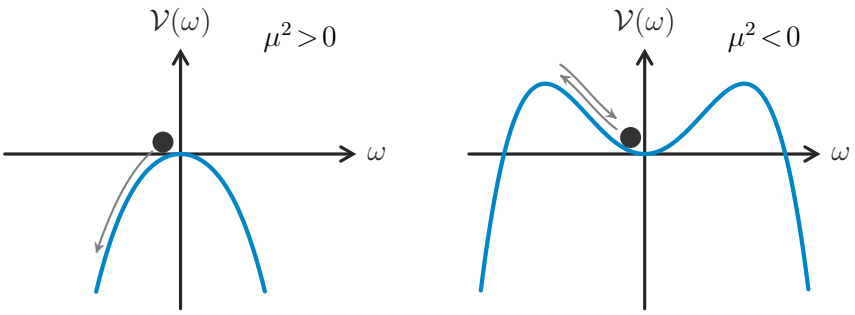

Figure 3.1: *Illustration of the upside-down potential $\mathcal{V}(\omega)$ for $\mu^2 > 0$ (left) and $\mu^2 < 0$ (right).*

with the damping term having opposite sign in the RS case, $\dot{\sigma}(\varphi) = -kr$, while the BC remain unchanged. This EOM can be understood as

$$\ddot{\omega}(\varphi) = 4\dot{\sigma}(\varphi)\,\dot{\omega}(\varphi) - r^2\frac{d\mathcal{V}(\omega)}{d\omega}, \tag{3.11}$$

where we have defined the upside-down potential

$$\mathcal{V}(\omega) \equiv -\frac{\mu^2}{2}\omega^2 - \frac{\lambda}{4!}\omega^4 = -\,V(\Sigma)\big|_{S=0}\,. \tag{3.12}$$

Equation (3.10) describes the damped motion of a particle in the potential $\mathcal{V}(\omega)$, see figure 3.1. The BC in (3.8) imply that the particle starts at the origin ($\omega = 0$) at "time" $\varphi = 0$ and returns to the origin after a time $\varphi = \pi$. For positive μ^2 the only solution satisfying the BC is the trivial one $\omega(\varphi) = 0$, since once it is displaced from the origin, the particle will roll down the potential and never return. Having a non-trivial solution thus requires $\mu^2 < 0$, as might have been expected from the start. However, as we will see later, this condition is not yet sufficient in the case of non-zero curvature.

It is instructive to rewrite (3.10) through the rescaling

$$\omega(\varphi) = \sqrt{\frac{6|\mu^2|}{\lambda}}\,v(\varphi), \tag{3.13}$$

where $v(\varphi)$ is a dimensionless field. With this rescaling the quartic coupling λ disappears from the EOM, contributing now just to the normalization factor. In terms of the dimensionless field $v(\varphi)$, relation (3.10) becomes

$$\ddot{v}(\varphi) - 4\dot{\sigma}(\varphi)\,\dot{v}(\varphi) + |\mu r|^2\left[v(\varphi) - v^3(\varphi)\right] = 0. \tag{3.14}$$

Note that the maximum of the inverted potential is now located at $v = \pm 1$. Moreover, the 4D energy density (3.9) takes the following form

$$\rho_E = -3r\frac{|\mu|^4}{\lambda}\int_0^\pi d\varphi\, e^{-4\sigma}v^4(\varphi). \tag{3.15}$$

In the following two subsections we consider two special cases where $\sigma(\varphi) = 0$, i.e. a flat extra dimension, and $\sigma(\varphi) = kr(\pi - \varphi)$, the RS warp factor (AdS geometry). In section 3.1.3 we employ a general warp function $\sigma(\varphi)$, which takes into account the backreaction due to the bulk scalar field.

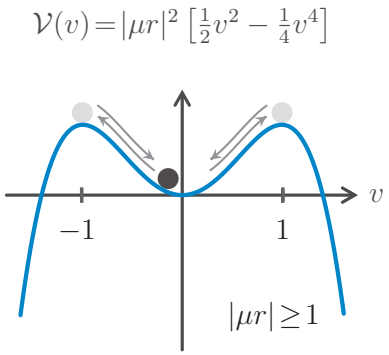

Figure 3.2: *Sketch of the potential $\mathcal{V}(v)$ and the motion of the particle in the flat case.*

3.1.1 Flat extra dimension

In order to build up intuition about the structure of the solutions for the VEV of an odd bulk scalar field, it is useful to review first the case of a flat metric, $\sigma(\varphi) = 0$. Similar studies for the flat extra dimension can be found in [24, 175, 176]. In this case there is no damping, since the $\dot{\sigma}$ term in (3.14) vanishes, as $\dot{\sigma} = 0$. The EOM for the dimensionless background field $v(\varphi)$ reads now

$$\ddot{v}(\varphi) + |\mu r|^2 \left[v(\varphi) - v^3(\varphi)\right] = 0. \tag{3.16}$$

This equation describes the undamped motion of a particle exposed to a non-linear conservative force. In the absence of the quartic term in the potential the motion would be harmonic,

$$v(\varphi) = N \sin\left(|\mu r|\varphi\right), \tag{3.17}$$

where N is an arbitrary normalization constant. The BC at $\varphi = 0$ is trivially satisfied. However, the BC at $\varphi = \pi$ is only satisfied for the very special parameter values $|\mu r| = n \in N$ and therefore only specific values of μ are solutions of our boundary-value problem. However, the anharmonic term in (3.16) has the effect of slowing down the motion as the particle climbs further up the potential, and hence the BC at $\varphi = \pi$ can *always* be satisfied as long as $|\mu r| \geq 1$, see figure 3.2. More generally, if $[|\mu r|] = n$ with some integer $n \geq 1$, with $[x]$ denoting the largest integer smaller than x, there will be exactly n solutions of (3.16) satisfying the BC, and the one with the lowest energy density is the one with the largest amplitude, corresponding to the motion where the particle climbs exactly once up the potential and has a turning point at $\varphi = \pi/2$.

In the flat case we can solve for the motion explicitly, using the energy conservation law (a first integral of the EOM)

$$E = \frac{1}{2}\dot{v}^2(\varphi) + \frac{|\mu r|^2}{2}\left[v^2(\varphi) - \frac{1}{2}v^4(\varphi)\right] = \frac{|\mu r|^2}{2}\left[v_m^2 - \frac{1}{2}v_m^4\right], \tag{3.18}$$

where $v_m < 1$ is the height of the turning point. Note that we cannot have $v_m > 1$, as in that case the particle would roll over the maximum of the inverted potential and roll away to infinity, thus violating the BC at $\varphi = \pi$. For $v_m = 1$ the particle would come to rest at the maximum of the inverted potential and stay there forever, violating as well the BC at $\varphi = \pi$.

We can integrate the above first-order differential equation, obtaining

$$|\mu r|\varphi = \int_0^{\frac{v(\varphi)}{v_m}} dx \frac{1}{\sqrt{1 - x^2 - \frac{v_m^2}{2}(1 - x^4)}} = \sqrt{\frac{2}{2 - v_m^2}}\, F\left(\arcsin\frac{v(\varphi)}{v_m}\middle|\, \frac{v_m^2}{2 - v_m^2}\right) \tag{3.19}$$

where $F(x|z)$ is the elliptic integral of the first kind. The condition that $\varphi = \pi/2$ at the turning point, i.e. where $v = v_m$, yields

$$|\mu r|\,\frac{\pi}{2} = \sqrt{\frac{2}{2-v_m^2}}\,K\left(\frac{v_m^2}{2-v_m^2}\right), \tag{3.20}$$

where $K(z) = F(\frac{\pi}{2}|z)$ is the complete elliptic integral of the first kind. In the limit where $|\mu r| \gg 1$, relation (3.20) implies

$$v_m \approx 1 - 4\exp\left(-\frac{\pi}{\sqrt{2}}|\mu r|\right), \tag{3.21}$$

up to exponentially suppressed terms. Solution (3.19) can then be approximated as (for $0 \leq \varphi < \pi/2$)

$$|\mu r|\,\varphi \approx \operatorname{arctanh}\frac{v(\varphi)}{v_m}, \tag{3.22}$$

and the reversed motion applies for $\pi/2 < \varphi \leq \pi$. Using (3.13), we recover for the original VEV Georgi *et al.*'s approximate solution [24]

$$\omega(\phi) \approx \sqrt{\frac{6|\mu^2|}{\lambda}}\tanh\left(\frac{|\mu r|}{\sqrt{2}}\phi\right)\tanh\left(\frac{|\mu r|}{\sqrt{2}}(\pi-\phi)\right), \tag{3.23}$$

which holds up to exponentially small terms.

3.1.2 Warped space

We now turn to the case of a WED and consider the RS metric with $\sigma(\varphi) = kr(\pi - \varphi)$. In this geometry the EOM for the background field $\omega(\phi)$ takes the form

$$\ddot{\omega}(\varphi) + 4kr\,\dot{\omega}(\varphi) + |\mu r|^2\omega(\varphi) - \frac{\lambda r^2}{6}\omega^3(\varphi) = 0, \tag{3.24}$$

where the damping term is now a linear function of $\dot{\omega}$. We can redefine $\omega(\varphi) = e^{-2\sigma}\,\bar{\omega}(\varphi)$, such that the single derivative term in the above equations is canceled. Therefore, the EOM for $\bar{\omega}$ reads

$$\ddot{\bar{\omega}} = (\mu^2 + 4k^2)\,r^2\,\bar{\omega} + \frac{\lambda r^2}{3!}\,e^{-4\sigma}\,\bar{\omega}^3\,, \tag{3.25}$$

which is analogous to the flat case of previous subsection. Analyzing solutions of (3.25) with small amplitude one finds that due to the damping term oscillations are possible only if $\mu^2 + 4k^2 < 0$. This is only a necessary condition for the problem to have a non-trivial solution, however, it is not a sufficient condition, as we will see below. For $-4k^2 < \mu^2 < 0$ there are no oscillations but exponentially damped motion, in which the particle returns to the origin only at infinite time.

Note that the *effective* mass parameter $(\mu^2 + 4k^2)$ in (3.25) corresponds to the BF bound in AdS space, as we discussed in section 2.3. However, the BF bound was obtained for a free bulk scalar theory, whereas in our case the scalar field has quartic interactions leading to the appearance of a non-trivial VEV in the bulk. As we argued above, the violation of the BF bound is a necessary condition for this to happen. Only in this case, the bulk scalar field condenses and acquires a ϕ-dependent VEV, which leads to emergence of a scale related to the bulk scalar and the loss of conformality of the dual theory [182].

It is instructive to recast (3.24) in terms of $v(\varphi)$, such that in the RS geometry we get

$$\ddot{v}(\varphi) + 4kr\,\dot{v}(\varphi) + |\mu r|^2\left[v(\varphi) - v^3(\varphi)\right] = 0. \tag{3.26}$$

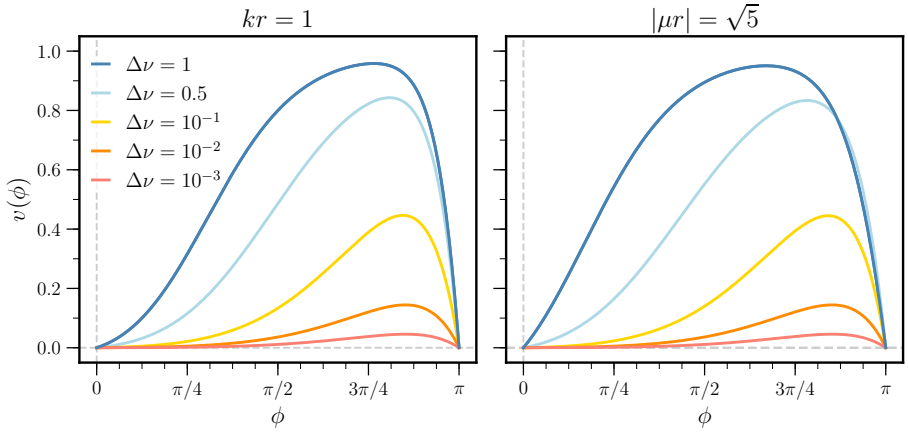

Figure 3.3: *Solutions for the scalar VEV $v(\phi)$, with $\phi = \pi - \varphi$, for different choices of $\Delta\nu = \nu - 1$ and fixed values of kr (left) and $|\mu r|$ (right).*

In the absence of the quartic term in the potential the motion would be a damped harmonic oscillation,

$$v(\varphi) = Ne^{-2kr\varphi}\sin(\nu\,\varphi), \tag{3.27}$$

where the frequency $\nu \equiv \sqrt{|\mu r|^2 - 4(kr)^2}$ is real and N is again an arbitrary normalization factor. While the BC at $\varphi = 0$ is trivially satisfied, the BC at $\varphi = \pi$ is only satisfied for the very special parameter values $\nu = n \in N$. By the same arguments as for the flat case, but now for another definition of ν, the BC at $\varphi = \pi$ can always be satisfied as long as $\nu \geq 1$. More generally, for $[\nu] = n$ with some integer $n \geq 1$ there will be exactly n solutions of (3.26) satisfying the BC, and the one with the lowest energy density (3.15) is the one with the largest amplitude, corresponding to the motion where the particle climbs exactly once up the potential and then falls down to satisfy the BC at $\varphi = \pi$. Note that in this case the turning point will not be placed at $\varphi = \pi/2$ but will be slightly shifted onto a lower value of φ due to the damping. It follows from this discussion that the correct condition for having a non-trivial background solution reads

$$\nu^2 = |\mu r|^2 - 4(kr)^2 > 1, \tag{3.28}$$

as for the values in $1 > |\mu r|^2 - 4(kr)^2 > 0$ the movement can not be completed by the particle, and it will not be able to come back to $v = 0$ at "time" $\varphi = \pi$.

In a natural setup, one would assume that the dimensionless quantities $|\mu r|$ and kr are chosen to be of $\mathcal{O}(1)$, leading therefore to values of $\nu \sim \mathcal{O}(1)$. Some representative solutions for the scalar VEV $v(\phi)$ in this case are shown in figure 3.3 for fixed values of kr (left) and $|\mu r|$ (right) and different values of $\Delta\nu \equiv \nu - 1$. Note that the maximum possible value of the VEV, $v_m = 1$, is only approached for values of $\Delta\nu \gtrsim 1$, whereas the amplitude of the oscillation gets smaller as $\Delta\nu$ gets closer to zero. One can also see that small values of $\Delta\nu$ not only result in smaller amplitudes, but also lead to very asymmetric VEV profiles, which look rather different from a step function. However, in realistic versions of RS models the product kr is chosen such that the hierarchy problem is solved, leading to the condition that $L = kr\pi \approx 33$. In this case the quantities $|\mu r|$ and kr on the left-hand side of the bound (3.28) are both much larger than 1. It is then useful to rewrite $\nu^2 \equiv (kr)^2\, b^2$, such that the bound is recast in the form

$$b = \sqrt{\frac{|\mu^2|}{k^2} - 4} > \frac{1}{kr}\,, \tag{3.29}$$

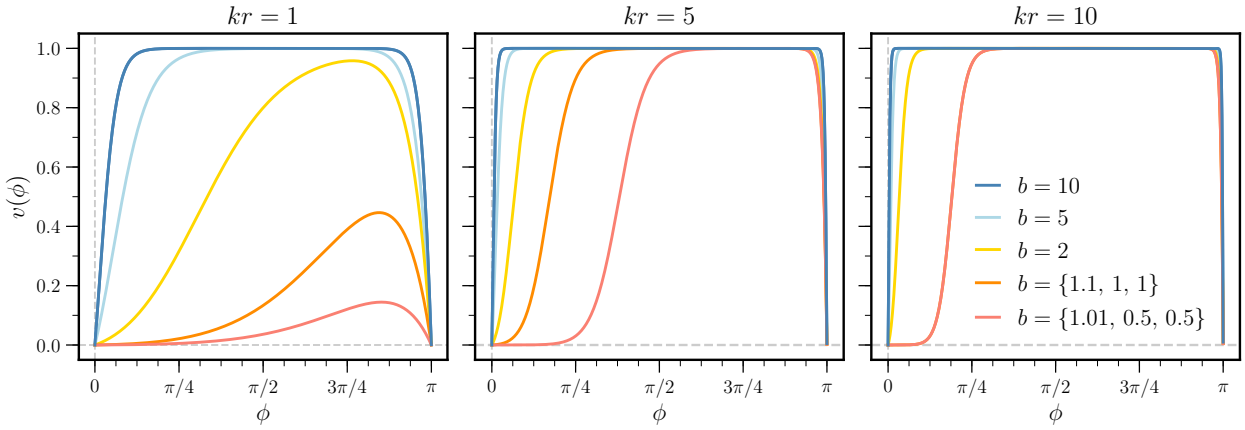

Figure 3.4: *Solutions for the scalar VEV $v(\phi)$ for different choices of kr and $b > 1/kr$. In the legend, we show in brackets the values of b used for the different figures, from left to right, such that the constraint $b > 1/kr$ is satisfied.*

where the right-hand side is close to 0.1 for $L \approx 33$. This bound is reminiscent of the BF bound $\beta = \sqrt{\mu^2/k^2 + 4} > 0$ for a free bulk scalar without SSB. Likewise, we can rewrite the differential equation (3.26) as

$$\frac{d^2v(z)}{dz^2} - 4\,\frac{dv(z)}{dz} + \left(4 + b^2\right)\left[v(z) - v^3(z)\right] = 0\,, \tag{3.30}$$

where $z = kr\phi = kr(\pi - \varphi)$. It is natural to assume that the parameter b^2 in this equation, which is given in terms of a ratio of two Planck-scale parameters μ and k, is of $\mathcal{O}(1)$. The equation must then be solved with the BC $v(z_i) = 0$ for $z_{\rm UV} = 0$ and $z_{\rm IR} = L$. Note that the large parameter $L \approx 33$ only enters via the size of the interval on which one solves the differential equation, while the parameter b^2 is still naturally of $\mathcal{O}(1)$. Under these conditions, we can see that the quantity $\nu^2 = (kr)^2\, b^2 \gg 1$ is naturally much larger than 1, and consequently the VEV develops a profile with a broad plateau approaching the value $v_m = 1$, resulting in a shape that closely resembles a step function, with an asymmetric behavior near the branes. In figure 3.4, we show solutions for the scalar VEV $v(\phi)$ for different values of b consistent with the bound (3.29) for $kr = 1$, 5 and 10. While the first plot is just a different representation of figure 3.3, in the last two plots the presence of the large parameter $L = kr\pi \gg 1$ gives rise to a prominent plateau, whereas the behavior close to the boundaries is only controlled by the parameter b. Note that the asymmetries near the branes reduce as b increases. If we plotted these results as functions of $z = kr\phi$, the behavior of the various lines in the last two plots near the two branes would be identical, and only the width of the plateau would be different. In the mechanical analogue of figure 3.1, solutions with a wide plateau correspond to fine-tuned motions where the point-mass comes to rest infinitesimally close to the maximum of the potential, staying there for a long time before coming down. Therefore, the motion from the origin to the maximum and back are independent of how long the particle stays at the top. We find the solutions obtained for large kr to look much closer to the traditional case of a step function, showing that solving the hierarchy problem helps to obtain kink-like solutions for the VEV. While this is particularly true near the IR brane (for $\phi \lesssim \pi$), to obtain a kink-like solution also near the UV brane (for $\phi \gtrsim 0$) requires large values of b. Indeed, there is a decoupling limit, in which $b \to \infty$ and the scalar VEV $v(\phi)$ approaches $\text{sgn}(\phi)$, such that one recovers the $\mathbb{Z}_2$-odd bulk masses of the conventional RS model.

3.1.3 Warped space with backreaction on the metric

The presence of a non-zero VEV of the bulk scalar field has an impact on the background geometry of the warped space, in the same fashion as we discussed in section 2.6 for the GW field. In this section, we calculate the backreaction caused by the bulk scalar by solving the coupled scalar-gravity system, the action of which reads

$$S_{\Sigma}^{(5\mathrm{D})} = \int d^4x \int_{-\pi}^{\pi} d\phi \sqrt{g} \Big\{ -\frac{\mathcal{R}}{2\kappa^2} + \frac{1}{2} g^{MN} (\partial_M \Sigma)(\partial_N \Sigma) - V(\Sigma) - \sum_i \frac{\sqrt{|\hat{g}_i|}}{\sqrt{g}} V_i(\Sigma) \delta(\phi - \phi_i) \Big\}, \quad (3.31)$$

where $\mathcal{R}$ is the 5D Ricci scalar, $\kappa^{-2} \equiv 2M_*^3$ with M_* being the 5D Planck mass, $V(\Sigma)$ is the bulk scalar potential for scalar field $\Sigma(x, \phi)$, and $V_i(\Sigma)$ are the brane potentials. We consider (3.2) as an ansatz for the metric where $\sigma(\phi)$ is a generic ϕ-dependent warp function. Note that the 5D Planck mass M_* is related to the reduced 4D Planck mass $M_{\mathrm{Pl}} \simeq 2 \cdot 10^{15}$ TeV by

$$M_{\mathrm{Pl}}^2 = M_*^3 \, r \int_0^{\pi} d\phi \, e^{-2\sigma(\phi)} = \frac{M_*^3}{2k} \left(1 - e^{-2kr\pi}\right), \quad (3.32)$$

where the second equality only holds for the RS case $\sigma(\phi) = kr|\phi|$.

Here we focus on the background solutions for the metric and bulk scalar field, i.e. $\Sigma(x, \phi) = \omega(\phi)$. The Einstein's equation and the EOM for $\omega(\phi)$ resulting from the action (3.31) are

$$\begin{aligned} \mathcal{R}_{MN} - \frac{1}{2} g_{MN} \mathcal{R} &= \kappa^2 \, T_{MN}, \\ -\frac{1}{\sqrt{g}} \partial_M \left(\sqrt{g} g^{MN} \partial_N \omega \right) &= \frac{\partial V(\omega)}{\partial \omega} + \sum_i \frac{\sqrt{|\hat{g}_i|}}{\sqrt{g}} \frac{\partial V_i(\omega)}{\partial \omega} \delta(\phi - \phi_i), \end{aligned} \quad (3.33)$$

where the energy-momentum tensor T_{MN} for $\omega(\phi)$ is,

$$T_{MN} = \partial_M \omega \partial_N \omega - g_{MN} \left[\frac{1}{2} g^{PQ} \partial_P \omega \partial_Q \omega - V(\omega) \right] + \sum_i \frac{\sqrt{|\hat{g}_i|}}{\sqrt{g}} V_i(\omega) \hat{g}^i_{\mu\nu} \delta^{\mu}_M \delta^{\nu}_N \delta(\phi - \phi_i), \quad (3.34)$$

with $\hat{g}^i_{\mu\nu}$ and $\hat{g}_i$ being the 4D induced metric and its determinant at the brane i, respectively. From equation (3.33), we get the EOM for the warp function $\sigma(\phi)$ and scalar VEV $\omega(\phi)$ as

$$\begin{aligned} \sigma'^2 &= \frac{\kappa^2}{6} \Big[\frac{1}{2} \omega'^2 - r^2 V(\omega) \Big], \\ \sigma'' &= \frac{\kappa^2}{3} \Big[\omega'^2 + r \sum_i V_i(\omega) \, \delta(\phi - \phi_i) \Big], \\ \omega'' - 4\sigma' \omega' &= r^2 \frac{\partial V(\omega)}{\partial \omega} + r \sum_i \frac{\partial V_i(\omega)}{\partial \omega} \delta(\phi - \phi_i), \end{aligned} \quad (3.35)$$

where the scalar potential has been given in (3.6) and includes the 5D bulk cosmological constant Λ_B. The brane localized potentials are constant brane tensions, since the odd bulk scalar field vanishes on the branes, and therefore

$$V_{\mathrm{UV}}(\omega) = V_{\mathrm{UV}}, \qquad V_{\mathrm{IR}}(\omega) = V_{\mathrm{IR}}. \quad (3.36)$$

These brane potentials are crucial in order to ensure that the 4D cosmological constant vanishes, so that the proposed RS metric in (3.2) is a solution of Einstein's equations, as was previously discussed in section 2.2. The above equations have singularities due to the presence of 3-branes at $\phi = 0$ and $\phi = \pi$, therefore the warped function $\sigma(\phi)$ and the scalar field $\omega(\phi)$ satisfy the conditions

$$\big[\sigma'(\phi)\big]_i = \frac{\kappa^2}{3} r V_i, \qquad \big[\omega'(\phi)\big]_i = 0, \quad (3.37)$$

where the "jump" of a function, $[f(x)]$, was defined in (2.10).

The evolution of the fields in the bulk is described by (3.35) after dropping the brane-localized terms. However, the three resulting equations are not independent. Indeed, the background solution is completely determined by

$$\begin{aligned} \sigma'' - \frac{\kappa^2}{3}\omega'^2 &= 0, \\ \omega'' - 4\sigma'\omega' - r^2\frac{\partial V(\omega)}{\partial \omega} &= 0. \end{aligned} \tag{3.38}$$

Note that $\sigma(\phi)$ only appears through its derivatives both in (3.37) and (3.38). Hence, we have a system of two coupled differential equations of first order in $\sigma'(\phi)$ and second order in $\omega(\phi)$, which only requires three integration constants to be solved. However, note that we have four constraints coming from BC and the jump conditions (3.37). Three of these constraints fix the three integration constants, whereas the remaining one corresponds to the usual fine-tuning required to make the ansatz (3.2) a solution, which guarantees in particular a vanishing 4D cosmological constant. This should not come as a surprised as it was a feature in the original RS model, as can be seen in (2.12) and (2.13). The relations between the 5D bulk cosmological constant and brane tensions, which is required by 4D Poincaré invariance, gets modified in our case compared with the original RS model. In particular, for a non-trivial scalar VEV the RS relation $V_{\rm UV}^{\rm RS} = -V_{\rm IR}^{\rm RS} = 6k/\kappa^2$ is in conflict with the bulk EOM (3.38). This can be seen by integrating (3.38) over the extra dimension ϕ. One obtains

$$\sigma'(\pi_-) = \sigma'(0_+) + \frac{\kappa^2}{3}\int_{0_+}^{\pi_-} d\phi\, \omega'^2(\phi), \tag{3.39}$$

which implies that the RS solution with $\sigma'(\pi_-) = \sigma'(0_+) = kr$ will no longer solve the system of equations in the presence of a non-trivial VEV. As a consequence, the first jump condition in (3.37) implies that the two brane tensions

$$V_{\rm UV} = \frac{6\sigma'(0_+)}{r\kappa^2}, \qquad V_{\rm IR} = -\frac{6\sigma'(\pi_-)}{r\kappa^2} \tag{3.40}$$

are not longer equal and opposite as in the RS case. One can fix one of the integration constants by choosing the boundary value of the warp function on the UV brane, such that in the UV the background geometry asymptotes to the AdS space, i.e. $\sigma'(0_+) = kr$. Hence, the brane tensions in our model are

$$V_{\rm UV} = \frac{6k}{\kappa^2}, \qquad V_{\rm IR} = -V_{\rm UV} - \frac{2}{r}\int_{0_+}^{\pi_-} d\phi\, \omega'^2(\phi). \tag{3.41}$$

The bulk cosmological constant Λ_B introduced in (3.6) can now be obtained by inserting the solutions from (3.38) into (3.35) and evaluating the fields near the UV brane, leading to

$$\sigma''^2(0_+) = \frac{\kappa^2}{6}\Big[\frac{1}{2}\omega'^2(0_+) - r^2\Lambda_B\Big]. \tag{3.42}$$

Doing the replacement $\sigma'(0_+) \to kr$, we get

$$\Lambda_B = -\frac{6k^2}{\kappa^2} - \frac{\omega'^2(0_+)}{2r^2}. \tag{3.43}$$

This new contribution to Λ_B leads to modifications of the background geometry in the IR w.r.t. the case of a RS space.

Summarizing, for a non-trivial scalar VEV with Dirichlet BC we need to solve the coupled equations (3.38), which in terms of the dimensionless VEV $v(\phi)$ take the form

$$\begin{aligned} \sigma''(\phi) - \gamma\, v'^2(\phi) &= 0, \\ v''(\phi) - 4\,\sigma'(\phi)\, v'(\phi) + |\mu r|^2\left[v(\phi) - v^3(\phi)\right] &= 0, \end{aligned} \tag{3.44}$$

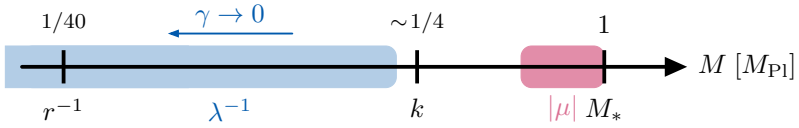

Figure 3.5: *Illustration of the parametric values of the dimensionful parameters of our model in units of the fundamental scale $M_{\rm Pl} \simeq M_*$. Note that the small hierarchy between k and $1/r \approx 0.1\,k$ is required for the model to address the gauge hierarchy problem. The relation between the parameters k, $|\mu|$ and M_* is in principle arbitrary, however our dynamical mechanism requires that $|\mu| > 2k$ with good approximation, see* (3.28).

along with BC,

$$v(0) = v(\pi) = 0, \qquad \sigma'(0) = kr. \tag{3.45}$$

For (3.44) we have defined the dimensionless parameter

$$\gamma \equiv \frac{|\mu|^2}{\lambda M_*^3} = \frac{2|\mu|^2\kappa^2}{\lambda}, \tag{3.46}$$

which parametrizes the scalar-gravity interaction, i.e. the strength of the backreaction. The limit $\gamma \to 0$ corresponds to the case of zero backreaction on the metric, where we recover the solutions of section 3.1.2 for the odd scalar VEV and the RS solution for the metric.

The value of γ is a free parameter of our model, which depends on a ratio involving three parameters that are naturally set by the Planck scale. Assuming that $|\mu|$ and λ^{-1} are not trans-Planckian, i.e. the values of $|\mu|$ and λ^{-1} are not greater than M_*, values of γ moderately smaller than 1 can be arranged without much fine tuning. For our analysis we will consider the scenarios of strong and negligible backreaction, for which we will set $\gamma = 0.5$ and $\gamma = 0$, respectively. During our numerical study, we found the results obtained for $\gamma \lesssim 0.1$ to be very close to those found for $\gamma = 0$.

Before discussing the numerical solutions of the coupled scalar-gravity system a few comments could help the reader understand our strategy for solving the coupled system of equations as well as for setting the values for the parameters of the model. In this work, we obtain the numerical solutions by the shooting method of initial conditions, using equation (3.44). In particular, we choose the initial conditions by varying the values of $\sigma'(0)$ and $v'(0)$ at the UV brane, i.e. for $\phi = 0$, such that our boundary-value problem is solved. The choices of values for other parameters appearing in this chapter are natural in the sense that all the dimensionless parameters have $\mathcal{O}(1)$ values, whereas the dimensionful parameters (e.g. $\mu, k, \ldots$) have $\mathcal{O}(1)$ values in units of the 5D Planck mass M_*, which we may identify with the physical Planck scale $M_{\rm Pl}$. Furthermore, the value of the compactification radius r of the extra dimension is chosen such that it solves the gauge hierarchy problem. In particular, we take $r = 40 M_{\rm Pl}^{-1}$, such that $k \sim 33/(\pi r)$ and $|\mu| \in [20, 40]/r$ are both below $M_{\rm Pl}$. In figure 3.5 we schematically summarize the different choices for the values of the parameters appearing in the model.

In figure 3.6, we show the numerical solutions for the coupled system (3.44) for different values of γ, in particular we plot results using $\gamma = 0$ (no backreaction limit, dashed lines) and $\gamma = 0.5$ (strong backreaction, solid lines), for input values of $|\mu r| = 25$ (red), 30 (light blue) and 40 (dark blue). The upper panels show the profile of the scalar VEV $v(\phi)$ for these cases, together with the RS case of a $\mathrm{sgn}(\phi)$ function (black dashed), both in the whole extra dimension (left panel) and in a "zoomed" region near the branes (right panels). The lower panels show the warp function, $\sigma(\phi)$ (left panel), and the ratio of the warp function w.r.t. the RS solution, $\sigma(\phi)/(kr\phi)$

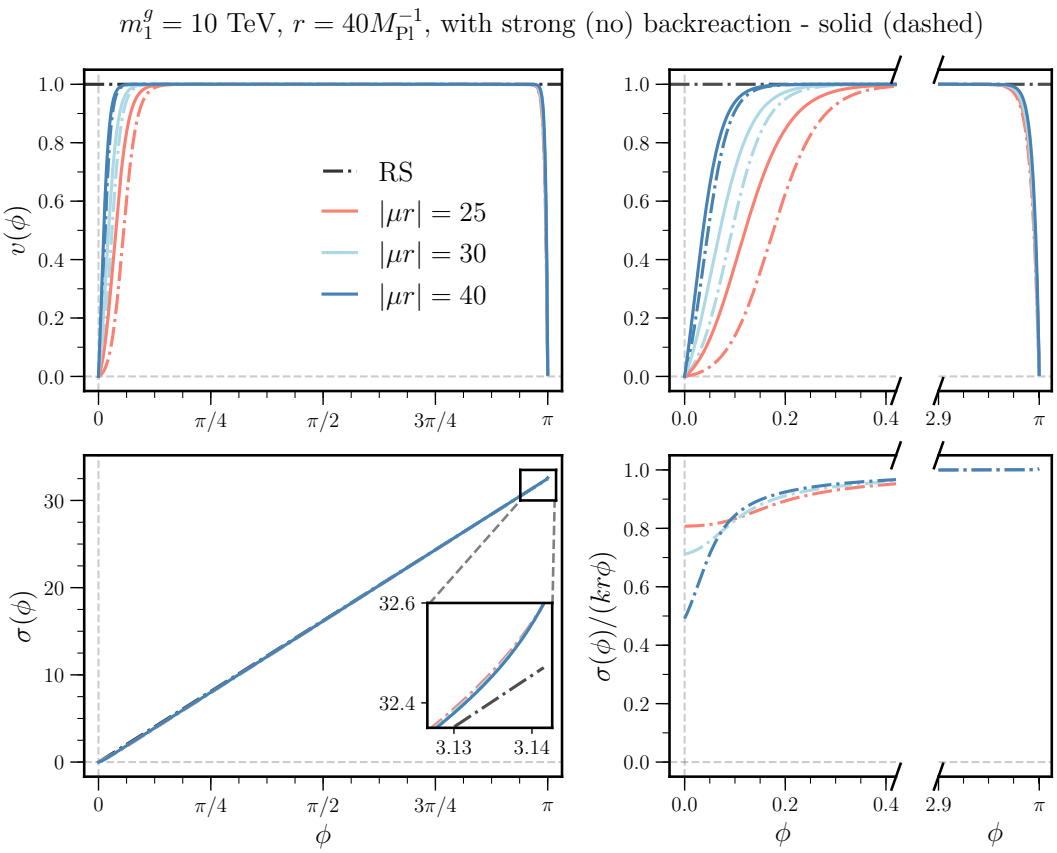

Figure 3.6: *Background solutions for $\gamma = 0$ (no backreaction limit) and $\gamma = 0.5$ (strong backreaction) and different values of $|\mu r|$. Upper panels show the scalar VEV solutions for RS (with sgn(ϕ) function) and $|\mu r| = 25, 30$ and 40, with the upper right figure emphasizing the behavior of the VEV near the branes. Analogous plots are shown for the warp function $\sigma(\phi)$ in the lower panels, where on the right panels we show the ratio $\sigma(\phi)/(kr\phi)$ instead of just $\sigma(\phi)$.*

(right panels), again the latter only showing values of ϕ close to the branes. Note that again for $\mu \to \infty$ (corresponding to $b \to \infty$ if no tuning is assumed) we reach the decoupling limit where $v(\phi) \to \text{sgn}(\phi)$, i.e. the dynamics of the bulk scalar freezes. Therefore, for a generic case with a fixed value of radius of extra dimension r, with increasing $|\mu r|$ the solutions in the bulk get closer to the original RS assumption.

Furthermore, it is instructive to set the scale of the model parameters in terms of some TeV-scale observable. It is common in the literature to define the so-called KK mass scale

$$M_{\rm KK} \equiv \frac{\sigma'(\pi)}{r} e^{-\sigma(\pi)}, \tag{3.47}$$

which in the context of RS models sets the mass scale for low-lying KK excitations of the SM particles. For the non-backreaction case, $M_{\rm KK}$ has the well-known expression

$$M_{\rm KK} = k e^{-kr\pi}. \tag{3.48}$$

However, as we will show in section 3.2.3, once the backreaction is taken into account the ratio between e.g. the first vector resonance in the spectrum and $M_{\rm KK}$ changes dramatically, which makes

the use of $M_{\rm KK}$ for phenomenological studies problematic. Therefore, for the rest of this chapter we will use a physical mass instead of $M_{\rm KK}$ to define the scale of NP. In particular, we chose the mass of the first KK gluon, m_1^g, as it does not depend on other input parameters, but is fixed only by the metric. This will become clear later in section 3.2, where the gluon mass appears as the eigenvalue solution of equation (3.56). For all solutions shown in figure 3.6 this mass is set to $m_1^g = 10$ TeV.

Comments on the stability of the WED with an odd bulk scalar field

We briefly comment here on the issue of stability of the extra dimension once an odd bulk scalar field is introduced to the theory. In any realistic warped extra-dimensional model that solves the gauge hierarchy problem, it is essential to have a dynamical mechanism to stabilize the radius r of the extra dimension, i.e. the distance between the two branes, as this size is the main parameter that sets to which scale $M_{\rm Pl}$ gets "warped-down" to. Without such a mechanism, the quantum perturbations of the metric (3.2), the so-called *radion*, remain massless, as as discussed in section 2.6. However, as shown by GW [162], the radius of extra dimension can be dynamically stabilized by a 5D bulk scalar which has non-trivial potentials in the bulk and at both branes (see section 2.6). Given the fact that the bulk scalar field $\Sigma(x, \phi)$, which we have introduced in our model to generate the fermion bulk masses, affects the background geometry in a non-trivial way, it is natural to ask whether such a bulk scalar could also serve as a stabilizing GW field.

In order to answer this question, one needs to solve Einstein equations to linear order in perturbations of the metric as well as the bulk scalar field, see e.g. [116]. After this exercise, one ends up with a bulk scalar, which is a linear combination of metric and scalar field perturbations, and it has a zero mode, corresponding to the light radion, and a tower of KK modes. However, it was shown in [183] that a scalar field with an extremum point in the bulk of the extra dimension cannot stabilize the size of the extra dimension and that, in fact, it introduces an instability in the system as it develops a tachyonic mode. We have explicitly verified this result and found a tachyonic mode in the spectrum of scalar perturbations. Hence, an odd bulk scalar alone cannot stabilize the extra dimension. However, one can argue that introducing a second bulk scalar acting as a GW stabilizing field can not only stabilize the size of extra dimension but also remove the tachyonic mode from the scalar spectrum. This analysis was beyond the scope of our work, but we note that partial progress has been made along these lines in [177], see also [176, 184].

Hence, for simplicity we study the backreaction of the background solutions assuming the geometry to be static, for both the weak and strong backreaction scenarios, i.e. we do not consider the scalar perturbations of the metric but only consider the fluctuations of the odd bulk scalar around its background VEV as in (3.4). We simplify the problem this way, as considering the scalar perturbations of the metric would require us to introduce, in addition, a GW field to get rid of any possible tachyons appearing in the system. This would make our system too complicated to be solved using the techniques we previously discussed, while it is also beyond the scope of our work.

3.2 Gauge bosons and EW precision tests

In this section we calculate the impact on EW precision observables due to the backreaction from the $\mathbb{Z}_2$-odd bulk scalar on the metric. We consider both the minimal RS case and its custodial extension in the presence of a brane-localized Higgs sector. Moreover, we present the EOM for the gauge bosons, necessary for us to use m_1^g as the scale of NP throughout the rest of the chapter.

3.2.1 Minimal case

We closely follow the treatment of the KK decomposition for the EW sector from [110, 111]. We start by considering a $SU(2)_L \times U(1)_Y$ bulk gauge group, spontaneously broken to $U(1)_Q$ by the VEV of an IR-localized Higgs. In order to have SM gauge bosons as the zero modes of bulk gauge bosons, we require the vector components W^a_μ and B_μ to be even under the $\mathbb{Z}_2$ orbifold symmetry, whereas for the scalar components W^a_ϕ and B_ϕ we require them to be odd. We can write the gauge-sector bulk action as

$$S_V^{(5\mathrm{D})} = \int d^4x \int_{-\pi}^{\pi} d\phi \, \sqrt{g}\, g^{KM} g^{LN} \Big(-\frac{1}{4} W^a_{KL} W^a_{MN} - \frac{1}{4} B_{KL} B_{MN} \Big) + S_{\mathrm{Higgs}} + S_{\mathrm{GF}} + S_{\mathrm{FP}} \,, \tag{3.49}$$

where W^a_{MN} and B_{MN} are the 5D field strength tensors for $SU(2)_L$ and $U(1)_Y$. S_{GF} and S_{FP} are the gauge fixing and the Faddeev-Popov ghost actions, respectively. For simplicity, the Higgs-sector is localized on the IR brane. The action for the canonically normalized Higgs doublet $H(x)$ reads

$$S_H^{(4\mathrm{D})} = \int d^4x \, \Big\{ (D_\mu H)^\dagger (D^\mu H) - (m\, e^{-\sigma(\pi)})^2 \left(H^\dagger H\right) - \lambda_H \left(H^\dagger H\right)^2 \Big\} , \tag{3.50}$$

see section 2.3 for a detailed explanation. After the EWSB, $H(x)$ can be decomposed as

$$H(x) = \frac{1}{\sqrt{2}} \begin{pmatrix} -i\sqrt{2}\, G^+(x) \\ v_h + h(x) + i G^3(x) \end{pmatrix} , \tag{3.51}$$

with $v_h \simeq 246\,\mathrm{GeV}$ the SM Higgs VEV, $h(x)$ is the Higgs field and $G^\pm$ and G^3 the associated Goldstone bosons. The covariant derivative D_μ is defined as

$$D_\mu = \partial_\mu - i\frac{g_5}{2} \tau^a W^a_\mu - i g'_5 B_\mu , \tag{3.52}$$

in similarity with (1.4), with τ^a the Pauli matrices, and g_5 and g'_5 the 5D gauge couplings of $SU(2)_L$ and $U(1)_Y$, respectively. Note that now $[g_5] = [g'_5] = -1/2$ (see section 2.4). How we can define the 4D effective gauge couplings from these quantities will become clear later this section.

We write the KK decomposition of the 5D gauge fields in the form of 4D vector bosons and scalars as [110]

$$\mathbb{A}_\mu(x,\phi) = \frac{1}{\sqrt{r}} \sum_n \mathbb{A}^{(n)}_\mu(x)\, \chi^{\mathbb{A}}_n(\phi) \,, \qquad \mathbb{A}_\phi(x,\phi) = \frac{-1}{\sqrt{r}} \sum_n \frac{1}{m^{\mathbb{A}}_n} \mathbb{A}^{(n)}_\phi(x)\, \partial_\phi \chi^{\mathbb{A}}_n(\phi) \,, \tag{3.53}$$

where $\mathbb{A} = A, Z, W^\pm$ are the usual field redefinitions of the EW gauge bosons, as

$$\begin{aligned} W^\pm_M &= \frac{1}{\sqrt{2}} \left(W^1_M \mp i W^2_M \right) , \\ Z_M &= \frac{1}{\sqrt{g_5^2 + g_5'^2}} \left(g_5 W^3_M - g'_5 B_M \right) , \\ A_M &= \frac{1}{\sqrt{g_5^2 + g_5'^2}} \left(g'_5 W^3_M + g_5 B_M \right) . \end{aligned} \tag{3.54}$$

Above $\mathbb{A}^{(n)}_\mu(x)$ and $\mathbb{A}^{(n)}_\phi(x)$ are the 4D KK mass eigenstates, and the dimensionless $\chi^{\mathbb{A}}_n(\phi)$ are the KK wave-functions, which form a complete basis on the orbifold. These KK wave-functions satisfy the orthonormality condition

$$2 \int_0^\pi d\phi \, \chi^{\mathbb{A}}_m(\phi)\, \chi^{\mathbb{A}}_n(\phi) = \delta_{mn} \,. \tag{3.55}$$

Note that both the kinetic terms for the gauge fields and the Higgs field in the action (3.49) contain mixed terms involving the gauge bosons with their scalar companions and the Goldstone

fields, respectively. These mixings can be removed by introducing appropriate gauge-fixing terms in the Lagrangian, see for instance [110]. Inserting the KK decompositions into the action (3.49) leads to the EOM

$$-\frac{1}{r^2}\,\partial_\phi\Big(e^{-2\sigma(\phi)}\,\partial_\phi\,\chi_n^{\mathbb{A}}(\phi)\Big) = (m_n^{\mathbb{A}})^2\,\chi_n^{\mathbb{A}}(\phi)\,, \tag{3.56}$$

along with the BC

$$\partial_\phi\,\chi_n^{\mathbb{A}}(0) = 0\,, \qquad \Big(\partial_\phi + \pi r^2 \tilde{m}_{\mathbb{A}}^2 e^{2\sigma(\phi)}\Big)\,\chi_n^{\mathbb{A}}(\pi^-) = 0. \tag{3.57}$$

The parameter appearing in the BC from (3.57), $\tilde{m}_{\mathbb{A}}$, corresponds to the mass term arising from the interaction with the brane-localized Higgs field, being

$$\tilde{m}_W^2 = \frac{g_5^2}{2\pi r}\frac{v_h^2}{4}, \qquad \tilde{m}_Z^2 = \frac{(g_5^2+g_5'^2)}{2\pi r}\frac{v_h^2}{4}, \qquad \tilde{m}_A^2 = 0. \tag{3.58}$$

As we discussed previously in section 2.4, this term will make the zero-mode solution deviate from the flat profile for the fields with non-vanishing $\tilde{m}_{\mathbb{A}}$. However, this can be treated as a $\mathcal{O}(v_h/M_{\rm KK})$ perturbation and the effects are expected to be small. Moreover, we can define the 4D gauge couplings as

$$g_4^2 \equiv \frac{g_5^2}{2\pi r}, \qquad g_4'^2 = \frac{g_5'^2}{2\pi r}. \tag{3.59}$$

The equations for the gluon and the photon are trivially the same, and they only depend on the metric, therefore the possible importance of the backreaction effects on the gauge boson profiles. For the case of negligeable backreacion, we have

$$\chi_0^A(\phi) = \chi_0^g(\phi) = \frac{1}{\sqrt{2\pi}}. \tag{3.60}$$

For $\mathbb{A} = Z, W^\pm$, we obtain the following expressions for the physical zero-mode masses

$$m_0^{\mathbb{A},2} = \tilde{m}_{\mathbb{A}}^2\left[1 - \frac{r^2\tilde{m}_{\mathbb{A}}^2}{\pi}\int_0^\pi d\phi_1 e^{2\sigma(\phi_1)}\phi_1^2 + \mathcal{O}\left(\frac{v_h^4}{M_{\rm KK}^4}\right)\right], \tag{3.61}$$

while the photon and the gluon remains massless, as expected.

The momentum-space 5D gauge boson propagator for $\mathbb{A}_\mu$ is defined by the EOM [150, 185] (see also [12, 124, 172])

$$\left[\frac{1}{r^2}\,\partial_\phi e^{-2\sigma(\phi)}\,\partial_\phi + p^2\right] D_{\mathbb{A}}(\phi,\phi';p) = \delta(\phi-\phi'), \tag{3.62}$$

together with the BC

$$\partial_\phi D_{\mathbb{A}}(\phi,\phi';p)\Big|_{\phi=0} = 0, \qquad \Big(\partial_\phi + \pi r^2\tilde{m}_{\mathbb{A}}^2 e^{2\sigma(\phi)}\Big)\,D_{\mathbb{A}}(\phi,\phi';p)\Big|_{\phi=\pi^-} = 0, \tag{3.63}$$

where similar EOM and BC apply for ϕ'. Equivalently, the 5D propagator is defined by its KK decomposition [103, 104, 110]

$$D_{\mathbb{A}}(\phi,\phi';p) = \sum_n \frac{\chi_n^{\mathbb{A}}(\phi)\chi_n^{\mathbb{A}}(\phi')}{p^2-(m_n^{\mathbb{A}})^2} = D_{\mathbb{A}}^{(0)}(\phi,\phi';p) + \tilde{D}_{\mathbb{A}}(\phi,\phi';p), \tag{3.64}$$

where in the last step we have separated the propagator into the contribution coming from the zero mode (massless before EWSB) and the contributions of the rest of the KK tower [56]. This

separation is useful since only the term $\tilde{D}_{\mathbb{A}}(\phi,\phi';p)$, evaluated at zero-momentum $p=0$ and in the limit $\tilde{m}_{\mathbb{A}}\to 0$, is relevant for EWPT at the level of dimension-6 operators. This quantity reads

$$\tilde{D}_{\mathbb{A}}(\phi,\phi';0)=\frac{r^2}{2}\left[\int_0^{\phi_>}d\phi_1 e^{2\sigma(\phi_1)}-\frac{1}{\pi}\left(\int_0^{\phi}+\int_0^{\phi'}\right)d\phi_1 e^{2\sigma(\phi_1)}\phi_1 \right. \\ \left. -\int_0^{\pi}d\phi_1 e^{2\sigma(\phi_1)}\left(1-\frac{\phi_1}{\pi}\right)^2\right]+\mathcal{O}\left(\frac{\tilde{m}_{\mathbb{A}}^2}{M_{\rm KK}^2}\right), \tag{3.65}$$

where $\phi_>=\max(\phi,\phi')$. This expression can be obtained by integrating over the EOM for the profiles and then using the definition in (3.64) together with the orthogonality condition (3.55).

Using this expression for the 5D propagator we get

$$\frac{G_F}{\sqrt{2}}=\frac{1}{2v_h^2}\left[1+\pi r^2\tilde{m}_W^2\int_0^{\pi}d\phi_1 e^{2\sigma(\phi_1)}+\mathcal{O}\left(\frac{v_h^4}{M_{\rm KK}^4}\right)\right], \tag{3.66}$$

as well as the following expressions for the oblique parameters T and S [54, 56, 124]

$$S=8v_h^2\pi^2r^2\int_0^{\pi}d\phi_1 e^{2\sigma(\phi_1)}\left(1-\frac{\phi_1}{\pi}\right), \qquad T=\frac{v_h^2\pi^2r^2}{c_w^2}\int_0^{\pi}d\phi_1 e^{2\sigma(\phi_1)}. \tag{3.67}$$

Note that at zeroth-order in $v_h/M_{\rm KK}$, the contribution to the S and T parameters only depend on the metric and on the radius of extra dimension r.

3.2.2 Custodial case

One possibility of reducing the tree-level contribution to the T parameter [133] and at the same time relaxing the deviations on the $Z\bar{b}_Lb_L$ coupling usually predicted in RS models [134] is to enlarge the bulk gauge symmetry to include the custodial group $SU(2)_L\times SU(2)_R$ [132, 135, 136]. In particular, one can assume an $SU(2)_L\times SU(2)_R\times U(1)_X$ bulk gauge symmetry that gets broken to $SU(2)_L\times U(1)_Y$ at the UV brane by the UV BC, and to $SU(2)_V\times U(1)_X$ by the VEV of the Higgs at the IR, as

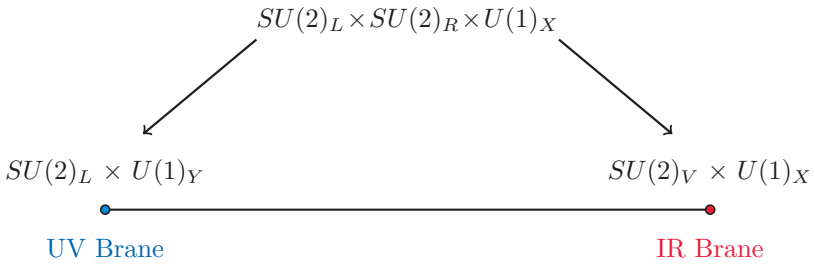

In this case, one obtains the following relations for the 4D masses for $\mathbb{A}=Z,W^{\pm}$

$$m_{\mathbb{A}}^2=\tilde{m}_{\mathbb{A}}^2\left[1-\frac{r^2\tilde{m}_{\mathbb{A}}^2}{\pi}\int_0^{\pi}d\phi_1 e^{2\sigma(\phi_1)}\left(\phi_1^2+\pi^2\rho_{\mathbb{A}}\right)+\mathcal{O}\left(\frac{v_h^4}{M_{\rm KK}^4}\right)\right], \tag{3.68}$$

where now

$$\tilde{m}_W^2=\frac{g_{5L}^2}{2\pi r}\frac{v_h^2}{4}, \qquad \tilde{m}_Z^2=\frac{(g_{5L}^2+g_{5Y}^2)}{2\pi r}\frac{v_h^2}{4}, \tag{3.69}$$

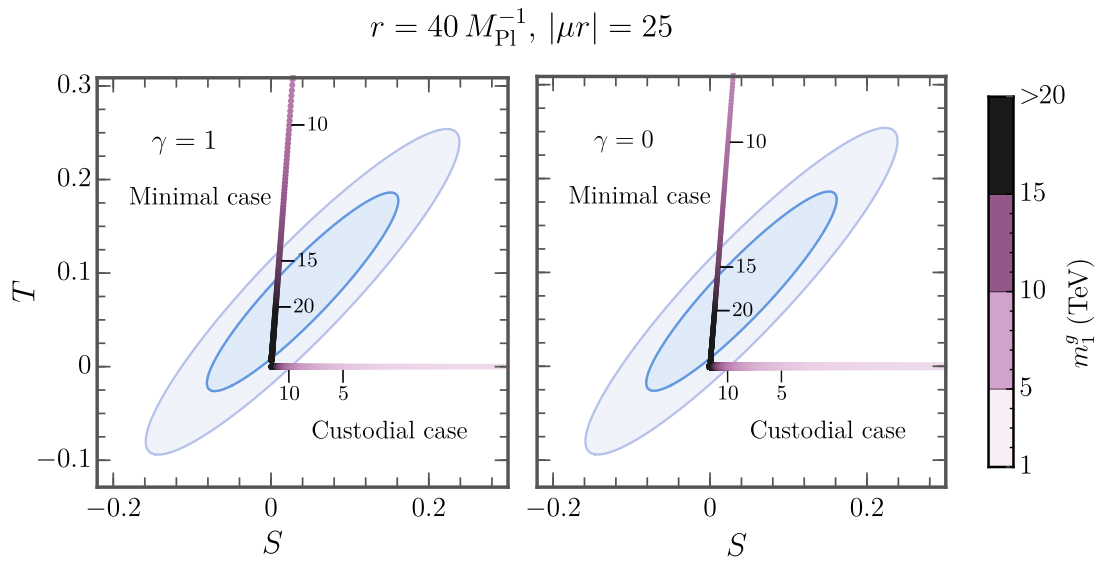

Figure 3.7: *Values of the S and T parameters for the scan performed on the mass of the first KK gluon m_1^g. The color bar shows the values of the mass of the first KK gluon m_1^g in TeV. The blue contours show the 68% and 95% CL regions in the TS-plane allowed by EWPT. We fix $|\mu r| = 25$ for both plots. For the left panel we have fix $\gamma = 1$ and the right panel shows the no backreaction limit, i.e. $\gamma = 0$. The horizontal $T = 0$ points refer to the custodial case, whereas vertically inclined points are for the minimal case.*

and we have defined for convenience $\rho_W = t_W^2$ and $\rho_Z = t_W^2 c_w^2 c_\theta^2$ (see Appendix C for more details). The different mixing angles are defined as

$$t_W = \frac{g_{5R}}{g_{5L}}, \qquad t_\theta = \frac{g_{5X}}{g_{5R}}, \qquad t_w = \frac{g_{5Y}}{g_{5L}}, \tag{3.70}$$

with

$$g_{5Y} = \frac{g_{5R} g_{5X}}{\sqrt{g_{5R}^2 + g_{5X}^2}}. \tag{3.71}$$

One also obtains

$$\frac{G_F}{\sqrt{2}} = \frac{1}{2v_h^2}\left[1 + \pi r^2 \tilde{m}_W^2 \left(1 + \rho_W\right) \int_0^\pi d\phi_1 e^{2\sigma(\phi_1)} + \mathcal{O}\left(\frac{v_h^4}{M_{\rm KK}^4}\right)\right], \tag{3.72}$$

whereas the T parameter now vanishes and the S parameter remains unchanged as in (3.67).

3.2.3 Numerical study

We now derive the constraints on the KK mass scale from the prediction of the S and T parameters, for both the minimal and the custodial RS models and considering the backreaction on the metric from the VEV of the bulk scalar field. In figure 3.7, we show contours the 68% and 95% CL contours allowed by the S and T parameters, as reported by Gfitter group [58]. For the fit performed by fixing $U = 0$, this corresponds to the values

$$S|_{U=0} = 0.04 \pm 0.08, \qquad T|_{U=0} = 0.08 \pm 0.07, \tag{3.73}$$

γ	m_1^g (TeV) Minimal case	m_1^g (TeV) Custodial case	$M_{\rm KK}$ (TeV) Minimal case
1	14.3	9.6	21.5
0.5	14.0	9.6	12.9
0.1	13.9	9.6	7.0
0.01	13.8	9.5	5.8
0	13.6	9.5	5.6

Table 3.1: *Mass of the lightest KK gluon satisfying the constraints from EWPT at 95% CL for the minimal case and the custodial case. The parameter γ, which is varied between 1 and 0, determines the strength of the backreaction. We fixed $|\mu r| = 25$ and $r = 40 M_{Pl}^{-1}$. The last column shows M_{KK} as defined in* (3.47) *for the minimal case.*

with a correlation coefficient of $+0.92$, see [58].

As mentioned earlier, we use the mass of the first KK gluon resonance, m_1^g, to display the bounds, where m_1^g is obtained from the solution of the gauge boson EOM (3.56) with Neumann BC. We perform a numerical scan, where for given values of $|\mu r|$, kr and γ we determine the KK gluon mass, as well as the warp function and the VEV of the bulk scalar from the coupled equations (3.44). We then obtain S and T from (3.67) for the minimal model, and the corresponding ones for the custodial case, i.e. using the same value for the S parameter and setting $T = 0$. In figure 3.7, the colored legend shows the values of the first KK-gluon mass. The size of the extra dimension is fixed to $r = 40 M_{\rm Pl}^{-1}$. For both plots we have fixed $|\mu r| = 25$ and we use $\gamma = 1$ for the left panel, whereas the right panel corresponds to the case where no backreaction is considered, i.e. $\gamma = 0$. Comparing the two plots one sees that backreaction only has a minor impact on the numerical results. Also, the results are rather insensitive to changes in $|\mu r|$, as one can infere from figure 3.6.

We collect the EWPT 95% CL bounds on the lightest KK-gluon mass m_1^g in table 3.1. One observes that regardless of the model parameters the bounds on m_1^g are rather stringent and out of the reach of LHC. Note that custodial versions of the RS model are favored over models with minimal particle content in that they allow for lighter KK resonances, minimal versions of the RS model are favored by Higgs phenomenology [109, 150, 186]. We should emphasize however that our analysis of EWPT bounds was based on tree-level calculations. In some regions of parameters space, positive one-loop corrections to the T parameter could help to eliminate the bounds. For the custodial RS model, this has been studied in [107, 108]. The backreaction of the scalar VEV on the metric only has a minor impact on the bounds on m_1^g. Note, however, that this would not be true if one considers the "unphysical" KK mass scale as defined in terms of the derivative of the metric in (3.47), which varies strongly with γ. However, we know that physical masses are not directly dependent on $M_{\rm KK}$, which is a parameter defined strictly at the IR brane, but that also depend strongly on the value of the metric th the bulk, therefore the results of table 3.1 should not be considered as surprising.

3.3 KK excitations of the bulk scalar field

The profiles of the scalar KK resonances can be computed by inserting the KK decomposition

$$S(x, \phi) = \sum_{n=1}^{\infty} S_n(x)\, \chi_n^S(\phi), \tag{3.74}$$

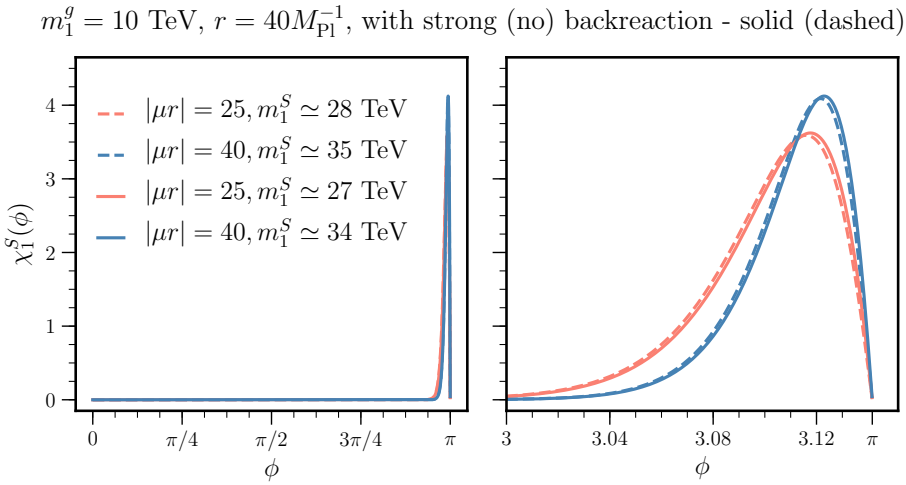

Figure 3.8: *Profiles of the first KK resonance of the bulk scalar field for $|\mu r| = 25$ (red) and 40 (blue), for $\gamma = 0.5$ (solid lines) and $\gamma = 0$ (dashed lines). The different mass eigenvalues are shown in the legend. In all cases we have fixed $m_1^g = 10$ TeV.*

into the action (3.5) and keeping the quadratic terms in the field. This allows us to obtain the EOM

$$\left[\partial_\phi^2 - 4\,\sigma'(\phi)\,\partial_\phi - |\mu r|^2\left(3v^2(\phi) - 1\right) + r^2 (m_n^S)^2 e^{2\sigma(\phi)}\right] e^{\sigma}\chi_n^S(\phi) = 0, \tag{3.75}$$

that together with the normalization condition for the scalar profiles

$$2\int_0^\pi d\phi\; \chi_n^{S\dagger}(\phi)\,\chi_m^S(\phi) = \delta_{mn}\,, \tag{3.76}$$

defines the Sturm-Liouville problem.

In figure 3.8 we show the numerical solutions of the lightest odd scalar KK modes for strong (solid) and no (dashed) backreaction for the input values $|\mu r| = 25$ (red) and $|\mu r| = 40$ (blue). We have fixed the mass of first KK gluon $m_1^g = 10$ TeV, whereas the corresponding eigenvalue, i.e. the mass of the first KK scalar mode, which is obtained as a solution of the Sturm-Liouville problem, is shown in the legend for each case considered. Note that the Dirichlet BC for the scalar field are incompatible with the existence of a zero-mode solution. We find the first KK excitation of the scalar field to have a mass of order 30 TeV for the input parameters leading to $m_1^g = 10$ TeV. This means, in particular, that the masses of the scalar KK resonances are out of the reach of the LHC and that the fermion and vector KK resonances would be the first to be accesible for future direct search experiments. Note that the main difference both in the profiles and the scalar masses are caused by the different values of the dimensionless parameter $|\mu r|$, with $-|\mu|$ the scalar 5D mass parameter, whereas the solutions do not seem to notice whether backreaction effects on the metric are present or not.

Even if our estimates for the mass of the lowest-lying scalar resonances are beyond the kinematic reach of the LHC, it is illustrative to investigate which are the main decay channels. Therefore, we computed some of the relevant decay modes for the first KK mode of the bulk scalar, which from now on we will denote by $S \equiv S^1$, and show the different branching ratios (BR) in table 3.2. We work in the massless quark limit $v_h \to 0$ and use the notation where q stands for the (u, d, c, s, b) quarks, while Q denotes the KK excitations of all SM fermion chiral fields besides t_R, whose KK excitation is denoted by T. This is justified by the fact that, for the cases at hand,

$(\lvert\mu r\rvert, \gamma)$	$S \to qQ$	$S \to tQ$	$S \to tT$	$S \to QQ$	$S \to TT$	$S \to gg$	m_S (TeV)	m_T (TeV)
(25, 0)	0.07	0.04	0.01	0.86	$2 \cdot 10^{-5}$	0.011	28	14
(40, 0)	0.06	0.03	0.01	0.89	$7 \cdot 10^{-4}$	0.008	35	14
(25, 0.5)	0.16	0.05	0.03	0.75	0	0.009	27	20
(40, 0.5)	0.06	0.03	0.12	0.77	0	0.007	34	22

Table 3.2: *Main BR for the first KK resonance of the $\mathbb{Z}_2$-odd scalar, S, for all cases under consideration. Last two columns show the values of m_S and m_T while $m_Q \sim \mathcal{O}(10)$ TeV for all the cases shown, see main text for more details.*

all the KK resonances besides T share approximately the same mass $m_Q \approx 10$ TeV. Remember that the tree-level decay into two SM quarks is forbidden in the massless quarks limit, i.e. when $v_h/M_{\text{KK}} \to 0$, as in this case there is no mixing between the zero modes and KK fermions, and the S scalar field only couples to modes belonging to the same 5D field.

We find the preferred decay channel to be the one where S decays into two KK resonances, with BR($S \to QQ$) $\sim 80 - 90\%$. Decays into one SM quark and the KK quark have significantly smaller BR. The decay channel $S \to TT$ is open for $\gamma = 0$ and closed for $\gamma = 0.5$, where $2m_T > m_S$. For the decay into gluons, $S \to gg$, we have estimated the BR by summing over the first few KK fermions in the loop. As one can see from the table, this mode has a small BR of approximately 1%. In principle, the decay channel $S \to GG$, with G being the first KK excitation of the gluon, is kinematically open and should be taken into account. While its calculation is highly non trivial we expect a BR not much larger than that for $S \to gg$, which is already pretty small. We also neglect EW loop processes like $S \to \gamma\gamma, S \to W^+W^-$, $S \to ZZ$, $S \to \gamma Z$, and similar ones involving their KK resonances. We find the total decay width of the scalar to be $\Gamma/m_S \sim (2-4) \cdot 10^{-4}$ for the different cases presented in table 3.2, due to the small couplings of the scalar to the different fermions. For computing 3.2 we have solved the background solutions resulting in $m_g^1 = 10$ TeV and set $\lambda/r = 1$, for computing the couplings of the S scalar to the different particles. Note that the ratio Γ/m_S can be adjusted by changing the value of λ/r, which defines the effective coupling of the 4D fermion resonances to the S scalar (this will become relevant next chapter).

The discovery of such particle, even at a possible 100 TeV collider [187], seems extremely challenging. We have checked that the leading-order cross-section $\sigma(gg \to S)$ for a center-of-mass energy $\sqrt{s} = 100$ TeV and the PDF set `CT14nlo` is of the order of $\mathcal{O}(10^{-7})$ pb. Associated Q production $pp \to SQ$ via the t-channel exchange of a Q resonance and the subsequent $S \to QQ$ decay seems the more promising channel to discover such an elusive resonance. However, the collider study necessary to precisely address this question is beyond the scope of our work.

3.4 Dynamical bulk fermion masses

As previously mentioned, one of the main motivations behind this work is to provide a dynamical mechanism to generate fermion bulk masses and therefore to solve the flavor puzzle using the mechanism described in section 2.7. The bulk fermion bilinear $\bar{\Psi}\Psi$ has to be odd under $\phi \to -\phi$ transformations in order to respect the $\mathbb{Z}_2$ symmetry of the model. What we have proposed is that these masses arise *à la* bulk "Higgs mechanism", i.e. through the coupling to $\mathbb{Z}_2$-odd scalar field which acquires a VEV along the extra dimension $\langle\Sigma\rangle = \omega(\phi)$. Contrary to the usual *ad-hoc* approach, where the bulk mass parameters are multiplied by sgn(ϕ) to make the 5D mass term of

the Lagrangian $\mathbb{Z}_2$ invariant, now both the profile along the extra dimension and the parity of the VEV are a byproduct of the parity assignment and the dynamics of the 5D field. In this section, we present this mechanism of generating bulk fermion masses for a single fermion Ψ, singlet under the gauge group. We will generalize it to the three-generation case and the SM gauge group in the next section.

Taking the terms involving the sgn(ϕ) from the action (2.78), and replacing them for Yukawa coupling terms of the fermion 5D fields with the bulk scalar, the fermion action can be written as

$$S_\Psi^{(5\mathrm{D})} = 2\int d^4x \int_0^\pi d\phi \sqrt{g}\left\{ E_a^N \left[\frac{i}{2}\bar{\Psi}\,\Gamma^a(\partial_N - \overleftarrow{\partial}_N)\Psi + \frac{\omega_{bcN}}{8}\,\bar{\Psi}\{\Gamma^a,\sigma^{bc}\}\Psi \right] - \mathcal{Y}\bar{\Psi}\Sigma\Psi \right\}, \qquad (3.77)$$

where again $\Gamma_A = (\gamma_\mu, i\gamma_5)$ are the 5-dimensional Dirac matrices, E_a^N is the inverse fünfbein, and ω_{bcN} is the spin connection, as in section 2.5. The last term in the action is the 5D Yukawa interaction of the fermion Ψ with the odd scalar Σ with Yukawa coupling $\mathcal{Y}$. Remember that the mass dimensions of the fields and couplings in the above action are $[\Psi] = 2$, $[\Sigma] = 3/2$, and $[\mathcal{Y}] = -1/2$.

After the scalar field develops its VEV, the above action for the fermion field can be rewritten as

$$S_\Psi^{(5\mathrm{D})} = 2\int d^4x \int_0^\pi d\phi \sqrt{g}\left\{ E_a^N \left[\frac{i}{2}\bar{\Psi}\Gamma^a(\partial_N - \overleftarrow{\partial}_N)\Psi \right] - \omega(\phi)\mathcal{Y}\bar{\Psi}\Psi \right\} + S_{\Psi,\mathrm{int}}^{(5\mathrm{D})}, \qquad (3.78)$$

where $S_{\Psi,\mathrm{int}}^{(5\mathrm{D})}$ contains the terms defining the fermion interactions with the odd scalar fluctuation $S(x,\phi)$.

We KK-decompose the bulk fermions into the 4D chiral fermion modes as in (2.82),

$$\Psi(x,\phi) = \sum_{\substack{n=0 \\ A=L,R}}^{\infty} \psi_n^A(x)\frac{e^{2\sigma(\phi)}}{\sqrt{r}} f_n^A(\phi), \qquad (3.79)$$

where $\psi_n^{L,R}(x)$ are the left- and right-handed 4D chiral fermions with their corresponding ϕ-dependent profiles $f_n^{L,R}(\phi)$. The prefactor $e^{2\sigma(\phi)}/\sqrt{r}$ is introduced to ensure the canonical normalization of the KK modes and to make the wave-functions $f_n^{L,R}(\phi)$ dimensionless. As a consequence of the above KK decomposition, the $f(\phi)$-profiles satisfy the orthogonality condition

$$2\int_0^\pi d\phi\, e^{\sigma(\phi)} f_m^{L,R*}(\phi)\, f_n^{L,R}(\phi) = \delta_{mn}. \qquad (3.80)$$

Using the variational principle and integrating by parts in the action (3.78), we obtain the EOM for the fermion profiles

$$\left[\pm\frac{1}{r}\,\partial_\phi - \mathcal{Y}\omega(\phi)\right] f_n^{L,R}(\phi) = -m_n\, e^{\sigma(\phi)} f_n^{R,L}(\phi), \qquad (3.81)$$

along with BC

$$e^{-4\sigma}\delta\bar{\Psi}\gamma_5\Psi\Big|_{\phi=0,\pi} = 0. \qquad (3.82)$$

The plus (minus) sign on the left-hand side of (3.80) refers to f_n^L (f_n^R). The masses of the KK resonances are denoted by m_n. It is instructive to introduce a dimensionless quantity

$$c \equiv \mathcal{Y}\sqrt{\frac{6}{\lambda}}\,\frac{|\mu r|}{\sigma'(\pi)} \qquad (3.83)$$

such that (3.81) can be recast in the dimensionless form

$$\Big[\pm\partial_\phi - c\,\sigma'(\pi)\,v(\phi)\Big] f_n^{L,R}(\phi) = -r m_n e^{\sigma(\phi)} f_n^{R,L}(\phi), \qquad (3.84)$$

where we have replaced $\omega(\phi)$ with $v(\phi)$ as in (3.13). Note that the definition of c has been done so that in the case where $v(\phi)$ is replaced by sgn(ϕ), we recover the conventional dimensionless bulk mass parameter $c = m/k$, as was introduced in (2.84).

Following the same arguments as in section 2.5, the BC in (3.82) guarantees either $f_m^{L*}(0)\, f_n^R(0) = 0$, or $f_m^{L*}(\pi)\, f_n^R(\pi) = 0$, i.e. for a given field and assuming the same $\mathbb{Z}_2$ behavior at both branes, either the LH or the RH component of the field has to be $\mathbb{Z}_2$-odd. That allows us to define a $\mathbb{Z}_2$-parity on the orbifold to be given by $\pm\gamma_5$. The zero-mode profiles are obtained by solving (3.81) with $m_n = 0$. The equation then determines the $\mathbb{Z}_2$-even profile functions, while the $\mathbb{Z}_2$-odd functions vanish.

3.4.1 Fermion zero modes

The fermion profiles are now given by (3.84) and, in contrast to what was obtained in section 2.5.1, they can only be obtained numerically. From (3.84) the expression for the zero-mode profiles read

$$f_0^{L,R}(\phi) = f_0^{L,R}(0)\, \exp\left(\pm c\, \sigma'(\pi) \int_0^\phi v(z)\, dz\right). \tag{3.85}$$

As usual, the chirality chosen to vanish for a given fermion field at one of the branes, e.g. $f_0^R(0) = 0$ or $f_0^L(0) = 0$, will not have a zero mode, since the differential equation along with the BC from (3.84) cannot be satisfied for a non-trivial solution.

We would like to compare the solutions for the fermion zero modes computed using the background solutions shown in figure 3.6, including strong and no backreaction effects on the metric. With this idea in mind we will define the profile "tilde" and "hat" functions, $\tilde{f}_{\text{UV,IR}}(\phi)$ and $\hat{f}_{\text{UV,IR}}(\phi)$, where UV and IR denote the brane at which the profile has a stronger presence, while $\tilde{f}(\phi)$ and $\hat{f}(\phi)$ will be defined in (3.86) and (3.87), respectively. We show these profile functions in figure 3.9 for values of the dimensionless 5D mass parameter c such that the fermion profiles have the same value on the IR brane. This will be particularly pertinent for the next section, where we would like to study the impact on the flavor structure of the model arising from the non-trivial VEV profile, $v(\phi)$, and the modification of the metric, $\sigma(\phi)$, since the values of the fermion profiles at the IR brane are the relevant parameters to reproduce the quark masses and mixing angles, for a given 5D Yukawa matrix in the brane-localized Higgs scenario. Note that for a bulk Higgs scenario the mechanism would be similar but, however, fermion masses would be given by the integral of the overlap of the different profiles. Moreover, we represent in the upper panels the rescaled profiles

$$\tilde{f}^{L,R}(\phi) \equiv \sqrt{\frac{2}{\sigma'(\pi)}}\, e^{\sigma(\pi)/2}\, f_0^{L,R}(\phi)\,, \tag{3.86}$$

defined in such a way that their values at the IR brane, $\tilde{f}(\pi) \equiv F(c)$, are the factors responsible for the exponential hierarchies expected in the 4D effective Yukawa matrices, obtained after weighting these factors with the different entries of the anarchic 5D Yukawa couplings, see (3.93) below. On the other hand, the lower panels represent the "properly normalized" fermion profiles

$$\hat{f}^{L,R}(\phi) = e^{\sigma(\phi)/2} f^{L,R}(\phi), \qquad \text{with} \qquad \int_{-\pi}^{\pi} \hat{f}^{L,R}(\phi)^2 d\phi = 1\,, \tag{3.87}$$

see (2.91). Such profiles are useful to visualize the changes on flavor observables, since are precisely these functions the ones that enter (convoluted with the corresponding 5D gauge propagators) in $\Delta F = 1$ and $\Delta F = 2$ processes [119,178–180]. Since these convolutions are very sensitive to the behavior of the functions near the IR brane, observing the change of these profiles in the

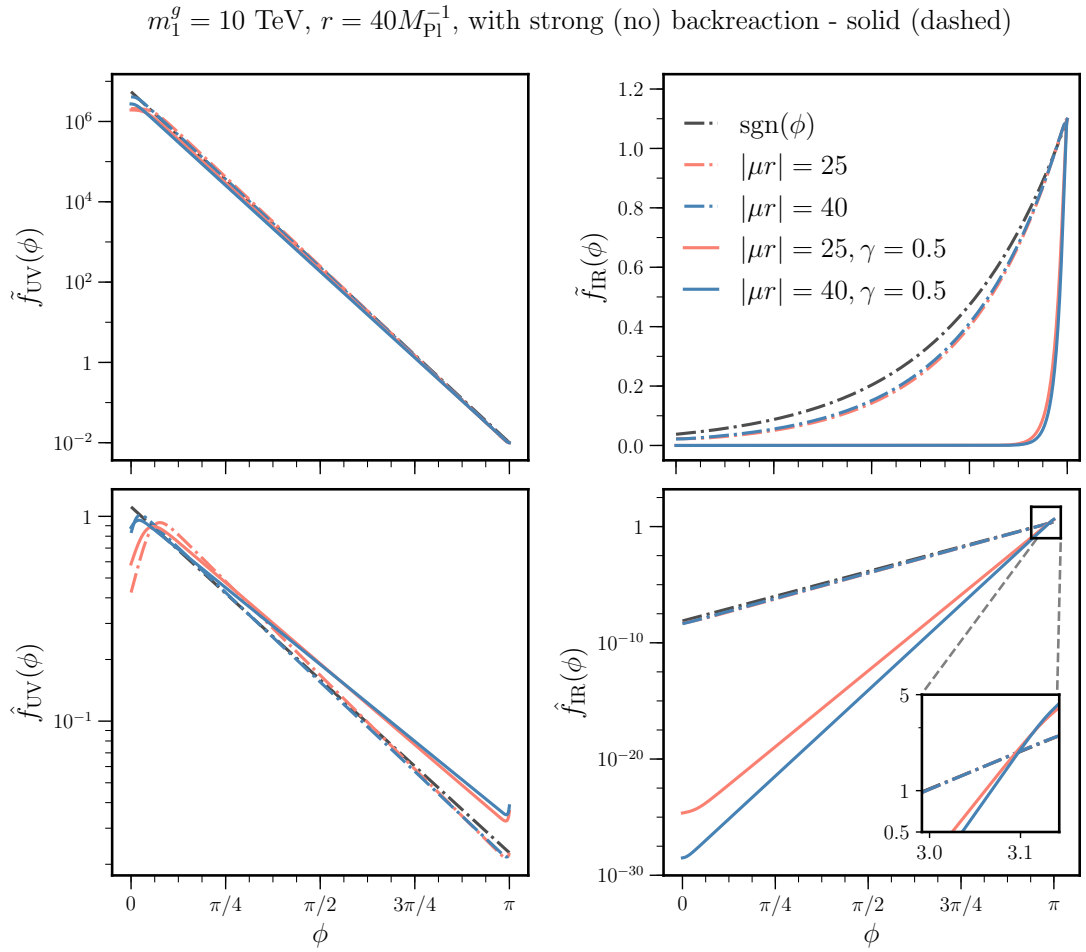

Figure 3.9: *Profiles of fermion zero modes obtained in the original RS model (black), i.e. using a sgn(ϕ) function in front of the bulk masses, and in our model, where bulk masses are generated dynamically through the VEV of a scalar field, considering both strong and no backreaction (solid and dashed lines, respectively) and using the background solutions shown in figure 3.6. The left (right) panels show profiles which are localized near the UV (IR) brane. In each case, we adjust the dimensionless couplings c such that the values of the profiles on the IR brane are the same in all cases, with $F(c) = \tilde{f}(\pi) = 0.01$ and 1.1 for the left and right panels, respectively. In the upper panels we show the rescaled profiles, $\tilde{f}(\phi)$, defined in* (3.86)*, whereas the lower panels display the "properly normalized" solutions, $\hat{f}(\phi)$, defined in* (3.87)*. See text for more details.*

vicinity of the IR brane gives a good idea of the impact the scenarios examined here may have on flavor-violating processes.

The black dashed line in the different panels shows, for comparison, the profiles obtained in the conventional RS model without the bulk scalar field, i.e. the case for which fermion 5D bulk masses are simply multiplied by sgn(ϕ). We observe that in the case of no backreaction our solutions lie rather close to the black dashed line, meaning that our dynamical mechanism for generating brane-localized fermion profiles succeeds to give profile functions which are numerically close to those

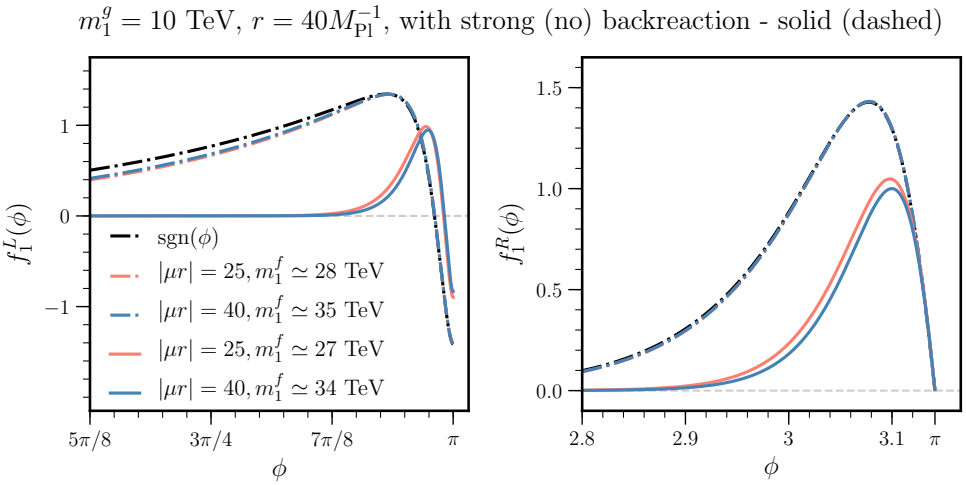

Figure 3.10: *Profiles of the first KK resonances of a fermion 5D field with a LH zero mode, obtained in the original RS model (black), i.e. using a sgn(ϕ) and in our model, where 5D bulk masses are generated dynamically through the VEV of a scalar field, considering strong and no backreaction (solid and dashed lines, respectively). We use the background solutions shown in figure 3.6. The left (right) panels show the profiles for the LH (RH) chiralities.*

of the conventional RS model. However, in contrast to what we found in the previous section for the scalar field, the backreaction on the metric can have a significant impact on the shapes of the profiles. This is specially noticeable for the profiles pointing towards the IR brane, see the right panels in figure 3.9. The phenomenological consequences of this observation will be studied later.

3.4.2 Fermion KK modes

As discussed previously in section 2.5 the EOM for higher KK resonances can be obtained from (3.84) by taking a derivative w.r.t. the fifth coordinate. This decouples the EOM and gives

$$\Big[\partial_\phi^2 - \sigma'(\phi)\,\partial_\phi \mp c\,\sigma'(\pi)v'(\phi) + r^2 m_n^2\, e^{2\sigma(\phi)} \pm c\,\sigma'(\pi)\sigma'(\phi)v(\phi) - c^2\,\sigma'^2(\pi)v^2(\phi)\Big] f_n^{L,R}(\phi) = 0. \tag{3.88}$$

As an example, we present in figure 3.10 numerical solutions for the RH and LH profile functions for the first KK excitation of a fermion with LH zero mode. The meaning and labeling of the various curves is the same as in figure 3.9. For each choice of parameters, we also give the value of the corresponding KK fermion mass.

3.5 A dynamical solution to the flavor puzzle

One of the major strengths of RS models is that they not only provide a solution to the hierarchy problem but also naturally explain the large hierarchies observed in the spectrum of SM quark masses and mixing angles. We introduced the mechanism that allows us to reproduce the observed quark structure in section 2.7. Moreover, we commented that for the leptonic sector such a

mechanism is not directly applicable, since the PMNS mixing matrix features large mixing angles. However, in section 2.7 we implemented this framework using sgn(ϕ) for making the fermion bulk masses $\mathbb{Z}_2$ dependent. In this section, we will investigate whether this continues to be the case in scenarios where the bulk masses are generated dynamically. We will also study the implications of the dynamical approach for flavor physics. In particular, we will explore how the modifications of the fermion profiles affect the usual RS-GIM mechanism [21, 170, 188] and study their impact on the $\Delta F = 2$ observable ϵ_K, measuring CP violation in $K - \bar{K}$ mixing, which typically sets the strongest flavor constraint in models with WED [119, 178–180].

The Yukawa interactions with the Higgs field, localized on the IR brane, induce a mixing between the would-be zero modes and the KK excitations of different 5D fields. These contributions are of $\mathcal{O}(v_h^2/M_{\text{KK}}^2)$ for both the mass eigenvalues and the CKM mixing matrix. In order to simplify the calculations and have approximate expressions describing fermion mixings we will restrict ourselves to the ZMA, in a similar manner as we presented it in section 2.7. Remember that in this approximation fermion bulk profiles are solved with the Yukawa couplings "switched-off", and these couplings are included as a $\mathcal{O}(v_h^2/M_{\text{KK}}^2)$ perturbation. Actually, since the overlaps of the different quark profiles with the Higgs profiles are proportional to the corresponding quark masses, up to some common multiplicative factor. Therefore this approximation holds best for the light SM quarks, for which the neglected terms are indeed much smaller than $\mathcal{O}(v_h^2/M_{\text{KK}}^2)$.

3.5.1 Hierarchies of fermion masses and mixings

We now consider three generations of 5D fermions in the bulk interacting with a scalar sector consisting of the odd scalar in the bulk and the Higgs doublet on the IR brane. If we denote by Q and q^c the three-component vectors in flavor space belonging to $SU(2)_L$ doublets and singlets, respectively, the quadratic terms in the 5D action can be written in the form

$$\begin{aligned} S^{(5\text{D})}_{\text{ferm, 2}} = \int d^4x \int_{-\pi}^{\pi} d\phi \sqrt{g} \Bigg\{ & \frac{i}{2} E_a^N \Big[\bar{Q}\, \Gamma^a (D_N - \overleftarrow{D}_N) Q + \sum_{q=u,d} \bar{q}^c\, \Gamma^a (D_N - \overleftarrow{D}_N) q^c \Big] \\ & - \omega(\phi) \Big[\bar{Q} \boldsymbol{\mathcal{Y}}_Q Q - \sum_{q=u,d} \bar{q}^c \boldsymbol{\mathcal{Y}}_q q^c \Big] \\ & - \delta(|\phi| - \pi) \frac{\sqrt{|\hat{g}_i|}}{g} \frac{v_h\, e^{\sigma(\pi)}}{\sqrt{2}} \Big[\bar{u}_L\, \boldsymbol{Y}_u^{(5\text{D})}\, u_R^c + \bar{d}_L\, \boldsymbol{Y}_d^{(5\text{D})}\, d_R^c + \text{h.c.} \Big] \Bigg\} \,, \end{aligned} \tag{3.89}$$

similar to (2.126), where now the 5D fermion masses have a dynamical origin. Without loss of generality we work in the "bulk-mass basis", where $\boldsymbol{\mathcal{Y}}_{Q,q}$ denote diagonal matrices leading to real bulk masses, see the discussion in section 2.7, and $\boldsymbol{Y}_q^{(5\text{D})}$ are the 5D Yukawa matrices which couple different 5D fermion fields to the Higgs field.

The 5D up-type quarks can be KK-decomposed as follows

$$\begin{aligned} u_L(x,\phi) &= \frac{e^{2\sigma(\phi)}}{\sqrt{r}} \sum_n \boldsymbol{\mathcal{C}}_n^{(Q)}(\phi)\, u_L^{(n)}(x) \,, \qquad u_R(x,\phi) = \frac{e^{2\sigma(\phi)}}{\sqrt{r}} \sum_n \boldsymbol{\mathcal{S}}_n^{(Q)}(\phi)\, u_R^{(n)}(x) \,, \\ u_L^c(x,\phi) &= \frac{e^{2\sigma(\phi)}}{\sqrt{r}} \sum_n \boldsymbol{\mathcal{S}}_n^{(u)}(\phi)\, u_L^{(n)}(x) \,, \qquad u_R^c(x,\phi) = \frac{e^{2\sigma(\phi)}}{\sqrt{r}} \sum_n \boldsymbol{\mathcal{C}}_n^{(u)}(\phi)\, u_R^{(n)}(x) \,, \end{aligned} \tag{3.90}$$

where the diagonal matrices $\boldsymbol{\mathcal{C}}_n^{(Q,u)}$ denote $\mathbb{Z}_2$-even profiles, while $\boldsymbol{\mathcal{S}}_n^{(Q,u)}$ are also diagonal matrices and correspond to odd profiles. The index n labels the mass eigenstates, with fermion masses m_n and spinor fields $u_{L,R}^{(n)}(x)$. The spinor fields on the left-hand side of the equations are three-component vectors in flavor space. The equations of motion for the different profiles in the ZMA correspond to those presented in section 3.4.

Inserting these decompositions into the action, the Yukawa interaction on the IR brane reads

$$S^{(4D)} \supset -\int d^4x \, \frac{v_h \, e^{\sigma(\pi)}}{\sqrt{2}\, r} \left[\bar{u}_L^{(n)}(x) \, \boldsymbol{\mathcal{C}}_n^{(Q)}(\pi) \, \boldsymbol{Y}_u^{(5D)} \, \boldsymbol{\mathcal{C}}_m^{(u)}(\pi) \, u_R^{(m)}(x) + \text{h.c.} \right], \tag{3.91}$$

where it is convenient to use the fermion fields normalized as in (3.86). It is clear from (3.85) that, for a given pair of background solutions $\sigma(\phi)$ and $v(\phi)$, the values of the profiles of the different zero modes on the IR brane depend only on the dimensionless quantity c, defined in (3.83). Therefore, it is useful to define the functions

$$F(c_{X,i}) = \left(\tilde{\boldsymbol{\mathcal{C}}}_0^X(\pi) \right)_{ii} , \tag{3.92}$$

i.e., the value of the zero-mode profile of the field $X = Q, u, d$ on the IR brane, which depend only on the parameter $c_{X,i}$. Using this convention, we define the dimensionless Yukawa and the effective 4D Yukawa of the SM fields

$$\boldsymbol{Y}_q^{(5D)} = \frac{2\, \boldsymbol{Y}_q \, r}{\sigma'(\pi)}, \qquad (\boldsymbol{Y}_q^{\text{eff}})_{ij} = F(c_{Q,i}) \, (\boldsymbol{Y}_q)_{ij} \, F(c_{q,i}), \tag{3.93}$$

as in [110], but with the subtlety of trading kr for $\sigma'(\pi)$. The Yukawa entries $\boldsymbol{Y}_q$ are again considered to have modulo of order unity, i.e. $|\boldsymbol{Y}_q| \sim \mathcal{O}(1)$. Once the Yukawa couplings on the IR brane are "switched on" a mass matrix is obtained for the SM fields. The physical masses are obtained by solving the eigenvalue equation

$$\det\left(\boldsymbol{I}\, m_n^2 - \frac{v_h^2}{2} (\boldsymbol{Y}_q^{\text{eff}})(\boldsymbol{Y}_q^{\text{eff}})^\dagger \right) = 0 \, . \tag{3.94}$$

The eigenvectors of the matrices $\boldsymbol{Y}_q^{\text{eff}} \left(\boldsymbol{Y}_q^{\text{eff}}\right)^\dagger$ and $\left(\boldsymbol{Y}_q^{\text{eff}}\right)^\dagger \boldsymbol{Y}_q^{\text{eff}}$ (with $n = 1, 2, 3$ and $Q = U, D$, $q = u, d$) form the columns of the unitary matrices $\boldsymbol{U}_q$ and $\boldsymbol{W}_q$ appearing in the singular-value decomposition

$$\boldsymbol{Y}_q^{\text{eff}} = \boldsymbol{U}_q \, \boldsymbol{\lambda}_q \, \boldsymbol{W}_q^\dagger \, , \tag{3.95}$$

where

$$\boldsymbol{\lambda}_u = \frac{\sqrt{2}}{v_h} \, \text{diag}(m_u, m_c, m_t) \, , \qquad \boldsymbol{\lambda}_d = \frac{\sqrt{2}}{v_h} \, \text{diag}(m_d, m_s, m_b) \, . \tag{3.96}$$

In this approximation, the fields are mixed because of the Yukawa interactions on the IR brane. The 5D mass eigenstates and the SM mass eigenstates are related through the matrices $\boldsymbol{U}_q$ and $\boldsymbol{W}_q$, and the CKM mixing matrix is given by

$$\boldsymbol{V}_{\text{CKM}} = \boldsymbol{U}_u^\dagger \, \boldsymbol{U}_d \, . \tag{3.97}$$

We fit the bulk mass parameters $\boldsymbol{c}_X$ from the values of $F(\boldsymbol{c}_X)$ for a randomly generated Yukawa matrices $\boldsymbol{Y}_u$ and $\boldsymbol{Y}_d$. Assuming a hierarchical structure of the zero-mode profiles on the IR brane, i.e.

$$|F(c_{X_1})| < |F(c_{X_2})| < |F(c_{X_3})| \, , \tag{3.98}$$

the system is not determined and the different $F(c_{X,i})$ parameters can be expressed in terms of a single one, which we chose to be $F_2 \equiv F(c_{Q_2})$, as in [110]. See section 2.7 and appendix B, for the complete formulae.

3.5.2 Impact on flavor constraints: ϵ_K

We now explore how the changes in the fermion profiles caused by the non-trivial ϕ dependence of the VEV of the bulk scalar field, see e.g. figure 3.9, affect physical observables in flavor physics.

Because of the RS-GIM mechanism, most of the flavor violating observables are suppressed below the current experimental limits, see [114, 119, 181, 189, 190]. However, this mechanism is not enough to suppress NP contributions to CP violation in the Kaon sector below it current experimental limits. Therefore, we will focus our study to the particular case of the ϵ_K parameter, since CP violation in K–$\bar{K}$ mixing, as measured by this parameter, provides the most stringent flavor constraint in models with WED [119, 178–180, 191].

We follow closely the analyzes on ϵ_K in RS models from [110,179–181] and adopt the following parametrization for NP [192]

$$\mathcal{L}_{\text{eff}}^{\Delta S=2} = \sum_{i=1}^{5} C_i\, Q_i + \sum_{i=1}^{3} \tilde{C}_i\, \tilde{Q}_i\,, \tag{3.99}$$

where the operators relevant for K–$\bar{K}$ mixing are

$$\begin{aligned} Q_1 &= (\bar{d}_L\gamma^\mu s_L)\,(\bar{d}_L\gamma_\mu s_L)\,, \quad & \tilde{Q}_1 &= (\bar{d}_R\gamma^\mu s_R)\,(\bar{d}_R\gamma_\mu s_R)\,, \\ Q_4 &= (\bar{d}_R s_L)\,(\bar{d}_L s_R)\,, & Q_5 &= (\bar{d}_R^\alpha s_L^\beta)\,(\bar{d}_L^\beta s_R^\alpha)\,. \end{aligned} \tag{3.100}$$

A summation over color indices α, β is understood. In our convention the Wilson coefficients include only the NP contributions, i.e. $C_i \equiv C_i^{\text{NP}}$. For simplicity we only consider the leading contribution, arising from the tree-level exchange of KK gluons, and neglect contributions involving the exchange of other gauge bosons or scalar fields. In the ZMA, these contributions take the form

$$\begin{aligned} C_1 &= 4\pi^2\alpha_s\, r^2 \left(1 - \frac{1}{N_c}\right) (\widetilde{\Delta}_D)_{12} \otimes (\widetilde{\Delta}_D)_{12}\,, & \tilde{C}_1 &= C_1\big|_{D\to d}\,, \\ C_4 &= -4\pi^2\alpha_s\, r^2\, (\widetilde{\Delta}_D)_{12} \otimes (\widetilde{\Delta}_d)_{12}\,, & C_5 &= -\frac{C_4}{N_c}\,, \end{aligned} \tag{3.101}$$

where α_s is the strong coupling constant and $N_c = 3$ stands for the number of colors. The notation $(\widetilde{\Delta}_X)_{12} \otimes (\widetilde{\Delta}_Y)_{12}$ is defined as

$$\begin{aligned} (\widetilde{\Delta}_X)_{12} \otimes (\widetilde{\Delta}_Y)_{12} = (\mathcal{U}_X^\dagger)_{1j}(\mathcal{U}_X)_{j2}(\mathcal{U}_Y^\dagger)_{1k}(\mathcal{U}_Y)_{k2} \\ \times \int_0^\pi d\phi \int_0^\pi d\phi' \int_0^{\phi_<} d\bar{\phi}\, e^{2\sigma(\bar{\phi})} e^{\sigma(\phi)} e^{\sigma(\phi')} \left(\tilde{\mathcal{C}}_{0,j}^X(\phi)\right)^2 \left(\tilde{\mathcal{C}}_{0,k}^Y(\phi')\right)^2\,, \end{aligned} \tag{3.102}$$

where $\mathcal{U}_D = U_d$ and $\mathcal{U}_d = W_d$. Note that in this limit the Wilson coefficients relevant for computing ϵ_K only depend on the background solutions and the fermion profiles, and therefore on the Yukawa couplings. It can be seen from (3.65) that only the first term in the gauge propagator appears in (3.102), since the other terms cancel due to orthogonality and unitarity of the fermion profiles and the $\mathcal{U}$-matrices, respectively. It is clear from (3.102) that the more a particular fermion has its "properly normalized" profile $e^{\sigma(\phi)/2}\mathcal{C}_0(\phi)$ shifted away from the IR brane, the smaller its contribution to the Wilson coefficients would be. Moreover, one can readily conclude from this and from the behavior of the fermion profiles shown in the lower panels of figure 3.9, that large values of the backreaction tend to worse the RS-GIM mechanism. This is the case as the "properly normalized" profiles grow in the vicinity of the IR brane for both UV-localized and IR-localized fermions, when compared to the profiles obtained for none or negligeable backreaction.

In terms of the effective Lagrangian (3.99), the quantity ϵ_K is given by

$$\epsilon_K = \frac{-\kappa_\epsilon\, e^{i\varphi_\epsilon}}{\sqrt{2}\,(\Delta m_K)_{\text{exp}}}\, \text{Im}\,\langle K^0|\,\mathcal{L}_{\text{eff}}^{\Delta S=2}\,|\bar{K}^0\rangle\,. \tag{3.103}$$

The current experimental value [46] and SM prediction [3, 193] for $|\epsilon_K|$ are

$$|\epsilon_K|^{\text{exp}} = (2.228 \pm 0.011) \times 10^{-3}\,, \qquad |\epsilon_K|^{\text{SM}} = (2.16 \pm 0.18) \times 10^{-3}\,. \tag{3.104}$$

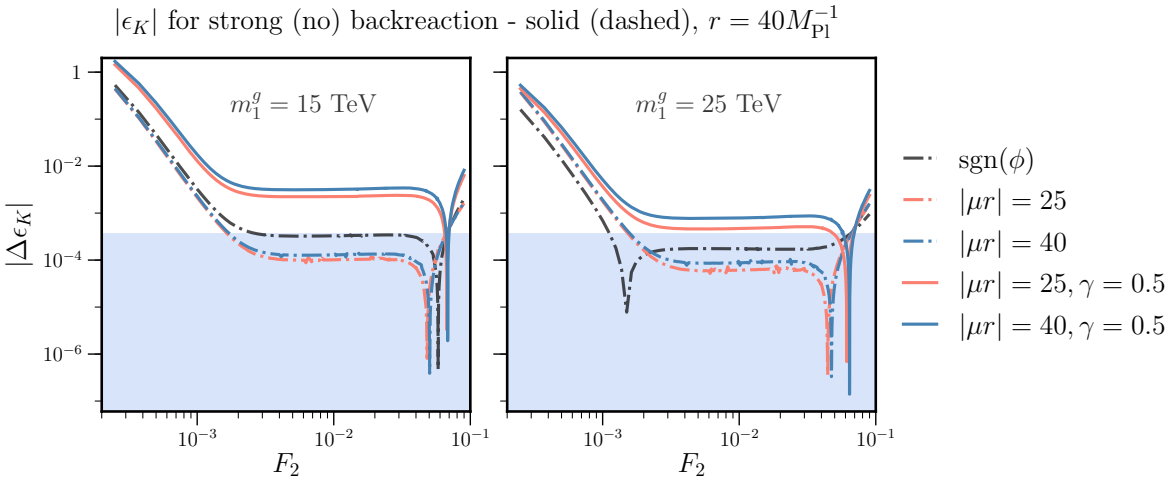

Figure 3.11: *$|\Delta\epsilon_K|$ as a function of F_2, computed with fermion profiles obtained by using sgn(ϕ) (black) and in our model, i.e. with dynamical 5D fermion masses, for different values of $|\mu r|$ and considering strong and no backreaction (solid and dashed lines, respectively). In the left (right) figure we have fixed $m_1^g = 15$ TeV (25 TeV). We show in blue the area allowe from*

To get a better understanding for the different contributions playing a role in ϵ_K, it is useful to note that

$$|\epsilon_K - \epsilon_K^{\rm SM}| \propto {\rm Im}\left[C_1 + \tilde{C}_1 + 213\left(C_4 + \frac{C_5}{N_c}\right)\right] \tag{3.105}$$

for a matching scale $\mu_{\rm NP} = 15\,$TeV.

For our numerical analysis we generate random Yukawa matrices with complex entries of norm in the interval $[1/3, 3]$ and use a χ^2 distribution to select parameter sets for which the quark masses and CKM parameters are reproduced within 95% CL. In figure 3.11 we plot the prediction for $\Delta\epsilon_K \equiv |\epsilon_K| - |\epsilon_K|^{\rm exp}$ assuming different values of $|\mu r|$, for strong and no backreaction, as a function of F_2. The left and right panels correspond to $m_1^g = 15$ TeV and 25 TeV, respectively. Moreover, for comparison we also show with a black dashed line the conventional RS case, corresponding to bulk fermion masses multiplied by a sgn(ϕ) function. We also show with a blue band the constraint

$$\Delta\epsilon_K \lesssim 4.2 \times 10^{-4}\,, \tag{3.106}$$

note that this quantity corresponds to the 2σ uncertainty of the SM prediction for ϵ_K derived in [3, 193]. We use this value as the main uncertainty for our prediction and demand that the central value of the experimental measurement lies within that range. Note that the uncertainty of the SM prediction is one order of magnitude larger than the experimental error, as can be seen in (3.104). We chose this uncertainty rather than the experimental error as in the defintion of $\Delta\epsilon_K$ we are already carrying such an uncertainty, and therefore the NP contribution is sensitive to this value, even if its not the origin.

For the purposes of making this figure, we consider a benchmark point defined by the following Yukawa matrices

$$\begin{aligned} \boldsymbol{Y}_u &= \begin{pmatrix} 0.109 + 1.865\,i & 2.000 - 1.324\,i & -0.706 + 1.514\,i \\ -2.163 - 0.615\,i & -0.695 - 0.483\,i & 2.299 - 1.604\,i \\ 1.517 + 1.399\,i & -0.928 + 0.065\,i & 2.204 + 0.970\,i \end{pmatrix}, \\ \boldsymbol{Y}_d &= \begin{pmatrix} 1.888 - 1.915\,i & 1.181 - 2.696\,i & 0.294 + 0.530\,i \\ 1.827 - 0.057\,i & 2.210 - 0.413\,i & 0.591 + 0.951\,i \\ 1.264 + 2.004\,i & -0.829 - 1.309\,i & -1.326 + 0.510\,i \end{pmatrix}. \end{aligned} \tag{3.107}$$

One can see from the left plot in figure 3.11 (i.e. for $m_1^g = 15$ TeV) that large values of the backreaction are disfavored by the current experimental measurement of ϵ_K. However, if we increase the KK scale to $m_1^g = 25$ TeV (right plot in figure 3.11), we find that it is only the model with $|\mu r| = 40$ and when we take the strong backreaction limit that remains in slight tension with the measured value of ϵ_K for a wide range of F_2 values. Note that our modified case without backreaction slightly improves the ϵ_K constraints as compared to the conventional RS case. However, as one can see from the above figure, considering a strong backreaction (we show results for $\gamma = 0.5$) leads to a larger contribution to ϵ_K and hence to more stringent constraints on the mass of the first KK gluon mode. This is a direct consequence of the behavior of the different "properly normalized" profiles shown in the lower panels of figure 3.9. For both UV and IR-localized fermions (corresponding to the lower left and right panels in figure 3.9, respectively), the inclusion of the backreaction results in an increase of the profiles in the vicinity of the IR brane. The values of these profiles near the IR brane play a central role for flavor-violating processes, because the different vector mediators inducing flavor-changing interactions are localized near the IR brane (when weighted with the appropriate powers of the metric). Thus, this results in a smaller flavor protection and hence a weakening of the RS-GIM mechanism [21, 170, 188], in agreement with figure 3.11. On the other hand, the shape of all curves in Figure 3.11 can be easily understood by taking into account that, for small values of F_2, all LH doublets are more and more UV localized, which makes their RH counterparts more and more IR localized in order to still produce the observed spectrum of fermion masses. Therefore, very small values of F_2 correspond to values where $\tilde{C}_1$ gets arbitrarily large to the point that can overcome the factor 213 in front of C_4 in (3.105). On the contrary, large values of F_2 correspond to values where exactly the opposite happens, leading to more and more IR-localized LH doublets and therefore to very large values of C_1. Note however, that both of these limits are constrained by reproducing the top-quark mass. For values where this arbitrary enhancement of one particular chirality ceases to occur, the dominant contributions to ϵ_K arise from C_4 and C_5, both of which are more or less constant, since they involve both fermion chiralities and are therefore expected to be controlled by the different fermion masses. This is due to the fact that, as one can readily see from (3.93), the effective Yukawa couplings and the corresponding SM fermion masses depend on the product of the profiles of both fermion chiralities on the IR brane. In the RS case, this leads to [119, 180]

$$C_4 = -N_c C_5 \sim 4\pi\alpha_s(kr\pi/M_{\text{KK}}^2)(2m_s m_d/v_h^2), \tag{3.108}$$

which explains the large plateau obtained for intermediate values of F_2 in all curves. Finally, the dips present in $\Delta\epsilon_K$ for some values of F_2 are the result of a cancellation between $\text{Im}(C_1)$ and $\text{Im}(C_4)$, which turn out to have opposite signs for our particular choice of Yukawa matrices.

Finally, in order to have a broader picture of the flavor impact of the non-trivial ϕ dependence of the bulk scalar VEV and the changes in the warp factor due to the backreaction, we computed the value of ϵ_K for a set of randomly generated Yukawa matrices. We choose a value of $F_2 = 0.01$, such that C_4 and C_5 give the leading contributions to ϵ_K and no large cancellations among the different contributions occur. Again, we used a χ^2 distribution for the generation of the Yukawa matrices. In figure 3.12 we show the histograms for the values of $|\epsilon_K|$ obtained from a set of $N_T = 500$

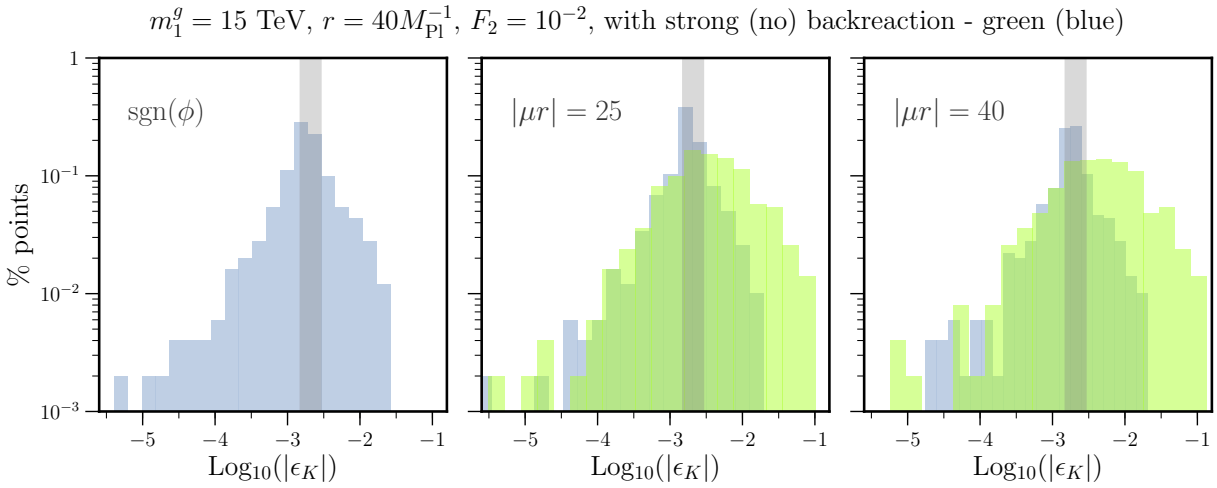

Figure 3.12: *Histogram showing the values of $|\epsilon_K|$ in the original RS model, and in our model for $|\mu r| = 25$ and 40, both in the case of zero and strong backreaction (blue and yellow bins respectively). In all these figures we fix $F_2 = 10^{-2}$ and $m_1^g = 15$ TeV.*

pairs of Yukawa matrices $\boldsymbol{Y}_u$ and $\boldsymbol{Y}_d$, for the different values of $|\mu r|$ and γ under consideration. For generating these points we have fixed $m_1^g = 15$ TeV. It can be seen that, as we found for the benchmark point given in (3.107), a small backreaction on the metric leads to a better agreement with $|\epsilon_K|^{\rm exp}$, whereas the strong backreaction case leads to a broader distribution and therefore to larger tension with data.

3.5.3 Flavor structure of low-lying scalar resonances

In extensions of the SM featuring a WED, the presence of TeV-scale KK resonances offers new possibilities for inducing flavor-changing interactions among the fermions of the SM. The flavor-changing couplings of KK gluons and other KK gauge bosons have been explored in detail in the literature, see e.g. [110, 119, 170, 178, 180, 191, 194]. At low energies, they give rise to various dimension-6 interactions in the effective weak Hamiltonian, whose contributions are suppressed by two powers of the KK mass scale ($\sim 1/M_{\rm KK}^2$).

In our model, the presence of scalar KK excitations provides a new source of flavor violation, and it is interesting to study the low-energy manifestations of this effect. The couplings of the lowest-lying scalar KK resonance S_1 to SM quarks can be parameterized in the form

$$\mathcal{L}_{\rm ferm} = -\sum_{q=u,d}\sum_{m,n} S_1(x)\left[g_{mn}^{(q)}\,\bar{q}_L^{(m)}(x)\,q_R^{(n)}(x) + \text{h.c.}\right], \tag{3.109}$$

where $m, n = 1, 2, 3$ are generation indices. Analogous couplings can be written in the lepton sector. An explicit expression for the quantities $g_{mn}^{(q)}$ has been presented in equation (3.26) of [154], where a model profile $\chi_1^S(\phi) \propto \exp\{(1+\beta_S)\,kr|\phi|\}$ was assumed, with a free parameter β_S. For our purposes, all we need to do is to replace this profile by the function $\chi_1^S(\phi)$ we have obtained from the solution to the EOM (3.75). For simplicity, we will neglect the effects of backreaction in the following discussion. Using the ZMA for the SM fermion profiles and using the fermion profiles

computed using sgn(ϕ) as the ϕ-dependence function for their 5D masses, we obtain

$$g^{(u)}_{mn} = \int_\epsilon^1 dt\, \chi_1^S(t) \left[x_n\, \hat{a}^{(U)\dagger}_m\, F(\boldsymbol{c}_Q)\, t^{\boldsymbol{c}_Q}\, \frac{\boldsymbol{\mathcal{Y}}_Q}{\sqrt{r}}\, F(\boldsymbol{c}_Q)\, \frac{t^{1+\boldsymbol{c}_Q} - \epsilon^{1+2\boldsymbol{c}_Q}\, t^{-\boldsymbol{c}_Q}}{1+2\boldsymbol{c}_Q}\, \hat{a}^{(U)}_n \right. \\ \left. - x_m\, \hat{a}^{(u)\dagger}_m\, F(\boldsymbol{c}_u)\, \frac{t^{1+\boldsymbol{c}_u} - \epsilon^{1+2\boldsymbol{c}_u}\, t^{-\boldsymbol{c}_u}}{1+2\boldsymbol{c}_u}\, \frac{\boldsymbol{\mathcal{Y}}_u}{\sqrt{r}}\, F(\boldsymbol{c}_u)\, t^{\boldsymbol{c}_u}\, \hat{a}^{(u)}_n \right]. \tag{3.110}$$

Here $x_n = m_n/M_{\text{KK}}$, with m_n denoting the masses of the three up-type quarks. An analogous expression holds for the couplings $g^{(d)}_{mn}$. Using the expressions for the various objects valid in the ZMA [110], combined with the fact that the profile function $\chi_1^S(t) \equiv \chi_1^S(\phi(t))$ peaks for values $t = \mathcal{O}(1)$, it is straightforward to derive the scaling laws

$$g^{(u)}_{mn} = \mathcal{O}(1)\, \frac{v_h}{M_{\text{KK}}}\, F(c_{Q_m})\, F(c_{u_n})\,, \\ g^{(d)}_{mn} = \mathcal{O}(1)\, \frac{v_h}{M_{\text{KK}}}\, F(c_{Q_m})\, F(c_{d_n})\,. \tag{3.111}$$

The above couplings display the familiar RS-GIM mechanism [170], which states that the couplings of low-lying KK resonances to light SM fermions are suppressed by an overlap factor $F(c_i)$ for each fermion, which is much smaller than 1 if the fermion is light compared with the weak scale and $\mathcal{O}(1)$ for the heavy fermions. Importantly, however, the couplings of scalar KK resonances are *in addition* suppressed by a factor v_h/M_{KK}, since for these coupling to be present a mass insertion for the fermions is needed. As a result, the exchange of a scalar resonance between four SM fermions gives rise to interactions proportional to

$$\frac{v_h^2}{M_{\text{KK}}^4}\, F(c_{Q_{n_1}})\, F(c_{q_{n_2}})\, F(c_{Q_{n_3}})\, F(c_{q_{n_4}})\,, \tag{3.112}$$

which are suppressed by *four* powers of M_{KK} and hence correspond to dimension-8 operators in the low-energy effective weak Hamiltonian. With M_{KK} in the range of 10 TeV, these effective interactions are highly suppressed and irrelevant for all practical purposes.

3.6 Higgs portal coupling to the bulk scalar and modified Higgs couplings

An interesting possibility which we have omitted so far is to add a portal coupling $\lambda\Sigma^2 H^\dagger H$ to the integrand of the 5D action in (3.3), connecting the new the $\mathbb{Z}_2$-odd bulk scalar with the Higgs doublet. After EWSB and once the odd scalar develops a VEV $\omega(\phi)$, such an interaction induces a mixing between the Higgs field h of the SM and the first scalar KK resonance S_1 (as well as higher KK resonances). This, in turn, has the effect of reducing the couplings of the Higgs boson to SM particles by a factor $\cos\theta_{hS}$, where θ_{hS} denotes the corresponding mixing angle.

In the setup discussed in this chapter, where the 5D Higgs field is confined to live on the IR brane, the portal coupling in the Lagrangian vanishes, since the $\mathbb{Z}_2$-odd bulk scalar field is strictly zero on the IR brane. However, such a coupling is inevitably induced by loops involving bulk fermions, which couple to the scalar field Σ as well as to the Higgs field, residing on the IR brane. Figure 3.13 shows some representative diagrams. For the mixing angle relating the physical Higgs boson h^{phys} to the Higgs field h in the Lagrangian, we then expect

$$\tan\theta_{hS} \sim \frac{N_c}{16\pi^2}\, \frac{v_h \hat{\omega}}{M_S^2} \sim \frac{N_c}{16\pi^2}\, \frac{v_h}{M_{\text{KK}}}\,. \tag{3.113}$$

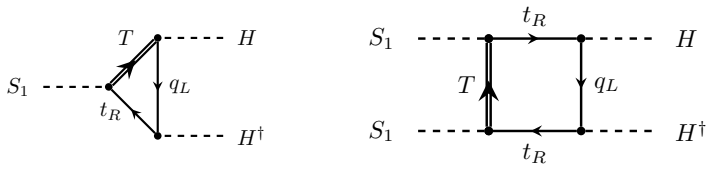

Figure 3.13: *Loop diagrams leading to effective interactions of the first KK resonance of the bulk scalar, S_1, to the higgs boson, in the brane-localized Higgs scenario.*

The parameter $\hat{\omega} \sim M_{\text{KK}}$ is given in terms of an angular integral of the relevant profile functions appearing in the loops, and is naturally of order the KK mass scale, M_{KK}. The mixing angle is thus expected to be very small in this setup, due to the double suppression by a loop factor and the ratio v_h/M_{KK}. It was therefore justified to neglect this mixing for our purposes in this chapter.

We emphasize, however, that the assumption of a brane-localized Higgs sector is neither required nor particularly natural in the context of RS models and it is by now well known that one can construct realistic RS models in which the Higgs doublet, like all other fields, lives in the bulk of the extra dimension [2,112,113,149,151,152,195,196]. In the context of such bulk-Higgs models, the portal interaction between the Higgs field and the $\mathbb{Z}_2$-odd scalar fields becomes a generic feature, and one expects the mixing angle to appear without a loop factor suppresion. In this case the mixing angle can naturally be of order a few percent, which might bring it to the sensitivity level of future precision Higgs measurements, see e.g. [197, 198]. As from a phenomenological point of view, this may be the most significant imprint of this class of models, we would explore this possibility in the next chapter.

3.7 Discussion

The RS model was originally proposed to solve the gauge hierarchy problem. However, soon after its inception, it was realized that it also allows for an explanation of the flavor puzzle, by means of a specific pattern of localization of the SM fermions in the bulk of the RS geometry, thus connecting the hierarchy of fermion masses to the one existing between the EW and Planck scales.

Notwithstanding, the issue concerning the coordinate dependence of the bulk fermion mass parameters has not been assessed carefully. As discussed in section 2.5, fermion bulk masses have to be odd under the $\mathbb{Z}_2$ orbifold symmetry of the RS geometry, and have been traditionally implemented as a constant parameter appearing together with an *ad-hoc* sgn(ϕ) function. In this chapter, we demonstrated that it is indeed possible to obtain these masses dynamically, via the VEV of a $\mathbb{Z}_2$-odd scalar with bulk Yukawa couplings to the different 5D fermion fields. In particular, we have shown in section 3.1 that an odd bulk scalar can develop a non-trivial background solution both for flat and WED. We have shown that kink-like solutions are only found for realistic scenarios, where the hierarchy problem is solved and the product $kr \gg 1$, and that these solutions approach the sgn(ϕ) for large values of $|\mu r|$. We have considered non-trivial effects of the ϕ-dependent VEV on the background geometry in the case of a WED, solving the coupled gravity-scalar Einstein equations and computing the background solutions for both the warp factor and the scalar field. It turns out that a non-negligible backreaction is induced on the AdS metric, which modifies the warp function in the vicinity of the UV and IR branes for reasonable values of the gravity-scalar coupling, $\gamma = |\mu|^2/(\lambda M_*^3)$. This is a consequence of the profile of the odd bulk scalar VEV being approximately constant in the bulk, while strongly changing in the vicinity of both branes. Hence,

the effects of the backreaction are especially visible in those regions. Moreover, we also briefly discussed the stability of the background geometry in the presence of an odd bulk scalar.

In section 3.2, we have analyzed the gauge sector of the minimal RS model with an $SU(2)_L \times U(1)_Y$ bulk gauge symmetry and the custodial case, where the bulk symmetry is enlarged. We have calculated the oblique parameters S and T in the presence of a general warp function $\sigma(\phi)$ and considering backreaction effects, and compared the results with those obtained in the conventional RS model, i.e. using the linear AdS warp function $kr\phi$. We have shown that presently allowed values of the S and T parameters set a stringent constraint on the masses of the first KK resonances. In particular, the mass of the first KK gluon state (which is often the lightest KK resonance in the model) has to be $\mathcal{O}(10)$ TeV, irrespectively of whether the backreaction on the metric is included or neglected in the study. We have also calculated the KK spectrum of the $\mathbb{Z}_2$-odd bulk scalar and studied its main decay channels for several benchmark cases.

Our mechanism for dynamically generating the fermion bulk masses has been presented in section 3.4, where for simplicity we consider a single 5D Dirac fermion Ψ which couples to the bulk odd scalar Σ through a 5D Yukawa coupling, $\mathcal{Y}\bar{\Psi}\Sigma\Psi$. After the KK decomposition of the bulk fermion, a KK tower of LH and RH chiral fermions is generated, where a zero mode exists for only one of the two chiralities, due to the BC. As usual, SM fermions correspond to the chiral zero modes of these bulk fermion fields. We show how the zero-mode profiles of the bulk fermions depend on the Yukawa coupling along with the ϕ-dependent VEV of the bulk scalar. By choosing appropriate values of the bulk Yukawa couplings, the zero-mode fermions can be localized towards either one of the branes, as is common in RS models. We have calculated the deviations of the zero-mode and KK-mode profiles in our model as compared to the conventional RS case, finding that these deviations can become sizable when the effects of the backreaction are taken into account. This deviations are particularly interesting since they can have an impact on flavor observables, and therefore on flavor bounds.

We then study the viability of our model when the full SM fermion content is considered, and reproduce the SM fermion masses after EWSB. The localization of the zero-mode profiles determines these masses in the effective theory. In section 3.5, we illustrated this mechanism for the case of a ϕ-dependent VEV and a modified warp factor, obtaining the hierarchical SM quark masses and mixing angles. Furthermore, we studied the impact of the dynamical generation of bulk fermion masses on flavor observables and the RS-GIM mechanism. We have examined, in particular, the flavor observable ϵ_K, which typically sets one of the most stringent bounds on models with a WED. We have compared our predictions with those obtained in the conventional RS model. We have also studied the dependence of our results on the model parameters and the strength of the backreaction on the metric. We have shown that the current experimental value of ϵ_K puts a severe constraint on the mass of the first KK gluon state, which has to be above $\mathcal{O}(10)$ TeV. Moreover, we have also shown that the presence of a non-negligible backreaction slightly tends to weaken the RS-GIM mechanism and, in particular, enhances the NP contribution to ϵ_K. However, the impact is very modest overall, showing that the dynamical origin of the different fermion masses via an odd scalar field is not only an appealing possibility, but also a phenomenologically viable one. In extensions of the SM with a WED, the presence of TeV-scale KK resonances introduces new sources of flavor-changing interactions among the SM fermions. In our particular model, scalar mediated four SM fermions can be described by effective dimension 8 interactions, which are v_h^4/M_{KK}^4 suppressed and can therefore be neglected for practical purposes.

Finally, in section 3.6 we briefly comment the portal coupling of the bulk scalar to the Higgs doublet, which in our model only appears at loop level. However, we pointed out that in realistic RS models the Higgs doublet should be allowed to propagate in the bulk of the extra dimension and. Therefore, in the context of such bulk-Higgs models the portal interaction between the Higgs field and the $\mathbb{Z}_2$-odd scalar fields becomes a generic feature. We should thus move on to the next chapter.

4 | A warped scalar portal to fermionic DM

We have shown in the previous chapter that extending the SM with a WED featuring a $\mathbb{Z}_2$-odd scalar singlet can provide a natural explanation to the hierarchy problem and at the same time explain the nature of fermion bulk masses, where the odd scalar plays the key role of giving an origin to such bulk masses. Here, we introduce another striking example of the SM not being able of accommodating some of the observed phenomena, i.e. the nature of DM and the necessary existence of a mediator connecting the DM sector with the SM. We know as a fact that there is no viable DM candidate in the SM, thus requiring the presence of NP. Moreover, together with any DM sector, there should be an intermediary connecting the dark sector with the SM. In this chapter, we argue that extensions of the SM with a WED compactified on an $S_1/\mathbb{Z}_2$ orbifold together with the odd scalar field not only introduce a geometrical origin to the previously presented issues, i.e. the flavor puzzle and the hierarchy problem, but that it simultaneously addresses the problem of the absence of a viable DM mediator within the SM. In particular, the KK excitations of the new scalar particle can be the leading portal to any fermion propagating into the bulk of the extra dimension, fields that could act as a suitable DM candidate, therefore, contributing to reproduce the observed DM relic abundance. Since the odd scalar field is responsible for all fermion bulk masses, it represents a unique window into any femionic dark sector propagating into the bulk of the WED. Models with WEDs already feature an irreducible mediator between visible and dark sectors, since gravity couples to matter through the energy-momentum tensor. However, as we will see, when the DM candidates are fermionic weakly interacting particles (WIMPs) with masses of $\mathcal{O}$(TeV), the resonances arising from the 5D $\mathbb{Z}_2$-odd scalar field can provide the most important mediators for the DM coannihilation cross section.

Moreover, we are aware that the derivations that took place in chapter 3 were restricted to the brane localized Higgs scenario, where the Higgs boson does not mix at tree-level with the $\mathbb{Z}_2$-odd scalar field. We argue that in a more general case the Higgs should be promoted to a bulk field and thus a natural question which arises concerns the possible interplay between the two scalar fields. The presence of the Higgs boson in the bulk will lead to the scalar excitations the Higgs boson to necessarily mix with the odd scalar. We study the modifications of the Higgs couplings and BR in this chapter, together with the new contributions to the relic density from Higgs-mediated coannihilations of the fermionic DM. Due to the scalar mixing, we will see that the fermionic dark sectors considered here are mostly Higgs-mediated for DM masses below the TeV scale. We examine thoroughly the resulting model of scalar-mediated fermionic DM for a large range of DM masses. We focus on the case where the DM particle is a vector-like (VL) fermion, corresponding to the first KK excitation of a 5D dark fermion. However, most of our results also hold in the case

where the DM candidate gets an external mass, which can be chiral, VL or even of Majorana type. We analyze these effects and explore the viability of fermionic DM in the presence of these new heavy scalar mediators both in the usual freeze-out scenario and in the case where the freeze-out happens during an early period of matter domination.

This chapter is organized as follows: we solve the coupled system of field equations in section 4.1, obtained after switching on the portal coupling between the two bulk scalar fields, by diagonalizing the resulting 4D mass matrix perturbatively. In section 4.2 we proceed to discuss the phenomenology assuming a non-negligible portal coupling and the presence of N_χ dark fermion bulk fields. First, we discuss the impact of the scalar mixing on the SM Higgs couplings. We then continue by examining the impact of the dark fermions on the Higgs invisible decay width. Then, we discuss the predictions for the DM coannihilation cross-section mediated by the Higgs field and the first KK resonance of the $\mathbb{Z}_2$-odd scalar field, comparing these contributions with the ones mediated by KK gravitons. We compute the prediction for the DM relic abundance as a function of the velocity-averaged coannihilation cross section in the usual freeze-out scenario as well as in the case of a matter-dominated universe [199–201]. Finally, we compute the constraints arising from direct detection using data from the Xenon1T experiment, showing that for a $\mathcal{O}(10$ TeV) fermionic WIMP we can reproduce the observed DM relic abundance in the scenario of matter domination, without conflicting with current data from Xenon1T. In the case of radiation domination and DM masses of ~ 15 TeV, these scalar mediators can provide a non-negligible fraction of the required coannihilation cross section, even though additional mediators would be required.

4.1 Bulk Higgs and Odd scalar mixing

We are here interested in the case where the two bulk scalar fields, i.e. the Higgs and the new $\mathbb{Z}_2$-odd scalar, mix with each other. In this case the action reads

$$S = \int d^5x\sqrt{g}\left\{ g^{MN}\left(D_M H\right)^\dagger D_N H + \frac{1}{2} g^{MN}\left(D_M \Sigma\right)\left(D_N \Sigma\right) - V(H,\Sigma) \right. \\ \left. - \frac{\sqrt{|\hat{g}_{\text{UV}}|}}{\sqrt{g}}\hat{V}^{\text{UV}}(H)\,\delta(t-\epsilon) - \frac{\sqrt{|\hat{g}_{\text{IR}}|}}{\sqrt{g}}\hat{V}^{\text{IR}}(H)\,\delta(t-1)\right\}. \tag{4.1}$$

We consider mixed BCs for the Higgs field, while the odd scalar field satisfies Dirichlet BCs. Such BCs for the bulk Higgs are a consequence of the brane-localized potentials, which are forbidden for the odd scalar, since it vanishes on the two branes. In our model, both bulk scalar fields develop a VEV. We can express the two 5D scalar in terms of their background configurations, $\varphi_H(t)$ and $\varphi_S(t)$, and their 5D excitations, $h(x,t)$ and $S(x,t)$, as

$$H(x,t) = \frac{t}{\epsilon\sqrt{2r}}\begin{pmatrix}0\\1\end{pmatrix}\left[\varphi_H(t) + h(x,t)\right], \qquad \Sigma(x,t) = \varphi_S(t) + \frac{t}{\epsilon\sqrt{r}}\,S(x,t). \tag{4.2}$$

The bulk potential now reads

$$V(H,\Sigma) = \mu_H^2|H|^2 - \frac{\mu_S^2}{2}\Sigma^2 + \frac{\lambda_S}{4}\Sigma^4 + \lambda_{HS}|H|^2\Sigma^2, \tag{4.3}$$

where μ_H, μ_S are the mass parameters and λ_S, λ_{HS} the quartic couplings. Note that in (4.3), in contrast to the convention we chose in chapter 3, μ_S appears in the potential with a minus sign, thus in this convention $\mu_S > 0$. We use the same definition for the brane-localized potentials of the bulk Higgs doublet as in (2.29). Following the same lines as in section 2.3, a quartic term for the Higgs field is only introduced at the IR brane. This configuration is enough to induce EWSB near that brane. The assumption that the profile of the Higgs is peaked towards the IR brane makes other quartic term contributions negligible and therefore, the UV and bulk quartic couplings can be omitted for any practical purpose [113, 149–155].

4.1.1 Background solutions

First, we want to determine the profiles of the two VEVs. We can derive the coupled EOM from (4.1) and (4.3), reading

$$\begin{aligned}\left[t^2\partial_t^2 - 3t\partial_t + \frac{\mu_S^2}{k^2}\Big(1 - v_S^2 - \bar{\lambda}\frac{k^4}{\mu_S^4}\frac{\lambda_S}{r}t^2\frac{\varphi_H^2}{M_{\text{KK}}^2}\Big)\right]v_S(t) = 0,\\ \left[t^2\partial_t^2 + t\partial_t - \beta^2 - \bar{\lambda}v_S^2\right]\frac{\varphi_H(t)}{t} = 0,\end{aligned} \tag{4.4}$$

where we have defined the dimensionless coupling

$$\bar{\lambda} \equiv \frac{\mu_S^2}{k^2}\frac{\lambda_{HS}}{\lambda_S}, \tag{4.5}$$

and redefined the VEV of the odd field as in [1], i.e.

$$\varphi_S(t) = \frac{\mu_S}{\sqrt{\lambda_S}}\, v_S(t). \tag{4.6}$$

In order to obtain an inverted one-dimensional Mexican-hat potential for v_S and guarantee the existence of non-trivial solutions, we demand that

$$\bar{\lambda}\frac{k^4}{\mu_S^4}\frac{\lambda_S}{r}t^2\frac{\varphi_H^2(t)}{M_{\text{KK}}^2}\bigg|_{t=1} \leq 1. \tag{4.7}$$

Since the Higgs VEV is monotonic in t (at least at leading order in $\bar{\lambda}$), once this condition is fulfilled it will also hold for $t < 1$. Therefore, in practice, we can translate (4.7) into an upper bound on the combination $\bar{\lambda}\lambda_S/r$. Plugging in the solution for the free Higgs VEV from (2.41), i.e. the solution for the VEV obtained for a vanishing portal coupling, this constraint translates into

$$\bar{\lambda}\frac{\lambda_S}{r} \lesssim \frac{x_4^{-2}}{10(1+\beta)}\left(\frac{\mu_S}{k}\right)^4, \tag{4.8}$$

with $x_4 = v_4/M_{\text{KK}}$ and v_4 defined as in (2.42).

We can solve the coupled system of equations iteratively. The starting point are the solutions we already know for the decoupled equations, which we denote by $v_{S,0}(t)$ and $\varphi_{H,0}(t)$. These solutions correspond to the ones previously obtained. In particular, $v_{S,0}(t)$ was computed in sections 3.1.2 and 3.1.3 (see e.g. figure 3.6), and the solution for the free case, $\varphi_{H,0}(t)$, was introduced in section 2.3, reading

$$\varphi_H(t) \simeq \varphi_H(1)\, t^{1+\beta}, \tag{4.9}$$

as in (2.41). Then, at every step, we insert the solution from the previous iteration for each VEV in the EOM corresponding to the other one in (4.4). This method is convenient, since the potential for the odd VEV and the strategy to solve its EOM is well understood to us, being the one we presented in chapter 3, see also [1]. Indeed, as we can see from figure 4.1, the potential does not differ much from the potential obtained in the decoupled case, i.e. for $\bar{\lambda} = 0$. Moreover, we have checked numerically that the solution obtained for $v_S(t)$ fits the one obtained for the decoupled case with high accuracy.

We display in figure 4.1 the one-dimensional effective potential $\tilde{V}(v_S)$ defined by

$$\frac{\delta\tilde{V}(v_S)}{\delta v_S} = \Big(1 - v_S^2(t) - \bar{\lambda}\frac{k^4}{\mu_S^4}\frac{\lambda_S}{r}t^2\frac{\varphi_H^2(t)}{M_{\text{KK}}^2}\Big)v_S(t), \tag{4.10}$$

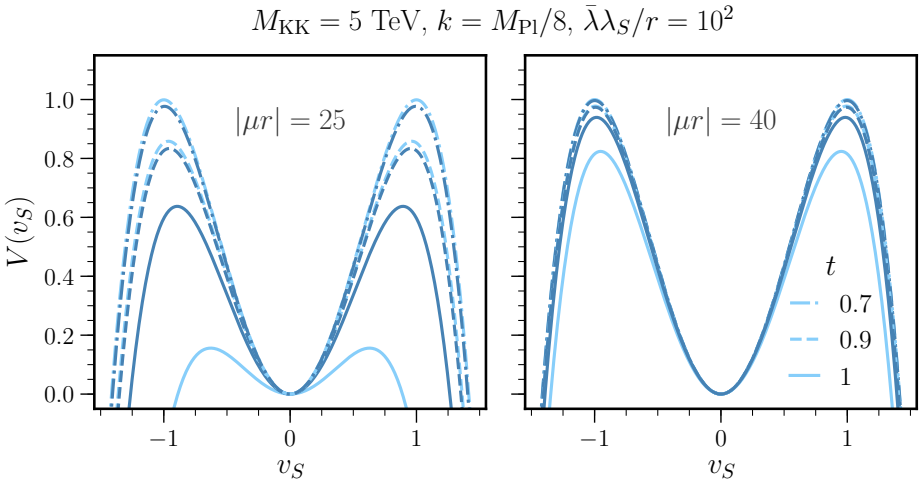

Figure 4.1: *Effective potential $\tilde{V}(v_S)$ computed using the leading-order solution $\varphi_{H,0}(t)$, for different values of t and $M_{KK} = 5$ TeV, $k/M_{\rm Pl} = 1/8$ and $\bar{\lambda}\lambda_S/r = 100$, for $\beta = 2$ (dark blue) and $\beta = 8$ (light blue).*

which determines the EOM for v_S once a known profile for φ_H is used as an input, see (4.4). We show this potential for $\bar{\lambda}\lambda_S/r = 100$ and different values of t, μ_S and β, using the leading-order solution for the Higgs profile $\varphi_H = \varphi_{H,0}$, in order to explore how its maxima change with increasing t and different values of μ_S and β. Here and below we choose $M_{\rm KK} = 5\,$TeV, which is motivated to avoid tensions with EW precision data, see chapter 3 or [1] for more details. Similarly, we take $k = M_{\rm Pl}/8$ where $M_{\rm Pl} = 2.4 \cdot 10^{18}$ GeV is the reduced Planck mass. This value corresponds to $kr \approx 10.1$, or equivalently $\Lambda_\pi \equiv M_{\rm Pl}\, e^{-kr\pi} = 40\,$TeV. We observe that both maxima decrease for increasing t. These two maxima would eventually collapse into the maximum of an inverted parabola if values of $\bar{\lambda}\lambda_S/r$ larger than the ones given by equation (4.8) were considered. In that case, only the trivial solution would exist and the study and discussion of the previous chapter will no longer be valid. In practice, we will never reach such large values due to perturbativity constraints on the first KK excitation of S, since the Yukawa couplings of this particle to the different fermions scale with $\sqrt{\lambda_S/r}$, see below. On the other hand, reproducing a value of the DM coannihilation cross section required to account for the observed relic abundance demands a large portal coupling between the different fermion sectors. For this reason, we will consider $\lambda_S/r \lesssim \mathcal{O}(100)$ for phenomenological reasons hereafter. In particular, we choose $\bar{\lambda}\lambda_S/r = 100$ for figure 4.1, in order to saturate the bound given by equation (4.8).

4.1.2 Scalar excitations

We now move on to the study of the scalar KK excitations. The profiles of these resonances can be computed by inserting the KK decompositions

$$\begin{aligned} h(x,t) &= \sum_{n=0}^{\infty} h_n(x)\chi_n^h(t), \\ S(x,t) &= \sum_{n=1}^{\infty} S_n(x)\chi_n^S(t) \end{aligned} \tag{4.11}$$

into the action (4.1) and keeping quadratic terms in the fields.

Our approach for solving the coupled system would be to compute the 4D mass matrix, obtained after integrating the quadratic terms in the action. Then, we can determine the eigenmodes and eigenvalues of the coupled system by diagonalizing the resulting matrix. Besides the KK scalar masses for the non-mixed case, non-diagonal entries only arise because of the terms in the potential, once we integrate the profiles over the fifth dimension. These terms are

$$\int d^5x\sqrt{g}\,V(H,\Sigma) \supset \bar{\lambda}\int d^4x\int_\epsilon^1 \frac{dt}{t^3}\left[\frac{M_{\text{KK}}^2}{kr}v_S^2(t)\,h(x,t)^2 + \frac{kr}{(\mu_S r)^2}\frac{\lambda_S}{r}t^2\varphi_H^2(t)S(x,t)^2 + 4\frac{M_{\text{KK}}}{\mu_S r}\sqrt{\frac{\lambda_S}{r}}\,t\,\varphi_H(t)v_S(t)h(x,t)S(x,t)\right]. \tag{4.12}$$

Inserting the KK decompositions for $h(x,t)$ and $S(x,t)$, and using the profiles for the decoupled case, we can write down the mass matrix to first order in $\bar{\lambda}$. In this case, the profiles need to satisfy the following EOM

$$\begin{aligned}\left[t^2\partial_t^2 + t\partial_t + x_n^2t^2 - \beta^2\right]\frac{\chi_n^h}{t} &= 0,\\ \left[t^2\partial_t^2 + t\partial_t + x_n^2t^2 + \frac{\mu_S^2}{k^2}(1-3v_S^2) - 4\right]\frac{\chi_n^S}{t} &= 0,\end{aligned} \tag{4.13}$$

together with BC

$$\begin{aligned}\partial_t\left[t\,\chi_n^h(t)\right]_{t=\epsilon^+} &= m_{\text{UV}}\,\chi_n^h(\epsilon), & \chi_n^S(\epsilon) &= 0\\ \partial_t\left[t\,\chi_n^h(t)\right]_{t=1^-} &= m_{\text{IR}}\,\chi_n^h(1) - \frac{6\lambda_{\text{IR}}}{M_{\text{KK}}^2}\varphi_H(1)^2\chi_n^h(1), & \chi_n^S(1) &= 0.\end{aligned} \tag{4.14}$$

The profile for the KK modes of the Higgs, $\chi_n^h(t)$ at zeroth order in $\bar{\lambda}$ were given in (2.50), reading

$$\chi_n^h(t) = \sqrt{\frac{L}{\pi}}\frac{tJ_\beta(x_{h_n}t)}{\sqrt{J_\beta^2(x_{h_n}) - J_{\beta+1}(x_{h_n})J_{\beta-1}(x_{h_n})}}, \tag{4.15}$$

where $J_\beta(x)$ is a Bessel function and the eigenvalues x_{h_n} satisfy

$$\frac{x_{h_n}J_{\beta+1}(x_{h_n})}{J_\beta(x_{h_n})} = 2\,(m_{\text{IR}} - 2 - \beta) \equiv 2\delta. \tag{4.16}$$

In particular, we saw that in the special case of the Higgs zero-mode, $\chi_0^h(t)$, the expression for the profile is approximately given by

$$\chi_0^h(t) \simeq \sqrt{\frac{L}{\pi}(1+\beta)}\,t^{1+\beta}, \tag{4.17}$$

up to $\mathcal{O}(x_{h_0}^2)$ corrections. In the case of the odd scalar, the solutions for the profiles need to be obtained numerically, because of the presence of v_S^2 in the EOM, which has no analytical expression. The solutions were presented in the previous chapter for ϕ-coordinates. The translation is straightforward. In both cases, the orthogonality condition for the scalar profiles is given by [113, 150]

$$\frac{2\pi}{L}\int_\epsilon^1 \frac{dt}{t}\chi_m^h(t)\chi_n^h(t) = \delta_{mn}. \tag{4.18}$$

We can now write the mass matrix to first order in $\bar{\lambda}$ as

$$\mathcal{M}^2 = \left[\begin{pmatrix} x_{h_0}^2 & 0 & 0 & \cdots\\ 0 & x_{S_1}^2 & 0 & \cdots\\ 0 & 0 & x_{h_1}^2 & \cdots\\ \vdots & \vdots & \vdots & \ddots\end{pmatrix} + \bar{\lambda}\begin{pmatrix} \kappa_{h_0}^2 & \kappa_{h_0S_1}^2 & \kappa_{h_0h_1}^2 & \cdots\\ \kappa_{h_0S_1}^2 & \kappa_{S_1}^2 & \kappa_{h_1S_1}^2 & \cdots\\ \kappa_{h_0h_1}^2 & \kappa_{h_1S_1}^2 & \kappa_{h_1}^2 & \cdots\\ \vdots & \vdots & \vdots & \ddots\end{pmatrix}\right] M_{\text{KK}}^2. \tag{4.19}$$

Here, x_{h_n} and x_{S_n} correspond to the unperturbed mass eigenvalues in units of M_{KK} of the decoupled system, i.e. for $\bar{\lambda} = 0$. Note that only light zero mode of the model corresponds to the profile with eigenvalue x_{h_0}, since the odd scalar field can have no zero modes, see section 3.3. One could argue that at zeroth order in $\bar{\lambda}$ non-diagonal terms should appear in terms relating different modes of the Higgs boson. However, since the Higgs zero-mode and VEV profiles are equivalent up to $\mathcal{O}(v_4^2/M_{\text{KK}}^2)$, these corrections appear at the same order and are neglected in our study, see e.g. [202].

Diagonalizing the mass matrix once the mixing is switched on, i.e. for $\bar{\lambda} \neq 0$, the mass of the lightest scalar becomes

$$m_h^2 \approx \left(x_{h_0}^2 + \bar{\lambda}\,\kappa_{h_0}^2\right) M_{\text{KK}}^2 \,. \tag{4.20}$$

The contributions to the mass matrix at first order in $\bar{\lambda}$ can be computed from (4.12). Using the parametrization from (4.19), these terms read

$$\begin{aligned}
\kappa_{S_m}^2 &= \frac{2\,kr}{(\mu_S r)^2}\frac{\lambda_S}{r}\int_\epsilon^1 \frac{dt}{t}\frac{\varphi_H^2(t)}{M_{\text{KK}}^2}[\chi_m^S(t)]^2 \,, \\
\kappa_{h_n S_m}^2 &= \frac{4}{\mu_S r}\sqrt{\frac{\lambda_S}{r}}\int_\epsilon^1 \frac{dt}{t^2}\frac{\varphi_H(t)}{M_{\text{KK}}} v_S(t)\chi_n^h(t)\chi_m^S(t) \,, \\
\kappa_{h_n h_m}^2 &= \frac{2}{kr}\int_\epsilon^1 \frac{dt}{t^3} v_S^2(t)\chi_n^h(t)\chi_m^h(t) \,,
\end{aligned} \tag{4.21}$$

where used $\kappa_{h_n}^2 \equiv \kappa_{h_n h_n}^2$. The different powers of t in the denominator result from our particular normalization of the VEV of the odd scalar field in (4.2), which differs from the normalization of the Higgs VEV.

A priori, both x_{h_0} and κ_{h_0} are naturally $\mathcal{O}(1)$ numbers, so in order to obtain a 125 GeV Higgs boson one needs to tune

$$\frac{m_h^2}{M_{\text{KK}}^2} \approx x_{h_0}^2 + \bar{\lambda}\,\kappa_{h_0}^2 \sim \left(\frac{0.125}{5}\right)^2 \sim 10^{-3}, \tag{4.22}$$

where we have used our benchmark value of $M_{\text{KK}} = 5$ TeV. Independently of the exact value of M_{KK}, this is a well-known feature of bulk Higgs models in WEDs [112, 113, 150–152, 195, 196] and it is commonly referred to as the *little hierarchy problem*. In our model we can achieve such a value in two different ways. For positive values of $\bar{\lambda}$, both terms in the sum need to be small simultaneously. In the case of $x_{h_0}^2$, this can be achieved by tuning the parameters in the Higgs potential accordingly in (4.16), as it is customary for bulk Higgs models with no additional scalars, see e.g. [113, 150]. For $\bar{\lambda}\,\kappa_{h_0}^2$ the only possibility is to make $\bar{\lambda}$ small enough, since $\kappa_{h_0}^2$ is an $\mathcal{O}(1)$ number unless very large values of β are chosen. The limit $\beta \to \infty$ corresponds to a brane-localized Higgs and the particular implementation of this limit not be considered here. Therefore, for positive values of $\bar{\lambda}$ we have

$$0 \leq \bar{\lambda}\,\kappa_{h_0}^2 \sim \bar{\lambda} \lesssim 10^{-3}. \tag{4.23}$$

As a result, in this case values of $\bar{\lambda}$ larger than 10^{-3} are not allowed, regardless of the value for $x_{h_0}^2$.

One could also entertain the possibility of considering solutions in which both quantities $x_{h_0}^2$ and $\kappa_{h_0}^2$ are simultaneously $\mathcal{O}(1)$, but they cancel each other out leading to a light Higgs mass. Since $\kappa_{h_0}^2 > 0$ by definition, one would need to have either $x_{h_0}^2$ or $\bar{\lambda}$ negative. The first possibility corresponds to a tachyonic Higgs field in the free case, i.e. before turning on the mixing with the odd scalar. This particular choice leads to the following requierement for the BC

$$\frac{x_{h_n} I_{\beta+1}(x_{h_n})}{I_\beta(x_{h_n})} = -2\,(m_{\text{IR}} - 2 - \beta) \equiv -2\delta \tag{4.24}$$

on the IR brane, where $I_n(x)$ are modified Bessel functions. This condition is similar to that in (4.16), but with a relative minus sign. However, such a path leads nowhere since, as can be proven, this equation is incompatible with the presence of a Higgs VEV [112, 113]. Therefore, the only viable option is to allow for negative values of $\bar{\lambda}$. In that case, equation (4.20) becomes

$$m_h^2 \approx \left(x_{h_0}^2 - |\bar{\lambda}|\,\kappa_{h_0}^2\right) M_{\rm KK}^2, \tag{4.25}$$

and we can always reproduce the Higgs mass regardless of the value of $\bar{\lambda} < 0$, by choosing the appropriate value of $x_{h_0}^2$.

For any choice of the model parameters, we can always parametrize the mixing between the even and odd bulk scalars as

$$h_0(x) = h_{\rm phys}(x) + \sin\theta_{h\mathcal{S}}\,\mathcal{S}(x) + \sin\theta_{h\mathcal{H}}\,\mathcal{H}(x), \tag{4.26}$$

where $\mathcal{H}(x) = h_1(x) + \mathcal{O}(\bar{\lambda})$ and $\mathcal{S}(x) = S_1(x) + \mathcal{O}(\bar{\lambda})$ are the profiles of the first KK modes in the limit where $\bar{\lambda} = 0$, and the mixing angles in our model are defined as

$$\begin{aligned} \sin\theta_{h\mathcal{S}} &= \bar{\lambda}\frac{\kappa_{h_0 S_1}^2}{x_{S_1}^2 - x_{h_0}^2} \approx \bar{\lambda}\frac{\kappa_{h_0 S_1}^2}{x_{S_1}^2}\,, \\ \sin\theta_{h\mathcal{H}} &= \bar{\lambda}\frac{\kappa_{h_0 h_1}^2}{x_{h_1}^2 - x_{h_0}^2} \approx \bar{\lambda}\frac{\kappa_{h_0 h_1}^2}{x_{h_1}^2}\,. \end{aligned} \tag{4.27}$$

In general, the mixing of the lightest Higgs eigenmode with the first odd excitation can be expressed as

$$\sin\theta_{h\mathcal{S}} \simeq 4\bar{\lambda}\sqrt{\frac{\lambda_S}{r}}\frac{x_4}{x_{S_1}^2}\frac{kr}{\mu_S r}(1+\beta)\int_\epsilon^1 dt\; t^{2\beta} v_S(t)\chi_1^S(t)\,, \tag{4.28}$$

and a similar expression can be derived for $\sin\theta_{h\mathcal{H}}$, i.e.

$$\sin\theta_{h\mathcal{H}} \simeq \frac{2\bar{\lambda}}{x_{h_1}^2}\sqrt{\frac{1+\beta}{kr}}\int_\epsilon^1 dt\, t^{\beta-2} v_S^2(t)\chi_1^h(t). \tag{4.29}$$

As we can see, when $\bar{\lambda}$ is positive the constraint set by the physical Higgs mass does not allow for a large mixing. Its upper bound is saturated when one assumes that the whole contribution to the Higgs mass is given by the $\bar{\lambda}\,\kappa_{h_0}^2$ term in (4.22). Then, we can infer the maximum value for $\bar{\lambda}$ from (4.22), being

$$\bar{\lambda}_{\rm max} = \frac{x_h^2}{\kappa_{h_0}^2} = \frac{x_h^2}{2(\beta+1)}\left[\int_\epsilon^1 dt\; t^{2\beta-1} v_S^2(t)\right]^{-1}. \tag{4.30}$$

In this case, plugging in the expression for $\kappa_{h_0 S_1}^2$ and $x_{S_1}^2$ in (4.28), we get

$$(\sin\theta_{h\mathcal{S}})_{\rm max} \simeq 2\frac{x_h^2 x_4}{x_{S_1}^2}\frac{k}{\mu_S}\sqrt{\frac{\lambda_S}{r}}\frac{\int_\epsilon^1 dt\; t^{2\beta} v_S(t)\chi_1^S(t)}{\int_\epsilon^1 dt\; t^{2\beta-1} v_S^2(t)}\,. \tag{4.31}$$

Now, we can use the upper bound on λ_S/r that we derived in (4.8), necessary for the potential of the odd VEV to allow for non-trivial solutions, in the equation for $\bar{\lambda}_{\rm max}$ to saturate its upper bound. In other words, we can insert (4.30) into equation (4.8) to obtain

$$\frac{\lambda_S}{r} \leq \frac{\mu_S^4}{k^4}\frac{2}{kr\, x_4^2\, x_h^2}\int_\epsilon^1 dt\; t^{2\beta-1} v_S^2(t). \tag{4.32}$$

This inequality for λ_S/r leads to

$$(\sin\theta_{h\mathcal{S}})_{\rm max} \simeq \frac{x_h}{x_{S_1}^2}\frac{2^{3/2}\,\mu_S r}{(kr)^{3/2}}\frac{\int_\epsilon^1 dt\; t^{2\beta} v_S(t)\chi_1^S(t)}{\left(\int_\epsilon^1 dt\; t^{2\beta-1} v_S^2(t)\right)^{1/2}}\,, \tag{4.33}$$

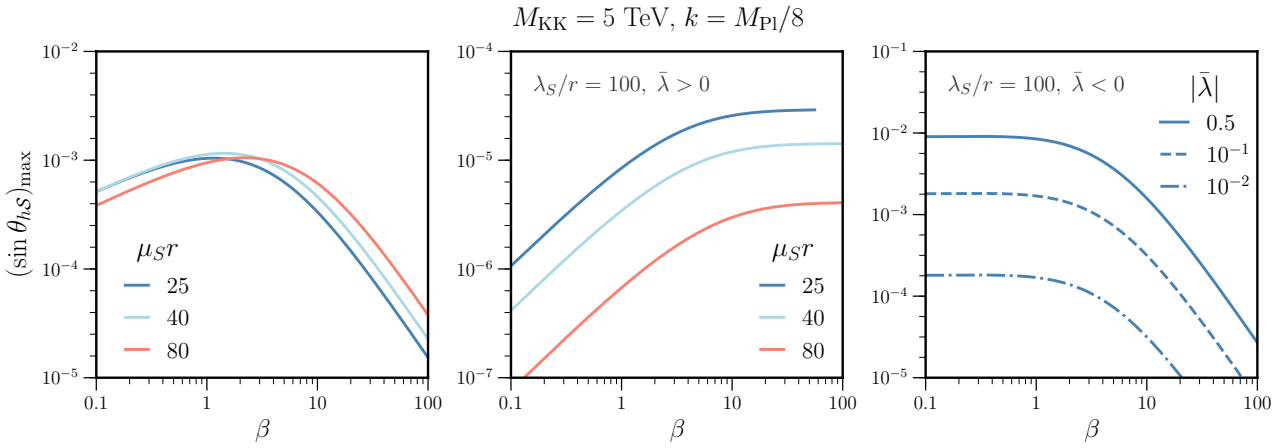

Figure 4.2: *Maximum allowed value for the parameter $\sin\theta_{h\mathcal{S}}$ describing the mixing between the lightest Higgs mode and the first KK resonance of the $\mathbb{Z}_2$-odd scalar, as a function of β and for fixed values of M_{KK} and $k/M_{\rm Pl}$. In the left and middle plots, we show this dependence for different values of $\mu_S r$ and positive $\bar{\lambda}$. In the left plot, we consider the maximum possible values of $\bar{\lambda} > 0$ and λ_S/r, whereas we fix λ_S/r to 100 in the middle plot, while still saturating the resulting upper bound for $\bar{\lambda}$. Finally, in the right plot we fix both $\mu_S r$ and λ_S/r and consider three different negative values of $\bar{\lambda}$.*

which only depends on β and $\mu_S r$, given that $kr \sim \mathcal{O}(10)$ in order to solve the hierarchy problem and that the eigenvalues x_i and the scalar profiles are determined once these parameters have been fixed.

When $\bar{\lambda}$ is negative, on the other hand, λ_S/r is unconstrained by relation (4.8). In this case, an upper bound on λ_S/r arises if one wants to prevent the theory from becoming strongly coupled, since the couplings of the KK scalar field $\mathcal{S}$ to the different fermions are proportional to $\sqrt{\lambda_S/r}$, as one can see from equation (4.41), see also section 4.2.1. Moreover, in this case sizable values of $|\bar{\lambda}| \sim \mathcal{O}(1)$ are allowed, since constraint (4.22) and therefore (4.23) do not apply anymore. For all these reasons, we find that $\sin\theta_{h\mathcal{S}}$ can be much larger than in the case of a positive $\bar{\lambda}$.

In figure 4.2, we show the different predictions for the maximum allowed value of the parameter $\sin\theta_{h\mathcal{S}}$, which measures the mixing between the lightest Higgs scalar and the first KK mode of the $\mathbb{Z}_2$-odd scalar as a function of β. In the left plot, we show this dependence for different values of $\mu_S r$ after saturating the upper bounds on λ_S/r and $\bar{\lambda}$, where positive values of $\bar{\lambda}$ have been considered. In the middle plot, we display the maximum allowed value of $\sin\theta_{h\mathcal{S}}$ for the same values of $\mu_S r$ and a fixed value $\lambda_S/r = 100$, together with $\bar{\lambda} = \bar{\lambda}_{\rm max} > 0$. Note that for $\mu_S r = 25$ and $\beta \sim 50$, $\lambda_S/r = 100$ takes its maximum value. This explains why, in this case, the line stops before one can reach $\beta = 100$, as using larger values for β requires making λ_S/r smaller, because of the constraint (4.32). Moreover, the reason why the values of $\sin\theta_{h\mathcal{S}}$ increase for smaller values of $\mu_S r$ can be easily understood from equation (4.31), where $\mu_S r$ appears in the denominator when λ_S/r is not saturated. Finally, in the right plot we show $(\sin\theta_{h\mathcal{S}})_{\rm max}$ for different values of $\bar{\lambda} < 0$ and fixed values $\mu_S r = 25$ and $\lambda_S/r = 100$. In all these plots we assume $M_{\rm KK} = 5$ TeV and $k = M_{\rm Pl}/8$. One can readily see that, for a given value of λ_S/r, the maximum allowed value for $\sin\theta_{h\mathcal{S}}$ is much more significant in the case $\bar{\lambda} < 0$, since larger values of $|\bar{\lambda}|$ can be taken. In addition, when $\bar{\lambda}$ is negative one could also consider higher values of λ_S/r than in the $\bar{\lambda} > 0$ case. All this results into larger mixing angles when $\bar{\lambda}$ is negative compared to the $\bar{\lambda} > 0$ case.

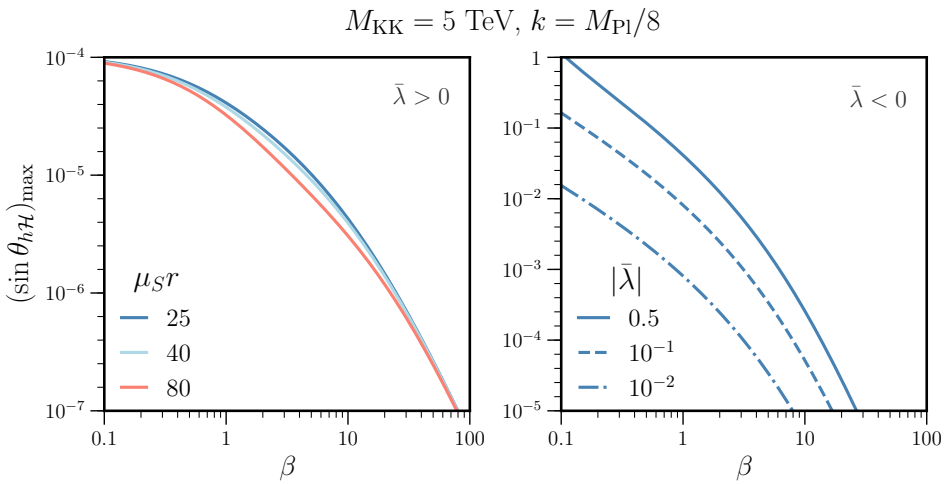

Figure 4.3: *Maximum allowed value for the parameter $\sin\theta_{h\mathcal{H}}$, describing the mixing between the lightest Higgs mode with its first KK resonance, as a function of β. In the left figure, we exhibit three different values of $\mu_S r$ for $\bar{\lambda} = \bar{\lambda}_{\rm max} > 0$, whereas in the right panel we consider three different negative values for $\bar{\lambda}$ and fixed the parameter $\mu_S r = 25$.*

For the Higgs mixing with its first KK mode, which we have parametrized by $\sin\theta_{h\mathcal{H}}$, we find a monotonic behavior, with $\sin\theta_{h\mathcal{H}}$ getting smaller for large values of β independently of the $\mu_S r$ parameter. This can be seen in figure 4.3, where we show $(\sin\theta_{h\mathcal{H}})_{\rm max}$ as a function of β for $M_{\rm KK} = 5$ TeV and $k = M_{\rm Pl}/8$. In particular, we display on the left panel this functional dependence for three different values of $\mu_S r$, after saturating $\bar{\lambda}$ to its upper bound. In the right panel we exhibit the case where $\mu_S r = 25$ is kept fixed, while $\lambda < 0$ takes different negative values. Comparing this panel with the right panel of the previous figure, we can see that $(\sin\theta_{h\mathcal{H}})_{\rm max}$ is a steeper function of β than $(\sin\theta_{h\mathcal{S}})_{\rm max}$ when $\bar{\lambda} < 0$. For the choice of parameters at hand, and depending on the value of $|\bar{\lambda}|$, $\sin\theta_{h\mathcal{H}}$ becomes bigger than $\sin\theta_{h\mathcal{S}}$ for β smaller than values between 1 and 10, depending on the other parameters of the model, whereas the opposite happens when β takes larger values.

4.2 Phenomenology

We have seen that once the Higgs boson is allowed to propagate into the bulk of the extra dimension, its mixing with the $\mathbb{Z}_2$-odd scalar becomes unavoidable. This mixing will leave its imprint on different aspects of the phenomenology, studying the possible signatures is the scope of this section. Firstly, it can lead to effects that could be tested at high-energy collider experiments, both present and future ones. Moreover, as we will see, assuming the presence of dark fermions, it can naturally contribute to reproduce the observed DM relic abundance and leave its imprint on DM direct-detection experiments.

We have seen how the quartic coupling leads to a mass mixing of the Higgs-boson zero mode with both its first KK resonance h_1 and the lowest-lying $\mathbb{Z}_2$-odd scalar, S_1. In this section, for practical purposes, we will neglect the differences between $\mathcal{S}$ and S_1, as well as between $\mathcal{H}$ and h_1, when discussing the phenomenology and couplings of the scalars to other particles, since the errors we would be making are proportional to the (small) mixing angles $\sin\theta_{h\mathcal{S}}$ and $\sin\theta_{h\mathcal{H}}$, respectively. Moreover, these mixing induce modifications on the Higgs-boson couplings to SM

particles, we will explore these modifications and study its impact on current and future colliders in section 4.2.1.

A key aspect of our model is that the odd scalar field constitutes a unique window into dark sectors featuring fermions propagating into the bulk. Indeed, since all the 5D fermion bulk masses are generated through Yukawa-like interactions with the odd scalar, the scalar KK modes necessarily connect any dark fermionic sector with the SM if the former is genuinely five dimensional. Such a connection is ineludible and constitutes a defining feature of the model. In the presence of a dark fermionic sector, the required Yukawa couplings between the odd scalar field and the bulk fermions have two interesting consequences. On the one hand, for light enough dark fermion masses, it contributes to enhance the Higgs invisible decay width, therefore, setting a constraint on the size of the scalar mixing between both 5D scalar fields. We study this in detail in section 4.2.2. On the other hand, as the dynamical generation of the 5D fermion masses naturally connects the visible and the invisible sectors via the KK resonances of the odd scalar field, it introduces an efficient coannihiliation channel for the lightest dark fermion, which is naturally stable and therefore a good DM candidate, where $\mathcal{S}$ can provide the leading contribution. We study this possibility both in the regular freeze-out scenario and in the case of a matter-dominated freeze-out in section 4.2.3. Finally, in section 4.2.4 we study in detail the constraints coming from direct-detection experiments using recent Xenon1T data [203, 204].

4.2.1 Modified Higgs couplings

As we have seen in the previous section, the physical Higgs boson can be expressed with very good approximation as a linear combination of the interaction eigenstates h_0, h_1 and S_1, as in (4.26). Since these interaction eigenstates couple differently to the SM particles, this mixing induces modifications of the SM Higgs couplings. Here, we study in detail the implications of such modifications.

The 4D effective couplings of the different scalars to fermions are obtained by integrating the profiles of the different fields over the fifth dimension and a subsequently rotation into the mass basis. In particular, the coupling of the Higgs-boson zero and KK modes to a pair of fermion chiral zero modes, $\bar{\Psi}_a \Psi_b$, is given by

$$y_{abh_n} = \frac{y_*}{\sqrt{kr}} \frac{2+\beta}{\sqrt{2(1+\beta)}} \int_\epsilon^1 dt \tilde{f}_a(t) \tilde{f}_b(t) \chi_n^h(t)\,, \tag{4.34}$$

where the EOM for a fermion field with a 5D bulk mass generated dynamically, in t-coordinates, reads

$$\Big[\pm t\partial_t - c\, v_S(t) \Big] \tilde{f}_0^{L,R}(t) = 0, \tag{4.35}$$

for $n = 0$ and

$$\Big[t^2\partial_t^2 + x_n^2 t^2 \mp c\, t\, v_S'(t) + c\, v_S(t) \Big(\pm 1 - c\, v_S(t) \Big) \Big] \tilde{f}_n^{L,R}(t) = 0, \tag{4.36}$$

for the heavier KK modes, where c is the usual dimensionless 5D mass, as introduced in (3.83). Here, we are following the definition from section 2.5.1 where $f_0(t) = \sqrt{kr\epsilon}\tilde{f}(t)$. Moreover, the KK decomposition now reads

$$\Psi_{L,R} = \sum_{n=0} \Psi_n^{L,R}(x) \left(\frac{t}{\epsilon}\right)^2 \sqrt{M_{\text{KK}}}\, \tilde{f}_n^{L,R}(t), \tag{4.37}$$

where these profiles must fulfill the following normalization conditions

$$2\int_\epsilon^1 \tilde{f}_m^{L*}(t) \tilde{f}_n^L(t) = 2\int_\epsilon^1 \tilde{f}_m^{R*}(t) \tilde{f}_n^R(t) = \delta_{mn}. \tag{4.38}$$

The quantity y_* in (4.34) is defined as a function of the 5D dimensionful Yukawa coupling $Y_{5\mathrm{D}}$ [110, 150]

$$y_* = \frac{\sqrt{k(1+\beta)}}{2+\beta} Y_{5\mathrm{D}}, \tag{4.39}$$

Note that for an up-type quark field Ψ_{Rb}, the Higgs-boson field H must be replaced by $\tilde{H}$. In (4.39), the parameter $Y_{5\mathrm{D}}$ is defined by

$$S_Y \supset -\int d^5x \sqrt{g}\, Y_{5\mathrm{D}} \bar{\Psi}_{La}(x,t) H(x,t) \Psi_{Rb}(x,t) + \mathrm{h.c.}\,. \tag{4.40}$$

On the other hand, the coupling of two light SM fermions to the scalar $\mathcal{S}$ only appears through a mass insertion. Indeed, before EWSB there is no direct coupling between $\mathcal{S}$ and two SM-like fermion fields, as the odd bulk scalar only couples to modes belonging to the same 5D field. Such a coupling is only generated after taking into account the fermion mixing induced by the Higgs VEV, v_{SM}.[1] We will compute the corresponding coupling perturbatively, as it is expected to be suppressed by a factor of $\mathcal{O}(v_{\mathrm{SM}}/M_{\mathrm{KK}})$. This effective coupling arises from the interactions of the $\mathcal{S}$ scalar to the different fermion zero modes and the first KK resonance with opposite chirality, once we rotate to the fermion mass basis after EWSB. Specifically, the coupling between $\mathcal{S}$, a chiral fermion zero mode a, and its first KK resonance A with opposite chirality, is given by

$$\begin{aligned} y_{aA\mathcal{S}} &= 2\, c_a \sqrt{\frac{\lambda_S}{r}} \frac{k}{\mu_S} \int_\epsilon^1 dt \tilde{f}_a(t) \tilde{f}_A^R(t) \chi_1^S(t), \quad \text{or} \\ y_{Aa\mathcal{S}} &= 2\, c_a \sqrt{\frac{\lambda_S}{r}} \frac{k}{\mu_S} \int_\epsilon^1 dt \tilde{f}_A^L(t) \tilde{f}_a(t) \chi_1^S(t), \end{aligned} \tag{4.41}$$

depending on the zero-mode chirality, where the dimensionless coupling c_a was defined in (3.83) for our model and in (2.84) for the original RS setup. Then, after rotating the fermion fields to the mass basis, we induce an interaction term $y_{f\mathcal{S}} \mathcal{S} \bar{f}_L f_R$ between the SM-like chiral fields, f_L and f_R, and $\mathcal{S}$.

We can write

$$\delta y_{fh}^{\mathrm{phys}} \equiv 1 - \frac{y_{fh}^{\mathrm{phys}}}{y_{fh}^{\mathrm{SM}}} \simeq (1 - \varkappa_f) + \Delta_{f\mathcal{H}} + \Delta_{f\mathcal{S}}, \tag{4.42}$$

where we have defined $\varkappa_f \equiv y_{f_L f_R h_0}/y_{fh}^{\mathrm{SM}}$. Here, y_{fh}^{phys} is the resulting Higgs Yukawa coupling

$$\mathcal{L} \supset -\frac{1}{\sqrt{2}} y_{fh}^{\mathrm{phys}} h \bar{f}_L f_R + \mathrm{h.c.}, \tag{4.43}$$

and y_{fh}^{SM} denotes the corresponding parameter in the SM. Moreover

$$\Delta_{f\mathcal{H}} = \sin\theta_{h\mathcal{H}} \frac{y_{f_L f_R h_1}}{y_{f_L f_R h_0}}, \qquad \Delta_{f\mathcal{S}} = \sin\theta_{h\mathcal{S}} \frac{y_{f\mathcal{S}}}{y_{f_L f_R h_0}}. \tag{4.44}$$

The quantity $\varkappa_f$ measures the ratio of the Yukawa coupling of the Higgs-boson zero mode relative to that of the SM Higgs boson, whereas the parameters $\Delta_{f\mathcal{H}}$ and $\Delta_{f\mathcal{S}}$ describe the admixtures of the Higgs-boson and $\mathbb{Z}_2$-odd scalar KK modes into the physical Higgs. At this order in $\bar{\lambda}$, $\varkappa_f$ is blind to the Higgs mixing with the odd scalar, since the contributions to this quantity in our model are a second order effect in the $\bar{\lambda}$ expansion. However, the quantity $\varkappa_f$ receives non-zero contributions that are independent of $\bar{\lambda}$, these are a byproduct of the induced light-heavy fermion mixing after EWSB and the shift in the 5D Higgs VEV. Such effects have been studied e.g. in [113], for the RS case. In particular, for $M_{\mathrm{KK}} = 5$ TeV, $\varkappa_b$ never exceeds $2.5 \cdot 10^{-2}$ when $1 \leq \beta \leq 10$. In the case of

[1] Note that $v_4 = v_{\mathrm{SM}}$ at first order in v_4/M_{KK} and ϵ.

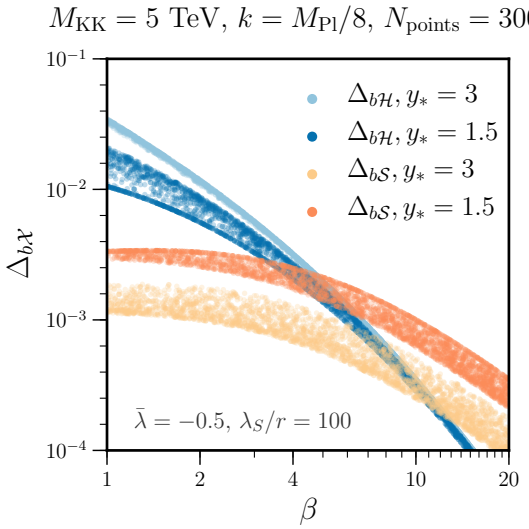

Figure 4.4: *$\Delta_{b\mathcal{H}}$ and $\Delta_{b\mathcal{S}}$ as functions of β for two different values of y_* and fixed values of $\bar{\lambda}$, λ_S/r, M_{KK} and $k/M_{\rm Pl}$. For each case, we have generated $N_{\rm points} = 3000$ random values of $c_{t_R} \in [-0.6, 0.2]$ and obtained $c_{q_L^3}$ and c_{b_R} by correctly reproducing the top- and bottom-quark masses.*

lighter quarks, even smaller values are expected. In this work we concentrate on $\Delta_{f\mathcal{S}}$ and $\Delta_{f\mathcal{H}}$, since they are direct probes of the mixing of the bulk Higgs field with the $\mathbb{Z}_2$-odd scalar field. Note that we have taken $y_{fh}^{\rm SM}$ equal to $y_{f_L f_R h_0}$ in the denominator of $\Delta_{f\mathcal{H}}$ and $\Delta_{f\mathcal{S}}$, since the difference here would be $\mathcal{O}(\bar{\lambda}\, v_{\rm SM}^2/M_{\rm KK}^2)$, and thus subleading.

Hereafter, we will focus on the bottom quark. The reasons for this are twofold. On the one hand, we expect the modifications of the Yukawa couplings to be larger for heavier quarks, while on the other hand, the bottom Yukawa coupling is among those measured most accurately, having in addition the most promising prospects [198, 205]. Indeed, existing measurements of the $h \to b\bar{b}$ signal strength (relative to the SM expectation) lead to $\mu_{h\to bb} = 1.01 \pm 0.12\,(\text{stat.})\,^{+0.16}_{-0.15}\,(\text{syst.})$ [205]. Assuming SM-like production, this translates into a measurement of $(y_{bh}^{\rm phys}/y_{bh}^{\rm SM})^2$ with an uncertainty of about 20%. However, the expected relative precision to be reached at future particle colliders such as the ILC, CLIC and the FCC is projected to be about 1% for the initial stages, reaching the 0.5% level in later stages of the experiments [198].

Figure 4.4 shows a scatter plot with values of $\Delta_{b\mathcal{H}}$ and $\Delta_{b\mathcal{S}}$ as a function of β, for $\bar{\lambda} = -0.5$ and $\lambda_S/r = 100$. For both quantities we display two different scenarios, corresponding to $y_* = 3$ and $y_* = 1.5$, where y_* is taken the same for both third-generation quarks, i.e. $y_* = y_*^t = y_*^b$. For each case, we have generated random values of $c_{t_R} \in [-0.6, 0.2]$, and obtained $c_{q_L^3}$ and c_{b_R} by fitting the top- and bottom-quark masses. One can see that for small values of β the impact on $\Delta_{b\mathcal{H}}$ of changing y_* is magnified. This is expected since, for values of $\beta \sim \mathcal{O}(1)$, the Higgs boson profile, χ_0^h, is less IR-localized and changes in β have a stronger effect in the overlap integrals in (4.34). Indeed, regardless of the value of y_*, the prediction for the bottom mass $m_b \approx v_4\, y_{b_L b_R h_0}/\sqrt{2}$ needs to remain unchanged. Since $y_{b_L b_R h_0}$ is proportional to y_*, see (4.34), changes in y_* have to be compensated by different fermion localizations and therefore a different value of the overlap integral in that relation, in such a way that $y_{b_L b_R h_0}$ remains approximately constant. The integral present in $y_{b_L b_R h_1}$ will change accordingly, but will deviate from the other integral as β decreases. This

effect is reversed for $\Delta_{b\mathcal{S}}$, since y_* is not explicitly present in the numerator of (4.44), and the effect of changing y_* is solely transfered to $\Delta_{b\mathcal{S}}$ via the different localizations of the third-generation fermion profiles. Since a smaller value of y_* requires a more IR-localized q_L^3 to reproduce the top-quark mass, one expects a bigger overlap between $\mathcal{S}$ and the third-generation LH doublet q_L^3, together with its first KK mode. This leads to a larger value of $y_{b\mathcal{S}}$ and $\Delta_{b\mathcal{S}}$, as one can see in the figure. Note that $\Delta_{b\mathcal{S}}$ scales with $\sqrt{\lambda_S/r}$, so one can readily obtain $\Delta_{b\mathcal{S}}$ for alternative choices of this parameter. Moreover, to a good approximation, both quantities scale linearly with $\bar{\lambda}$ for small values of $\bar{\lambda}$, because $\sin\theta_{h\mathcal{X}} \propto \bar{\lambda}$, as can be seen from (4.27).

Taking into account the projected sensitivity for the bottom Yukawa coupling, one can see that we will be able to probe sizable values of the scalar portal coupling $\bar{\lambda}$ for moderately small values of β. In particular, as can be seen from figure 4.4, for our chosen value $\bar{\lambda} = -0.5$, the predicted modifications $\Delta_{b\mathcal{H}}$ and $\Delta_{b\mathcal{S}}$ can be probed as long as β is less than about 4. The smaller the parameter $\bar{\lambda}$ gets, smaller would be the values of β that could be accessed at experiments.

If we analyze the couplings of the Higgs KK modes to the SM gauge bosons W and Z, which are described as zero modes of some corresponding 5D bulk gauge fields, we find that the effective 4D couplings are proportional to the integrals

$$g_{h_n VV} \propto \int_\epsilon^1 \frac{dt}{t} \varphi_H(t) \chi_n^h(t)\,, \tag{4.45}$$

where we have used that, to a good approximation, these zero-mode profiles are flat along the extra dimension, as we showed in section 2.4 (see also [103, 104, 110]). Since $\varphi_H(t) \simeq v_4 \chi_0^h(t)$, the orthogonality condition for the scalar profiles given in (4.18) makes this integral vanish for $n \neq 0$, therefore only allowing the coupling of the SM gauge bosons to the Higgs-boson zero mode to be non-vanishing, whereas couplings of higher KK modes of the Higgs boson to the gauge-boson zero modes only appear as $\mathcal{O}(v_4/M_{\text{KK}})$ corrections. Therefore, modifications of the Higgs couplings to gauge bosons caused by the mixing of the zero mode with heavier KK modes are strongly suppresed, being at most $\mathcal{O}(\bar{\lambda} v_4^2/M_{\text{KK}}^2)$. For the case of the S_1 scalar, which is a SM singlet, the couplings to EW gauge bosons would only appear at the loop level. Therefore, it will not modify the Higgs couplings to gauge bosons in an noticeable way, since these changes are suppressed by a small mixing angle $\mathcal{O}(10^{-2})$, see figure 4.2, and a loop factor.

4.2.2 Invisible Higgs decays

The mixing between the Higgs and the $\mathbb{Z}_2$-odd bulk scalar field induces an effective coupling of the Higgs boson to any 5D bulk fermion present in the theory which is not localized on the UV or IR brane. This includes the possibility of fermions not charged under the SM group, the so-called dark fermions. Hereafter, we will consider such a sector exists and will study its potential signatures, including its role in explaining the observed DM relic abundance.

We could consider two different scenarios, depending on the origin of the dark fermion masses. In the first scenario, the dark fermion mass arises purely from orbifolding, i.e. from the compactification of the WED, and it is thus proportional to its curvature, $m_\chi \propto M_{\text{KK}}$. The simplest possibility is to add a 5D fermion with no zero mode, whose first KK resonance is automatically stable and a good DM candidate. In the case where one of the chiralities of the corresponding 5D field has a Dirichlet (Neumann) BC on the UV (IR) brane, the first KK mode can be parametrically lighter than M_{KK} [206], potentially light enough to be accessible in Higgs-boson decay. In this case, the DM candidate is VL even though it can have non-trivial quantum numbers under a possible new dark group. We thus allow for N_χ copies of such VL fermion. In the second scenario the fermion mass term connects two zero modes with opposite chiralities, arising from two different 5D fields. In this scenario, the fermion mass can either come through a dark Higgs mechanism or a brane-localized VL mass. If the dark Higgs is localized towards the IR brane, or alternatively the VL

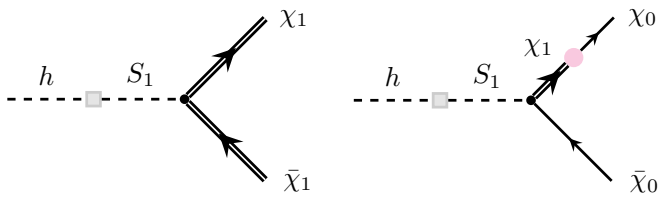

Figure 4.5: *Diagrams responsible for the generation of the Higgs coupling to dark fermions in the two main scenarios discussed in the text. The left figure corresponds to the case where the DM candidate is the first KK mode of a single 5D fermion field. The right figure corresponds to the case where the different chiralities of the DM candidate are zero modes of different 5D fields and the mediation via heavy KK modes is required.*

mass is localized on the IR brane, the fermion mass is proportional to $M_{\rm KK}$, even though a large hierarchy can arise for UV-localized dark fermions. Either way, in this case S_1 does not interact directly with these two chiral zero modes (in the same way S_1 does not couple directly to b_L and b_R, as discussed previously), since they are zero modes of two different 5D fields. However, such a coupling can be generated after a mass insertion through the mediation of the heavy KK modes (whether the mass comes from the spontaneous breaking of the dark gauge group or a VL mass is irrelevant to this discussion), as we described in the previous section. We also assume a possible multiplicity of dark fermions given by N_χ as before. We illustrate these two scenarios in figure 4.5. Note that in the second case we expect the coupling of the Higgs boson to the dark fermion to be $\mathcal{O}(m_\chi/M_{\rm KK})$ suppressed. Moreover, this calculation is rather model dependent. Alternatively, one could leave the nature of the dark fermion mass unspecified and define an effective Yukawa coupling, taking into account the mixing of the heavy modes with the zero mode.

There is an additional instance, which can be thought of as an intermediate scenario between the previous two cases. There one adds a 5D gauge-singlet fermion field with no additional flavor quantum numbers, which has a chiral zero mode and a Majorana mass term localized on the IR brane. The coupling of this field to $\mathcal{S}$ is generated analogously to the second case described above, via the involvement of a heavy KK mode and a mass insertion. Therefore, at the end of the day, this case is rather similar to the previous one, besides the difference in the multiplicities of fermionic d.o.f. for a Majorana field.

We have computed the mass of the first KK mode for a 5D field with mixed BC, i.e. for VL dark fermions as in the first case described above. This result is well known for non-dynamical bulk masses but has never been explored when these are generated by the VEV of a $\mathbb{Z}_2$-odd scalar. Therefore, we show here the results obtained in the model at hand, where the different fermion bulk masses are generated by the VEV of the odd scalar field, and compared it to the non-dynamical case, where such bulk fermion masses are introduced by hand and where the dimensionless mass parameter reads $c_\chi = M_\chi/k$, with M_χ the 5D bulk mass. We show in the left panel of figure 4.6 the first mass eigenvalue $x_1 \equiv m_1^\chi/M_{\rm KK}$, as a function of the usual dimensionless bulk-mass parameter, which we denote by c_χ for the dark fermions. In the common RS scenario, the first KK mass m_1^χ can be made arbitrarily light by adjusting the c_χ parameter [206]. However, in our model a lower bound on the mass value arises due to behavior of v_S close to the branes, where it vanishes. We find this bound to be $x_1 \sim 6 \cdot 10^{-3}$, corresponding to 30 GeV for our reference value $M_{\rm KK} = 5$ TeV. We also show in the right panel of figure 4.6 the coupling of the VL fermions to the scalar $\mathcal{S}$, defined analogously to (4.41), but now involving two KK profiles instead of one,

$$y_{\chi\mathcal{S}} = 2\, c_\chi \sqrt{\frac{\lambda_S}{r}} \frac{k}{\mu_S} \int_\epsilon^1 dt \tilde{f}^L_{1,\chi}(t) \tilde{f}^R_{1,\chi}(t) \chi_1^S(t), \tag{4.46}$$

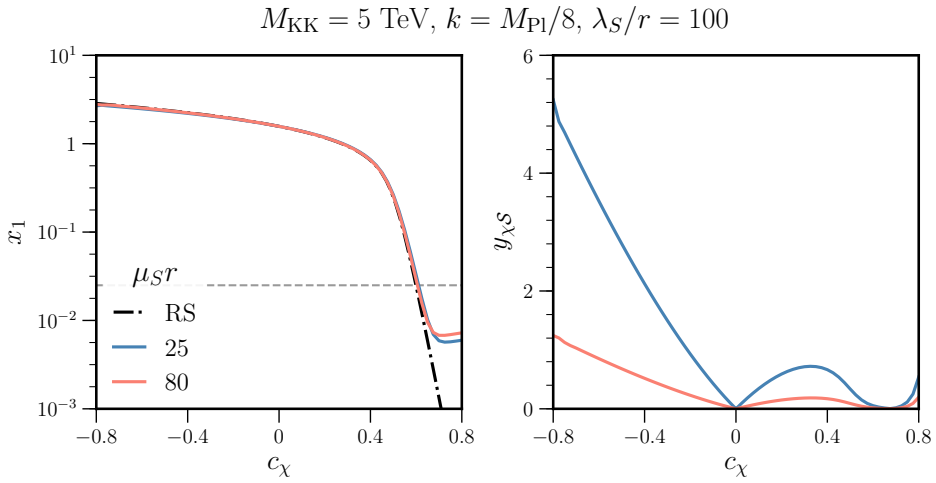

Figure 4.6: *Left panel: Mass fraction $x_1 = m_1/M_{KK}$ of the first VL fermion KK mode in terms of the 5D dimensionless bulk-mass parameter c_χ for the case of a LH chirality, with Dirichlet and Neumann BC on the UV and the IR brane, respectively, for two different values of $\mu_S r$. The black-dashed line corresponds to the case where the fermion bulk masses are obtained as it is customary in RS models. We also show the value for which $m_\chi = m_h/2$ with a dashed gray line. Higgs decays into a pair of DM particles $\chi_1\bar{\chi}_1$ are kinematically allowed only if x_1 falls below this line. Right panel: Value of $y_{\chi\mathcal{S}}$ as a function of c_χ for the same choice of BC and values of $\mu_S r$. Note that there is no black-dashed line, as the odd bulk scalar is not a feature of the traditional RS model.*

as a function of c_χ for different values of $\mu_S r$. In both panels we have set $M_{\rm KK} = 5$ TeV, $k = M_{\rm Pl}/8$ and $\lambda_S/r = 100$. We can see that, for large values of m_χ, sizable values of $y_{\chi\mathcal{S}}$ are expected. Note that the VL fermions could also have a contribution to their mass coming from the dark sector, for instance because of an IR-localized Majorana mass term. However, such modifications would not affect their couplings to the scalar $\mathcal{S}$.

Once we have determined the coupling of the VL dark fermions to the odd scalar, $\mathcal{S}$, we can proceed to compute the effective coupling to the Higgs boson. This coupling, to the first dark KK fermion, reads

$$y_{\chi h} \equiv y_{\chi\mathcal{S}} \sin\theta_{h\mathcal{S}}. \tag{4.47}$$

It is now straightforward to compute the decay width of the Higgs boson into dark fermions, as it is given by

$$\Gamma(h \to \bar{\chi}\chi) = \frac{y_{\chi h}^2 N_\chi}{8\pi} m_h \left(1 - \frac{4m_\chi^2}{m_h^2}\right)^{3/2}. \tag{4.48}$$

Using that $\mathcal{B}(H \to \text{inv}) < 0.33$ at 95% CL [207] and $\Gamma_H^{\rm SM} \approx 4$ MeV, we can set an upper limit on the effective coupling of the Higgs boson to dark fermions. We find the upper bound on $y_{\chi h}$ to be $y_{\chi h} \lesssim 0.02/\sqrt{N_\chi}$ for DM candidates with mass $m_\chi < m_h/2$. Note that this constraint does not apply to heavier fermions.

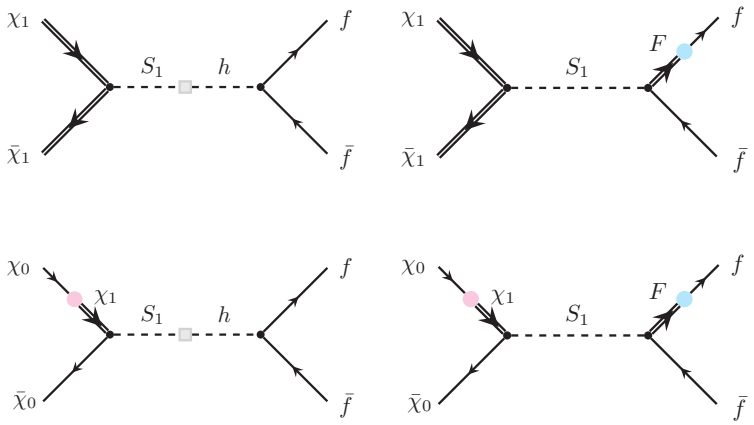

Figure 4.7: *Diagrams contributing to the DM coannihilation cross section with SM fermions in the final state. The diagrams shown in the first line correspond to the case where the DM candidate is a (potentially light) KK fermion χ_1, whereas the diagrams in the second line correspond to the case where a mass insertion on a dark fermion line is needed in order to generate an effective interaction $S_1\bar{\chi}_0\chi_0$.*

4.2.3 Scalar-mediated fermionic DM

As discussed in the previous section, the $\mathbb{Z}_2$-odd scalar field will couple to any fermion field propagating in the bulk of the WED. This provides a robust bridge between the SM and any dark sector having fermions arising from 5D bulk fermion fields. In the case where these dark fermions are stable and make for a viable DM candidate, the KK excitations of the odd scalar field thus constitute efficient mediators for DM coannihilation into SM particles. Moreover, as we have already seen, the mixing between both scalar bulk fields induces a Higgs coupling to dark fermions, thereby turning the Higgs boson into an additional scalar mediator. We will explore these contributions here.

We illustrate in figure 4.7 the relevant diagrams for the coannihilation $\bar{\chi}\chi \to \bar{f}f$ in the two cases, with and without a "dark mass insertion", that were discussed in the previous section. We represent by a blue blob the heavy-light mass mixing induced after EWSB in the visible sector, whereas the possible light-heavy mass mixing in the dark sector is depicted by a pink blob. For the sake of concreteness, we will focus on the first scenario (top row of figure 4.7), i.e. of N_χ copies of a 5D VL dark fermion field, which could potentially have parametrically light KK modes. We assume that these potentially light KK modes – the lightest dark particles – are stable and therefore a viable DM candidate. In this case, both the mass of the DM candidate m_χ and its couplings to the physical Higgs and the $\mathbb{Z}_2$-odd scalar, $y_{\chi h}$ and $y_{\chi\mathcal{S}}$, respectively, depend only on a single c_χ parameter from the dark sector (in addition to other model parameters such as e.g. M_{KK}, kr or $\mu_S r$), as shown in figure 4.6. This is the main advantage of this scenario, as there is no need of specifying any further dynamics in the dark sector. Considering the alternative case, where the interaction of $\mathcal{S}$ to the dark fermions requires a mass insertion on a dark fermion line, would just lead to a different shape of the curve $y_{\chi S} = F(m_\chi)$ and, by virtue of (4.47), also the value of $y_{\chi h} = \sin\theta_{h\mathcal{S}}\, y_{\chi S}$ (modulo a different count of d.o.f., in the case of Majorana fermions), but the new curve would have to specified in term of new parameters, and would depend on the nature of the dark sector.

For Higgs-mediated processes, the dominant coannihilation final state will be $t\bar{t}$, if kinematically accessible (i.e. for $m_\chi > m_t$), or $b\bar{b}$, together with the vector final states W^+W^- and ZZ. In the

case of diagrams mediated by S_1, $t\bar{t}$ or $b\bar{b}$ are the dominant coannihilation channels for moderately small values of m_χ. However, for larger values of m_χ, coannihilation into a SM fermion and its first KK resonance is also possible and can become the dominant coannihilation channel.

The relic abundance for a radiation-dominated freeze-out regime can be computed using [199] (see also e.g. [208, 209])

$$\Omega_\chi h^2 \simeq \frac{x_f}{2\sqrt{g_{\star S}(m_\chi/x_f)}} \frac{10^{-9}\text{GeV}^{-2}}{\langle\sigma v\rangle}, \tag{4.49}$$

where $\Omega_\chi h^2 = 0.120 \pm 0.001$ [210]. Here, $g_{\star S}(T_f)$ denotes the effective number of d.o.f. in entropy as function of the freeze-out temperature T_f, and we have defined a parameter $x_f = m_\chi/T_f$, to be determined below. $\langle\sigma v\rangle$ is the velocity-averaged cross section at the freeze-out temperature, which can be calculated as [199]

$$\begin{aligned}\langle\sigma v\rangle = &\frac{1}{8m_\chi^4 T_f K_2^2(m_\chi/T_f)} \times \\ &\int_{4m_\chi^2}^{\infty} ds\, \sigma(s)\left(s-4m_\chi^2\right)\sqrt{s} K_1(\sqrt{s}/T_f),\end{aligned} \tag{4.50}$$

where $K_n(x)$ are modified Bessel functions. The parameter x_f in (4.49) is obtained by solving the implicit equation

$$x_f = \ln\left(g_\chi \frac{m_\chi}{2\pi^3}\sqrt{\frac{45}{8x_f\, g_{\star S}(m_\chi/x_f)}}\, M_{\rm Pl}\langle\sigma v\rangle\right), \tag{4.51}$$

where $g_\chi = 4N_\chi$ is the number of DM d.o.f..

Alternatively, one can also consider that DM freeze-out happens in an early period of matter domination, as proposed in [200, 201]. Indeed, nothing prevents this from happening if radiation becomes dominant again before big-bang nucleosynthesis. The fact that DM decoupling happens during matter domination changes the freeze-out dynamics, since the Hubble rate has a different parametric dependence compared to the usual case, with $H \propto T^{3/2}$ versus $H \propto T^2$. We do not elaborate here in detail on the dynamics behind this scenario, as it is not crucial for our current analysis. We assume the existence of a scalar field ϕ (in our setup, one possibility would be to have this scalar localized on the UV brane) which starts behaving like matter at a critical temperature $T_\star \sim m_\phi$, much larger than $M_{\rm KK}$. If ϕ is sufficiently long-lived, its contribution to the energy density grows until it ultimately dominates the total energy density regardless of its initial contribution $(1-\tau)$ at $T_\star$, where $\tau \in [0,1]$ denotes the fraction of energy in radiation at $T = T_\star$. Following [200, 201] we will take $\tau = 0.99$ as a benchmark value. Freeze-out happens at a temperature T_f, in a matter-dominated universe, before ϕ instantaneously decays at $T_\Gamma < T_f < T_\star$, reheating the bath to $T_{\rm RH}$ and further diluting the DM freeze-out abundance. Hereafter we will assume $T_{\rm RH} \sim 1$ GeV. See appendix D.2 for more details.

We show in figure 4.8 the velocity averaged coannihilation cross section $\langle\sigma v\rangle$ at the freeze-out temperature as a function of m_χ, for $N_\chi = 1$, $M_{\rm KK} = 5$ TeV and $k = M_{\rm Pl}/8$. In the top panels, we consider benchmarks with different values of β, y_* as well as c_{t_R}, the parameter fixing the localization of the RH top. In both top panels, we consider $\sin\theta_{h\mathcal{S}} = 10^{-5}$ and $\lambda_S/r = 75$, as well as two different values of β and c_{t_R}. In particular, we show $\beta = 2$ (orange), $\beta = 10$ (blue), $c_{t_R} = -0.2$ (dashed line) and $c_{t_R} = -0.4$ (solid line). In the top-left panel we fix $y_* = 3$ for both the up and the down third-generation quark sector, with $c_{q_L^3}$ and c_{b_R} being determined by reproducing the top and bottom quark masses for a given choice of c_{t_R}. The same is done in the top-right panel but this time for $y_* = 1.5$. In both cases, for the sake of simplicity, light quark masses are reproduced with UV localized fermions with identical bulk mass parameters (modulo a sign difference between opposite chiralities) and different values of y_* compared to the third generation quarks, in particular we set $y_*^s = 1/2$ (for our purposes, such a not-so-refined study is more than

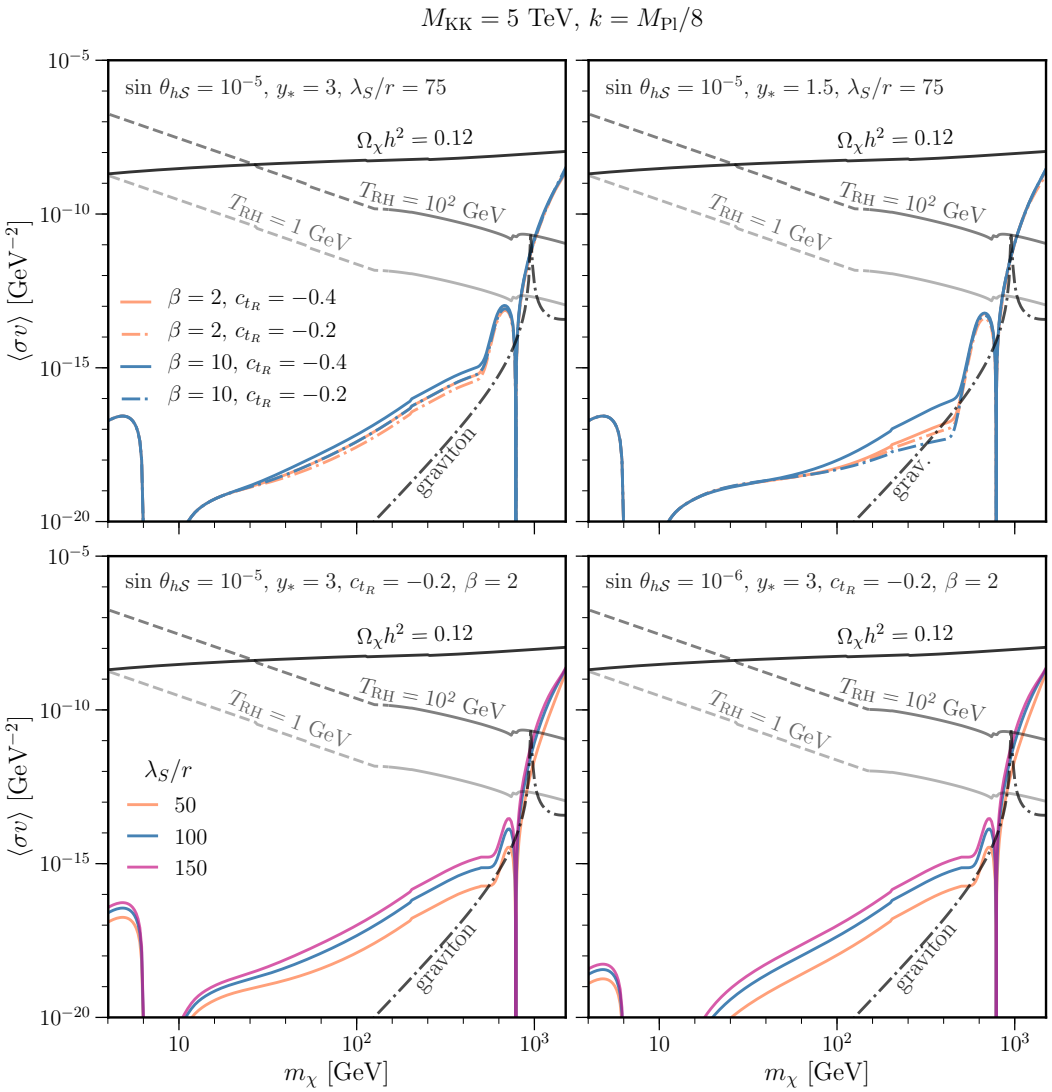

Figure 4.8: *Velocity-averaged coannihilation cross section $\langle\sigma v\rangle$ at the freeze-out temperature as a function of the DM mass m_χ, for $N_\chi = 1$, $M_{KK} = 5$ TeV and $k = M_{\rm Pl}/8$. In the top panels, we fix $\sin\theta_{h\mathcal{S}}$ and λ_S/r and consider two different values of y_*. In both cases, we take two different values of β and c_{t_R}. In the bottom panels, we fix β, y_* and c_{t_R} and consider different values of λ_S/r for $\sin\theta_{h\mathcal{S}} = 10^{-5}$ (left) and $\sin\theta_{h\mathcal{S}} = 10^{-6}$ (right). In all four panels, we show in dot-dashed gray the $\langle\sigma v\rangle$ prediction for diagrams mediated by the exchange of the first KK graviton. We also show the velocity averaged cross section reproducing the relic density experimental value from Planck with a black line, and the equivalent for a matter dominated freeze out in gray, for two different values of $T_{\rm RH}$, after using $T_\star = 10^5$ GeV and $\tau = 0.99$. For these lines the section in dashed gray corresponds to predictions for which $x_f < 3$, and therefore in this regime the DM decouples relativistically [200, 201].*

enough). We can see that increasing the IR localization of the RH top, i.e. having bigger values of $|c_{t_R}|$, leads to a bigger cross section for most DM masses when $y_* = 3$. Since y_* is large enough

in this case, changes in c_{t_R} does not have a dramatic impact on $c_{q_L^3}$ and c_{b_R}, which remain almost unchanged. Therefore, the increase of the coannihilation cross section is mostly due to a larger $\mathcal{S}t_Lt_R$ coupling, which is indeed the leading one for DM masses below about 10 TeV. Such a larger coupling is the consequence of a bigger overlap with $\mathcal{S}$ and the increase in the Yukawa coupling $\mathcal{Y}$ coming with c. In the case of $y_* = 1.5$, on the contrary, changes in $|c_{t_R}|$ do have a dramatic impact on $c_{q_L^3}$, since the RH top can not account for the top mass alone, requiring a fairly IR-localized third-generation quark doublet. Therefore, the contribution to $\mathcal{S}t_Lt_R$ coming from the mixing of both top chiralites are similar, which results in bigger changes in the cross section for the region of DM masses between 1 and 4 TeV as one can see from figure 4.8 top-right panel. On the other hand, bigger values of β lead in general to a larger mixing between fermion-zero modes and their KK resonances after EWSB, increasing the effective coupling $y_{f\mathcal{S}}$ after diagonalization. Therefore, in general, one expects a larger coannihilation cross section for $m_\chi \lesssim 10$ TeV and increasing values of β. Changing β also affects the $\mathcal{S}t_Lt_R$ coupling indirectly, since reproducing the observed quark masses results in different values of the mass parameters c. This explains why the dashed blue line in the top-right panel of figure 4.8 is below the other ones, since $c_{q_L}^3$ accidentally gets close to zero and thus reduces the LH doublet contribution to the $\mathcal{S}t_Lt_R$ coupling, as can be seen in equation (4.41).

In the bottom panels of figure 4.8, on the other hand, we show $\langle\sigma v\rangle$ for different values of λ_S/r as a function of m_χ. In both bottom panels, we fix $\beta = 2$, $y_* = 3$ for both third-generation quark sectors, as well as $c_{t_R} = -0.2$. The left-bottom panel corresponds to the choice $\sin\theta_{h\mathcal{S}} = 10^{-5}$, whereas for the bottom-right one we take $\sin\theta_{h\mathcal{S}} = 10^{-6}$. By reducing the mixing, one effectively suppress the Higgs mediated contribution to the coannihilation cross section, which is mostly relevant for small DM masses, specially around $m_\chi \approx m_h/2$. This will have an impact on direct detection as we will see later, since the Higgs provides the leading contribution in such experiments, and therefore larger values of $\sin\theta_{h\mathcal{S}}$ will typically lead to more severe bounds from these experiments. The parameter λ_S/r controls the effective Yukawa coupling of the $\mathcal{S}$ scalar to fermions $y_{\chi\mathcal{S}}$, see equations (4.41) and (4.46). We consider $\lambda_S/r = 50$ (orange), $\lambda_S/r = 100$ (blue) and $\lambda_S/r = 150$ (purple). Increasing λ_S/r has the effect of increasing the coannihilation cross section in general, besides for values of $m_\chi \lesssim m_{\mathcal{S}}/2$ where the rise in the coupling is offset by the increase of its decay width. One should note that the resonant-like peak starting around $7-8$ TeV is not only due to the $\mathcal{S}$ resonance but also to the fact that new heavy-light final states become kinematically accessible in the coannihilation process. They consist of a first KK fermion resonance of mass ~ 15 TeV together with a SM-like fermion. We do not show values of m_χ beyond ~ 15 TeV since the DM mass can not be made heavier than this value for $M_{\rm KK} = 5$ TeV, as in our model the DM candidate is the first KK mode of a VL field and these fields cannot be made heavier by tuning the parameters of the model, see the plateau for large negative values of c_χ in figure 4.6. One could entertain the possibility of adding brane-localized masses or kinetic terms for this to happen, but for the sake of concreteness we do not explore such possibilities here. At any rate, for such large values of m_χ, one would need to eventually include the decays of $\mathcal{S}$ to a pair of low-lying KK fermions, which will make $\mathcal{S}$ much wider of what is sensible in a perturbative theory.

In addition, we display for comparison the contribution due to diagrams mediated by the first KK graviton, which are also irreducible in models with WEDs (see e.g. [209,211] for useful expressions). We can see that, for the chosen values of $M_{\rm KK}$ and $k/M_{\rm Pl}$, corresponding to $M_{\rm KK} = 5$ TeV and $\Lambda_\pi = M_{\rm Pl}e^{-k\pi r} = 40$ TeV, the contribution of the odd scalar resonance $\mathcal{S}$ dominates over the KK graviton one. In particular, this happens for all values of m_χ, with the exception of the small regions where the coupling $y_{\chi\mathcal{S}}$ goes to zero and, in some cases depending on the model parameters, at the peak appearing for $m_\chi \sim m_1^G/2$. The relative importance of each contribution and the location of the graviton peak can be changed by modifying the ratio $\Lambda_\pi/M_{\rm KK}$ and/or by including brane kinetic terms [212]. We will not explore such possibilities, being our aim here to show that the scalar contribution can naturally be the leading one, as one can readily see from the figure. In addition to the KK-graviton contribution, one also expects a contribution to the coannihilation

cross section arising from the radion exchange. However, such contribution is rather model dependent, since the radion mass is subject to the specifics of the stabilization mechanism. A natural expectation is that the radion will be much lighter than the first KK graviton. Such exchange has been discussed e.g. in [211, 213]. In particular, the authors of [213] found the radion contribution to be mostly irrelevant for a rather light radion and IR-localized matter. A similar result is expected here, for a light radion that does not mix with the other bulk scalars (that one can always assume). The interesting case where the stabilizing scalar mixes with both the Higgs and the $\mathbb{Z}_2$-odd scalar leads to an extensive case study that was out of the scope of this thesis.

Finally, we also show the values of the velocity averaged cross section for which the observed DM relic abundance is reproduced, both in the usual scenario and in the case of an early period of matter domination. In particular, we show with a solid black line the values of $\langle\sigma v\rangle$ for which a value of $\Omega_\chi h^2 = 0.12$ is reproduced, in the case of a regular freeze-out mechanism, and in the scenario of matter domination in gray, for $\tau = 0.99$, $T_\star = 10^5$ GeV and two values of $T_{\rm RH}$, 1 and 10^2 GeV, respectively. The lines in dashed gray correspond to regions where $x_f < 3$, i.e. for a region in parameter space where the DM is expected to decouple relativistically and the current treatment loses validity, see [200, 201] for more details. We can see that the observed relic abundance can be reproduced in the case of matter domination for masses $m_\chi \sim 8 - 10$ TeV. In the usual case of radiation domination, $\langle\sigma v\rangle$ can be a non-negligible fraction of the total averaged cross section required to reproduce the observed relic abundance for $m_\chi \sim 15$ TeV, which is in the ballpark of the naturally expected fermion masses in RS models.

4.2.4 Direct detection

Direct detection experiments can also set very important constraints on the parameter space in scalar-mediated models of DM. In fact, these experiments can constrain most of the parameter space in the case of Higgs-mediated DM, with the exception of a small region around the Higgs resonance, see e.g. [210, 214]. We study here the constraints from direct detection experiments in our model. In particular, we will compare our predictions with the current constraints from the Xenon1T experiment [203, 204].

We are interested in the spin-independent cross section. This quantity can be computed as

$$\sigma_{\chi N} \approx \frac{4}{\pi}\mu_{\chi N}^2 \left[Z f_p + (A - Z) f_n\right]^2 \simeq \frac{4}{\pi}\mu_{\chi N}^2 A^2 f_n^2, \tag{4.52}$$

with Z and A the atomic number and atomic mass of the target nucleus, respectively, and $\mu_{\chi N}$ the reduced mass of the DM and nucleus system [208, 209, 215]. In order to compute such cross section we use following effective Lagrangian

$$\mathcal{L}_{\rm eff} = f_p(\bar\chi\chi)(\bar p p) + f_n(\bar\chi\chi)(\bar n n). \tag{4.53}$$

The terms f_p and f_n in (4.52) and (4.53) are effective coupling constants and can be written as

$$\frac{f_{p,n}}{m_{p,n}} = \sum_{q=u,d,s} f_{Tq}^{(p,n)} \frac{\alpha_q}{m_q} + \frac{2}{27} f_{Tg}^{(p,n)} \sum_{q=c,b,t} \frac{\alpha_q}{m_q}, \tag{4.54}$$

where α_q stands for the effective four-fermion interaction vertex, obtained by considering the scalar t-channel exchange. In our model α_q has the following form

$$\alpha_q = y_{\chi\mathcal{S}} \left\{ \frac{y_{q\mathcal{S}}}{m_{\mathcal{S}}^2} + \frac{y_{qh} \sin\theta_{h\mathcal{S}}}{m_h^2} \right\}. \tag{4.55}$$

Finally, $f_{Tg}^{(p,n)}$ is defined as

$$f_{Tg}^{(p,n)} = 1 - \sum_{q=u,d,s} f_{Tq}^{(p,n)}, \tag{4.56}$$

and the values for f_p^q and f_n^q are [209, 216]

$$\begin{aligned} &f_p^u = (20.8 \pm 1.5) \cdot 10^{-3}, \quad f_p^d = (41.1 \pm 2.8) \cdot 10^{-3}, \\ &f_n^u = (18.9 \pm 1.4) \cdot 10^{-3}, \quad f_n^d = (45.1 \pm 2.7) \cdot 10^{-3}, \\ &f_p^s = f_n^s = 0.043 \pm 0.011. \end{aligned} \tag{4.57}$$

One can compare the contribution of each scalar to the direct detection cross section by computing the ratio between the terms appearing in equation (4.55). We find that the channel mediated by the Higgs boson is dominant provided that

$$\sin\theta_{h\mathcal{S}} > \frac{m_h^2}{m_{\mathcal{S}}^2} \frac{y_{q\mathcal{S}}}{y_{qh}} \sim 10^{-7}, \tag{4.58}$$

i.e. we expect the Higgs mediated interaction to be the leading contribution for $\sin\theta_{h\mathcal{S}} > 10^{-7}$. This tells us in particular that we can relax the constraints coming from direct detection by making this mixing smaller, while keeping the same coupling $y_{\chi\mathcal{S}}$ to the DM fermions. However, this is only possible up to the point when the odd scalar contribution becomes dominant. In this case

$$\alpha_q \approx \frac{y_{\chi\mathcal{S}} y_{q\mathcal{S}}}{m_{\mathcal{S}}^2}, \tag{4.59}$$

which can be considered as the minimum value of α_q, depending just on these three quantities.

We show in figure 4.9 the constraints from direct detection and invisible Higgs decays on the velocity averaged coannihilation cross section $\langle\sigma v\rangle$ as a function of m_χ. We used $N_\chi = 1$, $M_{\text{KK}} = 5$ TeV, $k = M_{\text{Pl}}/8$ and different values for the mixing angles between the odd scalar and the Higgs boson, in particular $\sin\theta_{h\mathcal{S}} = \{10^{-3}, 10^{-4}, 10^{-5}, 10^{-6}\}$, ordered from top left to bottom right. The first two mixing angles, i.e. the two largest ones, can only be achieved for $\bar{\lambda} < 0$, whereas the last two can be obtained for positive and negative values of $\bar{\lambda}$. We display in each figure the prediction from our model with blue lines for two different benchmarks, corresponding to the choices of $y_* = 3$ (solid line) and $y_* = 1.5$ (dot-dashed line) for the third generation quarks t and b. As we did in previous sections, light generations have identical bulk mass parameters in absolute value and different values of y_*, starting with $y_*^s = 1/2$). In both cases, we have set $\beta = 2$ and $c_{t_R} = -0.2$, while λ_S/r has been chosen in such a way that $\Gamma_{\mathcal{S}}/m_{\mathcal{S}} \approx 0.7$. More specifically, we have taken $\lambda_S/r = 120$ and $\lambda_S/r = 65$, for $y_* = 3$ and $y_* = 1.5$, respectively. Since the width is mostly given by the decay of $\mathcal{S}$ into a third generation quark and its first KK resonance, such assignment ensures that the overall coupling of the odd scalar field to the visible sector is roughly the same in both cases. However, the smaller value of y_* in the benchmark $\{y_* = 1.5,\ \lambda_S/r = 65\}$ leads to a more IR-localized third-generation LH doublet q_L^3 and to a much larger coupling of $\mathcal{S}$ to $\bar{b}_L b_R$ and $\bar{q}_L^3$ plus its first KK resonance, even with a smaller value of λ_S/r. At the end of the day, however, the solid lines are above the dashed ones for most values of m_χ, since the DM coupling $y_{\chi\mathcal{S}}$ is smaller by a factor $\sqrt{120/65} \sim 1.4$, which makes up for the small differences existing among the couplings to the visible sector. The differences between both benchmarks are magnified once the purely $\mathcal{S}$-mediated channel, corresponding to the right column of figure 4.7, is the most dominant one. This happens in particular for large DM masses and/or small values of $\sin\theta_{h\mathcal{S}}$, as one can readily see by comparing the different panels in figure 4.9.

The gray region shows the area excluded by the LHC experimental limits on the Higgs invisible decay width, whereas the purple region corresponds to the Xenon1T constraints, where we are using the same convention as for our predictions, i.e. the solid line corresponds to the values of

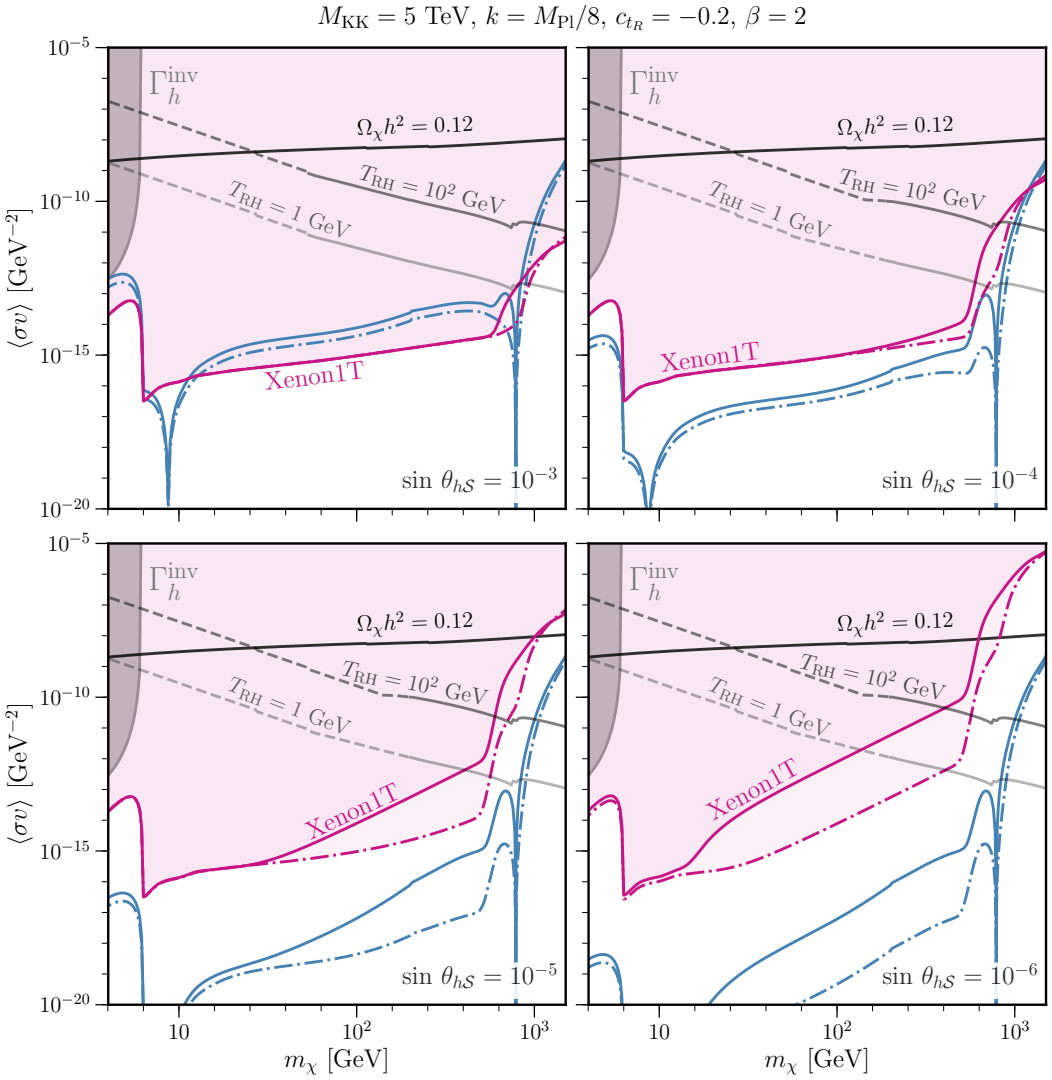

Figure 4.9: *Velocity averaged coannihilation cross section at the freeze-out temperature for different values of the mixing between the odd scalar and the Higgs boson, $\sin\theta_{h\mathcal{S}} = \{10^{-3}, 10^{-4}, 10^{-5}, 10^{-6}\}$, from top left to bottom right. The first two cases correspond to negative values of $\bar{\lambda}$. We have set $N_\chi = 1$, $M_{KK} = 5$ TeV and $k = M_{\rm Pl}/8$. We show in blue the predictions for two different benchmarks with different values of y_* and λ_S/r (see the text). In both cases, we have fixed $c_{t_R} = -0.2$ and $\beta = 2$. We show the constraints coming from the Higgs invisible decay width in gray and the limits from Xenon1T in purple. Moreover, we include the velocity averaged cross section reproducing the relic density experimental value from Planck in black, and the equivalent for a matter dominated freeze out in gray, for two different values of $T_{\rm RH}$, where we used $T_\star = 10^5$ GeV and $\tau = 0.99$. For these lines the section in dashed gray corresponds to predictions for which $x_f < 3$, and therefore in this regime the DM decouples relativistically [200, 201].*

$y_* = 3$ and the dot-dashed line stands for $y_* = 1.5$. The latter are found by plotting the velocity averaged coannihilation cross section obtained after rescaling $y_{\chi\mathcal{S}}$ such that $\sigma_{\chi N}$ saturates the

Xenon1T experimental bound, what we could denote as $\langle\sigma v\rangle_{\rm Xenon1T}$. For the values of $\sin\theta_{h\mathcal{S}}$ shown in this figure, the leading contribution to the DM-nucleon cross section is by far the one arising from the t-channel exchange of a Higgs boson, with the exception of the last case where $\sin\theta_{h\mathcal{S}} = 10^{-6}$ and the $\mathcal{S}$ contribution, while still being subleading, starts to become relevant. This explains why the Xenon1T bound for the $\{y_* = 3,\ \lambda_S/r = 120\}$ benchmark is weaker than the limit obtained for $\{y_* = 1.5,\ \lambda_S/r = 65\}$, whenever the coannihilation cross section is dominated by the $\mathcal{S}$ contribution. Indeed, in the former case, the couplings of $\mathcal{S}$ to the visible sector are slightly larger. This leads to a larger value of $\langle\sigma v\rangle_{\rm Xenon1T}$ after rescaling $y_{\chi\mathcal{S}}$ and to a weaker bound from direct detection. When $\langle\sigma v\rangle$ is dominated by the Higgs exchange, direct detection bounds become indistinguishable for both benchmarks, since the Higgs couplings to the SM quarks are mostly fixed and SM-like.

We also show the velocity averaged cross section reproducing the observed relic density both in the usual freeze-out scenario (black) and in the case of an early period of matter domination, for values of $T_{\rm RH} = 10^2$ GeV (dark gray) and 1 GeV (light gray). For both gray lines, we used $T_\star = 10^5$ GeV and $\tau = 0.99$. Similarly to figure 4.8, lines in dashed gray correspond to regions where $x_f < 3$ and the DM is expected to decouple relativistically. We can see that for $\sin\theta_{h\mathcal{S}} = 10^{-3}$, one can not explain the observed relic abundance without exceeding the bounds from Xenon1T. However, this is not the case in the matter dominated scenario with $T_{\rm RH} = 1$ GeV, where the required coannihilation cross section to explain the DM relic abundance does not exceed the Xenon1T bound for $y_* = 3$. In the case of $y_* = 1.5$, the required cross section is excluded by the Xenon1T bound. In the case of $\sin\theta_{h\mathcal{S}} = 10^{-4}$ we can reproduce the correct amount of DM for both values of $T_{\rm RH}$, in a scenario of matter domination, being the values of $\langle\sigma v\rangle$ corresponding to the top of the resonant peak excluded by direct detection bounds. For even smaller values of $\sin\theta_{h\mathcal{S}}$ like 10^{-5} or 10^{-6}, the data from Xenon1T never constrains the predictions for the coannihilation cross section obtained in both benchmarks, since the Higgs coupling to DM $y_{\chi h}$ becomes too small for such mixing angles. Therefore, by assuming an early period of matter domination, we are able to explain the observed DM relic abundance for moderately small values of $\sin\theta_{h\mathcal{S}}$ without conflicting current direct detection experiments. Even in the case of radiation domination, we can get to values of $\langle\sigma v\rangle$ relatively close to the ballpark of what is needed. In that case, $\mathcal{S}$ could potentially contribute with a non-negligible fraction to the coannihilation cross section necessary to reproduce the experimental value of the relic density. Nevertheless, additional mediators accounting for most of the coannihilation are certainly needed in the scenario of radiation domination.

4.3 Summary

In realistic models the Higgs scalar field should propagate in the bulk of the WED. We have seen that in this context a mixing of the Higgs with the odd bulk scalar responsible for bulk fermion masses is then unavoidable. In this chapter, we have studied the impact of the scalar mixing on precision measurements of Higgs couplings. In particular, we have computed the modifications of the Higgs couplings to EW gauge bosons and the bottom quark as a consequence of the mixing between the SM-like Higgs boson and the first KK resonances of both bulk fields, $\mathcal{H}$ and $\mathcal{S}$. We have demonstrated that planned future colliders could probe the induced modifications on the b-quark Yukawa in the case where $\beta \lesssim 4$, values for which the Higgs boson has a strong presence into the bulk.

In addition, we have demonstrated that the addition of a $\mathbb{Z}_2$-odd scalar field developing a VEV in extra-dimensional models can provide a unique window into any 5D fermionic dark sector. Given that the scalar field generates fermion bulk masses through Yukawa-like interactions with the different 5D fermions, it will also irrevocably connect the SM with any possible dark sector featuring bulk fermions. We have studied in detail the phenomenological consequences of such a

portal, showing that the lightest KK dark fermion is stable and can coannihilate efficiently thanks to the mediation of the odd-scalar resonances as well as the Higgs boson. Indeed, we have demonstrated that it is possible to reproduce the observed DM relic abundance for an $\mathcal{O}(10)$ TeV KK dark fermion assuming that freeze-out occurs during an early period of matter domination, and that we can naturally avoid the constraints from direct-detection experiments, which only become relevant when the parameter $\sin\theta_{h\mathcal{S}}$ controlling the mixing between the SM-like Higgs boson and the first KK resonance $\mathcal{S}$ of the $\mathbb{Z}_2$-odd scalar field is $\gtrsim 10^{-4}$. For smaller values of the mixing angle, the Higgs contribution to the direct-detection cross section gets reduced and loses importance, becoming comparable at some point to the one from the t-channel exchange of the $\mathcal{S}$ resonance, which is beyond the reach of current direct detection experiments. Even in the regular case of a radiation dominated freeze-out, this irreducible contribution to the coannihilation cross-section can account for a non-negligible part of the required value when the DM mass is ~ 15 TeV. We have also shown that these scalar contributions to the coannihilation cross section can be more important than those arising from the exchange of KK gravitons. We have also studied the constraints on the Higgs effective Yukawa coupling to DM when its mass is light enough to allow for the Higgs boson to decay into a pair of DM particles. We conclude that the effective Yukawa coupling to the dark fermions $y_{\chi h} \lesssim 0.02/\sqrt{N_\chi}$, with N_χ being the multiplicity of the 5D dark fermion.

5 | Conclusions

Research in particle physics focused on BSM have received lots of attention during the last decades, leading to many extensions of the SM being carefully analyzed. Motivated initially by the gauge hierarchy problem, scenarios such as supersymmetry, composite-Higgs models and models with extra dimensions arised, playing an important role. However, the current absence of any sign of NP at the LHC (the discrepancies in the flavour sector are not yet sufficient to claim evidence for physics BSM) lead to a broader diversification of both the motivations triggering the search for BSM physics both from the theoretical and experimental perspective. In this regard, models with extra dimensions, and in particular those considering a WED, offer a beautiful solution to several of the current open questions, as e.g. the flavor puzzle and DM. The RS model, even though it was originally proposed as a solution of the gauge hierarchy problem, also allows for an explanation of the flavor puzzle, as was realized soon after its birth. In this model, the flavor structure of the quark sector of the SM can be easily reproduced by means of a specific pattern of localization of the SM fermions in the bulk of the RS geometry. In other words, a similar mechanism provides a natural explanation of both the hierarchy of fermion masses and mixings, and the one existing between the EW and Planck scales. In addition, because of the AdS/CFT correspondence, models with WED offer a precious window into strongly interacting sectors. This correspondence offers a suitable framework where many predictions, that otherwise could only be pursued using a lattice approach, can be made.

However, as we point out, an important question that has not received much attention in RS models with bulk matter fields is why do 5D fermion masses, which are responsible for the different fermion localizations along the extra dimension and therefore for solving the flavor puzzle, have such a coordinate dependence. Fermion bulk masses have to be odd under the $\mathbb{Z}_2$ orbifold symmetry, and commonly they are introduced as a constant parameter with an *ad-hoc* $\text{sgn}(\phi)$ function, in RS models. The main scope of this thesis has been to demonstrate whether it is possible to obtain these masses dynamically, and analyze the phenomenological viability.

In chapter 3, we have demonstrated that it is indeed possible to do so, via the VEV of a $\mathbb{Z}_2$-odd scalar with bulk Yukawa couplings to the different 5D fermion fields. In this chapter we have shown that an odd bulk scalar can develop non-trivial background solutions in a WED and that the background solutions resemble the sign function in realistic scenarios, i.e. for the same values of the model parameters that solve the hierarchy problem. In addition, we considered the possible backreaction effects of the VEV on the metric, and found that the RS warp function gets modified in the vicinity of the UV and IR branes for natural values of the gravity-scalar coupling. Moreover,

we analyzed the gauge sector of the minimal RS model with an $SU(2)_L \times U(1)_Y$ bulk gauge symmetry and its extension to a bulk custodial symmetry. We calculated the oblique parameters S and T and set constraints on the masses of the first KK resonances considering both gauge sectors, and under different configurations of our model. We found that the mass of the first KK gluon state, which is often the lightest KK resonance in the model, must be at least $\mathcal{O}(10)$ TeV, irrespectively of whether backreaction effects on the metric are included or neglected. We have also calculated the KK spectrum of the $\mathbb{Z}_2$-odd bulk scalar, and found that it corresponds to one of the heaviest first KK resonances of the model, with $m_S \sim 30$ TeV. We studied how fermion bulk masses are generated in our dynamical mechanism, where 5D bulk fermions couple to the bulk odd scalar through 5D Yukawa couplings, and how the fermion profiles depend on these Yukawa couplings together with the shape of the scalar VEV profile. We checked that, similarly to the usual RS setup, fermion zero-modes can be localized towards either of the branes. We calculated the deviations of the fermion zero-mode and KK-mode profiles in our model when compared to the traditional case, where a sgn(ϕ) function is used. We find that these deviations can become sizable when backreaction effects are taken into account. Moreover, the magnificence of dynamically generating bulk fermion masses is manifested when one considers the full SM fermion content and calculates the SM fermion masses after EWSB. As usual, the idea is to describe SM fermions with corresponding chiral zero modes of the bulk fermion fields. In that case, the localization of the zero-mode profiles determines the 4D masses spectrum. Using the idea of the framework presented previously for the traditional RS setup, we have illustrated how this mechanism works for the case of a ϕ-dependent VEV and a modified warp factor, by reproducing the hierarchical structure of SM quark masses and mixing angles. Given that the deviations in the fermion profiles can potentially affect the model predictions, we studied the impact of such behavior on flavor observables and on the RS-GIM mechanism. In particular, we computed the flavor observable ϵ_K, which typically sets one of the most stringent bounds on models with a WED, under different configurations of the model parameters and different strengths of the backreaction on the metric, and compared our predictions with those obtained in the conventional RS model. The experimental values of ϵ_K put constrain the mass of the first KK gluon state to be above $\mathcal{O}(10)$ TeV, in agreement with the S and T bounds. Moreover, we saw that the presence of a non-negligible backreaction tends to slightly weaken the RS-GIM mechanism, enhancing the NP contribution to ϵ_K. Moreover, we checked if the presence of new TeV-scale KK resonances could lead to flavor-changing interactions among the SM fermions. The exchange of the scalar KK resonances between four SM fermions gives rise to effective dimension 8 interactions which are suppressed by four powers of v_h/M_{KK}, and are therefore negligible.

In chapter 4, we demonstrated that the inclusion of the $\mathbb{Z}_2$-odd scalar field in WED models not only provides a viable origin for the 5D fermion masses, but that it can also act as a mediator connecting the SM with any 5D fermionic dark sector. Being the odd bulk scalar responsible for the bulk mass of any fermion propagating in the WED, the bulk scalar will inevitably connect the SM with such other 5D field. Therefore, assuming that the lightest KK fermion is stable and can coannihilate efficiently due to the mediation of the odd-scalar resonance, it would automatically become a DM candidate. In addition, in realistic models the Higgs scalar field propagates into the bulk of the WED, and thus a mixing with the new scalar field becomes unavoidable. Not only this could lead to modifications of the SM-like behavior for the Higgs boson, but it makes the Higgs become another potential mediator of the fermionic DM. We studied the impact of the scalar mixing on precision measurements of Higgs couplings. In particular, we have computed the modifications of the Higgs couplings to EW gauge bosons and the bottom quark as a consequence of the mixing between the SM-like Higgs boson and the first KK resonances of both bulk fields, finding that planned future colliders could probe the induced modifications on the b-quark Yukawa for some values of the model parameters, specially as the Higgs moves away from the IR brane. We have also studied the constraints on the Higgs effective Yukawa coupling to DM when its mass is light enough to allow for the Higgs boson to decay into a pair of DM particles. We also demonstrated that the mediation of the first odd-scalar resonance together with the Higgs boson contribution

can reproduce the observed DM relic abundance for an $\mathcal{O}(10)$ TeV KK dark fermion, assuming that freeze-out occurs during an early period of matter domination. On the other hand, for the regular case of a radiation dominated freeze-out, the scalar contribution to the coannihilation cross section can account for a non-negligible part of the required value, when the DM mass is ~ 15 TeV. We have also compared the scalar contributions to the coannihilation cross section with those arising from the exchange of KK gravitons, finding that the odd scalar contribution be more important for most DM masses. Moreover, we have shown that our predictions are not in conflict with current data from direct-detection experiments, for most of the chosen benchmarks. In particular, we found that these bounds are only relevant when the scalar mixing parameter, $\sin\theta_{h\mathcal{S}}$, takes values larger than $\mathcal{O}(10^{-4})$, whereas for smaller values, the contribution to the direct-detection cross section given by t-channel Higgs exchange becomes less and less important, finding a lower limit at the moment the $\mathcal{S}$ exchange t-channel takes over, at around $\sin\theta_{h\mathcal{S}} \sim \mathcal{O}(10^{-7})$.

In summary, the results presented in this work put RS models with bulk matter fields on firmer theoretical ground. They provide a viable mechanism for dynamically generating a crucial ingredient for the RS solution of the flavor puzzle, i.e. 5D fermion bulk masses, which here appear as the VEV of a bulk scalar field. This mechanism comes together with the prediction of the existence of heavy scalar KK resonances, much heavier than the other KK states, being this a feature of the model. These scalar resonances are too heavy to be produced in possible high-energy extensions of the LHC. However, they would infer modifications on Higgs couplings when both scalars are allowed to mix, therefore, offering a promising window into the model, and making it testable at future colliders. Moreover, we have shown that models with a WED naturally feature a DM mediator, as the odd scalar can connect any fermion dark sector to the SM. This scalar, together with the Higgs boson, can contribute to explain of the observed relic abundance of DM, specially when we consider heavy VL fermions, without conflicting with current data from colliders, flavor experiments and cosmology and while still providing natural solutions to the hierarchy problem and the flavor puzzle.

A | Coordinates dictionary

We discussed in section 2.1 that the WED is described by an $S^1/\mathbb{Z}_2$ topology, i.e. that it is compactified on an orbifold, and that therefore, the coordinates must satisfy the identifications appearing in (2.2). This allows for a different choice of coordinates, all of them satisfying the requirements from (2.2). We summarize here the different choice of coordinates that have been used throughout this thesis. This appendix could serve as a dictionary for translating from any one choice of coordinates to another.

We know that a generic 5D metric that respects 4D Poincaré invariance can be written as

$$ds^2 = a(x_5)^2 \eta_{\mu\nu} dx^\mu dx^\nu - b(x_5)^2 dx_5^2. \tag{A.1}$$

From (A.1), we can easily summarize some of coordinate choices for describing the AdS$_5$ spacetime

$$\begin{aligned} ds^2 &= e^{-2k|y|}\eta_{\mu\nu}dx^\mu dx^\nu - dy^2 \\ &= e^{-2kr|\phi|}\eta_{\mu\nu}dx^\mu dx^\nu - r^2 d\phi^2 \\ &= \frac{\epsilon^2}{t^2}\left(\eta_{\mu\nu}dx^\mu dx^\nu - \frac{1}{M_{\text{KK}}^2}dt^2\right), \end{aligned} \tag{A.2}$$

where the translations between them are

$$y = r\phi, \qquad \text{and} \qquad t = \epsilon\, e^{kr|\phi|}, \qquad \text{with} \qquad \epsilon = e^{-kr\pi}, \tag{A.3}$$

and $M_{\text{KK}} = k\epsilon = ke^{-kr\pi}$.

Knowing that the extra dimension has end-points at $y = y_{\text{UV}} = 0$ and $y = y_{\text{IR}} = r\pi$, corresponding to the UV and IR branes respectively, we can infer the brane positions for the different coordinates. We summarize this in table A.1, together with the expressions for $\sqrt{g}$.

Moreover, the derivatives are related by

$$\frac{\partial y}{\partial \phi} = r, \qquad \text{and} \qquad \frac{\partial t}{\partial \phi} = \text{sgn}(\phi)\, kr\epsilon\, e^{kr\phi} = \text{sgn}(\phi)\, krt, \tag{A.4}$$

in such a way that

$$dy = r d\phi, \qquad \text{sgn}(\phi)\, d\phi = \frac{dt}{krt}, \tag{A.5}$$

Coordinates	UV brane	IR brane	$\sqrt{g}$
y	0	$y_{\rm IR} = r\pi$	$e^{-4k\|y\|}$
ϕ	0	π	$re^{-4kr\|\phi\|}$
t	ϵ	1	$\epsilon^5/\left(t^5 M_{\rm KK}\right)$

Table A.1: *Dictionary for the different coordinates.*

and

$$\partial_y = \frac{1}{r}\partial_\phi, \qquad\qquad \partial_\phi = \text{sgn}(\phi)\, krt\partial_t\,, \tag{A.6}$$

where $\partial_x \equiv \partial/\partial x$.

We can now check how the integrals on the fifth dimensions can be performed using these coordinates. Starting from the integral in y

$$\int_{-y_{\rm IR}}^{y_{\rm IR}} dy\Big(\dots\Big) = 2\int_0^{y_{\rm IR}} dy\Big(\dots\Big), \tag{A.7}$$

where we have denoted by $(\dots)$ any possible term of the action, which has to be invariant under $\mathbb{Z}_2$ transformations, and therefore it allows for the integral to be only performed in the $[0, y_{\rm IR}]$ interval. In term of the other coordinates, this reads

$$\int_{-y_{\rm IR}}^{y_{\rm IR}} dy\Big(\dots\Big) = 2\int_0^{\pi} rd\phi\Big(\dots\Big) = \frac{2}{k}\int_\epsilon^1 dt\Big(\dots\Big) = \frac{2\pi r}{L}\int_\epsilon^1 dt\Big(\dots\Big), \tag{A.8}$$

where we have used $L \equiv kr\pi$. In addition, we can see that the δ-functions must transform with opposite factor as the differential, therefore they come together with a factor $b(x_5)^{-1}$, as

$$\delta(y - y_z) \;\longleftrightarrow\; r^{-1}\delta(\phi - \phi_z) \;\longleftrightarrow\; \delta(t - t_z)\, kt\,, \tag{A.9}$$

where, e.g. z might stand for the IR brane location, leading to $y_{\rm IR} = r\pi$, $\phi_{\rm IR} = \pi$ and $t_{\rm IR} = 1$.

B | Complementary formulae for fermions in WED

In this appendix we want to complement section 2.7 of the text with some useful formulae. Most of this formulae has been obtained from [110].

First of all, in that section we discussed how dealing with brane-localized Yukawa interactions for the 5D fermions make the usual orthonormality conditions not valid anymore, because of inconsistencies caused by the delta function. Therefore, we need to promote such conditions to the following

$$\int_{-\pi}^{\pi} d\phi\, e^{\sigma(\phi)}\, \boldsymbol{A}_m^{(Q,u)}(\phi)\, \boldsymbol{A}_n^{(Q,u)}(\phi) = \delta_{mn}\, \mathbf{1} + \boldsymbol{\Delta A}_{mn}^{(Q,u)}\,, \qquad \text{with } \boldsymbol{A} = \boldsymbol{C}, \boldsymbol{S}. \tag{B.1}$$

Here, we sumarize the results for $\boldsymbol{\Delta C}_{mn}^{(Q,u)}$ and $\boldsymbol{\Delta S}_{mn}^{(Q,u)}$ obtained in [110], where these quantities were derived, reading

$$\begin{aligned} \boldsymbol{\Delta C}_{mn}^{(Q,u)} &= \pm\, \frac{2}{r}\, \frac{m_m\, \boldsymbol{C}_n^{(Q,u)}(\pi)\, \boldsymbol{S}_m^{(Q,u)}(\pi^-) - m_n\, \boldsymbol{C}_m^{(Q,u)}(\pi)\, \boldsymbol{S}_n^{(Q,u)}(\pi^-)}{m_m^2 - m_n^2}\,, \\ \boldsymbol{\Delta S}_{mn}^{(Q,u)} &= \mp\, \frac{2}{r}\, \frac{m_m\, \boldsymbol{C}_m^{(Q,u)}(\pi)\, \boldsymbol{S}_n^{(Q,u)}(\pi^-) - m_n\, \boldsymbol{C}_n^{(Q,u)}(\pi)\, \boldsymbol{S}_m^{(Q,u)}(\pi^-)}{m_m^2 - m_n^2}\,, \end{aligned} \tag{B.2}$$

for $m \neq n$, while for $m = n$ we have

$$\boldsymbol{\Delta C}_{nn}^{(Q,u)} = -\boldsymbol{\Delta S}_{nn}^{(Q,u)} = \pm \frac{1}{m_n r}\, \boldsymbol{C}_n^{(Q,u)}(\pi)\, \boldsymbol{S}_n^{(Q,u)}(\pi^-)\,. \tag{B.3}$$

Moving forward to the implementation of the Froggat-Nielsen mechanism [110, 174], we assumed the projection of the zero-mode profiles at the IR brane to have the following hierarchical structure

$$|F(c_{A_1})| < |F(c_{A_2})| < |F(c_{A_3})|\,. \tag{B.4}$$

which is a natural assumption for us, that can be easily obtained even by considering small differences in the c_{A_i} parameters. Then, we showed the explicit formulae for how the products of up- and down-type quark masses can be written in terms of the dimensionless 5D Yukawa and the $F(c_{A_i})$ parameters in (2.156), in such a way that we obtained the expression for the different quark masses in terms of these entries, which we presented in (2.157). Moreover, we introduced the recipe for computing elements of the $\boldsymbol{U}_q$ and $\boldsymbol{W}_q$ matrices in (2.158), where we did so in terms

of $\boldsymbol{u}_q$ and $\boldsymbol{w}_q$ coefficientes plus phases, which we denoted by ϕ_j. We would like to ellaborate on this idea here and complement the results presented in section 2.7.

We can rewrite the $\boldsymbol{u}_q$ and $\boldsymbol{w}_q$ elements in terms of the entries of the dimensionless 5D Yukawa matrices, $(Y_q)_{ij}$, and their minors $(M_q)_{ij}$, [110]. In this case, the matrices $\boldsymbol{u}_q$ and $\boldsymbol{w}_q$ read

$$\boldsymbol{u}_q = \begin{pmatrix} 1 & \frac{(M_q)_{21}}{(M_q)_{11}} & \frac{(Y_q)_{13}}{(Y_q)_{33}} \\ -\frac{(M_q)^*_{21}}{(M_q)^*_{11}} & 1 & \frac{(Y_q)_{23}}{(Y_q)_{33}} \\ \frac{(M_q)^*_{31}}{(M_q)^*_{11}} & -\frac{(Y_q)^*_{23}}{(Y_q)^*_{33}} & 1 \end{pmatrix}, \qquad \boldsymbol{w}_q = \begin{pmatrix} 1 & \frac{(M_q)^*_{12}}{(M_q)^*_{11}} & \frac{(Y_q)^*_{31}}{(Y_q)^*_{33}} \\ -\frac{(M_q)_{12}}{(M_q)_{11}} & 1 & \frac{(Y_q)^*_{32}}{(Y_q)^*_{33}} \\ \frac{(M_q)_{13}}{(M_q)_{11}} & -\frac{(Y_q)_{32}}{(Y_q)_{33}} & 1 \end{pmatrix}, \tag{B.5}$$

while the phases ϕ_j are given by

$$e^{i\phi_j} = \text{sgn}\left[F(c_{Q_j})\, F(c_{q_j})\right]\, e^{-i(\rho_j - \rho_{j+1})}\,, \tag{B.6}$$

with

$$\rho_1 = \arg\left(\det(\boldsymbol{Y}_q)\right), \qquad \rho_2 = \arg\left((M_q)_{11}\right), \qquad \rho_3 = \arg\left((Y_q)_{33}\right), \qquad \rho_4 = 0. \tag{B.7}$$

Now, the leading-order expressions for λ, A, $\bar{\rho}$, and $\bar{\eta}$ can be derived in terms of the entries for the matrices we just defined. Recalling definitions of the Wolfenstein parameters of the CKM matrix

$$\lambda = \frac{|V_{us}|}{\sqrt{|V_{ud}|^2 + |V_{us}|^2}}, \qquad A = \frac{1}{\lambda}\left|\frac{V_{cb}}{V_{us}}\right|, \qquad \bar{\rho} - i\bar{\eta} = -\frac{V^*_{ud}V_{ub}}{V^*_{cd}V_{cb}}\,, \tag{B.8}$$

we have

$$\begin{aligned} \lambda =& \frac{|F(c_{Q_1})|}{|F(c_{Q_2})|}\left|\frac{(M_d)_{21}}{(M_d)_{11}} - \frac{(M_u)_{21}}{(M_u)_{11}}\right|, \\ A =& \frac{|F(c_{Q_2})|^3}{|F(c_{Q_1})|^2\,|F(c_{Q_3})|}\left|\left(\frac{(Y_d)_{23}}{(Y_d)_{33}} - \frac{(Y_u)_{23}}{(Y_u)_{33}}\right) \Big/ \left(\frac{(M_d)_{21}}{(M_d)_{11}} - \frac{(M_u)_{21}}{(M_u)_{11}}\right)^2\right|, \\ \bar{\rho} - i\bar{\eta} =& \frac{(Y_d)_{33}\,(M_u)_{31} - (Y_d)_{23}\,(M_u)_{21} + (Y_d)_{13}\,(M_u)_{11}}{(Y_d)_{33}\,(M_u)_{11}\left[\frac{(Y_d)_{23}}{(Y_d)_{33}} - \frac{(Y_u)_{23}}{(Y_u)_{33}}\right] \times \left[\frac{(M_d)_{21}}{(M_d)_{11}} - \frac{(M_u)_{21}}{(M_u)_{11}}\right]}\,. \end{aligned} \tag{B.9}$$

We see that the relation $\bar{\rho} - i\bar{\eta}$ is independent of the zero-mode profiles $F(c_{A_i})$ to first order.

We would like now to determine the zero-mode profiles in terms of the quark masses and Wolfenstein parameters from the expressions (2.157) and (B.9). However, it was shown in [110] that the model is not determined and that we have the freedom to express the different $F(c_{A_i})$ parameters in terms of a single one, which we chose to be $F(c_{Q_2})$, following their recipe.

Therefore, expressing the $F(c_{A_i})$ parameters of the different quark fields in terms of $F(c_{Q_2})$, we find

$$|F(c_{Q_1})| = \frac{\lambda}{\left|\frac{(M_d)_{21}}{(M_d)_{11}} - \frac{(M_u)_{21}}{(M_u)_{11}}\right|}\,|F(c_{Q_2})|\,, \qquad |F(c_{Q_3})| = \frac{\left|\frac{(Y_d)_{23}}{(Y_d)_{33}} - \frac{(Y_u)_{23}}{(Y_u)_{33}}\right|}{A\lambda^2}\,|F(c_{Q_2})|\,, \tag{B.10}$$

for the LH fields and

$$
\begin{aligned}
|F(c_{u_1})| =& \frac{\sqrt{2}m_u}{v_h} \frac{|(M_u)_{11}|\left|\frac{(M_d)_{21}}{(M_d)_{11}} - \frac{(M_u)_{21}}{(M_u)_{11}}\right|}{\lambda|\det(\boldsymbol{Y}_u)|} \frac{1}{|F(c_{Q_2})|}\,, \\
|F(c_{u_2})| =& \frac{\sqrt{2}m_c}{v_h} \frac{|(Y_u)_{33}|}{|(M_u)_{11}|} \frac{1}{|F(c_{Q_2})|}\,, \\
|F(c_{u_3})| =& \frac{\sqrt{2}m_t}{v_h} \frac{A\lambda^2}{|(Y_u)_{33}|\left|\frac{(Y_d)_{23}}{(Y_d)_{33}} - \frac{(Y_u)_{23}}{(Y_u)_{33}}\right|} \frac{1}{|F(c_{Q_2})|}\,, \\
|F(c_{d_1})| =& \frac{\sqrt{2}m_d}{v_h} \frac{|(M_d)_{11}|\left|\frac{(M_u)_{21}}{(M_u)_{11}} - \frac{(M_d)_{21}}{(M_d)_{11}}\right|}{\lambda|\det(\boldsymbol{Y}_d)|} \frac{1}{|F(c_{Q_2})|}\,, \\
|F(c_{d_2})| =& \frac{\sqrt{2}m_s}{v_h} \frac{|(Y_d)_{33}|}{|(M_d)_{11}|} \frac{1}{|F(c_{Q_2})|}\,, \\
|F(c_{d_3})| =& \frac{\sqrt{2}m_b}{v_h} \frac{A\lambda^2}{|(Y_d)_{33}|\left|\frac{(Y_u)_{23}}{(Y_u)_{33}} - \frac{(Y_d)_{23}}{(Y_d)_{33}}\right|} \frac{1}{|F(c_{Q_2})|}\,,
\end{aligned}
\tag{B.11}
$$

for the RH fields.

These relations lead to a hierarchical structure between the quark profiles evaluated at the IR brane, as was shown in (2.159) and (2.159).

However, note that all the relations in (B.10) and (B.10) have a dependence on $|F(c_{Q_2})|$, being opposite for the LH profiles and RH profiles. This makes the system invariant under the following transformations

$$
F(c_{Q_i}) \to \eta\, F(c_{Q_i})\,, \qquad F(c_{q_i}) \to \frac{1}{\eta}\, F(c_{q_i})\,, \tag{B.12}
$$

where the $SU(2)_L$ doublet fields are rescaled by a η factor, and at the same time the singlet fields are rescaled with an opposite factor $1/\eta$. Note that this relation holds while leaving the 5D Yukawa couplings invariant.

Moreover, there are more transformations that can be implemented leaving the system invariant if we allow the 5D dimensionless Yukawa couplings to rescale. One possibility would be

$$
F(c_{Q_i}) \to \eta\, F(c_{Q_i})\,, \qquad F(c_{q_i}) \to \eta\, F(c_{q_i})\,, \qquad \boldsymbol{Y}_q \to \frac{1}{\eta^2}\, \boldsymbol{Y}_q, \tag{B.13}
$$

for which we rescale all of the RH fields with the same factor. However, we could rescale them using different η_q for each q, and absorb that factor with the 5D Yukawas as follows

$$
F(c_{Q_i}) \to \eta\, F(c_{Q_i})\,, \qquad F(c_{q_i}) \to \eta_q\, F(c_{q_i})\,, \qquad \boldsymbol{Y}_q \to \frac{1}{\eta\eta_q}\, \boldsymbol{Y}_q. \tag{B.14}
$$

Note that this set of transformations (or any combination of them) leave the masses and mixing angles in the quark sector unchanged. However, they could lead do completely different bulk profiles for the fermions, and therefore the prediction for any possible observable that depends on the bulk profiles would change accordingly, as e.g. observables for flavor-changing interactions or the prediction for $\Delta\epsilon_K$, see section 3.5.2.

C | EW precision observables in the custodial model

Here we expand on the discussion from section 3.2, where we have studied the impact of the deviations from the original RS metric (caused by the backreaction) on EWPT and present general expressions for the gauge boson masses, the Fermi constant and the EW observables. Since the minimal case has been presented in greater detail on section 3.2 and analogous expressions for this case can be found in the literature (see e.g. [124]), we focus here on the extended model with a custodial symmetry in the bulk. In this case the gauge-sector bulk action reads [111]

$$S_{5\mathrm{D}}^{\mathrm{gauge}} = \int d^4x \int_{-\pi}^{\pi} d\phi \, \sqrt{g}\, g^{KM} g^{LN} \Big[-\frac{1}{4} L^a_{KL} L^a_{MN} - \frac{1}{4} R^a_{KL} R^a_{MN} - \frac{1}{4} X_{KL} X_{MN} \Big] + S_{\mathrm{Higgs}} + S_{\mathrm{GF}} + S_{\mathrm{FP}} \,, \tag{C.1}$$

where L_{MN}, R_{MN}, and X_{MN} are the field-strength tensors for the bulk gauge groups $SU(2)_L$, $SU(2)_R$, and $U(1)_X$ respectively, and $a = 1, 2, 3$. Employing the usual redefinition of the Higgs field to canonically normalize its kinetic term, the action for the Higgs sector S_{Higgs} takes the form

$$S_{\mathrm{Higgs}} = \int d^4x \int_{-\pi}^{\pi} d\phi \left[\frac{1}{2} \mathrm{Tr} \left[(D_\mu H)^\dagger (D^\mu H) \right] - V(H) \right] \delta(\phi - \pi) \,, \tag{C.2}$$

where the Higgs bi-doublet can be represented as

$$H(x) = \frac{1}{\sqrt{2}} \begin{pmatrix} v_h + h(x) - iG^3(x) & -i\sqrt{2}\, G^+(x) \\ -i\sqrt{2} G^-(x) & v_h + h(x) + iG^3(x) \end{pmatrix} . \tag{C.3}$$

The covariant derivative on the Higgs field is defined as

$$iD_\mu H = i\partial_\mu H + \frac{g_{5L}}{2} L^a_\mu \tau^a H - \frac{g_{5R}}{2} H \tau^a R^a_\mu \,, \tag{C.4}$$

with g_{5L} and g_{5R} denoting the 5D gauge couplings of $SU(2)_L$ and $SU(2)_R$, respectively. By means of the field redefinitions

$$L^\pm_\mu = \frac{1}{\sqrt{2}} (L^1_\mu \mp i L^2_\mu), \qquad R^\pm_\mu = \frac{1}{\sqrt{2}} (R^1_\mu \mp i R^2_\mu), \tag{C.5}$$

the EOM for the charged gauge bosons can be brought to the same form as for the minimal case, c.f. (3.56). We obtain

$$-\frac{1}{r^2} \partial_\phi \Big(e^{-2\sigma(\phi)} \, \partial_\phi \, \chi^{\mathbb{W}}_n(\phi) \Big) = (m^\pm_n)^2 \, \chi^{\mathbb{W}}_n(\phi) \,; \qquad \mathbb{W} = L^\pm, R^\pm, \tag{C.6}$$

with non-diagonal BC

$$\begin{matrix}\partial_\phi \chi_n^{L^\pm}(0) = 0 \\ \chi_n^{R^\pm}(0) = 0\end{matrix} \quad , \qquad \left[\mathbb{I}\,\partial_\phi + \pi e^{2\sigma(\pi)} r^2 \tilde{m}_{\tilde{A}}^2 \begin{pmatrix} c_W^2 & -s_W c_W \\ -s_W c_W & s_W^2 \end{pmatrix}\right] \begin{pmatrix} \chi_n^{L^\pm}(\pi^-) \\ \chi_n^{R^\pm}(\pi^-) \end{pmatrix} = 0, \quad \text{(C.7)}$$

where we have defined

$$\tilde{m}_{\tilde{A}}^2 = \frac{1}{2\pi r} \frac{(g_{L5}^2 + g_{R5}^2) v_h^2}{4}\,, \qquad s_W = \frac{g_{5R}}{\sqrt{g_{5L}^2 + g_{5R}^2}}\,. \quad \text{(C.8)}$$

Similarly, if one defines

$$\begin{pmatrix} Z_M \\ A_M \end{pmatrix} = \begin{pmatrix} c_w & -s_w \\ s_w & c_w \end{pmatrix} \begin{pmatrix} L_M^3 \\ B_M \end{pmatrix}, \qquad \begin{pmatrix} Z'_M \\ B_M \end{pmatrix} = \begin{pmatrix} c_\theta & -s_\theta \\ s_\theta & c_\theta \end{pmatrix} \begin{pmatrix} R_M^3 \\ X_M \end{pmatrix}, \quad \text{(C.9)}$$

with

$$s_\theta = \frac{g_{5X}}{\sqrt{g_{5R}^2 + g_{5X}^2}}\,, \qquad s_w = \frac{g_{5Y}}{\sqrt{g_{5L}^2 + g_{5Y}^2}}\,, \qquad g_{5Y} = \frac{g_{5R} g_{5X}}{\sqrt{g_{5R}^2 + g_{5X}^2}}\,, \quad \text{(C.10)}$$

the bulk EOM for the neutral gauge fields become

$$-\frac{1}{r^2}\,\partial_\phi\Big(e^{-2\sigma(\phi)}\,\partial_\phi\,\chi_n^{\mathbb{Z}}(\phi)\Big) = (m_n)^2\,\chi_n^{\mathbb{Z}}(\phi)\,; \qquad \mathbb{Z} = Z', Z, \quad \text{(C.11)}$$

$$-\frac{1}{r^2}\,\partial_\phi\Big(e^{-2\sigma(\phi)}\,\partial_\phi\,\chi_n^{A}(\phi)\Big) = (m_n^A)^2\,\chi_n^{A}(\phi)\,, \quad \text{(C.12)}$$

with BC

$$\begin{gathered}\partial_\phi\,\chi_n^A(0) = \partial_\phi\,\chi_n^A(\pi^-) = 0\,, \qquad \partial_\phi\,\chi_n^Z(0) = 0\,, \qquad \chi_n^{Z'}(0) = 0\,, \\ \left[\mathbb{I}\,\partial_\phi + \pi e^{2\sigma(\pi)} r^2 \tilde{m}_{\tilde{A}}^2 \begin{pmatrix} c_W^2/c_w^2 & -s_W c_W c_\theta/c_w \\ -s_W c_W c_\theta/c_w & s_W^2 c_\theta^2 \end{pmatrix}\right] \begin{pmatrix} \chi_n^Z(\pi^-) \\ \chi_n^{Z'}(\pi^-) \end{pmatrix} = 0\,.\end{gathered} \quad \text{(C.13)}$$

We can solve the EOM for the zero modes of the charged and neutral gauge bosons perturbatively in powers of v_h^2/M_{KK}^2. For the masses of the zero-mode gauge bosons, we then obtain

$$m_W^2 = \tilde{m}_{\tilde{A}}^2 c_W^2 \left[1 - \frac{r^2 \tilde{m}_{\tilde{A}}^2}{\pi} \int_0^\pi d\phi_1 e^{2\sigma(\phi_1)} \left(c_W^2 \phi_1^2 + \pi^2 s_W^2\right)\right] + \mathcal{O}\left(\frac{v_h^6}{M_{\text{KK}}^4}\right), \quad \text{(C.14)}$$

$$m_Z^2 = \tilde{m}_{\tilde{A}}^2 \frac{c_W^2}{c_w^2} \left[1 - \frac{r^2 \tilde{m}_{\tilde{A}}^2}{\pi} \int_0^\pi d\phi_1 e^{2\sigma(\phi_1)} \left(\frac{c_W^2}{c_w^2} \phi_1^2 + \pi^2 s_W^2 c_\theta^2\right)\right] + \mathcal{O}\left(\frac{v_h^6}{M_{\text{KK}}^4}\right), \quad \text{(C.15)}$$

while the photon remains massless and has a constant profile in the bulk. Moreover, we find for the Fermi constant

$$\begin{aligned}\frac{G_F}{\sqrt{2}} &= \frac{g_{5L}^2}{8 r m_W^2} \left[(\chi_0^{L\pm}(0))^2 - m_W^2 \tilde{D}_W(0,0;0)\right] \\ &= \frac{1}{2v_h^2}\left[1 + r^2 \tilde{m}_{\tilde{A}}^2 \pi \int_0^\pi d\phi_1 e^{2\sigma(\phi_1)} (1 + \rho_W) + \mathcal{O}\left(\frac{v_h^4}{M_{\text{KK}}^4}\right)\right].\end{aligned} \quad \text{(C.16)}$$

The oblique parameters $\hat{S}$, $\hat{T}$, $\hat{W}$ and $\hat{Y}$ defined in [54] can be expressed in terms of the quantities [56]

$$\hat{\alpha} = 2\pi \left[\tilde{D}_{\mathbb{A}}(\pi,\pi;0) - D^{(-)}(\pi,\pi;0)\right] = \pi r^2 \int_0^\pi d\phi_1\, e^{2\sigma(\phi_1)} \left(1 - \frac{\phi_1^2}{\pi^2}\right), \quad \text{(C.17)}$$

$$\hat{\beta} = 2\pi \tilde{D}_{\mathbb{A}}(0,\pi;0) = \pi r^2 \int_0^\pi d\phi_1\, e^{2\sigma(\phi_1)} \frac{\phi_1}{\pi} \left(1 - \frac{\phi_1}{\pi}\right), \quad \text{(C.18)}$$

$$\hat{\gamma} = 2\pi \tilde{D}_{\mathbb{A}}(0,0;0) = -\pi r^2 \int_0^\pi d\phi_1 e^{2\sigma(\phi_1)} \left(1 - \frac{\phi_1}{\pi}\right)^2, \quad \text{(C.19)}$$

where $\tilde{D}_{\mathbb{A}}(\phi,\phi';p)$ was defined in (3.64), and $D^{(-)}(\phi,\phi';0)$ is the 5D propagator for bulk gauge fields with UV Dirichlet BC, evaluated at zero momentum and before EWSB. One finds

$$D^{(-)}(\phi,\phi';0) = -\frac{r^2}{2}\int_0^{\phi_<} d\phi_1\, e^{2\sigma(\phi_1)}\,, \tag{C.20}$$

where $\phi_< = \min(\phi,\phi')$. This leads to

$$\hat{S} = \frac{g^2 v_h^2}{2}\big(\hat{\beta}-\hat{\gamma}\big) = \frac{2\alpha\pi v_h^2}{s_w^2}\,\pi r^2\int_0^{\pi} d\phi_1\, e^{2\sigma(\phi_1)}\left(1-\frac{\phi_1}{\pi}\right), \tag{C.21}$$

$$\hat{T} = \frac{g'^2 v_h^2}{4}\left(-\hat{\alpha}+2\hat{\beta}-\hat{\gamma}\right) = 0, \tag{C.22}$$

$$\hat{W} = \hat{Y} = -\frac{g^2 v_h^2}{4}\hat{\gamma} = \frac{\alpha v_h^2}{s_w^2}\,\pi^2 r^2\int_0^{\pi} d\phi_1 e^{2\sigma(\phi_1)}\left(1-\frac{\phi_1}{\pi}\right)^2, \tag{C.23}$$

where $g \equiv g_{5L}/\sqrt{2\pi r}$ and $g' \equiv g_{5Y}/\sqrt{2\pi r}$ are the EW gauge couplings of the SM.

In the limit of negligible backreaction on the metric, these low-energy observables in (C.14) and (C.16) take the familiar form

$$m_W^2 = c_W^2\tilde{m}_{\tilde{A}}^2\left[1-\frac{c_W^2\tilde{m}_{\tilde{A}}^2}{2M_{\rm KK}^2}\left(L-1+\frac{1}{2L}\right)-\frac{s_W^2\tilde{m}_{\tilde{A}}^2}{2M_{\rm KK}^2}L+\mathcal{O}\left(\frac{v_h^4}{M_{\rm KK}^4}\right)\right], \tag{C.24}$$

$$m_Z^2 = \frac{c_W^2}{c_w^2}\tilde{m}_{\tilde{A}}^2\left[1-\frac{c_W^2\tilde{m}_{\tilde{A}}^2}{2c_w^2 M_{\rm KK}^2}\left(L-1+\frac{1}{2L}\right)-\frac{s_W^2 c_\theta^2\tilde{m}_{\tilde{A}}^2}{2M_{\rm KK}^2}L+\mathcal{O}\left(\frac{v_h^4}{M_{\rm KK}^4}\right)\right], \tag{C.25}$$

$$\frac{G_F}{\sqrt{2}} = \frac{1}{2v_h^2}\left[1+\frac{\tilde{m}_{\tilde{A}}^2}{2M_{\rm KK}^2}L+\mathcal{O}\left(\frac{v_h^4}{M_{\rm KK}^4}\right)\right] = \frac{1}{2v_{\rm SM}^2}, \tag{C.26}$$

where $L \equiv kr\pi$. On the other hand, the expressions for the oblique parameters S and T simplify to

$$S = \frac{4s_w^2}{\alpha}\,\hat{S} = \frac{2\pi v_h^2}{M_{\rm KK}^2}\,, \qquad T = \frac{\hat{T}}{\alpha} = 0\,. \tag{C.27}$$

D | DM cross sections and Matter dominated freeze-out

D.1 Cross section expressions

The different coannihilation cross sections of a couple of DM fermion fields, $\bar{\chi}\chi$, into a pair of SM particles are given by (see e.g. [201])

$$\sigma(\bar{\chi}\chi \to \bar{f}f) = \frac{N_f\, y_{\chi\mathcal{S}}^2}{16\pi} s \left(1 - \frac{4m_f^2}{s}\right)^{3/2} \left(1 - \frac{4m_\chi^2}{s}\right)^{1/2} \times \left[\frac{y_{fh}^2 \sin^2\theta_{h\mathcal{S}}}{\left(s - m_h^2\right)^2} + \frac{y_{f\mathcal{S}}^2}{\left(s - m_{\mathcal{S}}^2\right)^2} + \frac{2\, y_{fh} y_{f\mathcal{S}} \sin\theta_{h\mathcal{S}}}{\left(s - m_{\mathcal{S}}^2\right)\left(s - m_h^2\right)}\right], \tag{D.1}$$

$$\sigma(\bar{\chi}\chi \to hh) = \frac{y_{\chi\mathcal{S}}^2}{32\pi} \left(1 - \frac{4m_h^2}{s}\right)^{1/2} \left(1 - \frac{4m_\chi^2}{s}\right)^{1/2} \times \left[\frac{9\sin^2\theta_{h\mathcal{S}} m_h^4}{v_4^2\left(s - m_h^2\right)^2} + \frac{\sin^2\theta_{h\mathcal{S}} x_{S_1}^4 M_{\text{KK}}^4}{v_4^2\left(s - m_{\mathcal{S}}^2\right)^2} + \frac{6\, m_h^2 \sin^2\theta_{h\mathcal{S}} x_{S_1}^2 M_{\text{KK}}^2}{v_4^2\left(s - m_{\mathcal{S}}^2\right)\left(s - m_h^2\right)}\right], \tag{D.2}$$

$$\sigma(\bar{\chi}\chi \to VV) = \frac{\delta_V y_{\chi\mathcal{S}}^2 \sin^2\theta_{h\mathcal{S}}}{8\pi} \left(1 - \frac{4m_V^2}{s}\right)^{1/2} \left(1 - \frac{4m_\chi^2}{s}\right)^{1/2} \times \frac{m_V^4}{v_4^2\left(s - m_h^2\right)^2}\left[2 + \frac{(s - 2m_V^2)^2}{4m_V^4}\right], \tag{D.3}$$

$$\sigma(\bar{\chi}\chi \to \bar{Q}q) = \frac{N_Q\, y_{\chi\mathcal{S}}^2 y_{Qq}^2}{16\pi} \frac{s}{\left(s - m_{\mathcal{S}}^2\right)^2} \left(1 - \frac{m_Q^2}{s}\right)^{3/2} \left(1 - \frac{4m_\chi^2}{s}\right)^{1/2}, \tag{D.4}$$

with $\delta_V = 1, 1/2$ for $V = W^\pm, Z$.

D.2 Matter dominated freeze-out

We review here the relevant formulae for the calculation of the current DM relic abundance after freeze-out during an early period of matter domination (see [200, 201] for more details).

We assume the presence of a long-lived heavy scalar field ϕ, which starts behaving like matter at a critical temperature $T_\star \sim m_\phi$, which we assumme to be much larger than $M_{\rm KK}$, i.e. $T_\star \gg M_{\rm KK}$. If ϕ is long-lived enough, its contribution to the energy density ρ_ϕ will grow until ultimately monopolize the total energy density regardless of its initial contribution at $T_\star$, given by $(1-\tau)$, with $\tau \in [0,1]$

$$\tau = \left.\frac{\rho_R + \rho_\chi}{\rho_R + \rho_\chi + \rho_\phi}\right|_{T=T_\star}, \tag{D.5}$$

and ρ_χ, ρ_R, the energy density of DM and the visible sector of the extra-dimensional theory.

Using the Friedmann equation

$$H^2 = \frac{1}{3m_{\rm Pl}^2}\left[\rho_R + \rho_\chi + \rho_\phi\right], \tag{D.6}$$

and defining $H_\star = H(T_\star)$ we obtain

$$H^2 = H_\star^2\left[\frac{g_*\tau}{g_* + g_\chi}\left(\frac{a_\star}{a}\right)^4 + (1-\tau)\left(\frac{a_\star}{a}\right)^3 + \frac{g_\chi\tau}{g_* + g_\chi}\left(\frac{a_\star}{a}\right)^4\right], \tag{D.7}$$

where g_* is the effective number of relativistic degrees of freedom of the visible sector of the extra-dimensional theory. Assuming that the entropy is conserved in this sector and taking into account that $g_* \gg g_\chi$, we can write

$$H = H_\star\sqrt{1-\tau}\left(\frac{x_\star}{x}\right)^{3/2}\left[\frac{r}{1-\tau}\left(\frac{x_\star}{x}\right) + 1\right]^{1/2}, \tag{D.8}$$

where we have defined $x = m_\chi/T$ and $x_\star = x(T_\star)$.

The annihilation rate $\Gamma_{\rm ann}$ can be written as

$$\Gamma_{\rm ann} = \frac{g_\chi m_\chi^3}{(2\pi x)^{3/2}} e^{-x}\langle\sigma v\rangle, \tag{D.9}$$

where $\langle\sigma v\rangle$ is the velocity-averaged coannihilation cross section. In our scenario of scalar mediated fermionic DM, after Taylor expanding (σv) with respect to v_r^2, we can write

$$(\sigma v) \simeq a + b v_r^2 = b v_r^2, \tag{D.10}$$

since $a = 0$ for the scalar-mediated cross sections considered in this thesis. Therefore, one can write the velocity-averaged coannihilation cross section as

$$\langle\sigma v\rangle \simeq \frac{6b}{x}, \tag{D.11}$$

which leads to

$$\Gamma_{\rm ann} = \frac{g_\chi m_\chi^3}{(2\pi)^{3/2}} e^{-x}\frac{6b}{x^{5/2}}. \tag{D.12}$$

We can define the freeze-out temperature by asking $H(x_f) = \Gamma_{\rm ann}(x_f)$, with $x_f = m_\chi/T_f$. This leads to

$$x_f = \log\left(\frac{g_\chi}{(2\pi)^{3/2}}\frac{m_\chi^3 6b}{H_\star x_\star^{3/2}}(1-\tau)^{-1/2}\left(x_f^2+\frac{r x_\star}{1-\tau}x_f\right)^{1/2}\right). \tag{D.13}$$

The yield $Y = n_\chi/s$, with s the entropy density, is given at freeze-out by

$$Y_f = \left(\lambda\int_{x_f}^{\infty} dx\left(1+\frac{\tau}{1-\tau}\frac{x_\star}{x}\right)^{-1/2}x^{-7/2}\right)^{-1}, \tag{D.14}$$

where

$$\lambda = \frac{2\pi^2 g_{*S} m_\chi^3 6b}{45 H_\star x_\star^{3/2}}, \tag{D.15}$$

with g_{*S} the number of effective entropic degrees of freedom. More explicitly, it reads

$$\begin{aligned}\frac{1}{Y_f} \approx \frac{\pi^2 g_{*S} m_\chi^3 \langle\sigma v\rangle}{90 H_\star x_\star^4}\left(\frac{1-\tau}{\tau}\right)^{5/2}\Bigg(&3x_f \sinh^{-1}\left(\sqrt{\frac{x_\star\tau}{x_f(1-\tau)}}\right)\\ &+\sqrt{\frac{x_\star}{x_f}}\left(\frac{\tau}{1-\tau}\right)^{3/2}\sqrt{1+\frac{x_\star\tau}{x_f(1-\tau)}}\left[2x_\star - 3x_f\frac{(1-\tau)}{\tau}\right]\Bigg),\end{aligned} \tag{D.16}$$

where we have approximated $\langle\sigma v\rangle \approx 6b/x_f$. Finally, the prediction for the DM relic abundance, assuming a matter dominated universe during freeze-out, reads

$$\Omega_\chi h^2 = \zeta\frac{s_0 m_\chi Y_f}{\rho_{\text{critical}}}, \tag{D.17}$$

where $\rho_{\text{critical}} = 8.13\cdot 10^{-47}$ GeV^4, $s_0 \simeq 2.29\cdot 10^{-38}$ GeV^3. In the above equation, ζ parametrizes the dilution of the DM abundance after freeze-out due to the decays of ϕ and the subsequent entropy injection

$$\zeta = \frac{s_{\text{before}}}{s_{\text{after}}} = \frac{\Omega_\chi}{\Omega_\chi^f}, \tag{D.18}$$

which can be expressed with good approximation as follows

$$\zeta \approx \frac{45}{4\pi^3}\frac{1}{(1-\tau)g_*}\frac{T_{\text{RH}}}{T_\star}. \tag{D.19}$$

List of Figures

List of Tables

Bibliography

[1] A. Ahmed, A. Carmona, J. Castellano Ruiz, Y. Chung, and M. Neubert, "Dynamical origin of fermion bulk masses in a warped extra dimension," *JHEP* **08** (2019) 045, [arXiv:1905.09833].

[2] A. Carmona, J. Castellano, and M. Neubert, "A warped scalar portal to fermionic dark matter," arXiv:2011.09492.

[3] D. M. Straub, "flavio: a Python package for flavour and precision phenomenology in the Standard Model and beyond," arXiv:1810.08132.

[4] A. Buckley, J. Ferrando, S. Lloyd, K. Nordström, B. Page, M. Rüfenacht, M. Schönherr, and G. Watt, "LHAPDF6: parton density access in the LHC precision era," *Eur. Phys. J. C* **75** (2015) 132, [arXiv:1412.7420].

[5] J. D. Hunter, "Matplotlib: A 2d graphics environment," *Computing in Science & Engineering* **9** no. 3, (2007) 90–95.

[6] **ATLAS** Collaboration, G. Aad *et al.*, "Observation of a new particle in the search for the Standard Model Higgs boson with the ATLAS detector at the LHC," *Phys. Lett. B* **716** (2012) 1–29, [arXiv:1207.7214].

[7] S. Chatrchyan, V. Khachatryan, A. Sirunyan, A. Tumasyan, W. Adam, E. Aguilo, T. Bergauer, M. Dragicevic, J. Erö, C. Fabjan, and et al., "Observation of a new boson at a mass of 125 gev with the cms experiment at the lhc," *Physics Letters B* **716** no. 1, (Sep, 2012) 30–61. http://dx.doi.org/10.1016/j.physletb.2012.08.021.

[8] D. B. Kaplan, H. Georgi, and S. Dimopoulos, "Composite Higgs Scalars," *Phys. Lett. B* **136** (1984) 187–190.

[9] R. Rattazzi and A. Zaffaroni, "Comments on the holographic picture of the Randall-Sundrum model," *JHEP* **04** (2001) 021, [hep-th/0012248].

[10] N. Arkani-Hamed, M. Porrati, and L. Randall, "Holography and phenomenology," *JHEP* **08** (2001) 017, [hep-th/0012148].

[11] R. Contino, Y. Nomura, and A. Pomarol, "Higgs as a holographic pseudoGoldstone boson," *Nucl. Phys. B* **671** (2003) 148–174, [hep-ph/0306259].

[12] R. Contino and A. Pomarol, "Holography for fermions," *JHEP* **11** (2004) 058, [hep-th/0406257].

[13] R. Contino and A. Pomarol, "The holographic composite Higgs," *Comptes Rendus Physique* **8** (2007) 1058–1067.

[14] R. Contino, "The Higgs as a Composite Nambu-Goldstone Boson," in *Theoretical Advanced Study Institute in Elementary Particle Physics: Physics of the Large and the Small*, pp. 235–306. 2011. arXiv:1005.4269.

[15] H. Georgi and D. B. Kaplan, "Composite Higgs and Custodial SU(2)," *Phys. Lett. B* **145** (1984) 216–220.

[16] M. J. Dugan, H. Georgi, and D. B. Kaplan, "Anatomy of a Composite Higgs Model," *Nucl. Phys. B* **254** (1985) 299–326.

[17] K. Agashe, R. Contino, and A. Pomarol, "The Minimal composite Higgs model," *Nucl. Phys. B* **719** (2005) 165–187, [hep-ph/0412089].

[18] L. Randall and R. Sundrum, "A Large mass hierarchy from a small extra dimension," *Phys. Rev. Lett.* **83** (1999) 3370–3373, [hep-ph/9905221].

[19] N. Arkani-Hamed, S. Dimopoulos, and G. Dvali, "The hierarchy problem and new dimensions at a millimeter," *Physics Letters B* **429** no. 3-4, (Jun, 1998) 263–272. http://dx.doi.org/10.1016/S0370-2693(98)00466-3.

[20] N. Arkani-Hamed and M. Schmaltz, "Hierarchies without symmetries from extra dimensions," *Phys. Rev. D* **61** (2000) 033005, [hep-ph/9903417].

[21] T. Gherghetta and A. Pomarol, "Bulk fields and supersymmetry in a slice of AdS," *Nucl. Phys.* **B586** (2000) 141–162, [hep-ph/0003129].

[22] M. Perez-Victoria, "Randall-Sundrum models and the regularized AdS / CFT correspondence," *JHEP* **05** (2001) 064, [hep-th/0105048].

[23] K. Agashe and A. Delgado, "A Note on CFT dual of RS model with gauge fields in bulk," *Phys. Rev. D* **67** (2003) 046003, [hep-th/0209212].

[24] H. Georgi, A. K. Grant, and G. Hailu, "Chiral fermions, orbifolds, scalars and fat branes," *Phys. Rev.* **D63** (2001) 064027, [hep-ph/0007350].

[25] Y. Grossman and M. Neubert, "Neutrino masses and mixings in nonfactorizable geometry," *Phys. Lett.* **B474** (2000) 361–371, [hep-ph/9912408].

[26] K. R. Dienes, E. Dudas, and T. Gherghetta, "Extra space-time dimensions and unification," *Phys. Lett. B* **436** (1998) 55–65, [hep-ph/9803466].

[27] K. R. Dienes, E. Dudas, and T. Gherghetta, "Grand unification at intermediate mass scales through extra dimensions," *Nucl. Phys. B* **537** (1999) 47–108, [hep-ph/9806292].

[28] C. N. Yang and R. L. Mills, "Conservation of isotopic spin and isotopic gauge invariance," *Phys. Rev.* **96** (Oct, 1954) 191–195. https://link.aps.org/doi/10.1103/PhysRev.96.191.

[29] D. J. Gross and F. Wilczek, "Ultraviolet Behavior of Nonabelian Gauge Theories," *Phys. Rev. Lett.* **30** (1973) 1343–1346.

[30] H. D. Politzer, "Reliable Perturbative Results for Strong Interactions?," *Phys. Rev. Lett.* **30** (1973) 1346–1349.

[31] G. 't Hooft and M. Veltman, "Regularization and Renormalization of Gauge Fields," *Nucl. Phys. B* **44** (1972) 189–213.

[32] G. 't Hooft and M. Veltman, "Combinatorics of gauge fields," *Nucl. Phys. B* **50** (1972) 318–353.

[33] A. Pich, "The Standard Model of Electroweak Interactions," in *2010 European School of High Energy Physics*, pp. 1–50. 1, 2012. arXiv:1201.0537.

[34] A. Pich, "Electroweak Symmetry Breaking and the Higgs Boson," *Acta Phys. Polon. B* **47** (2016) 151, [arXiv:1512.08749].

[35] G. Altarelli and S. Forte, "Gauge Theories and the Standard Model,".

[36] G. Altarelli and S. Forte, "The Standard Model of Electroweak Interactions,".

[37] M. D. Schwartz, *Quantum Field Theory and the Standard Model*. Cambridge University Press, 3, 2014.

[38] M. E. Peskin and D. V. Schroeder, *An Introduction to quantum field theory*. Addison-Wesley, Reading, USA, 1995.

[39] S. Glashow, "Partial Symmetries of Weak Interactions," *Nucl. Phys.* **22** (1961) 579–588.

[40] S. Weinberg, "A Model of Leptons," *Phys. Rev. Lett.* **19** (1967) 1264–1266.

[41] A. Salam, "Weak and Electromagnetic Interactions," *Conf. Proc. C* **680519** (1968) 367–377.

[42] P. W. Higgs, "Broken symmetries, massless particles and gauge fields," *Phys. Lett.* **12** (1964) 132–133.

[43] F. Englert and R. Brout, "Broken Symmetry and the Mass of Gauge Vector Mesons," *Phys. Rev. Lett.* **13** (1964) 321–323.

[44] G. Guralnik, C. Hagen, and T. Kibble, "Global Conservation Laws and Massless Particles," *Phys. Rev. Lett.* **13** (1964) 585–587.

[45] T. Kibble, "Symmetry breaking in non-Abelian gauge theories," *Phys. Rev.* **155** (1967) 1554–1561.

[46] **Particle Data Group** Collaboration, P. Zyla *et al.*, "Review of Particle Physics," *PTEP* **2020** no. 8, (2020) 083C01.

[47] N. Cabibbo, "Unitary Symmetry and Leptonic Decays," *Phys. Rev. Lett.* **10** (1963) 531–533.

[48] M. Kobayashi and T. Maskawa, "CP Violation in the Renormalizable Theory of Weak Interaction," *Prog. Theor. Phys.* **49** (1973) 652–657.

[49] L.-L. Chau and W.-Y. Keung, "Comments on the Parametrization of the Kobayashi-Maskawa Matrix," *Phys. Rev. Lett.* **53** (1984) 1802.

[50] L. Wolfenstein, "Parametrization of the Kobayashi-Maskawa Matrix," *Phys. Rev. Lett.* **51** (1983) 1945.

[51] **CKMfitter Group** Collaboration, J. Charles, A. Hocker, H. Lacker, S. Laplace, F. Le Diberder, J. Malcles, J. Ocariz, M. Pivk, and L. Roos, "CP violation and the CKM matrix: Assessing the impact of the asymmetric B factories," *Eur. Phys. J. C* **41** no. 1, (2005) 1–131, [hep-ph/0406184].

[52] A. Hocker, H. Lacker, S. Laplace, and F. Le Diberder, "A New approach to a global fit of the CKM matrix," *Eur. Phys. J. C* **21** (2001) 225–259, [hep-ph/0104062].

[53] M. E. Peskin and T. Takeuchi, "Estimation of oblique electroweak corrections," *Phys. Rev. D* **46** (1992) 381–409.

[54] R. Barbieri, A. Pomarol, R. Rattazzi, and A. Strumia, "Electroweak symmetry breaking after LEP-1 and LEP-2," *Nucl. Phys.* **B703** (2004) 127–146, [hep-ph/0405040].

[55] A. Carmona Bermúdez, *Collider implications of heavy fermions in models with extra dimensions*. PhD thesis, U. Granada (main), 2013.

[56] H. Davoudiasl, S. Gopalakrishna, E. Ponton, and J. Santiago, "Warped 5-Dimensional Models: Phenomenological Status and Experimental Prospects," *New J. Phys.* **12** (2010) 075011, [arXiv:0908.1968].

[57] M. Baak, M. Goebel, J. Haller, A. Hoecker, D. Kennedy, R. Kogler, K. Mönig, M. Schott, and J. Stelzer, "The electroweak fit of the standard model after the discovery of a new boson at the lhc," *The European Physical Journal C* **72** no. 11, (Nov, 2012) . http://dx.doi.org/10.1140/epjc/s10052-012-2205-9.

[58] J. Haller, A. Hoecker, R. Kogler, K. Mönig, T. Peiffer, and J. Stelzer, "Update of the global electroweak fit and constraints on two-Higgs-doublet models," *Eur. Phys. J. C* **78** no. 8, (2018) 675, [arXiv:1803.01853].

[59] R. Aoude, "Effective field theory phenomenology and scattering amplitudes," 2020.

[60] B. Pontecorvo, "Mesonium and anti-mesonium," *Sov. Phys. JETP* **6** (1957) 429.

[61] B. Pontecorvo, "Inverse beta processes and nonconservation of lepton charge," *Sov. Phys. JETP* **7** (1958) 172–173.

[62] Z. Maki, M. Nakagawa, and S. Sakata, "Remarks on the unified model of elementary particles," in *11th International Conference on High-energy Physics*, pp. 663–666. 1962.

[63] B. Pontecorvo, "Neutrino Experiments and the Problem of Conservation of Leptonic Charge," *Sov. Phys. JETP* **26** (1968) 984–988.

[64] F. Zwicky, "Die Rotverschiebung von extragalaktischen Nebeln," *Helv. Phys. Acta* **6** (1933) 110–127.

[65] V. C. Rubin and J. Ford, W.Kent, "Rotation of the Andromeda Nebula from a Spectroscopic Survey of Emission Regions," *Astrophys. J.* **159** (1970) 379–403.

[66] P. A. R. Ade, N. Aghanim, M. Arnaud, M. Ashdown, J. Aumont, C. Baccigalupi, A. J. Banday, R. B. Barreiro, J. G. Bartlett, and et al., "Planck 2015 results," *Astronomy & Astrophysics* **594** (Sep, 2016) A13. http://dx.doi.org/10.1051/0004-6361/201525830.

[67] N. Aghanim, Y. Akrami, M. Ashdown, J. Aumont, C. Baccigalupi, M. Ballardini, A. J. Banday, R. B. Barreiro, N. Bartolo, and et al., "Planck 2018 results," *Astronomy & Astrophysics* **641** (Sep, 2020) A6. http://dx.doi.org/10.1051/0004-6361/201833910.

[68] G. Bertone and D. Hooper, "History of dark matter," *Reviews of Modern Physics* **90** no. 4, (Oct, 2018) . http://dx.doi.org/10.1103/RevModPhys.90.045002.

[69] G. Bertone, D. Hooper, and J. Silk, "Particle dark matter: evidence, candidates and constraints," *Physics Reports* **405** no. 5-6, (Jan, 2005) 279–390. http://dx.doi.org/10.1016/j.physrep.2004.08.031.

[70] T. Katsuragawa and S. Matsuzaki, "Dark matter in modified gravity?," *Physical Review D* **95** no. 4, (Feb, 2017) . http://dx.doi.org/10.1103/PhysRevD.95.044040.

[71] N. C. Martens and D. Lehmkuhl, "Dark matter = modified gravity? scrutinising the spacetime–matter distinction through the modified gravity/ dark matter lens," *Studies in History and Philosophy of Science Part B: Studies in History and Philosophy of Modern Physics* **72** (2020) 237 – 250. http://www.sciencedirect.com/science/article/pii/S135521982030109X.

[72] K.-H. Chae, F. Lelli, H. Desmond, S. S. McGaugh, P. Li, and J. M. Schombert, "Testing the Strong Equivalence Principle: Detection of the External Field Effect in Rotationally Supported Galaxies," *Astrophys. J.* **904** no. 1, (2020) 51, [arXiv:2009.11525].

[73] J. Moffat, "Modified Gravity or Dark Matter?," arXiv:1101.1935.

[74] **SNO** Collaboration, Q. Ahmad *et al.*, "Measurement of the rate of $\nu_e + d \rightarrow p + p + e^-$ interactions produced by ${}^8B$ solar neutrinos at the Sudbury Neutrino Observatory," *Phys. Rev. Lett.* **87** (2001) 071301, [nucl-ex/0106015].

[75] **SNO** Collaboration, Q. Ahmad *et al.*, "Measurement of day and night neutrino energy spectra at SNO and constraints on neutrino mixing parameters," *Phys. Rev. Lett.* **89** (2002) 011302, [nucl-ex/0204009].

[76] **SNO** Collaboration, Q. Ahmad *et al.*, "Direct evidence for neutrino flavor transformation from neutral current interactions in the Sudbury Neutrino Observatory," *Phys. Rev. Lett.* **89** (2002) 011301, [nucl-ex/0204008].

[77] **KamLAND** Collaboration, K. Eguchi *et al.*, "First results from KamLAND: Evidence for reactor anti-neutrino disappearance," *Phys. Rev. Lett.* **90** (2003) 021802, [hep-ex/0212021].

[78] Y. Fukuda, T. Hayakawa, E. Ichihara, K. Inoue, K. Ishihara, H. Ishino, Y. Itow, T. Kajita, J. Kameda, S. Kasuga, and et al., "Evidence for oscillation of atmospheric neutrinos," *Physical Review Letters* **81** no. 8, (Aug, 1998) 1562–1567. http://dx.doi.org/10.1103/PhysRevLett.81.1562.

[79] R. N. Mohapatra and G. Senjanović, "Neutrino mass and spontaneous parity nonconservation," *Phys. Rev. Lett.* **44** (Apr, 1980) 912–915. https://link.aps.org/doi/10.1103/PhysRevLett.44.912.

[80] M. Magg and C. Wetterich, "Neutrino mass problem and gauge hierarchy," *Physics Letters B* **94** no. 1, (1980) 61 – 64. http://www.sciencedirect.com/science/article/pii/0370269380908254.

[81] T. P. Cheng and L.-F. Li, "Neutrino masses, mixings, and oscillations in $su(2) \times u(1)$ models of electroweak interactions," *Phys. Rev. D* **22** (Dec, 1980) 2860–2868. https://link.aps.org/doi/10.1103/PhysRevD.22.2860.

[82] G. Lazarides, Q. Shafi, and C. Wetterich, "Proton lifetime and fermion masses in an so(10) model," *Nuclear Physics B* **181** no. 2, (1981) 287 – 300. http://www.sciencedirect.com/science/article/pii/0550321381903540.

[83] R. N. Mohapatra and G. Senjanović, "Neutrino masses and mixings in gauge models with spontaneous parity violation," *Phys. Rev. D* **23** (Jan, 1981) 165–180. https://link.aps.org/doi/10.1103/PhysRevD.23.165.

[84] R. Foot, H. Lew, X. G. He, and G. C. Joshi, "See-saw neutrino masses induced by a triplet of leptons," *Zeitschrift für Physik C Particles and Fields* **44** no. 3, (1989) 441–444. https://doi.org/10.1007/BF01415558.

[85] Y. Cai, J. Herrero-García, M. A. Schmidt, A. Vicente, and R. R. Volkas, "From the trees to the forest: a review of radiative neutrino mass models," *Front. in Phys.* **5** (2017) 63, [arXiv:1706.08524].

[86] J. Pendlebury, S. Afach, N. Ayres, C. Baker, G. Ban, G. Bison, K. Bodek, M. Burghoff, P. Geltenbort, K. Green, and et al., "Revised experimental upper limit on the electric dipole moment of the neutron," *Physical Review D* **92** no. 9, (Nov, 2015) . http://dx.doi.org/10.1103/PhysRevD.92.092003.

[87] S. Weinberg, "A New Light Boson?," *Phys. Rev. Lett.* **40** (1978) 223–226.

[88] F. Wilczek, "Problem of Strong P and T Invariance in the Presence of Instantons," *Phys. Rev. Lett.* **40** (1978) 279–282.

[89] R. Peccei and H. R. Quinn, "CP Conservation in the Presence of Instantons," *Phys. Rev. Lett.* **38** (1977) 1440–1443.

[90] V. Kuzmin, V. Rubakov, and M. Shaposhnikov, "On anomalous electroweak baryon-number non-conservation in the early universe," *Physics Letters B* **155** no. 1, (1985) 36 – 42. http://www.sciencedirect.com/science/article/pii/0370269385910287.

[91] D. N. Spergel, L. Verde, H. V. Peiris, E. Komatsu, M. R. Nolta, C. L. Bennett, M. Halpern, G. Hinshaw, N. Jarosik, A. Kogut, M. Limon, S. S. Meyer, L. Page, G. S. Tucker, J. L. Weiland, E. Wollack, and E. L. Wright, "First-year wilkinson microwave anisotropy probe (WMAP) observations: Determination of cosmological parameters," *The Astrophysical Journal Supplement Series* **148** no. 1, (Sep, 2003) 175–194. https://doi.org/10.1086%2F377226.

[92] A. Sakharov, "Violation of CP Invariance, C asymmetry, and baryon asymmetry of the universe," *Sov. Phys. Usp.* **34** no. 5, (1991) 392–393.

[93] H. M. Lee, "Lectures on Physics Beyond the Standard Model," 7, 2019. arXiv:1907.12409.

[94] **LHCb** Collaboration, R. Aaij *et al.*, "Search for lepton-universality violation in $B^+ \to K^+\ell^+\ell^-$ decays," *Phys. Rev. Lett.* **122** no. 19, (2019) 191801, [arXiv:1903.09252].

[95] **Belle** Collaboration, A. Abdesselam *et al.*, "Test of lepton flavor universality in $B \to K^*\ell^+\ell^-$ decays at Belle," arXiv:1904.02440.

[96] **Belle** Collaboration, A. Abdesselam *et al.*, "Measurement of $\mathcal{R}(D)$ and $\mathcal{R}(D^*)$ with a semileptonic tagging method," arXiv:1904.08794.

[97] **LHCb** Collaboration, R. Aaij *et al.*, "Test of lepton universality with $B^0 \to K^{*0}\ell^+\ell^-$ decays," *JHEP* **08** (2017) 055, [arXiv:1705.05802].

[98] A. Crivellin and F. Saturnino, "Explaining the Flavor Anomalies with a Vector Leptoquark (Moriond 2019 update)," *PoS* **DIS2019** (2019) 163, [arXiv:1906.01222].

[99] G. Nordström, "On the possibility of unifying the electromagnetic and the gravitational fields," *ArXiv Physics e-prints* (Feb., 2007) , [physics/0702221].

[100] T. Kaluza, "On the Problem of Unity in Physics," *Sitzungsber. Preuss. Akad. Wiss. Berlin (Math. Phys.)* **1921** (1921) 966–972.

[101] O. Klein, "Quantentheorie und fünfdimensionale relativitätstheorie," *Zeitschrift für Physik* **37** no. 12, (Dec, 1926) 895–906. https://doi.org/10.1007/BF01397481.

[102] A. Pomarol and M. Quiros, "The Standard model from extra dimensions," *Phys. Lett. B* **438** (1998) 255–260, [hep-ph/9806263].

[103] A. Pomarol, "Gauge bosons in a five-dimensional theory with localized gravity," *Phys. Lett. B* **486** (2000) 153–157, [hep-ph/9911294].

[104] H. Davoudiasl, J. Hewett, and T. Rizzo, "Bulk gauge fields in the Randall-Sundrum model," *Phys. Lett. B* **473** (2000) 43–49, [hep-ph/9911262].

[105] M. Carena, A. Delgado, E. Ponton, T. M. P. Tait, and C. E. M. Wagner, "Precision electroweak data and unification of couplings in warped extra dimensions," *Phys. Rev.* **D68** (2003) 035010, [hep-ph/0305188].

[106] M. Carena, A. Delgado, E. Ponton, T. M. P. Tait, and C. E. M. Wagner, "Warped fermions and precision tests," *Phys. Rev.* **D71** (2005) 015010, [hep-ph/0410344].

[107] M. Carena, E. Ponton, J. Santiago, and C. E. M. Wagner, "Light Kaluza Klein States in Randall-Sundrum Models with Custodial SU(2)," *Nucl. Phys.* **B759** (2006) 202–227, [hep-ph/0607106].

[108] M. Carena, E. Ponton, J. Santiago, and C. E. M. Wagner, "Electroweak constraints on warped models with custodial symmetry," *Phys. Rev.* **D76** (2007) 035006, [hep-ph/0701055].

[109] M. Carena, S. Casagrande, F. Goertz, U. Haisch, and M. Neubert, "Higgs Production in a Warped Extra Dimension," *JHEP* **08** (2012) 156, [arXiv:1204.0008].

[110] S. Casagrande, F. Goertz, U. Haisch, M. Neubert, and T. Pfoh, "Flavor Physics in the Randall-Sundrum Model: I. Theoretical Setup and Electroweak Precision Tests," *JHEP* **10** (2008) 094, [arXiv:0807.4937].

[111] S. Casagrande, F. Goertz, U. Haisch, M. Neubert, and T. Pfoh, "The Custodial Randall-Sundrum Model: From Precision Tests to Higgs Physics," *JHEP* **09** (2010) 014, [arXiv:1005.4315].

[112] P. R. Archer, "The Fermion Mass Hierarchy in Models with Warped Extra Dimensions and a Bulk Higgs," *JHEP* **09** (2012) 095, [arXiv:1204.4730].

[113] P. R. Archer, M. Carena, A. Carmona, and M. Neubert, "Higgs Production and Decay in Models of a Warped Extra Dimension with a Bulk Higgs," *JHEP* **01** (2015) 060, [arXiv:1408.5406].

[114] S. J. Huber, "Flavor violation and warped geometry," *Nucl. Phys. B* **666** (2003) 269–288, [hep-ph/0303183].

[115] G. von Gersdorff, "Flavor Physics in Warped Space," *Mod. Phys. Lett. A* **30** no. 15, (2015) 1540013, [arXiv:1311.2078].

[116] C. Csaki, M. L. Graesser, and G. D. Kribs, "Radion dynamics and electroweak physics," *Phys. Rev.* **D63** (2001) 065002, [hep-th/0008151].

[117] C. Csaki, J. Erlich, and J. Terning, "The Effective Lagrangian in the Randall-Sundrum model and electroweak physics," *Phys. Rev.* **D66** (2002) 064021, [hep-ph/0203034].

[118] C. Csaki, G. Marandella, Y. Shirman, and A. Strumia, "The Super-little Higgs," *Phys. Rev. D* **73** (2006) 035006, [hep-ph/0510294].

[119] C. Csaki, A. Falkowski, and A. Weiler, "The Flavor of the Composite Pseudo-Goldstone Higgs," *JHEP* **09** (2008) 008, [arXiv:0804.1954].

[120] S. De Curtis, M. Redi, and A. Tesi, "The 4D Composite Higgs," *JHEP* **04** (2012) 042, [arXiv:1110.1613].

[121] M. Redi and A. Tesi, "Implications of a Light Higgs in Composite Models," *JHEP* **10** (2012) 166, [arXiv:1205.0232].

[122] M. Redi, "Implications of 125 GeV Higgs in Composite Models," *PoS* **ICHEP2012** (2013) 159.

[123] C. Csáki and P. Tanedo, "Beyond the Standard Model," in *Proceedings, 2013 European School of High-Energy Physics (ESHEP 2013): Paradfurdo, Hungary, June 5-18, 2013*, pp. 169–268. 2015. arXiv:1602.04228.

[124] J. A. Cabrer, G. von Gersdorff, and M. Quiros, "Suppressing Electroweak Precision Observables in 5D Warped Models," *JHEP* **05** (2011) 083, [arXiv:1103.1388].

[125] J. A. Cabrer, G. von Gersdorff, and M. Quiros, "Warped 5D Standard Model Consistent with EWPT," *Fortsch. Phys.* **59** (2011) 1135–1138, [arXiv:1104.5253].

[126] J. A. Cabrer, G. von Gersdorff, and M. Quiros, "Flavor Phenomenology in General 5D Warped Spaces," *JHEP* **01** (2012) 033, [arXiv:1110.3324].

[127] J. A. Cabrer, G. von Gersdorff, and M. Quiros, "Improving Naturalness in Warped Models with a Heavy Bulk Higgs Boson," *Phys. Rev. D* **84** (2011) 035024, [arXiv:1104.3149].

[128] A. M. Iyer, K. Sridhar, and S. K. Vempati, "Bulk Randall-Sundrum models, electroweak precision tests, and the 125 GeV Higgs," *Phys. Rev. D* **93** no. 7, (2016) 075008, [arXiv:1502.06206].

[129] B. M. Dillon and S. J. Huber, "Non-Custodial Warped Extra Dimensions at the LHC?," *JHEP* **06** (2015) 066, [arXiv:1410.7345].

[130] J. de Blas, A. Delgado, B. Ostdiek, and A. de la Puente, "LHC Signals of Non-Custodial Warped 5D Models," *Phys. Rev. D* **86** (2012) 015028, [arXiv:1206.0699].

[131] A. M. Iyer, "B anomalies: From warped models to colliders," in *53rd Rencontres de Moriond on QCD and High Energy Interactions*, pp. 97–100. 2018. arXiv:1805.06832.

[132] K. Agashe, A. Delgado, M. J. May, and R. Sundrum, "RS1, custodial isospin and precision tests," *JHEP* **08** (2003) 050, [hep-ph/0308036].

[133] P. Sikivie, L. Susskind, M. B. Voloshin, and V. I. Zakharov, "Isospin Breaking in Technicolor Models," *Nucl. Phys.* **B173** (1980) 189–207.

[134] K. Agashe, R. Contino, L. Da Rold, and A. Pomarol, "A Custodial symmetry for $Zb\bar{b}$," *Phys. Lett.* **B641** (2006) 62–66, [hep-ph/0605341].

[135] S. Casagrande, F. Goertz, U. Haisch, M. Neubert, and T. Pfoh, "The custodial randall-sundrum model: from precision tests to higgs physics," *Journal of High Energy Physics* **2010** no. 9, (Sep, 2010) . http://dx.doi.org/10.1007/JHEP09(2010)014.

[136] C. Csaki, C. Grojean, L. Pilo, and J. Terning, "Towards a realistic model of Higgsless electroweak symmetry breaking," *Phys. Rev. Lett.* **92** (2004) 101802, [hep-ph/0308038].

[137] J. M. Maldacena, "The Large N limit of superconformal field theories and supergravity," *Int. J. Theor. Phys.* **38** (1999) 1113–1133, [hep-th/9711200]. [Adv. Theor. Math. Phys. 2,231(1998)].

[138] S. S. Gubser, I. R. Klebanov, and A. M. Polyakov, "Gauge theory correlators from noncritical string theory," *Phys. Lett.* **B428** (1998) 105–114, [hep-th/9802109].

[139] E. Witten, "Anti-de Sitter space and holography," *Adv. Theor. Math. Phys.* **2** (1998) 253–291, [hep-th/9802150].

[140] C. Csaki, J. Hubisz, and P. Meade, "TASI lectures on electroweak symmetry breaking from extra dimensions," in *Physics in D >= 4. Proceedings, Theoretical Advanced Study Institute in elementary particle physics, TASI 2004, Boulder, USA, June 6-July 2, 2004*, pp. 703–776. 2005. hep-ph/0510275.

[141] C. Csaki, J. Hubisz, and S. J. Lee, "Radion phenomenology in realistic warped space models," *Phys. Rev. D* **76** (2007) 125015, [arXiv:0705.3844].

[142] B. Batell and T. Gherghetta, "Warped phenomenology in the holographic basis," *Phys. Rev. D* **77** (2008) 045002, [arXiv:0710.1838].

[143] T. Gherghetta, "A Holographic View of Beyond the Standard Model Physics," in *Physics of the large and the small, TASI 09, proceedings of the Theoretical Advanced Study Institute in Elementary Particle Physics, Boulder, Colorado, USA, 1-26 June 2009*, pp. 165–232. 2011. arXiv:1008.2570.

[144] L. Nilse, "Classification of 1D and 2D orbifolds," *AIP Conf. Proc.* **903** (2007) 411–414, [hep-ph/0601015]. [,411(2006)].

[145] M. Carena, E. Ponton, T. M. Tait, and C. Wagner, "Opaque Branes in Warped Backgrounds," *Phys. Rev. D* **67** (2003) 096006, [hep-ph/0212307].

[146] H. Davoudiasl, J. Hewett, and T. Rizzo, "Phenomenology of the Randall-Sundrum Gauge Hierarchy Model," *Phys. Rev. Lett.* **84** (2000) 2080, [hep-ph/9909255].

[147] S. J. Huber and Q. Shafi, "Higgs mechanism and bulk gauge boson masses in the Randall-Sundrum model," *Phys. Rev. D* **63** (2001) 045010, [hep-ph/0005286].

[148] R. Diener and C. Burgess, "Bulk Stabilization, the Extra-Dimensional Higgs Portal and Missing Energy in Higgs Events," *JHEP* **05** (2013) 078, [arXiv:1302.6486].

[149] J. Hahn, C. Hörner, R. Malm, M. Neubert, K. Novotny, and C. Schmell, "Higgs Decay into Two Photons at the Boundary of a Warped Extra Dimension," *Eur. Phys. J.* **C74** no. 5, (2014) 2857, [arXiv:1312.5731].

[150] R. Malm, M. Neubert, K. Novotny, and C. Schmell, "5D Perspective on Higgs Production at the Boundary of a Warped Extra Dimension," *JHEP* **01** (2014) 173, [arXiv:1303.5702].

[151] H. Davoudiasl, B. Lillie, and T. G. Rizzo, "Off-the-wall Higgs in the universal Randall-Sundrum model," *JHEP* **08** (2006) 042, [hep-ph/0508279].

[152] G. Cacciapaglia, C. Csaki, G. Marandella, and J. Terning, "The Gaugephobic Higgs," *JHEP* **02** (2007) 036, [hep-ph/0611358].

[153] F. Mahmoudi, U. Maitra, N. Manglani, and K. Sridhar, "A Higgs in the Warped Bulk and LHC signals," *JHEP* **11** (2016) 075, [arXiv:1608.07407].

[154] M. Bauer, C. Hörner, and M. Neubert, "Diphoton Resonance from a Warped Extra Dimension," *JHEP* **07** (2016) 094, [arXiv:1603.05978].

[155] R. Malm, M. Neubert, and C. Schmell, "Higgs Couplings and Phenomenology in a Warped Extra Dimension," *JHEP* **02** (2015) 008, [arXiv:1408.4456].

[156] P. Breitenlohner and D. Z. Freedman, "Positive Energy in anti-De Sitter Backgrounds and Gauged Extended Supergravity," *Phys. Lett.* **115B** (1982) 197–201.

[157] P. Breitenlohner and D. Z. Freedman, "Stability in Gauged Extended Supergravity," *Annals Phys.* **144** (1982) 249.

[158] E. Ponton, "TASI 2011: Four Lectures on TeV Scale Extra Dimensions," in *Theoretical Advanced Study Institute in Elementary Particle Physics: The Dark Secrets of the Terascale*, pp. 283–374. 2013. arXiv:1207.3827.

[159] K. Dienes, "New directions for new dimensions: An introduction to Kaluza-Klein theory, large extra dimensions, and the brane world," in *Theoretical Advanced Study Institute in Elementary Particle Physics (TASI 2002): Particle Physics and Cosmology: The Quest for Physics Beyond the Standard Model(s)*, pp. 447–545. 6, 2002.

[160] F. Goertz, *Warped Extra Dimensions: Flavor, Precision Tests and Higgs Physics*. PhD thesis, Mainz U., Inst. Phys., 2011. arXiv:1112.6387.

[161] R. Sundrum, "Effective field theory for a three-brane universe," *Phys. Rev. D* **59** (1999) 085009, [hep-ph/9805471].

[162] W. D. Goldberger and M. B. Wise, "Modulus stabilization with bulk fields," *Phys. Rev. Lett.* **83** (1999) 4922–4925, [hep-ph/9907447].

[163] C. Csaki, "TASI lectures on extra dimensions and branes," in *Theoretical Advanced Study Institute in Elementary Particle Physics (TASI 2002): Particle Physics and Cosmology: The Quest for Physics Beyond the Standard Model(s)*, pp. 605–698. 4, 2004. hep-ph/0404096.

[164] S. Raychaudhuri and K. Sridhar, *Particle Physics of Brane Worlds and Extra Dimensions*. Cambridge Monographs on Mathematical Physics. Cambridge University Press, 5, 2016.

[165] O. DeWolfe, D. Z. Freedman, S. S. Gubser, and A. Karch, "Modeling the fifth-dimension with scalars and gravity," *Phys. Rev.* **D62** (2000) 046008, [hep-th/9909134].

[166] C. Csaki, M. Graesser, L. Randall, and J. Terning, "Cosmology of brane models with radion stabilization," *Phys. Rev. D* **62** (2000) 045015, [hep-ph/9911406].

[167] K.-m. Cheung, "Phenomenology of radion in Randall-Sundrum scenario," *Phys. Rev. D* **63** (2001) 056007, [hep-ph/0009232].

[168] J. Garriga, O. Pujolas, and T. Tanaka, "Radion effective potential in the brane world," *Nucl. Phys. B* **605** (2001) 192–214, [hep-th/0004109].

[169] J. F. Gunion, M. Toharia, and J. D. Wells, "Precision electroweak data and the mixed Radion-Higgs sector of warped extra dimensions," *Phys. Lett. B* **585** (2004) 295–306, [hep-ph/0311219].

[170] K. Agashe, G. Perez, and A. Soni, "Flavor structure of warped extra dimension models," *Phys. Rev.* **D71** (2005) 016002, [hep-ph/0408134].

[171] S. J. Huber and Q. Shafi, "Fermion masses, mixings and proton decay in a Randall-Sundrum model," *Phys. Lett.* **B498** (2001) 256–262, [hep-ph/0010195].

[172] A. Carmona and J. Santiago, "The Effective Lagrangian for Bulk Fermions in Models with Extra Dimensions," *JHEP* **01** (2012) 100, [arXiv:1110.5651].

[173] C. Hörner, *Analyses of production and decay processes of the Higgs boson and of a new scalar in a warped extra dimension*. PhD thesis, Mainz U., 2018.

[174] C. Froggatt and H. B. Nielsen, "Hierarchy of Quark Masses, Cabibbo Angles and CP Violation," *Nucl. Phys. B* **147** (1979) 277–298.

[175] B. Grzadkowski and M. Toharia, "Low-energy effective theory from a nontrivial scalar background in extra dimensions," *Nucl. Phys.* **B686** (2004) 165–187, [hep-ph/0401108].

[176] M. Toharia and M. Trodden, "Metastable kinks in the orbifold," *Phys. Rev. Lett.* **100** (2008) 041602, [arXiv:0708.4005].

[177] M. Toharia, M. Trodden, and E. J. West, "Scalar Kinks in Warped Extra Dimensions," *Phys. Rev.* **D82** (2010) 025009, [arXiv:1002.0011].

[178] M. Blanke, A. J. Buras, B. Duling, S. Gori, and A. Weiler, "$\Delta F = 2$ Observables and Fine-Tuning in a Warped Extra Dimension with Custodial Protection," *JHEP* **03** (2009) 001, [arXiv:0809.1073].

[179] M. Bauer, S. Casagrande, L. Gründer, U. Haisch, and M. Neubert, "Little Randall-Sundrum models: ϵ_K strikes again," *Phys. Rev.* **D79** (2009) 076001, [arXiv:0811.3678].

[180] M. Bauer, S. Casagrande, U. Haisch, and M. Neubert, "Flavor Physics in the Randall-Sundrum Model: II. Tree-Level Weak-Interaction Processes," *JHEP* **09** (2010) 017, [arXiv:0912.1625].

[181] M. Bauer, R. Malm, and M. Neubert, "A Solution to the Flavor Problem of Warped Extra-Dimension Models," *Phys. Rev. Lett.* **108** (2012) 081603, [arXiv:1110.0471].

[182] D. B. Kaplan, J.-W. Lee, D. T. Son, and M. A. Stephanov, "Conformality Lost," *Phys. Rev.* **D80** (2009) 125005, [arXiv:0905.4752].

[183] J. Lesgourgues and L. Sorbo, "Goldberger-Wise variations: Stabilizing brane models with a bulk scalar," *Phys. Rev.* **D69** (2004) 084010, [hep-th/0310007].

[184] T. Gherghetta and M. Peloso, "Stability analysis of 5D gravitational solutions with N bulk scalar fields," *Phys. Rev. D* **84** (2011) 104004, [arXiv:1109.5776].

[185] L. Randall and M. D. Schwartz, "Quantum field theory and unification in AdS5," *JHEP* **11** (2001) 003, [hep-th/0108114].

[186] F. Goertz, U. Haisch, and M. Neubert, "Bounds on Warped Extra Dimensions from a Standard Model-like Higgs Boson," *Phys. Lett.* **B713** (2012) 23–28, [arXiv:1112.5099].

[187] **FCC** Collaboration, A. Abada *et al.*, "Future Circular Collider," CERN-ACC-2018-0058.

[188] K. Agashe, M. Papucci, G. Perez, and D. Pirjol, "Next to minimal flavor violation," hep-ph/0509117.

[189] J. Santiago, "Minimal Flavor Protection: A New Flavor Paradigm in Warped Models," *JHEP* **12** (2008) 046, [arXiv:0806.1230].

[190] S. Davidson, G. Isidori, and S. Uhlig, "Solving the flavour problem with hierarchical fermion wave functions," *Phys. Lett. B* **663** (2008) 73–79, [arXiv:0711.3376].

[191] M. Blanke, A. J. Buras, B. Duling, K. Gemmler, and S. Gori, "Rare K and B Decays in a Warped Extra Dimension with Custodial Protection," *JHEP* **03** (2009) 108, [arXiv:0812.3803].

[192] M. Ciuchini *et al.*, "Δm_K and ϵ_K in SUSY at the next-to-leading order," *JHEP* **10** (1998) 008, [hep-ph/9808328].

[193] J. Brod, M. Gorbahn, and E. Stamou, "Standard-model prediction of ϵ_K with manifest CKM unitarity," *Phys. Rev. Lett.* **125** no. 17, (2020) 171803, [arXiv:1911.06822].

[194] K. Agashe, G. Perez, and A. Soni, "B-factory signals for a warped extra dimension," *Phys. Rev. Lett.* **93** (2004) 201804, [hep-ph/0406101].

[195] A. Azatov, M. Toharia, and L. Zhu, "Higgs Mediated FCNC's in Warped Extra Dimensions," *Phys. Rev.* **D80** (2009) 035016, [arXiv:0906.1990].

[196] L. Vecchi, "A Natural Hierarchy and a low New Physics scale from a Bulk Higgs," *JHEP* **11** (2011) 102, [arXiv:1012.3742].

[197] **Physics of the HL-LHC Working Group** Collaboration, M. Cepeda *et al.*, "Higgs Physics at the HL-LHC and HE-LHC," arXiv:1902.00134.

[198] J. de Blas *et al.*, "Higgs Boson Studies at Future Particle Colliders," *JHEP* **01** (2020) 139, [arXiv:1905.03764].

[199] P. Gondolo and G. Gelmini, "Cosmic abundances of stable particles: Improved analysis," *Nucl. Phys.* **B360** (1991) 145–179.

[200] S. Hamdan and J. Unwin, "Dark Matter Freeze-out During Matter Domination," *Mod. Phys. Lett. A* **33** no. 29, (2018) 1850181, [arXiv:1710.03758].

[201] P. Chanda, S. Hamdan, and J. Unwin, "Reviving Z and Higgs Mediated Dark Matter Models in Matter Dominated Freeze-out," *JCAP* **01** no. 01, (2020) 034, [arXiv:1911.02616].

[202] M. Frank, N. Pourtolami, and M. Toharia, "Higgs Bosons in Warped Space, from the Bulk to the Brane," *Phys. Rev. D* **87** no. 9, (2013) 096003, [arXiv:1301.7692].

[203] **XENON** Collaboration, P. Di Gangi, "First dark matter search results of the XENON1T experiment," *Nuovo Cim. C* **41** no. 3, (2018) 109.

[204] **XENON** Collaboration, E. Aprile *et al.*, "Dark Matter Search Results from a One Ton-Year Exposure of XENON1T," *Phys. Rev. Lett.* **121** no. 11, (2018) 111302, [arXiv:1805.12562].

[205] **ATLAS** Collaboration, M. Aaboud *et al.*, "Observation of $H \to b\bar{b}$ decays and VH production with the ATLAS detector," *Phys. Lett. B* **786** (2018) 59–86, [arXiv:1808.08238].

[206] K. Agashe and G. Servant, "Warped unification, proton stability and dark matter," *Phys. Rev. Lett.* **93** (2004) 231805, [hep-ph/0403143].

[207] **CMS** Collaboration, A. M. Sirunyan *et al.*, "Search for invisible decays of a Higgs boson produced through vector boson fusion in proton-proton collisions at $\sqrt{s} = 13$ TeV," *Phys. Lett.* **B793** (2019) 520–551, [arXiv:1809.05937].

[208] Y. G. Kim and K. Y. Lee, "The Minimal model of fermionic dark matter," *Phys. Rev. D* **75** (2007) 115012, [hep-ph/0611069].

[209] G. Arcadi, A. Djouadi, and M. Raidal, "Dark Matter through the Higgs portal," *Phys. Rept.* **842** (2020) 1–180, [arXiv:1903.03616].

[210] **Planck** Collaboration, N. Aghanim *et al.*, "Planck 2018 results. VI. Cosmological parameters," arXiv:1807.06209.

[211] H. M. Lee, M. Park, and V. Sanz, "Gravity-mediated (or Composite) Dark Matter," *Eur. Phys. J. C* **74** (2014) 2715, [arXiv:1306.4107].

[212] H. Davoudiasl, J. Hewett, and T. Rizzo, "Brane localized curvature for warped gravitons," *JHEP* **08** (2003) 034, [hep-ph/0305086].

[213] M. G. Folgado, A. Donini, and N. Rius, "Spin-dependence of Gravity-mediated Dark Matter in Warped Extra-Dimensions," arXiv:2006.02239.

[214] M. Escudero, A. Berlin, D. Hooper, and M.-X. Lin, "Toward (Finally!) Ruling Out Z and Higgs Mediated Dark Matter Models," *JCAP* **12** (2016) 029, [arXiv:1609.09079].

[215] S. Kanemura, S. Matsumoto, T. Nabeshima, and N. Okada, "Can WIMP Dark Matter overcome the Nightmare Scenario?," *Phys. Rev. D* **82** (2010) 055026, [arXiv:1005.5651].

[216] M. Hoferichter, J. Ruiz de Elvira, B. Kubis, and U.-G. Meißner, "High-Precision Determination of the Pion-Nucleon σ Term from Roy-Steiner Equations," *Phys. Rev. Lett.* **115** (2015) 092301, [arXiv:1506.04142].